The University of Sheffield

Tumour cell-bone cell interactions in breast cancer bone metastases; mechanisms and effects of therapies

Hannah K Brown

PhD thesis

February 2012

DEPARTMENT OF ONCOLOGY
SCHOOL OF MEDICINE AND BIOMEDICAL SCIENCES

Permission of reproduction

Permission for reproduction in this thesis is granted for the following manuscripts:

Brown HK, Holen I. Anti-tumour effects of bisphosphonates--what have we learned from *in vivo* models? Curr Cancer Drug Targets. 2009 Nov;9(7):807-23. With kind permission from Bentham Science Publishers Ltd.

Brown HK, Ottewell PD, Evans CA, Holen I. Location matters: osteoblast and osteoclast distribution is modified by the presence and proximity to breast cancer cells *in vivo*. Clin Exp Metastasis. 2012 May 6. [Epub ahead of print]. With kind permission from Springer Science and Business Media.

Acknowledgements

Firstly, I would like to thank my supervisor Dr Ingunn Holen for all her help, guidance, encouragement and support in the last years. Thank you very much!!!

I would like to thank Dr Penny Ottewell who has taught me so many techniques and could not have done this without her. Also thank you for the moral support whenever it was needed.

A big thank you also goes to Alyson Evans, Diane Lefley, Natasha Wind, and Caroline Wilson who have all been brilliant in helping me out when I could not manage on my own and in answering my never ending questions…

Orla Gallagher, Holly Evans, Les Coulton and Darren Lath, thank you very much for cutting so many sections for me and answering my µCT and histomorphometry questions.

I would also like to say thank you to Shelly Lawson and Mark Jones who have helped me with the multiphoton microscopy and flow cytometry.

Of course I could not have done this without my wonderful friends Ewa Dudziec (!!), Louise Way and Ankita Agrawal. The many pub hours after work were always a pleasure :o)

Ευχαριστώ πολύ Νικόλας!!! You really were fantastic in supporting me, encouraging me, calming me down, helping me out, listening and sharing happy moments!

Und ganz zum Schluss ein riesen grosses DANKE an meine tolle Familie!! I hope I made you proud :o)

Summary

Metastasis to bone is a common complication of advanced breast cancer and is often associated with pain and high morbidity. Although effective therapeutic strategies are available for primary breast cancer, metastatic disease is currently incurable and associated with poor outcome. Detailed understanding of early stage disease in bone, supporting the development of effective treatment regimens at this point is therefore required. The vicious cycle of metastatic tumour growth and bone destruction is often targeted in patients presenting with osteolytic lesions by addition of anti-resorptive agents (bisphosphonates) to standard neoplastic therapy. In addition to the bone sparing effects, bisphosphonates have been shown to exert anti-tumour effects *in vitro* and *in vivo.* The main aim of this thesis was to identify bone cell-tumour cell interactions during disease progression, including stages prior to bone destruction. Furthermore, the anti-cancer effects of early sequence- and schedule-dependent combination therapy with doxorubicin followed by zoledronic acid were assessed, with particular focus on the bone microenvironment. In addition, the frequently asked question whether bisphosphonates are actively internalised by peripheral tumour cells (i.e. outside the skeleton) was investigated *in vivo*.

This thesis contributes important information to the field of bone metastases by showing for the first time that osseous tumour growth *in vivo* dramatically alters bone cell distribution depending on cell type, proximity to the tumour and disease stage. Treatment studies provided strong evidence that early administration of a single dose of combination treatment is effective in bone protection and in the inhibition of osseous tumour growth. It was furthermore shown for the first time that a small subset of peripheral breast cancer cells internalise fluorescently labelled bisphosphonate, suggesting a potential direct effect of the compounds on extra-skeletal tumour cells *in vivo*.

Collectively, the work presented in this thesis has provided strong evidence that the presence of tumour cells initiates significant changes to the bone microenvironment prior to the development of lesions. Treatment should therefore be initiated at an earlier stage of advanced disease. In addition, anti-tumour effects of combination therapy were found to be in part mediated through alterations to the bone microenvironment. It was furthermore shown that bisphosphonate treatment might redirect tumour growth to extraosseous sites, underlining the necessity to further investigate the effects of bone sparing agents on metastatic tumour growth.

List of abbreviations

ATCC	American Type Culture Collection
B	Bone
BM	Bone marrow
BP	Bisphosphonate
BrdU	Bromodeoxyuridine (5-bromo-2-deoxyuridine)
BV/TV	Bone volume per tissue volume
CBA	Cytometric bead array
cDNA	Complementary DNA
cm	Centimetre
cm^3	Centimetre cubed
CO_2	Carbon dioxide
CT	Cycle threshold
CTX	Collagen type-1 cross-linked C-telopeptide
CXCR4	C-X-C chemokine receptor type 4
DEPC	Diethyl pyrocarbonate
dH_2O	Deionised water
DKK	Dickkopf-related protein
DMSO	Dimethyl sulfoxide
DNA	Deoxyribonucleic acid
dNTPs	Deoxynucleotide triphosphates
Dox	Doxorubicin
EDTA	Ethylenediaminetetraacetic acid
ELISA	Enzyme-linked immunosorbant assays
EOP	End of procedure
FADD	Fas-Associated protein with Death Domain
FAM	6-carboxyfluorescin (fluorescent dye)
FCS	Foetal Calf Serum
g	Gram
GFP	Green fluorescent protein
GMCSF	Granulocyte-macrophage colony-stimulating factor
H&E	Hematoxylin and eosin
H_2O	Water
H_2O_2	Hydrogen peroxide
HCL	Hydrochloric acid
HRP	Horse Radish Peroxidise
i.c.	Intracardiac
IGF	Insulin-like growth factor
IL	Interleukin
M	Muscle
MCP-1	Monocyte chemotactic protein
mg	Milligram
MgCl2	Magnesium Chloride
min	Minute

ml	Millilitre
mRNA	Messenger RNA
NaCl	Sodium chloride
NBP	Nitrogen-containing bisphosphonate
ng	Nanogram
nu	nude
Ob	Osteoblast
Oc	Osteoclast
OPG	Osteoprotegerin
p.i.	Peritoneal
PBS	Phosphate buffered saline
PCR	Polymerase chain reactions
PFA	Paraformaldehyde
pg	Picogram
PTH	Parathyroid hormone
PTHrP	Parathyroid hormone-related protein
qRT-PCR	Quantitative Real Time Polymerase Chain Reaction
RANK	Receptor activator of NF-kappaB
RANKL	Receptor activator of NF-kappaB ligand
RNA	Ribonucleic acid
rpm	rounds per minute
RT	Room temperature
sec	Second
s.c.	Subcutaneous
SDF1	Stromal cell-derived factor-1
SEM	Standard error of the mean
SFRP	Secreted frizzled-related protein
T	Tumour
Taq	Thermus aquaticus
TGF	Transforming growth factor beta
TRAP	Tartrate-resistant acid phosphatase
Tris	Tris(hydroxymethyl)aminomethane
UK	United Kingdom
UV	Ultra-violet
VEGF	Vascular Endothelial Growth Factor
vs.	Versus
Zol	Zoledronic acid
β-Gal	beta-galactosidase
µCT	Micro-computed tomography
µg	Microgram
µl	Microlitre
µM	Micromolar
°C	Degree Celsius
4PL	4-parameter logistic

Table of Contents

Table of Figures

List of Tables

1. Introduction

1.1 Breast cancer and the metastatic process

Among women, breast cancer is the most common malignancy and represents the second leading cause of the high mortality rate for cancer patients. At least 70% of breast cancer patients with advanced disease develop bone metastases and death is often due to the formation and progression of metastatic lesions (Coleman, 2001). Over the past decades there has been great progress in the treatment of early breast cancer, but the current inability to cure metastatic disease emphasises the need for new treatment strategies for advanced cancer patients. The investigation of bone metastases in humans is greatly impeded due to the lack of available biopsies. Hence translational research using preclinical models plays an important role in identifying new treatment targets.

The process of metastasis, the dispersion of tumour cells through blood or lymphatic fluid and establishment at a new site, is comprised of a coordinated sequence of events. Most studies investigating the metastatic process have focussed on the cancer cells, however, more recent research is pointing out the significance of the tumour microenvironment for the metastatic process (Joyce and Pollard, 2009). Stephen Paget was the first to report that metastatic patterns of human cancers follow a preferred distribution to certain sites with close associations between the seed (tumour) and soil (microenvironment), an interaction that is now investigated frequently (Paget, 1889). Some cancer cells within the primary tumour alter their interactions with the surrounding extracellular matrix, which provides the cells with the potential to detach and enter the circulation but it still remains unclear what triggers these processes in detail. One important step in the release of tumour cells from the primary mass is the epithelial to mesenchymal transition (EMT or oncogenic EMT). In this reversible process, the polarised, sessile epithelial cells undergo several changes to become mesenchymal like cells with characteristics such as enhanced migration, invasion and protection from apoptosis (Kalluri and Weinberg, 2009). The EMT transition is therefore connected to increased tumourigenicity and increased cell survival and it has furthermore been shown that EMT is linked to expression of stem cell like markers. Once in the circulation, tumour cells are thought to bypass the immune system and mechanic forces through the formation of microthrombi with platelets (Jurasz et al., 2004). These structures may furthermore aid extravasation by lodging at sites of

capillary beds like the sinusoids in the bone marrow. The cells next have to attach to the new site in order to initiate tumour cell progression and blood vessel formation. Although the presence of disseminated breast tumour cells in the bone marrow has been associated with poor prognosis (Gebauer et al., 2001), not all of these cancer cells will develop into tumour colonies. Hence it is thought that only some specialised cancer cells, possibly those with stem like properties, are able to form metastatic foci. In addition, the complex interactions with the cells of the bone marrow is further highlighted by recent reports showing that cancer cells colonise to specialised sites in bone, the putative metastatic niches. The latter could help to explain the occasionally long period of time between primary tumour presentation and bone metastases development, a process that can last several years.

1.2 Tumour-induced bone disease

The following sections will describe the complex bone remodelling processes in a healthy setting as well as in the event of osseous tumour growth.

1.2.1 Differentiation of osteoblasts and osteoclasts

The unmineralised bone matrix (osteoid) consists primarily of collagen type-I, which is secreted by mesenchymal derived osteoblasts. Progenitor cells of the mesenchymal lineage interact with hormones, TGF-ß (transforming growth factor β) and BMPs (bone morphogenic proteins) leading to the activation of the canonical Wnt/ß-catenin pathway. Furthermore, expression of Runx2 (Runt-related transcription factor 2) (Ducy et al., 1999) and the downstream expression of osterix (Nakashima et al., 2002) were linked to the differentiation into pre-osteoblasts. Active osteoblasts then secrete collagen type I and alkaline phosphatase, both essential for the formation of osteoid, as well as factors involved in bone remodelling such as osteonectin, osteocalcin, osteopontin, SDF-1 (CXCL12), macrophage colony stimulating factor (M-CSF), osteoprotegerin (OPG) and receptor activator of nuclear factor kappa-B ligand (RANKL) (Harada and Rodan, 2003). The latter three molecules play a major role in the regulation of osteoclast differentiation, activation and survival and form together with RANK the main pathway of osteoclastogenesis (Boyle et al., 2003). On completion of bone formation the osteoblasts undergo apoptosis, develop into bone lining cells or become embedded in the osteoid, thus giving rise to osteocytes. An important negative regulator of osteoblast formation is the inhibition of the canonical Wnt

signalling pathway through antagonists like DKK1 (dickkopf 1) and sclerostin (expressed by osteocytes and osteoblasts) (Niehrs, 2006; Mendoza-Villanueva et al., 2011).

In contrast to the bone matrix secreting osteoblasts, the osteoclasts carry out bone resorption. Osteoclast precursors derive from haematopoietic stem cells of the monocyte lineage. In order to fuse and develop into multinucleated osteoclasts the progenitor cells require the interaction of RANKL (Receptor Activator of Nuclear factor κB Ligand), RANK and M-CSF (Teitelbaum, 2000). Osteoblasts and marrow stromal cells express RANKL whereas RANK is found on mononucleated osteoclast precursor cells. Together with OPG (osteoprotegerin), the soluble decoy receptor to RANK and therefore an inhibitor of the RANKL/RANK interaction, a system is generated to control formation and activity of mature osteoclasts (Lacey et al., 1998). The controlled interactions between osteoblast and osteoclast differentiation and activity are called "coupling" (Parfitt, 2000). A schematic overview of osteoblast and osteoclast differentiation is shown in Figure 1.1.

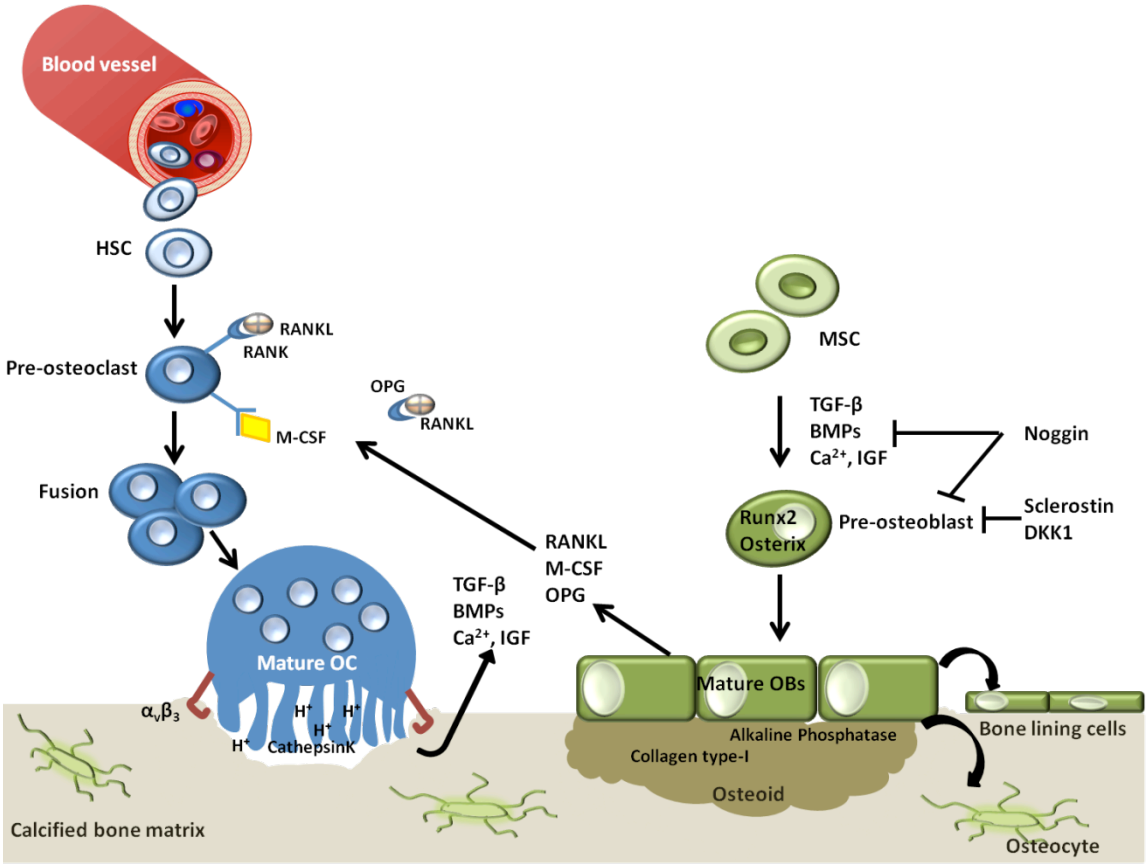

Figure 1.1 Osteoblast (Ob) and osteoclast (Oc) differentiation
Pre-osteoclasts interact with RANKL and M-CSF, which is followed by fusion of several precursors. The polykaryon is then attached to the bone matrix through $\alpha_v\beta_3$ integrin interactions. Mature osteoclasts form a ruffled border and release acid and proteolytic enzymes onto the calcified matrix triggering bone degradation and the formation of a resorption pit. During this process, TGF-ß, Ca^{2+} and other molecules are released from the matrix. Several of these factors then interact with osteoblast precursors resulting in the expression of Runx2 and osterix and thus the development into mature osteoblasts. During osteoid formation, osteoblasts also release RANKL, OPG and M-CSF, which in turn regulate osteoclastogenesis. Osteoblast differentiation is partly controlled by the expression of sclerostin and DKK1 by mature osteoblast and osteocytes as well as the BMP inhibitor noggin. HSC= haematopoietic stem cell, MSC=mesenchymal stem cell.

1.2.2 Bone remodelling in a healthy setting

In a healthy human approximately 5-10% of the bone matrix is replaced per year resulting in perpetual bone turnover. One cycle of trabecular bone remodelling lasts approximately 200 days in which around one quarter of this time is attributed to bone resorption and three quarters to bone formation. The process is closely regulated by a number of calciotropic hormones (for example parathyroid hormone (PTH) and oestrogen) (Harada and Rodan, 2003) and is carried out in a defined structural space, the bone-remodelling compartment (BRC) (Hattner et al., 1965; Parfitt, 2000). BRCs are

often enclosed by a canopy of bone lining cells and consist of osteoclasts, osteoblasts and blood vessels. During remodelling the osteoclasts adhere to the bone matrix through $\alpha_v\beta_3$ integrin, osteopontin and sialoprotein mediated interactions (Reinholt et al., 1990; Ross et al., 1993). The intimate contact between the ruffled border and the bone surface leads to the secretion of acid and proteolytic enzymes onto the bone matrix. During this process, collagen and stored growth factors (TGF-β, Ca^{2+}) are released, which is followed by osteoblast migration to the site of bone resorption. Osteoclast activity is terminated and osteoblast maturation commences before fresh osteoid is secreted (Boyle et al., 2003; Teitelbaum, 2000) (Fig. 1.2). This fine tuned process of bone remodelling is normally perfectly balanced in time and space but it may be disrupted in pathological conditions. Thus, bone remodelling can also carry risks: control-errors can cause either excessive bone resorption or formation. Aggressive cancers can induce an imbalance in bone turnover, a complication that is termed the vicious cycle.

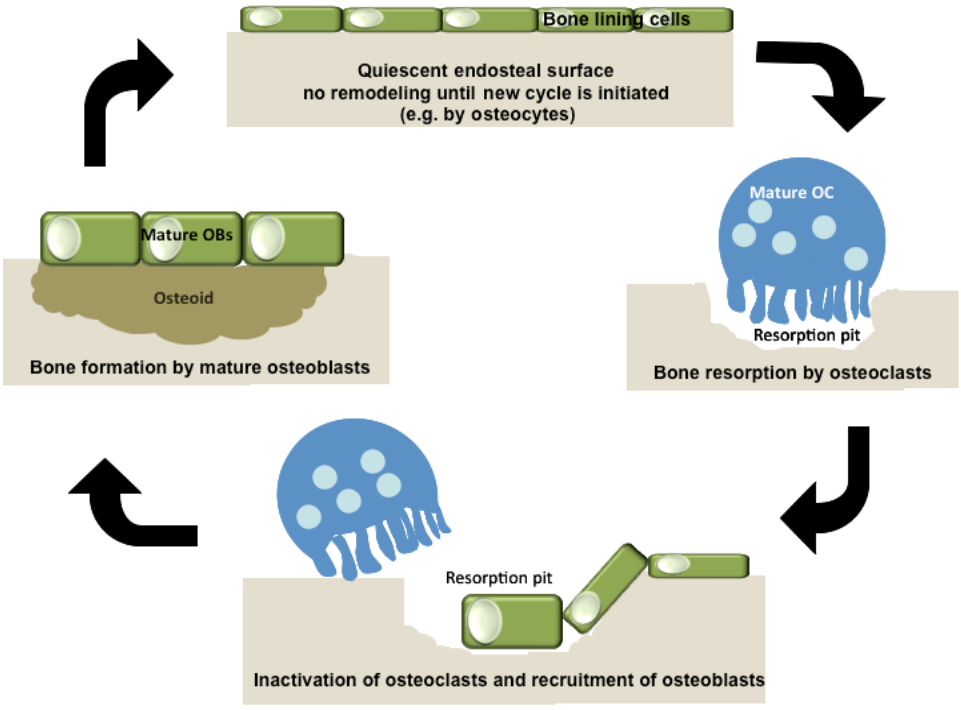

Figure 1.2 Bone turnover
Bone is regularly remodelled by osteoclasts, which are responsible for bone resorption, and osteoblasts, which replace the bone matrix with fresh osteoid. Oc=osteoclast, Ob=osteoblast.

1.2.3 The vicious cycle

Different types of solid tumours show a predilection of metastases to bone, with breast, prostate and lung cancer being the most common types. Tumour cells in bone result in the development of osteolytic, osteoblastic or mixed lesions, depending on the type of primary cancer. The associated skeletal morbidity is high, with a pathophysiology of bone fractures, hypercalcemia of malignancy and spinal cord compression.

Studies investigating metastatic tumour growth in bone have mainly focused on end stage disease with uncontrolled tumour growth and associated bone destruction. While these late stage studies only investigate a small area of the metastatic process they have greatly contributed to our understanding of the tumour-induced alterations to bone remodeling. The integrin $\alpha_v\beta_3$, which mediates osteoclast binding to bone, is also abundant in bone localised breast cancer cells and it is therefore likely that the integrin, in addition to other factors, assists towards the adherence of cancer cells to bone (Liapis et al., 1996). Once tumour cells have formed established colonies they disturb the normal bone remodelling through several factors, such as PTHrP (Parathyroid Hormone-related Protein), thus inducing osteoblasts to mediate osteoclast formation and activity through RANK/RANKL interactions (Roodman, 2001). In addition, tumour cells have been reported to express RANK and OPG, suggesting that the cells may actively alter the most relevant pathway of osteoclastogenesis (Thomas et al., 1999). RANK expressing tumour cells were furthermore shown to colonise tissues with high levels of RANKL, as was shown by tumour growth in bone (Jones et al., 2006). Other tumour derived factors that influence the osteoblast-osteoclast cross-talk are osteoclast enhancing cytokines such as IL-6 (Blanchard et al., 2009) and IL-8 (Bendre et al., 2003) as well as BMPs (Sato et al., 2010). Recently, it has been reported that osteoblast inhibitors such as the Wnt antogonist DKK1 as well as the BMP inhibitor noggin are selectively expressed in ostoelytic but not osteoblastic cell lines (Schwaninger et al., 2007). Furthermore, intraosseous PC3 xenografts (osteolytic prostate cancer) were shown to reduce bone formation *in vivo*, an effect that could be reversed after silencing noggin (Secondini et al., 2011). Tumour cells may therefore not only induce an increase in bone resorption but also inhibit bone formation, thus enhancing the osteolytic potential of the tumour. During the event of

bone resorption, TGF-β and Ca^{2+} ions are released from the bone matrix causing increased PTHrP secretion by breast cancer cells. This finally results in increased osteoclast formation connected with bone resorption and a vicious cycle of bone destruction and tumour cell growth is generated. However, before this microenvironment-independent stage of tumour growth is reached, the tumour cells firstly need to adapt and survive at the new site in order to initiate proliferation. The latter requires several interactions between the cancer cell and the bone microenvironment and will be discussed in the following section.

1.2.4 The bone marrow– a safe place for cancer cells?

Bone marrow contains mesenchymal stem cells (MSCs), haematopoietic stem cells (HSCs) and endothelial stem cells (EnSCs). MSCs have the ability to regenerate bone cells (osteoblasts, chondrocytes) and marrow stromal cells (fibroblasts, adipocytes) while HSCs regenerate cells of the lymphoid (B-, Natural Killer-, T-cells and lymphoid dendritic cells) and blood lineage (erythrocytes, platelets, granylocytes, monocytes, myeloid dendritic cells). The bone marrow is thus comprised of a high heterogeneity of cell types and several of them have been shown to have implications in tumour growth. For instance, bone marrow derived cells like hematopoietic progenitor cells are involved in the formation of the pre-metastatic niche (Kaplan et al., 2005) while monocytes and macrophages are recruited by the tumour due to their secretion of tumourigenic chemokines and MMPs (Rogers and Holen, 2011). The osteoclasts, which also derive from the hematopoietic lineage, are heavily involved in osseous breast tumour growth due to the involvement in the vicious cycle. Finally, mesenchymal derived cells, like fibroblasts are crucial components in the tumour stroma (Kalluri and Zeisberg, 2006), while osteoblasts have only recently been associated with breast tumour growth in bone as will be shown in the following section.

1.2.5 Interaction of tumour cells with cells of the bone marrow

Our understanding of the initiating stages of metastatic tumour growth in bone including homing, engraftment and the switch from micro- to macro-metastatic growth remains incomplete but are all areas of active research. A recent report has added to the complexity of the metastatic process by introducing the concept of the pre-metastatic niche. It was shown that before localisation of metastatic tumour cells to the lung, the primary tumour releases systemic factors, which subsequently target

the secondary site and make it more susceptible for tumour cell homing (Kaplan et al., 2005). The disseminated tumour cells next need to engraft, which has been shown to be a similar process to that of HSC homing and retention, including factors like osteopontin (Wai and Kuo, 2008) and CXCL12-CXCR4 interactions (Psaila and Lyden, 2009). The osteoblasts, and other stromal cells, play a major role in the HSC niche (also known as osteoblastic or endosteal niche) and increasing evidence suggests that these cells are also involved in tumour cell homing to bone. For example, osteoblasts highly express CXCL12 (SDF-1) while some breast cancer cells have been shown to express the receptor CXCR4 (Muller et al., 2001). In addition, the osteoblast derived adhesion molecule osteopontin was suggested to interact with $\alpha_v ß_3$ integrin expressing cancer cells (Takayama et al., 2005). A recent study by Shiozawa et al. (2011) was the first to show that disseminated prostate cancer cells directly compete with HSCs for engraftment into the osteoblastic niche at endosteal surfaces of an *in vivo* prostate cancer model. It was furthermore shown that experimental expansion and compression of the HSC niche was associated with increased or decreased numbers of disseminated cancer cells in the bone marrow. The spatial and temporal interactions between cancer cells and osteoblasts during tumour progression require further comprehensive *in vivo* studies in order to fully understand the complex cellular interactions. One important concept of the occupancy of the HSC niche by disseminated tumour cells may be the associated potential to induce a dormant state, thus enabling these cancer cells to escape cytotoxic challenges. In this respect, the study mentioned above has proposed a novel way of targeting these quiescent cells. Intriguingly the group could show that disseminated prostate cancer cells that had occupied HSC niches could be released into the circulation by using agents previously shown to mobilise engrafted HSCs (Shiozawa et al., 2011) thus possibly making them susceptible for treatment.

It is currently not known what triggers dormant tumour cells in the bone marrow to escape from quiescence and to eventually start proliferating. Cell-cell and cell-matrix interactions in the microenvironment may play a role. For example, the receptor CD44 (a cancer stem cell marker) has been shown to bind to several ligands in bone including hyaluronic acid, fibronectin, collagen type-I and osteopontin (Psaila and Lyden, 2009). Changes in expression patterns of these molecules by osteoblasts or other stromal

cells could potentially trigger tumour cells to progress. Endothelial cells and pericytes are furthermore recruited through tumour-derived pro-angiogenic factors (e.g. VEGF) eventually leading to the establishment of new vasculature and microenvironment-independent growth. Although angiogenesis is crucial for tumour progression, this process is not frequently studied because of difficulties in reproducible, quantitative analysis of (tumour associated) blood vessels in bone. The osteoclast is furthermore a cell type that is greatly involved in metastatic breast tumour growth in bone due to the crucial role in the vicious cycle. Breast cancer cells have also been shown to express the Wnt inhibitors DKK1 (Voorzanger-Rousselot et al., 2007) and sclerostin (Mendoza-Villanueva et al., 2011) leading to osteoblast suppression and increase in the osteolytic potential of the tumour.

It is therefore clear that the interactions between the multitude of cells present in the bone marrow and the tumour are of high complexity and require further analysis in order to develop new therapeutics for these crucial early stages of tumour progression. Especially the events involved in tumour cell engraftment, the initiating processes of tumour progression leading to bone destruction and the transition of micro- to macro-metastatic growth requires further investigation (Fig. 1.3). While the importance of the osteoblast in breast cancer has been shown for cancer cell homing to bone, the role of these cells at other stages of breast tumour growth remains greatly unknown. The osteoblast, in connection with the osteoclast, may be a key element in the switch from microenvironment-dependent to -independent growth. Investigation of newly established cancer colonies in bone and the cell-cell interactions with the surrounding bone cells during tumour progression may give insight into new treatment strategies.

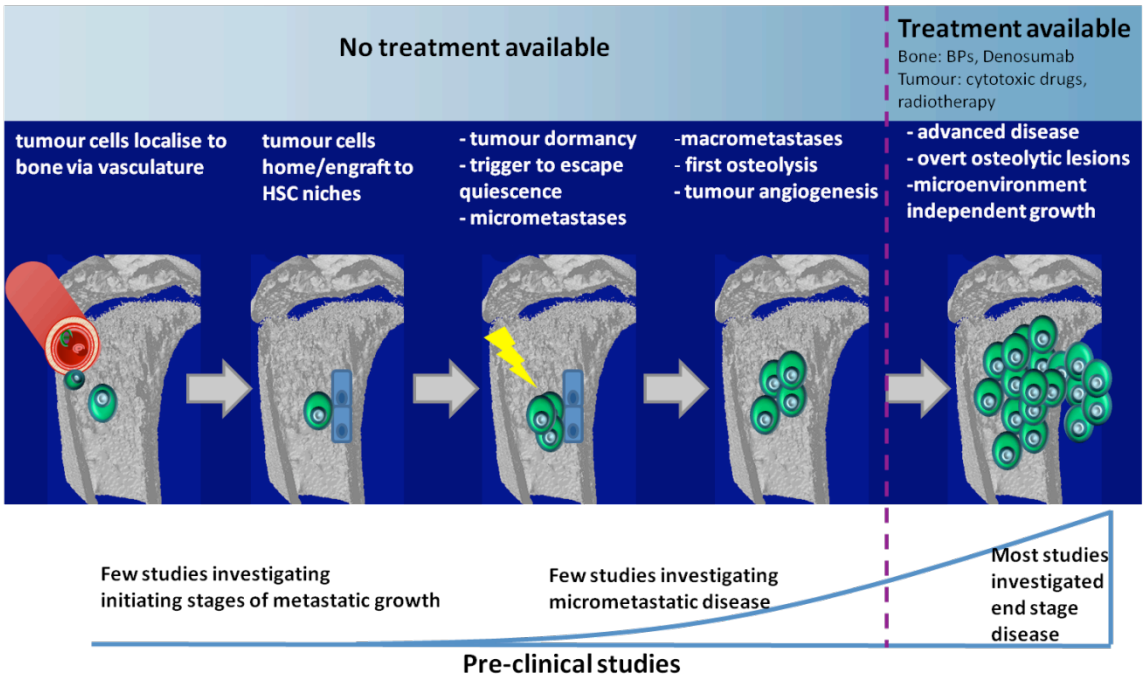

Figure 1.3 Overview of bone metastases development
The cartoon emphasises the lack of available treatment options for early stage disease and highlights the focus of preclinical studies on end stage disease. In order to develop new therapeutic strategies, more research has to be carried out at the earlier stages of tumour growth including homing, engraftment and the switch from micro- to macro-metastatic growth. BP=bisphosphonate, HSC=hematopoietic stem cell.

1.3 Treatment of cancer-induced bone disease

As shown above, bone homing tumour cells may interact with the bone microenvironment and use it to their favour, resulting in tumour growth progression and induction of the vicious cycle. Cancer-induced bone disease is generally treated with an anti-neoplastic and a palliative regimen, the latter including radiotherapy, administration of analgesia and occasionally orthopaedic surgery to improve quality of life. In addition, bisphosphonates (BPs) are effective inhibitors of bone resorption, resulting in pain relief and reduced incidence of skeletal-related events (Rosen et al., 2004; Kohno et al., 2005). The following sections will give an overview over some of the relevant agents used in breast cancer-induced bone disease.

1.3.1 Cytotoxic drugs

Breast cancer patients with recurrent disease can be separated into two groups, a high-risk and a low-risk group, based on clinical information regarding the probability of aggressive tumour progression. Low risk patients, with long disease-free survival,

confined metastatic sites and often ER+ (oestrogen receptor positive) tumours are most susceptible to hormone therapy. However, therapy resistance is not uncommon, thus necessitating the need for alternative treatments (chemotherapy) in this subgroup of patients. In addition, high-risk patients with multiple metastases and aggressive ER- (oestrogen receptor negative) tumours and patients requiring neoadjuvant therapy will be treated with a cytotoxic regimen. Due to the high heterogeneity of fast proliferating tumour cells, combination treatment with two or more of a variety of cytotoxic agents and/or other targeted compounds is common in clinical practice. While a number of chemotherapeutic agents are licensed for the treatment of breast cancer, the vast majority of patients will receive an anthracycline based treatment (for example doxorubicin or epirubicin) during the course of their disease, either as neoadjuvant/adjuvant or metastatic therapy.

1.3.1.1 Doxorubicin –mechanism of action

Doxorubicin is an anthracycline antibiotic produced by *Streptomyces peucetius varians caesius.* The planar structure of the tetracyclic ring system enables the compound to intercalate with the DNA double helix resulting in impairment of DNA- and RNA-polymerase activity and therefore leads to inhibition of DNA replication and transcription (Fornari et al., 1994). Apart from this, it was shown that doxorubicin can form DNA structures with topoisomerase II possibly causing the frequently found DNA strand breaks and it is thought that this mechanism is the main contributor to the drugs cytotoxicity (Silber et al., 1987). Doxorubicin has also been reported to induce the formation of hydroxyl free radicals (HO·) eventually leading to irreversible damage (Doroshow, 1983). As a result of the mechanisms described above cells exposed to doxorubicin eventually undergo apoptosis.

1.3.1.2 Doxorubicin in clinical practice

Because chemotherapeutic agents generally target fast proliferating cells, not only tumour cells but also hair follicle and cells lining the intestine etc. are affected, resulting in a number of side effects associated with cytotoxic drugs. In the case of doxorubicin, the most concerning adverse effect is its myocardial toxicity, which appears to increase in a dose-dependent manner. This toxic activity on cardiac cells is possibly connected to the drug's ability to generate free radicals (Shi et al., 2009).

The drug is most commonly administered in intervals of 21-days as monotherapy at 60-75mg/m^2 and in combination at 40-60mg/m^2 via a single intravenous injection. The duration of treatment and number of cycles is usually based on the individual case, and is limited by the cumulative cardic toxicity.

1.3.2 Bisphosphonates

Bisphosphonates are a substantial part of treatment regimens used for cancer-induced osteolysis and other malignant bone diseases due to their known anti-resorptive activity.

1.3.2.1 Chemical properties of bisphosphonates

Bisphosphonates are non-hydrolysable synthetic analogues of pyrophosphate (PPi) with a stable P-C-P backbone instead of the highly reactive phosphoanhydrid bonds (P-O-P) as found in PPi. There are a variety of different bisphosphonate structures with altering side chains, referred to as R^1 and R^2, which allow covalent binding of a number of molecules (Fig. 1.4). The P-C-P backbone structure comprises strong affinity to bind divalent cations like Ca^{2+}, Mg^{2+} and Fe^{2+} leading to binding of bisphosphonates to bone when administered *in vivo* (Masarachia et al., 1996).

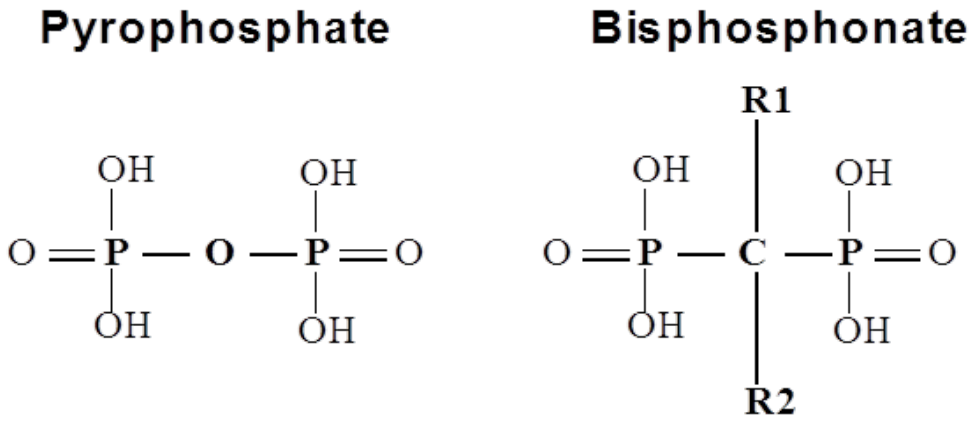

Figure 1.4 Structural differences between pyrophosphates and bisphosphonates
The P-C-P backbone of bisphosphonates is essential for binding to bone mineral while the side-chain R^1, usually -OH, -H or -Cl, enhances this effect. The R^2 side chain is more variable and enhances the anti-resorptive potency of the bisphosphonate.

1.3.2.2 Simple bisphosphonates and nitrogen-containing bisphosphonates

The varying chemical structure within the bisphosphonate group has been found to affect their anti-resorptive activity and the underlying mechanisms of action. This

divides the compounds into two classes: the simple bisphosphonates and the more complex nitrogen-containing bisphosphonates. Clodronate and etidronate, which closely resemble the structure of PPi and do not have complex side chains, have been reported to exhibit the weakest anti-resorptive activity *in vivo*. To date zoledronic acid (zol) is the most potent BP containing a ring structure with nitrogen at the R^2 side-chain and the drug is reported to have up to 10,000 fold higher anti-resorptive activity *in vitro* than the simpler counter parts (Fig. 1.5) (Widler et al., 2002).

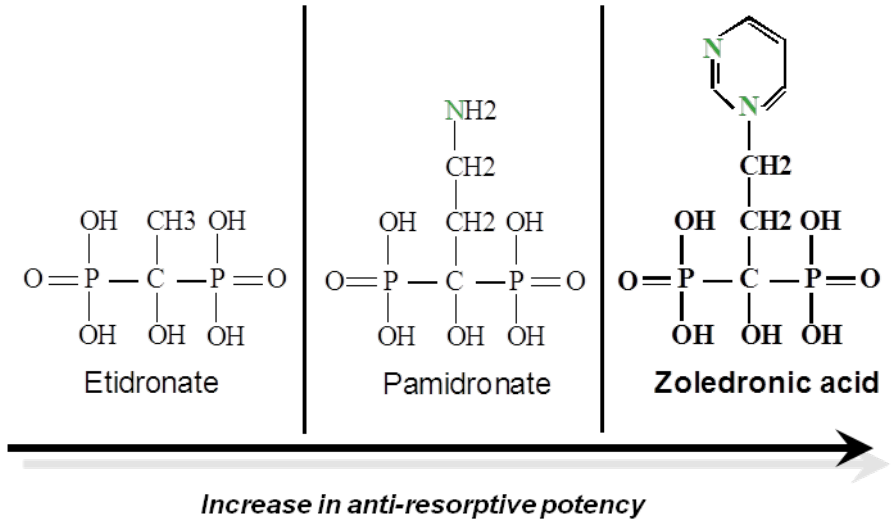

Figure 1.5 Structures of bisphosphonates
Clodronate resembles the structure of simple bisphosphonates. Increased length of the R^2 alkyl chain and the addition of a nitrogen residue enhance the potency of bone resorption with the most potent bisphosphonates being zoledronic acid and BPs with a similar structure.

1.3.2.3 Mechanism of action of nitrogen-containing bisphosphonates

In contrast to the simple bisphosphonates, the more complex nitrogen-containing bisphosphonates (NBPs) like zoledronic acid exert their mechanism of action through the inhibition of the mevalonate pathway. This ubiquitous pathway is responsible for isoprenoid and cholesterol production and is therefore required in every proliferating cell type. More precisely, NBPs have been shown to inhibit a key enzyme, the farnesyl diphosphate (FPP) synthase, which is responsible for conversion of IPP (isopentenyl diphosphate) to FPP (Fig. 1.6) (Martin et al., 1999). The lack of the downstream products FPP (farnesyl diphosphate) and GGPP (geranylgeranyl diphosphate) consequently leads to lack of substrates required for protein isoprenylation (Luckman et al., 1998). The main group of prenylated proteins is comprised of small GTPases,

such as Ras, Rho and Rac, and correct intracellular localisation and function of these proteins is dependent on the post-translational modification. It has been shown that the members of these protein families are essential for a variety of functions, especially in osteoclast activity and viability (Rogers et al., 2000). The drugs therefore inhibit osteoclastic bone resorption efficiently and thus find broad application in diseases of the bone. In addition, other prenylated proteins are likely to be affected by the drug. For example, the zoledronic acid-induced inhibition of prenylation was shown to cause delocalisation of the centromere protein F (Cenp-F) from the kinetochore resulting in impaired mitotic progression in a range of breast cancer cell lines (Brown et al., 2011).

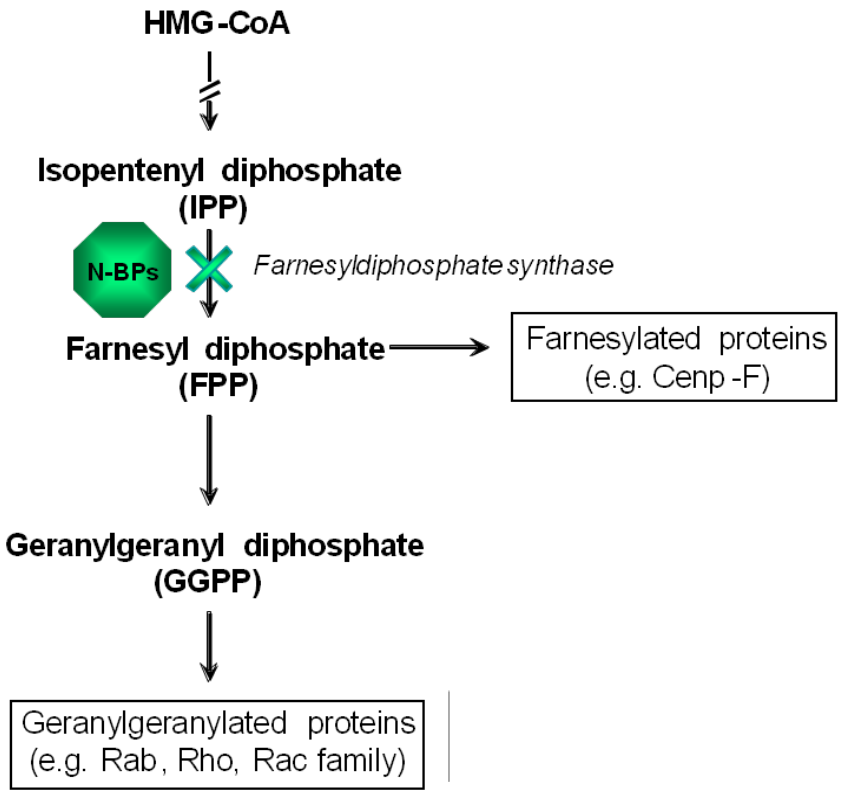

Figure 1.6 Mechanism of action of nitrogen-containing bisphosphonates
HMG-CoA is converted in several steps to IPP, the substrate for farnesyldiphosphate synthase. In the presence of NBPs, FPP synthase is inhibited consequently resulting in loss of the downstream products FPP and GGPP and inhibition of protein prenylation.

As soon as the effect of NBPs on the FPP synthase had been reported it was suggested that nitrogen-containing BPs might act on any cell type as long as sufficient amounts of the drug are internalised. To date, a number of cell types have been investigated in *in vitro* experiments revealing osteoclasts and macrophages to be the most sensitive to low zoledronic acid concentrations. The differing sensitivity between cell types is most likely reflected in their endocytic activity (Thompson et al., 2006), suggesting that cancer cells may also be affected. Indeed, the latter has been true for a number of cancer cell types in *in vitro* experiments showing a reduction in cell proliferation and induction of apoptosis (Fromigue et al., 2000; Clyburn et al., 2010). Whether the compound can also reach tumour cells *in vivo* and if the concentration is high enough to induce cytotoxic effects remains to be established.

1.3.2.4 Clinical use of bisphosphonates

Bisphosphonates are commonly used to treat breast cancer-induced bone disease, but also find application in other bone related malignancies to reduce the risk of skeletal related events (SREs) such as hypercalcemia, bone pain, pathological fractures and spinal cord compression. In an advanced cancer setting, zoledronic acid is currently administered intravenously at a dose of 4mg over 15 minutes every 3-4 weeks. Bisphosphonate treatment in the metastatic setting is only initiated when bone lesions have been confirmed radiologically.

In addition, new adjuvant applications of bisphosphonates are emerging. Breast cancer therapy can induce bone loss through alterations to the reproductive hormone levels. Chemotherapy in pre-menopausal women can induce menopause, ovarian function can be suppressed by therapies (e.g. goserelin) and aromatase inhibitors can cause a reduction in oestrogen levels resulting in bone reduction. The treatment-induced bone loss can be effectively treated with bisphosphonates, either at the point when increased bone loss is detected on DEXA scan, or as a preventive therapy in patients at high risk for bone loss (Conte and Frassoldati, 2007; Coleman et al., 2008).

1.4 Anti-tumour effects of bisphosphonates

Apart from the effects on bone resorption, there is increasing interest in the potential anti-tumour effects of bisphosphonates, and evidence is emerging from *in vitro* and *in vivo* studies supporting this. Numerous *in vitro* studies of a range of tumour cells have suggested induction of apoptosis, inhibition of proliferation, invasion and adhesion being involved in the molecular mechanisms (Neville-Webbe et al., 2002; Clezardin, 2005). For example, zoledronic acid, pamidronate and ibandronate treatment were shown to have anti-proliferative and pro-apoptotic effects on several breast cancer cell lines including MDA-MB-231 (Fromigue et al., 2000; Verdijk et al., 2007). Due to the strong anti-resorptive activity of bisphosphonates, indirect anti-tumour activity via the inhibition of the vicious cycle and thus depletion of bone-derived growth factors has also been proposed. Although the osteoblast is shown to be increasingly important in the role of cancer cell homing to bone, not much is known about whether the drugs also affect osteoblasts. A recent *in vitro* study reported, however, that bisphosphonate coated bone slices reduce the growth of primary rat osteoblasts, suggesting that the drugs may also interact directly with the bone forming cells (Cornish et al., 2011). The relevance of these data in an *in vivo* setting remains to be established. In addition, the coupling mechanism between osteoclasts and osteoblasts suggest that the bone forming cells may also be affected indirectly through impairment of the osteoclast.

The *in vivo* pharmacokinetic characteristics of bisphosphonates have been frequently questioned regarding the potential anti-tumour effects. *In vitro* studies showing anti-cancer efficacy of BPs often used very high dosing regimens with prolonged treatment times resulting in drug levels that are not achievable *in vivo*. This is due to the high affinity of the drugs to bone and thus bisphosphonates are rapidly cleared from the circulation effectively reducing the compounds availability in soft tissues. In clinical practice, zoledronic acid is administered as an infusion of 4mg over 15 minutes every 3-4 weeks. After intravenous administration, the majority of the drug (up to 60%) rapidly binds to bone resulting in a short serum half-life of about 1 hour (Chen et al., 2002; Brown et al., 2007). Hence, zoledronic acid peak plasma levels reach only concentrations of 1-2M and decline to approximately 1% after 24 hours. In bone, however, zoledronic acid is stored for years (Brown et al., 2007) and concentrations are thought to reach levels of up to 1000µM in the resorption pits underneath actively

resorbing osteoclasts (Sato et al., 1991), a level that may induce cytotoxic effects. It has therefore been proposed that tumour cells within bone could be exposed to a potentially cytotoxic concentration of bisphosphonates, compared to cancer cells localised in peripheral soft tissues. The difference in drug distribution between tissues consequently leads to the question whether bisphosphonate concentrations outside bone ever reach cytotoxic levels. In addition, the exact cellular and molecular mechanisms involved in the proposed anti-tumour activity of bisphosphonates remain to be elucidated. One major difficulty in pinpointing these effects is the separation between direct effects on cancer cells and those mediated through inhibition of bone resorption leading to reduced release of bone-derived growth factors or through other mechanisms.

1.4.1 Alternative mechanisms of action of BP-induced anti-tumour effects

In addition to the effects on the tumour cells and the osteoclasts, several alternative NBP-induced anti-cancer mechanisms have been proposed including the involvement of a range of prenylated proteins, γδT-cells, tumour-associated macrophages and effects on angiogenesis.

1.4.1.1 Prenylated proteins

NBP-induced inhibition of the MVA-pathway leads to lack of protein prenylation in proteins such as small GTPases. Disruption of the MVA-pathway consequently leads to faulty cellular signaling and impairment of angiogenesis, invasion and growth of cancer cells. *In vitro* experiments have shown that the accumulation of unprenylated proteins and of intermediates like isopentenylpyrophosphate (IPP) and a novel pyrophosphate analogue (ApppI) results in the induction of apoptosis (Monkkonen et al., 2006). In addition, mechanisms of metastatic dissemination, such as adhesion and invasion, as well as proliferation have been shown to be affected by the NBP-induced inhibition of the MVA pathway in cancer cells (Woodward et al., 2005). Whether the accumulation of unprenylated proteins plays a similarly important role *in vivo* is more difficult to establish. The administration of the MVA pathway intermediates FOH and GGOH are commonly used *in vitro* to reverse NBP-induced inhibition of prenylation. This method, however, is unfeasible *in vivo* and it therefore remains to be determined how much of the anti-tumour effects of NBPs are attributable to the *in vivo* accumulation of

unprenylated proteins. However, an indirect measurement through the detection of unprenylated Rap1A in tissue samples can be used as an indicator of the drug's effects on the MVA-pathway. It is noteworthy that there are about 300 prenylated proteins in the human proteome (Sebti, 2005), suggesting that there may be several proteins potentially involved in the drug's anti-tumour effects. Possible candidates could be proteins regulating the cell cycle and chromosome separation such as the farnesylated kinetochore protein Cenp-F, which has been shown to be affected by zoledronic acid treatment (Brown et al., 2011).

1.4.1.2 T-cell activation

Interactions between tumour cells and the immunological response are also thought to play a role in the anti-tumour effects of NBPs. A group of lymphocytes expressing the γδT-cell receptor identify specific antigens presented on tumour cells leading to cancer cell death *in vitro.* Interestingly, it was shown that one of these antigens is comprised of a MVA-pathway metabolite (IPP), which is known to accumulate in tumour cells, after NBP exposure (Gober et al., 2003). Thus, the drug-induced accumulation of mevalonate metabolites results in tumour cell recognition by γδT-cells and triggers an immune response against cancer cells. In this respect, lymphocytes expressing the Vγ9Vδ2T-cell receptor have been shown to recognise and kill tumour cells previously exposed to zoledronic acid, including breast, myeloma and lymphoma cells *in vitro* (Kunzmann et al., 2000; Gober et al., 2003). The relevance of these data *in vivo* has recently been assessed by Benzaid et al. (2011). NOD-SCID mice bearing T47D breast tumour xenografts were injected with human peripheral blood mononuclear cells, which trigger *in vivo* expansion of human Vγ9Vδ2T-cells. Animals with human Vγ9Vδ2T-cell and zoledronic acid + IL-2 (30μg/kg every 2 days for a total of 2 weeks) treatment were shown to have significantly reduced tumour growth and increased Vγ9Vδ2T-cell numbers compared to control mice. The data suggest that zoledronic acid treatment induced a significant anti-tumour effect mediated through phosphoantigen recognition by human Vγ9Vδ2T-cells.

1.4.1.3 Macrophages and tumour-associated macrophages (TAMs)

The role of macrophages in tumour growth and metastasis has become a growing field of interest with several studies showing an association of a variety of tumours with increased macrophage infiltration (Bingle et al., 2002). In general, two macrophage

phenotypes have been described (M1 and M2), each having different functions within the body but also in tumour progression. M2 polarised macrophages have been associated with pro-tumourigenic characteristics as they are shown to support tumour growth, migration, invasion and angiogenesis. Hypoxic tumour areas are known to release chemokines and cytokines such as IL-8, MMP-9, fibroblast growth factor 2 (FGF-2), VEGF and LOX (lysyl oxidase) to recruit TAMs in order to assist in new vessel formation (Murdoch et al., 2004) and metastatic growth (Erler et al., 2009). Importantly, it was shown that the primary tumour influences the polarisation of the recruited macrophages to its favour with most TAMS exhibiting pro-tumourigenic properties (Allavena et al., 2008). NBPs have been shown to inhibit macrophage proliferation and induce apoptosis via the mevalonate pathway *in vitro* (Luckman et al., 1998). The first *in vivo* study to report that TAMs are directly affected by bisphosphonate treatment was carried out by Coscia et al. (2010). The group could show that zoledronic acid treatment (100µg/kg/week zoledronic acid or PBS for 4 weeks followed by 3 weeks drug free interval, repeated cycles) reduced spontaneous mammary fat pad tumour growth in BALB-neuT mice as well as TAM infiltration and angiogenesis. Interestingly, the bisphosphonate induced a switch in macrophage phenotype from the pro-tumourigenic M2 to the tumouricidal M1 type. Taken together these studies suggest that the NBP-induced effects on macrophages could contribute to the reported anti-tumour effects.

1.4.1.4 Angiogenesis

The induction of new vessel formation is an essential step within the complicated sequence of metastatic tumour growth and there is a growing body of evidence suggesting that nitrogen-containing bisphosphonates may exhibit part of their anti-tumour effects through anti-angiogenic effects. Solid tumours with a diameter of less than 2mm are sufficiently supplied with nutrients through diffusion but tumour progression beyond this point requires additional blood supply. Zoledronic acid has been reported to inhibit neo-angiogenesis *in vivo* and *in vitro* (Wood et al., 2002), possibly mediated through inhibition of protein prenylation. In a clinical setting, Santini et al. (2003) could show that 4mg zoledronic acid administration to patients with advanced cancer and confirmed bone metastases resulted in decreased circulating VEGF levels up to 21 days after the drug was injected. In a more recent study, the use

of low-dose, high-frequent administration of zoledronic acid (1mg/week for 4 weeks followed by 3 cycles of 4mg every 28 days) confirmed the anti-angiogenic findings with reduced serum VEGF levels from seven to up to eighty-four days after the first treatment (Santini et al., 2007). Although these clinical studies suggest a bisphosphonate-induced anti-angiogenic effect, the involved cell type(s) remain to be established.

Taken together, NBPs may have a number of targets *in vivo* and it is likely that a combination of several mechanisms contribute to the reported anti-tumour effects. Several preclinical studies investigating these effects in models of breast cancer metastases to bone have been published and will be discussed in the following sections.

1.4.2 Potential anti-tumour activity of NBPs reported in *in vivo* studies

There is increasing preclinical evidence of anti-cancer effects of bisphosphonates in bone, reducing the extent of bone lesions as well as osseous tumour burden. In contrast, reports of the ability of bisphosphonates to affect tumours that have progressed to colonise bone-associated soft tissue and peripheral tumours are less consistent.

1.4.2.1 Bisphosphonate-induced effects on tumours in bone

As previously mentioned, bisphosphonates are commonly used to treat patients with confirmed metastatic bone disease and over the years, a growing number of publications report a potential anti-tumour activity of these compounds (Neville-Webbe et al., 2002; Clezardin, 2005; Caraglia et al., 2006; Winter et al., 2008). A range of tumour types that spread to bone, including breast, prostate and lung have been subject to investigation *in vivo*. The main body of studies has applied therapeutic protocols to assess the effects on established bone metastases. The drug-induced anti-tumour activity on early stages of bone metastases using preventive treatment regimens (before or at the same time as tumour cell implantation), were investigated less frequently.

Bisphosphonate-induced inhibition of osteolysis, reduced skeletal tumour burden and no effect on bone-associated soft tissue tumours

The effects of zoledronic acid or clodronate on tumours derived from the human breast cancer cells B02/GFP.2 in female balb/c athymic mice were investigated in a recent study (Daubine et al., 2007). The drugs were administered as daily, weekly or single regimens in either a preventative or therapeutic setting. The necessity of frequent drug administration was shown, as a single dose of zoledronic acid was not sufficient to reduce skeletal tumour burden. In contrast, administration of clodronate (daily) and zoledronic acid (daily or weekly) significantly reduced tumour burden, with zoledronic acid treatment being superior to clodronate. Bisphosphonate administration in adjuvant breast cancer therapy could therefore reduce cancer-induced bone disease and may be most effective at the early stages when tumour growth and expansion is still dependent on the microenvironment. A study investing the effects of ibandronate on intrafemural MDA-MB-231 tumour growth in athymic rats found that therapeutic ibandronate (10µg/kg/day) reduced progression of osteolytic lesions and metastases. However, complete elimination of tumour growth was not achieved, with bigger lesions staying unaffected (Neudert et al., 2003). When treatment was initiated prior to cancer cell injection, formation of new osteolytic lesions was decreased and animals had reduced incidence of metastases. A possible explanation of this differential effect could be that small metastatic foci consist of microenvironment-dependent cells and were therefore more sensitive towards the bisphosphonate-induced changes whereas larger tumours may achieve autocrine (microenvironment-independent) growth. In addition, treatment-induced alterations to the metastatic site may impede cancer cell engraftment to bone suggesting that adjuvant bisphosphonate treatment may be able to prevent bone metastases development.

A study underlining the suggestion that BPs do not exert their anti-tumour effects by direct mechanisms used the MDA-231-B/luc+ breast cancer model to investigate the effect of olpadronate on cancer-induced bone metastases (van der Pluijm et al., 2005). When olpadronate was given in a preventive way (s.c. 1.6µmol/kg/day), before intracardiac tumour cell injection, the formation of new bone metastases was significantly reduced. However, when given in a therapeutic protocol the drug did not

have significant impact on osseous tumour cell growth although a reduction in osteolysis was seen. In an intraosseous model, pamidronate (16µmol/kg/day) or olpadronate (1.6µmol/kg/day) were given daily following cancer cell implantation. Treatment reduced intraosseous colonies significantly but did not affect total tumour burden. The authors concluded that cancer cell growth was merely redirected from intra- to extraosseous sites due to space limitations caused by the drug-induced inhibition of bone resorption.

As shown above, a number of studies have reported that bisphosphonate treatment caused a reduction of skeletal tumour burden and inhibited osteolysis. However, in those studies investigating soft tissue tumour burden, no anti-tumour effect was reported at the extra-skeletal site suggesting a microenvironment-dependent anti-tumour effect.

Bisphosphonate-induced inhibition of osteolysis, reduced skeletal- but increased bone-associated soft tissue tumour burden

In contrast to the reports described in the previous section, a few studies have detected an increase of tumour mass in the soft tissue adjacent to affected bone in bisphosphonate treated animals. Sasaki and colleagues found that risedronate treatment increased soft tissue MDA-MB-231 human breast tumour burden in female balb/c-nu/nu mice, although there was a reduction in skeletal tumour colonisation (Sasaki et al., 1995). The data suggest that, while treatment with bisphosphonates does reduce skeletal tumour burden and osteolysis, it may cause an increased risk of developing tumours outside bone. These data are in agreement with the conclusion of van der Pluijm et al. (2005) who proposed that the bisphosphonate-induced limitation of space within bone causes tumours to spread to surrounding soft tissues. Sasaki et al. also investigated the effect of the new third generation bisphosphonate YH529 in the same breast cancer model (Sasaki et al., 1998). The drug significantly reduced number and area of osteolytic lesions and decreased osseous tumour volume in a dose-dependent manner. However, daily administration of 0.2 or 2µg YH529/mouse increased tumour volume in soft tissues surrounding bone while the higher dose of 20µg/mouse/day reduced it when compared to control. These results indicate that, in a clinical setting, prophylactic treatment with a low dose and continuous administration could benefit cancer patients with high risk of skeletal metastases by

reducing the incidence of bone metastases. The detection of increased bone-associated soft tissue tumour burden after bisphosphonate treatment requires further preclinical investigation.

Taken together, the majority of published data support that bisphosphonates exert their anti-tumour effects through inhibition of bone resorption, and that the drugs do not exhibit direct activity at non-osseous sites. However, most of these studies were not primarily designed to investigate the effects on soft tissue tumours, or in many cases the occurrence of extra-skeletal disease was not evaluated. In addition, preclinical studies reporting anti-tumour effects of bisphosphonates have frequently used high dosing regimens resulting in accumulated concentrations well beyond those used in clinic. However, frequent administration in a preventive schedule has been shown to be the most effective at protecting bone from metastatic breast cancer (Sasaki et al., 1995; Sasaki et al., 1998; Neudert et al., 2003; van der Pluijm et al., 2005; Daubine et al., 2007). Currently, clinical treatment with bisphosphonates alone will only be initiated once bone metastases are confirmed, although preclinical studies suggest that the best results would be obtained with an earlier treatment schedule. Despite the beneficial effects of a preventive treatment regimen, it is important to note that none of the studies could report a complete inhibition of tumour growth, suggesting that additional therapy with other anticancer agents is required. An overview of the different anti-tumour effects on bone-associated tumours reported from *in vivo* studies is given in Table 1.1.

Cells	BP	Effect on intraosseous tumour	Effect on bone-associated soft tissue tumour	Effect on osteolysis	Reference
Reduced osteolysis and skeletal tumour burden but no effect on bone-associated soft tissue tumours					
MDA-MB-231	Iban: 10µg/kg/d	T>P: reduced	—	T & P: reduced	(Neudert et al., 2003)
B02/GFP.2	Zol: cumulative dose of 100µg/mouse Clod: 530µg/kg/d	Zol single: no effect Zol (weekly, daily) > Clod: reduced	No effect	Zol: reduced Clod: reduced	(Daubine et al., 2007)
MDA-231-B/luc+					
Intracardiac	Olpa: 1.6µmol/kg/d	P: reduced	----	P&T: reduced	(van der Pluijm et al., 2005)
Intra-osseous	Olpa: 1.6µmol/kg/d Pam: 16µmol/kg/d	Olpa & Pam: reduced	Olpa & Pam: no effect	Reduced	
Inhibition of osteolysis, reduced skeletal but increased bone-associated soft tissue tumour burden					
MDA-MB-231	Ris: T: 4µg/m/d; 0.4, 4, 40µg/m/d; P: 4µg/m/d	Reduced	Increased	Reduced	(Sasaki et al., 1995)
MDA-MB-231	YH529: T: 0.2, 2, 20µg/m/d P: 2µg/m/d	Reduced	0.2, 2µg/m/d: increased 20µg/m/d: reduced	Reduced	(Sasaki et al., 1998)

Table 1.1 Effects of bisphosphonates on breast tumours in bone
Zol: zoledronic acid, Ris: risedronate, Iban: ibandronate, Clod: clodronate, Pam=pamidronate, Olpa=olpadronate, P= preventive, T=therapeutic, w= week, d= day, m=mouse. Reproduced and adapted with permission from Brown and Holen, 2009.

1.4.2.2 Bisphosphonates in combination with other drugs

The described preclinical studies of the effects of bisphosphonates on osseous tumour burden and in bone-associated soft tissues have reported somewhat conflicting results highlighting the need for new treatment regimens to improve quality of life. In clinical practice, treatment of cancer-induced bone disease commonly comprises the administration of cytotoxic drugs in combination with the palliative treatment offered by bisphosphonates. *In vitro* studies have shown that the combination of potent bisphosphonates, such as zoledronic acid, with other cytotoxic agents results in enhanced anti-tumour effects (Jagdev et al., 2001; Neville-Webbe et al., 2005; Neville-Webbe et al., 2006; Clyburn et al., 2010). These have been followed by *in vivo* studies investigating the effects of combination of a range of chemotherapeutic agents and

bisphosphonates, showing increased anti-tumour effects compared to single agent therapy (Hiraga et al., 2003; Duivenvoorden et al., 2007; van Beek et al., 2008; Ottewell et al., 2008a; Ottewell et al., 2008b). The cellular and molecular mechanisms underlying the increased anti-tumour effects caused by combined treatments remain to be identified. A number of studies using breast cancer models have reported reduced tumour growth following combination of a bisphosphonate with cytotoxic drugs as will be outlined below.

The anti-metastatic effect of the chemotherapeutic UFT (tegafur-uracil, 20mg/kg/day, days 14-21) in combination with zoledronic acid (i.v. 250µg/kg, day 7) or either drug alone was assessed using the murine 4T1 breast cancer model (Hiraga et al., 2003). The combined treatment regimen was reported to be superior in the reduction of metastatic bone areas but tumour burden at the orthotopic site (mammary fat pads) was not affected. The increased anti-tumour effects in bone support the theory that combined therapy might be more effective in clinical practice compared to single treatments. However, very high doses of zoledronic acid were used in this study, equivalent to a daily 15mg i.v. injection compared to the standard clinical administration of 4mg every 3-4 weeks. A different combination was investigated by Duivenvoorden et al. (2007) who assessed the effects of the antibiotic doxycycline in combination with zoledronic acid in a MDA-MB-231 human breast cancer model. Both single treatments and the combination resulted in decreased tumour burden in bone and surrounding soft tissues and reduced osteolysis. Interestingly it was reported that zoledronic acid alone resulted in a 93% reduction of tumour area in the soft tissue adjacent to the affected bones but only in 73% in total tumour burden, suggesting a direct effect of the drug on tumour cells outside the bone microenvironment. The combination of zoledronic acid and doxycycline may therefore be a possible therapeutic strategy for patients with advanced breast cancer.

In a study investigating early combination treatment, female balb/c nu/nu mice were inoculated intratibially with MDA-231-B/luc+ cells and treatment commenced 2 days later with zoledronic acid (i.p., 37.5, 75 or 150µg/kg, 5x/week) or risedronate (i.p., 150µg/kg, 5x/week), docetaxel (i.p., 2, 4, or 8 mg/kg, 2x/week) or a combination of both (docetaxel at 4mg/kg, 2x/week and risedronate at 150µg/kg, 5x/week) for a period of 5 weeks (van Beek et al., 2008). All concentrations of both bisphosphonates

and the combination schedule prevented osteolytic bone destruction, but docetaxel alone had no effect when compared to control. After combination treatment, no tumour growth in bone was detected in 6 out of 7 mice, while treatment with docetaxel alone prevented tumour growth in only 2 out of 7 mice and risedronate alone had no effect. The data show an enhanced anti-tumour effect in bone when bisphosphonates are used in combination with docetaxel, even at concentrations that were shown to be ineffective when given alone.

Several published studies have investigated the effects of combination treatments on tumours growing in bone, and it is therefore not possible to determine whether the reported anti-tumour effects are induced directly, indirectly or as a combination of both mechanisms. When using *in vivo* models, a separation of these effects is possible by e.g. subcutaneous implantation of tumour cells, which allows the investigation of the effects on cancer cells without bone involvement. Ottewell et al. (2008b) assessed the effects of doxorubicin (dox) and zoledronic acid (zol) on established subcutaneous tumours derived from MDA-G8 (MDA-MB-436-GFP) human breast cancer cells, to determine whether sequential and combined treatment can significantly inhibit subcutaneous tumour growth. Sequential treatment with dox followed 24 hours later by zol (once per week for a duration of six weeks) was shown to cause almost complete abolition of peripheral tumour growth and was reported to be the most effective of all treatment regimens tested. Pathway-specific gene array analysis performed to elucidate changes in gene expression induced by sequential treatment showed that 30 genes involved in cell cycle regulation and apoptosis had been changed in the subcutaneous tumour cells. Zoledronic acid (100µg/kg weekly for 6 weeks) alone had no effect on peripheral tumours, therefore not supporting the proposed direct anti-tumour activity of zoledronic acid monotherapy. The authors concluded that sequence-specific combination treatment might be beneficial to patients with early-stage breast cancer even in the absence of bone metastases. The effects of zoledronic acid combined with standard neoadjuvant chemotherapy on pathological response of the primary tumour were investigated in a subset of patients of the recent AZURE trial (Coleman et al., 2010). The addition of the bisphosphonate was shown to significantly reduce residual invasive breast tumour size compared to

women receiving standard therapy alone, supporting the proposed anti-tumour activity of doxorubicin and zoledronic acid outside the skeleton.

The effects of clinically relevant doses of zoledronic acid and doxorubicin on established extra- and intraosseous tumours was investigated using female balb/c nu/nu mice injected i.v. with B02 human breast cancer cells, which are known to home to bone (Ottewell et al., 2008a). While zoledronic acid alone significantly reduced osteolytic bone disease, only the sequential treatment resulted in significant reduction in intraosseous tumour volume and was shown to be the most effective in prolonging median survival ($p<0.0001$). Extraosseous tumour volume, defined as the tumour mass growing out of the bone marrow into the surrounding soft tissue, was not affected by any of the treatment schedules. In this respect, it was suggested that the surrounding microenvironment and the local drug concentration in different parts of the tumour could influence the response to treatment. The authors concluded that sequential administration of doxorubicin followed by zoledronic acid may be used in the treatment of advanced breast cancer patients, particularly for those with smaller bone metastases confined to the marrow space. Although significant synergistic anti-tumour effects could be detected when using the combination treatment, the study by Ottewell et al. (2008a) investigated advanced disease stages and used repeated dosing regimens. In addition, the effects of the treatment on the bone microenvironment were not addressed.

As shown above, several combination studies have been performed with zoledronic acid in combination with UFT (Hiraga et al., 2003), doxycycline (Duivenvoorden et al., 2007) and doxorubicin (Ottewell et al., 2008a; Ottewell et al., 2008b). Most studies investigated late stage bone disease and reported a significant reduction in osseous tumour burden following combination therapy, compared to using the single agents. In addition, therapeutic treatment regimens rather than preventive ones were used predominantly. The reported effects on visceral tumours or cancer cells in bone-associated soft tissue are more conflicting, with some studies showing no beneficial effects of drug combinations. The effects of treatment on metastatic prevention and possible associated risks have not been addressed in preclinical studies and further investigations are required to confirm these promising results.

1.4.2.3 Bisphosphonates alone vs. in combination – summary of findings

There is strong evidence that bisphosphonate treatment does reduce tumour growth in bone and inhibits the associated bone disease in a range of different cancer types *in vivo* (Brown and Holen, 2009). The effects on tumours spreading from the bone marrow cavity to the surrounding soft tissue, and effects on visceral tumours, are less conclusive. While some studies reported positive effects on extraosseous tumour growth and an increase in survival following bisphosphonate treatment, others did not observe a direct anti-metastatic effect. The most prominent anti-tumour activities are generated by regimens that include frequent drug administration, possibly due to the resulting high cumulative dose. Also, the need for repeated dosing indicates that bisphosphonates are unable to completely abolish cancer cell growth and merely cause a slowdown of the process. The most potent inhibition of tumour growth is seen when bisphosphonates are given in combination with cytotoxic drugs, suggesting that a similar approach may be utilized in the clinical setting, however, combination studies have previously focused on advanced disease models of cancer-induced bone disease.

1.5 Clinical application of bisphosphonates in adjuvant breast cancer therapy

Bisphosphonates are currently gold standard of care for patients with advanced disease and established bone metastases. Regarding the potential use of bisphosphonate in the adjuvant setting, the main areas of investigation include metastasis prevention and treatment-induced bone loss. The latter has been extensively investigated in breast cancer and much data is available supporting the administration of bisphosphonates to prevent/treat SREs in affected women (Wilson and Coleman, 2011). The use of the bone sparing agents in a preventive setting is less well established and is currently under investigation in a number of clinical trials.

The recent ABCSG-12 trial (n=1800) reported a significant increase in disease-free survival (DFS) in pre-menopausal women receiving endocrine therapy (goserelin and tamoxifen/anastrozole) and 4mg zoledronic acid once every 6 months for a duration of 3 years (Gnant et al., 2009). Interestingly, a reduction in loco-regional and extra-skeletal events was also reported. However, the survival benefit was confined to women >40 years of age, who would be expected to have complete suppression of

ovarian function with goserelin. The results suggest a beneficial effect of addition of bisphosphonate treatment to adjuvant endocrine therapy in this sub-population of patients.

A number of studies have investigated the adjuvant administration of clodronate for prevention of metastases in mixed cohorts of pre and postmenopausal women and have reported conflicting results. Direct anti-tumour effects on visceral tumours as well as reduction of tumour burden in bone and prolonged survival has been reported in a study investigating the effects of adjuvant oral clodronate administration in patients with early breast cancer and with confirmed disseminated tumour cells in the bone marrow (Diel et al., 2008). In contrast, Saarto et al. (2004) reported no decrease in skeletal tumour burden but an increase in visceral tumours, which was associated with reduced disease free survival (placebo 58% vs. clodronate 45%) after 10 years when administering oral clodronate in an adjuvant setting. The most recent, large NSABP-34 trial (n=3400) investigated the effects of daily oral clodronate (1600mg) or placebo in addition to standard therapy in stage I-II breast cancer patients (Paterson et al., 2011). The primary endpoint was disease free survival and secondary endpoints included incidence of metastases and overall survival. Subset analysis showed that addition of oral clodronate in women of 50 years or more significantly reduced metastatic disease including bone metastases.

The potential of combination therapy in prevention of bone metastases was also investigated in the recently completed AZURE trial (Coleman et al., 2011). A total of 3360 women with stage II/III breast cancer were randomly grouped to receive either standard therapy alone (including chemotherapy, endocrine and radiation therapy) or standard therapy in combination with zoledronic acid (4mg at 3-4 weeks for 6 weeks followed by 8 doses every 3 months and then 5 doses every 6 months). At a median follow-up of approximately 5 years, no changes in disease free survival (DFS, primary endpoint) and invasive DFS (secondary endpoint) were found when comparing patients receiving zol to those only receiving standard therapy. However, when differential sub-group analysis depending on menopausal status was carried out after completion of the trial, postmenopausal women (>5 years) receiving zol were found to have a 25% reduction in invasive DFS events when compared to younger women. In addition, postmenopausal women in this treatment arm exhibited a reduction in extra-skeletal

recurrences (30%) and improved overall survival rate (29%) when compared to pre- or perimenopausal women. Importantly, the latter group was found to have an increased risk, although not statistically significant, of extra-skeletal recurrences with increased numbers in visceral metastases and loco-regional recurrences, underlining the role of reproductive hormones in bone remodelling. In summary, the AZURE trial together with evidence from the ABCSG-12 and NSABP-34 trials, suggest that reproductive hormone levels play a role in the observed anti-tumour effects of bisphosphonates, and should be investigated in more detail. Furthermore, the NSABP-34 trial suggests that the anti-tumour effects are not limited to nitrogen-containing bisphosphonates.

Several other clinical breast cancer trials of adjuvant bisphosphonate treatment are currently ongoing and will help to identify the guidelines for future treatment with bone targeting agents. Alternative therapeutics for cancer-induced bone disease may be the recently developed fully humanised antibody to RANKL, denosumab, which has been shown to be an effective inhibitor of bone resorption (Stopeck et al., 2010).

1.6 Outstanding questions

The data from the clinical trials reflect the variable responses reported in *in vivo* studies, with the majority of reports observing anti-tumour effects and others reporting either no effect or increased cancer cell growth. The reported effects appear to be highly dependent on tumour type, treatment protocol and model system used. While most of the studies have reported the involvement of bone in the anti-cancer activity of bisphosphonates, there are some studies reporting evidence of direct effects using tumour models independent of bone. Despite this, more detailed trials are required to elucidate whether bisphosphonates exert their anti-cancer activity via direct, indirect or both mechanisms, and it remains to be established whether bisphosphonates are able to be internalised into cancer cells *in vivo*.

A greater effect of early compared to late bisphosphonate treatment was shown by a number of the preclinical studies. This is in agreement with the recently highlighted importance of early stages of tumour growth in bone. However, to date only very little preclinical data is available investigating the interactions between tumour and bone cells and especially the role of the osteoblasts requires further analysis.

1.7 Aims of the thesis

The main aims of this thesis were as follows:

- To assess whether the investigation of early tumour growth in bone is feasible and to establish the availability/suitability of methodologies for investigation of both the tumour and the bone microenvironment.
- To determine whether the cellular composition of bone metastases changes with disease progression.
- To characterise the interactions between breast cancer colonies and the surrounding cells of the microenvironment (systemic and local factors).
- To assess the effects of early sequence- and schedule-dependent therapy with a single dose of doxorubicin followed by zoledronic acid on early stage breast tumour growth in bone.
- To investigate the treatment-induced effects of a single dose of doxorubicin followed by zoledronic acid administered at an early stage (day 2) on bone-tumour cell interactions.
- To determine whether cells in subcutaneous breast tumour xenografts and host soft tissues internalise a fluorescently labelled bisphosphonate, AF647-RIS, using an *in vivo* model of breast cancer.

2. Materials and Methods

2.1 Materials

Laboratory equipment

ABI 7900 PCR System	Perkin-Elmer, Applied Biosystems
Agilent 2100 bioanalyzer	Agilent
Antigen retrieval bath	Dako
BD FACS Array™	Biosciences
Bio Vortexer	Biospec Products
Cryostat	5030 Microtome, Bright
Cytospin	Shandon
Desktop X-ray microtomograph	SkyScan 1172
Developer	Curix 60, AGFA
FACSCalibur	Becton Dickinson
Faxitron-cabinet-X-Ray system	Hewlett Packard
GPR centrifuge	Beckman
Imaging densitometer	GS-710, BIO-RAD
Improved Neubauer haemocytometer	Weber
Inverted light microscope	Olympus CK2, Japan
Inverted widefield fluorescence microscope	Leica DMI 4000B
IVIS® Lumina II	Caliper Life Sciences
Mammography film	MIN-R 181 1884, Kodak
Microtome	Bright
Mistral 2000, table centrifuge	MSE
MoFlo® Flow Cytometer	Beckman Coulter
Multiphoton Confocal Microscope	Zeiss LSM510 NLO Inverted
NanoDrop 2000 UV-Vis Spectrometer	Thermo Scientific
pH meter, SevenEasy	Mettler Toledo
Spectra Max M5e, plate reader	Molecular Devices
Technico Maxi, table centrifuge	Fischer Scentific
Thermal cycler, Mastercycler	Eppendorf
UV light source	Illumatool Lighting System, LightTools Research
X-ray microtomograph	SkyScan 1172

Software

Cell Quest™ Pro software	Version 3.3, BD Biosciences
CTAN software	CT-Analyser version 1.5.0.0, Skyscan
GraphPad Prism software	Version 5.0a, GraphPad
Living Image 4.0 software	Caliper Life Sciences
Osteomeasure software	Osteometrics
SoftMax Pro 5.2 software	Molecular Devices
Summit software	BD Biosciences
Volocity software	Version 4.3.2, Improvision

Plastic and disposable equipment

384-well PCR plate	Applied Biosystems
Autoclave tape, Comply™ Indicator Tape	3M
Cell strainer, 70µm and 100µm	BD Biosciences
Cryovials (1ml)	Nalgene Nunc Ltd.
Filter (32mm and 0.45µm membrane)	PALL Life Sciences
Filter cards	Thermo
Filter tips (10, 20, 100, 1000µl)	STARLAB
Flow cytometer tube	ELKAY LAB PRODUCTS UK
Glass bottom dishes (35mm, glass thickness N.0, uncoated)	MatTek Corporation
Insulin syringe (1ml) with needle (27G x ½")	Terumo Europe N.V.
Needle (25G x 5/8")	Becton Dickinson UK Ltd.
Optical adhesive covers, PCR compatible	Applied Biosystems
PCR tubes, 0.2ml, thin wall, flat cap	Fischer
Petri dishes, Nunclon™ surface	Nunc
Pipette tips (10, 200 and 1000µl)	Costar
Slide clips, CYTOCLIP™	Shandon
Strippets (5, 10 and 25ml)	Costar
SuperFrost®PLUS microscope slides	VWR International
Syringe (1ml, 10ml)	Becton Dickinson UK Ltd.
Tissue culture flasks T25, T75, T175	Nalgene Nunc Ltd.
Universal containers, Bijoux tubes	Starstedt

Laboratory chemicals and solutions

2-Propanol, >99%	Sigma
Acetic acid	BDH Chemicals Ltd.
Alexa Flour-647	Sigma
Alexa Flour-647-Risedronate	Kindly supplied by Prof M Rogers, University of Aberdeen
Aqueous eosin	VWR International Ltd.
Azowipe™ Hard Surface Disinfectant Irradiated Wipes	Synergy Health (UK) Ltd.
BrdU (5-Bromo-2'-deoxyuridine)	Sigma
Calcium carbonate	Sigma
Casein	Vector Laboratories Inc.
Chloroform, minimum 99%	Sigma
Concentrated hydrochloric acid	Fisher Scientific Ltd.
DEPC-treated water	Ambion
DePeX mounting medium	VWR International Ltd.
Dimethylformamide	VWR International Ltd.
DMSO	Sigma
Doxorubicin	PharmaChemie
EDTA	Sigma
Ethanol	Sigma
FCS	PAA Laboratories GmbH
Formaldehyde (37%)	Sigma

Geneticin (G148)	GIBCO
Gill's II haematoxylin	VWR International Ltd.
H_2O_2 (30%)	VWR International Ltd.
HCl	BDH Chemicals Ltd.
Hexane	VWR International Ltd.
Hygromycine , HygroGold™	InvivoGen
Isoflourane, IsoFlo®	Abbott
Ketamine	Fort Dodge Animal Health Ltd
Methanol	Fischer Scientific Ltd.
Naphthol AS-BI phosphate	Sigma
Normal Goat Serum	DakoCytomation, Denmark
OCT	Bright Instrument Company Ltd.
Paraformaldehyde	Sigma
Pararosaniline	Sigma
PBS tablets	OXOID Ltd.
PBS, pH 7.4	Gibco
Penicillin	PAA
Pentobarbiturate	LMV
ProLong® Gold antifade	Invitrogen
Puromycine	Sigma
RNAlater® solution	Ambion
RPMI-1640+ GlutaMAX-I medium	GIBCO
Sodium acetate trihydrate	VWR International Ltd.
Sodium dihydrogen orthophosphate dehydrate	BDH Chemicals Ltd.
Sodium nitrite	Sigma
Sodium tartrate dibasic trihydrate	Sigma
Streptomycin	PAA
TaqMan® Universal PCR Mastermix	Applied Biosystems
TE Buffer, pH8.0	Ambion
TRI REAGENT™	Sigma
Tri sodium citrate	BDH, VWR International Ltd.
Trypsin (0.05%) - EDTA (0.02%)	Gibco
Tween 20	BDH, VWR International Ltd.
Xylazine	Bayer Health Care
Xylene	Fisher Scientific Ltd.
Zoledronic acid	Novartis Pharma

Cell lines

B02	Dr P Clezardin, Lyon, France and Dr P Pujuguet, Paris, France
MDA-MB-231	ATCC
MDA-MB-231-GFP	Dr PD Ottewell and Dr I Holen
MDA-MB-436	ATCC
MDA-G8 (MDA-MB-436-GFP)	Dr PD Ottewell and Dr I Holen

Antibodies

Biotinylated horse anti-mouse	BA-2000, Vector Labs Inc.
Biotinylated goat anti-rabbit	BA-1000, Vector Labs Inc
Bromodeoxyuridine, monoclonal mouse	Clone Bu20a, M0744, DakoCytomation
Cam 5.2, anti-human	345779 and 349205, BD Biosciences
Caspase-3, polyclonal anti-active caspase-3	AF835, VectorLabs
GFP, polyclonal rabbit	A11122, Invitrogen, Oregon, USA
Goat anti-rabbit HRP	SC2004, Insight Biotec
Ki67, mouse monoclonal anti-human	Clone MIB-1, DakoCytomation
Rabbit IgG	X0936, DakoCytomation, Denmark
ß-galactosidase, Rabbit anti-mouse	AB161, AbCam

Commercial kits

Masson-Goldner trichrome staining kit	Merck
Mouse IL-1α Flex Set (Bead E4)	560157, BD Biosciences
Mouse IL-1β Flex Set (Bead E5)	560232, BD Biosciences
Mouse IL-6 Flex Set (Bead B4)	558301, BD Biosciences
Mouse KC Flex Set (Bead A9)	558340, BD Biosciences
Mouse MCP-1 Flex Set (Bead B7)	558342, BD Biosciences
Quantikine® Mouse TRANCE/RANKL/TNFSF11 Immunoassay	R&D Systems, Inc.
RANKL Immunoassay	Biomedica
Rat/Mouse PINP EIA	Immunodiagnosticsystems, IDS
RatLaps™ EIA for CTX	Immunodiagnosticsystems, IDS
RNA Cleanup, RNeasy Kit	Quiagen
Sclerostin Immunoassay	R&D Systems
SuperScript® III-Strand Synthesis SuperMix	Invitrogen
TaqMan® Pre Amp Cells-to-CT™ Kit	Applied Biosystems
Vectastain ABC-Kit	Vector Laboratories Inc.
VECTOR NovaRED Substrate Kit	Vector Laboratories Inc.

Human TaqMan® Assays

β-actin (HS01101944_s1)	Invitrogen	Not tested
B-cell chronic lymphocytic leukemia/lymphoma 2 (BCL2; Hs00236808_s1)	Applied Biosystems	Species specific[1]
BCL2-associated X protein (BAX; Hs99999001_m1)	Applied Biosystems	Species specific[1]
Caspase-2 (Hs00154240_m1)	Applied Biosystems	Species specific[1]
Caspase-2 and RIPK1 domain–containing adaptor with death domain (CRADD; Hs00388731_m1);	Applied Biosystems	Species specific[1]
CXCR4 (Hs00976734_m1)	Invitrogen	Not species specific[2]
CYCLIN D1 (Hs99999004_m1)	Applied Biosystems	Species specific[1]
CYCLIN D3 (Hs 01017690_g1)	Applied Biosystems	Species specific[1]
Cyclin-dependent kinase inhibitor 1A (P21; Hs00355782_m1)	Applied Biosystems	Species specific[1]
DKK-1 (Hs00931310)	Invitrogen	Species specific[2]

DKK-2 (Hs00205294)	Invitrogen	Species specific[2]
DKK-3 (Hs00951303)	Invitrogen	Species specific[2]
Fas-Associated protein with Death Domain (FADD; Hs00538709_m1)	Applied Biosystems	Species specific[1]
GapdH (Hs99999905_m1)	Invitrogen	Species specific[1]
GMCSF (Hs00171266)	Invitrogen	Species specific[2]
OPG (Hs00900358)	Invitrogen	Species specific[2]
Osteonectin (SPARC; Hs00277762)	Invitrogen	Species specific[2]
P53 (Hs99999147)	Invitrogen	Species specific[1]
RANK (Hs00187192)	Invitrogen	Species specific[2]
TNFRSF11 (RANKL; Hs00171068_m1)	Invitrogen	Not species specific[2]
SDF1 (CXCL12; Hs009340455)	Invitrogen	Species specific[2]
SFRP1 (Hs03928965)	Invitrogen	Species specific[2]
SFRP2 (Hs01564480)	Invitrogen	Species specific[2]

[1] Species specificity was tested in Ottewell et al. (2009), [2] species specificity was tested by Dr JK Woodward, University of Sheffield. Species specific=human. Not species specific=human assay cross reacts with mouse.

2.2 Methods

2.2.1 Cell lines

The oestrogen and progesterone receptor negative human breast cancer cell line MDA-MB-231 was transfected by Dr PD Ottewell to stably express the green-fluorescent protein (GFP). A bone homing subclone of the MDA-MB-231 cells, the B02 cell line, was used for some experiments. B02 cells, stably expressing GFP and beta-galactosidase (β-Gal), were kindly provided by Dr P Clezardin (INSERM, Lyon, France) and Dr P Pujuguet (Galapagos, Paris, France). For some experiments Dr PD Ottewell kindly provided the GFP expressing cell line MDA-G8 (derived from the human breast cancer cell line MDA-MB-436; Ottewell et al., 2008b).

2.2.2 Thawing and freezing of cells

For standard subculturing, cells were removed from liquid nitrogen and thawed quickly in a 37°C water bath before addition of 9ml of RPMI-1640 + 10% foetal calf serum (FCS). After centrifugation at 800rpm for 5 minutes the cell pellet was resuspended in 10ml of fresh medium and plated into a T75 flask. To freeze, cells were washed twice with PBS before trypsinising and dislodging from the bottom of the flask. Cells were pelleted by centrifugation (800rpm, 5 minutes) and the supernatant was removed prior to estimation of cell concentration using a hemocytometer. 10% DMSO in RPMI-1640 + 10% FCS were added to make a $1x10^6$cells/ml suspension. The cell suspension (1ml) was then transferred into cryovials and stored at -80°C over night before placing into liquid nitrogen.

2.2.3 Cell culture

Cells were grown in T75 flasks in RPMI-1640 medium supplemented with 10% heat inactivated foetal calf serum and were incubated at 37°C and 5% CO_2. Subculturing was undertaken in culture hoods under sterile conditions and took place approximately twice per week depending on confluence (about 80%). Culture medium was discarded and cells were rinsed twice with 5ml of sterile PBS. Cells were harvested by addition of 5ml trypsin (0.05%) - EDTA (0.02%) and incubation at 37°C and 5% CO_2 for 2-3 minutes. After dissociation, 5ml of sterile medium was added and adherent cells were dislodged by pipetting. Subsequently cells were transferred to a sterile tube and centrifuged for 5 minutes at 800 rpm and ambient temperature. The supernatant

was discarded and the cell pellet was gently resuspended in 10ml of fresh medium prior to plating the cells at the required concentration into a sterile T75 flask and incubation at 37°C and 5% CO_2. In some cases 5% penicillin and streptomycin was added to the medium to prevent infection. For *in vivo* experiments, antibiotic-containing medium was replaced with RPMI-1640 + 10% FCS for 24 hours prior to use.

In some cases B02 cells were grown in puromycine at 1µg/ml, hygromycine at 500µg/µl and/or G418 at 800µg/µl.

2.2.4 Estimation of cell number by haemocytometer

A single cell suspension was prepared prior to loading 10µl into the haemocytometer. Using an inverted light microscope, the number of cells in the four primary squares of each grid was counted. To calculate the total cell number, the sum of cells determined for four primary squares was divided by 4 and the resembling number multiplied by the original volume from which the cell sample was removed. The resulting number was multiplied by 10 000 to give the final cell number. Subsequently the suspension was spun down for 5 minutes at 800rpm and ambient temperature. The cell pellet was then gently resuspended in the appropriate amount of PBS or growth medium to make up the required cell concentration.

2.2.5 Flow cytometry - detection of GFP positive cells

In order to assess the percentage of GFP positive cells a confluent cell layer was washed twice with PBS before trypsinising and resuspending cells in PBS to give a concentration of $1x10^6$ cells/ml as described above. The cell suspension (0.5ml) was transferred through a 100µm cell strainer into a FACS tube. The same procedure was carried out for a corresponding GFP negative cell line as negative control. Samples were analysed using a flow cytometer and Cell Quest™ software. Samples from cell passages with 75% or lower GFP positive cells were sorted as described in the following section prior to use in *in vivo* experiments.

2.2.6 Cell sort

Cells of a confluent T75 flask were washed with PBS and trypsinised as described earlier before resuspending the cell pellet in 0.5ml of PBS. Cells were sorted for GFP positive cells using a FACSAria high performance cell sorter or the MoFlo® Flow Cytometer and a blue 488nm laser or a tunable Enterprise II Argon Ion laser (488nm),

respectively. GFP positive cells were sorted into 1ml of RPMI-1640 + 10% FCS and 10% penicillin/streptomycin before adding 9ml of medium and transferring into a T75 flask at 37°C and 5% CO_2.

2.2.7 B02 cell size

To specify tumour cell size for identification of tumour cells by multiphoton microscopy, an *in vitro* experiment was carried out measuring the diameter of B02 breast cancer cells. B02 human breast cancer cells were seeded at a density of $2x10^4$ cells/ml into 6-well-plates. Cells were left to settle over night at 37°C and 5% CO_2 before capturing images of randomly chosen fields using an inverted widefield fluorescence microscope and a 40x dry objective. Images were then analysed using Volocity software. The diameter of thirty-seven GFP positive cells was measured twice. An image showing the measurement of the cells is depicted in Figure 2.1. The mean cell diameter was found to be 34.66µm leading to the conclusion that GFP positive objects detected on multiphoton microscope scans were defined as cancer cells when larger than 30µm in diameter.

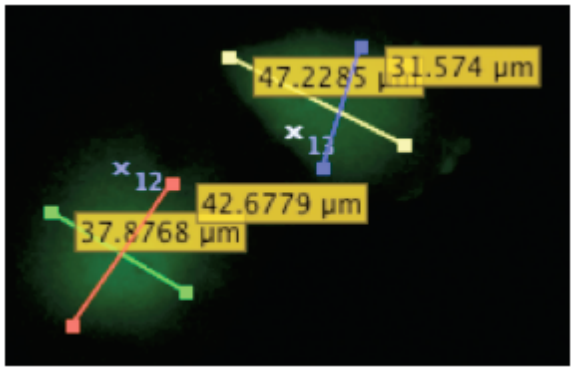

Figure 2.1 Measurement of cancer cell size using Volocity software
GFP expressing breast cancer cells were seeded into a 6-well plate and imaged using an inverted microscope before measuring with Volocity software as indicated on the image.

2.2.8 *In vivo* experiments

2.2.8.1 Ethics and animals

Animals were housed in the University of Sheffield Biological Service to the required guidelines. All experiments were conducted according to the institutional ethical guidelines and under the Home Office project licence 40/2972.

Female balb/c nude/nude mice were obtained from Charles River (UK) or Harlan (UK), as indicated in the experiments. Animals were ordered at an age of 4-5 weeks and were no older than 6-7 weeks at day of tumour inoculation for the intravenous and intracardiac models. For subcutaneous tumour models, animals were approximately 8 weeks of age at initiation of the experiment.

2.2.8.2 Preparation of injectables and *in vivo* procedures

2.2.8.2.1 Anaesthetic

Anaesthetic used for tumour cell injections was prepared by mixing ketamine with xylazine in autoclaved H_2O or sterile NaCl and was administered intraperitoneally at the either 116.0mg/kg ketamine, 7.3mg/kg xylazine, in NaCl or 56.5mg/kg ketamine, 5.5mg/kg xylazine, in H_2O. The solution was filter sterilised using filter and a 5ml syringe directly before use. Animals used for *in vivo* live imaging using the IVIS® Lumina II system were anaesthetised by isoflurane.

2.2.8.2.2 B02 cancer cell injection

On day of injection, GFP positive B02 cells were trypsinised, re-suspended in medium to inactivate the enzyme, spun down, re-suspended in sterile PBS to make a $1x10^6$ cells/ml suspension and placed on ice. Female, 6 week old balb/c nude mice were injected with ketamine/xylazine into the peritoneal cavity and placed into an incubator (33°C) to maintain body temperature and to ensure blood vessel dilation to facilitate injection. Complete anaesthesia was assessed by pinch reflex and the procedure was only carried out if animals did not withdraw the paw. Anaesthetised mice were placed onto the bench top and a piece of autoclave tape was placed over the abdomen to act as tunicae. The lateral tail artery was brought up by wiping the tail with an azowipe (a surface disinfectant) before 0.1ml of the $1x10^6$cells/ml suspension ($1x10^5$ cells per mouse) were slowly injected using a 1ml insulin syringe with a 27-gauge fitted needle. Clearing of the blood from the artery during injection and subsequent minor bleeding from the injection site were indications of successful administration. Animals were monitored closely and were placed back into the incubator to recover. Note that the literature to date mistakenly describes the B02 injection method as intravenous not intraarterial.

2.2.8.2.3 MDA-MB-231-GFP intracardiac injection

On day of injection, a $1x10^6$ cells/ml suspension of GFP positive MDA-MB-231-GFP cells was prepared as described for B02 cells and 6 week old balb/c nude female mice were anaesthetised using 56.5mg/kg ketamine and 5.5mg/kg xylazine. Complete anaesthesia was assessed by pinch reflex and the procedure was only carried out if animals did not withdraw the paw. Anaesthetised mice were slowly injected with 0.1ml of the cell suspension ($1x10^5$cells/mouse) directly into the left heart ventricle using a 1ml insulin syringe with a 27-gauge fitted needle. Successful administration was judged by the bright red colour of oxygenated blood drawn into the syringe bevel prior to injection of the cells. Animals were monitored closely and were placed back into the incubator to recover.

2.2.8.2.4 MDA-MB-231-GFP and MDA-G8 subcutaneous injection

GFP positive MDA-MB-231-GFP or MDA-G8 (GFP expressing clone of MDA-MB-436) cells were used for preparation of a $5x10^6$ cells/ml suspension in sterile PBS. The cells were placed on ice and female balb/c nude mice (8 weeks) were injected subcutaneously with 0.1ml of the cell suspension resulting in $5x10^5$ cells per mouse. Animals were monitored closely post injection and tumour size was measured once weekly using callipers. Tumour volume was then calculated from the mean of two measured diameters (mm) per tumour using the following formula: $¾ \times \pi \times r^3$, with r=mean diameter/2.

2.2.8.2.5 Doxorubicin injection

A 2mg/kg doxorubicin solution was prepared freshly in PBS and filter sterilised (32mm and 0.45µm membrane) prior to injection. Animals were placed into an incubator (35°C) to dilate the tail veins. Mice were then placed into a bench top restrainer and 0.1ml of the solution was drawn up into a 1ml insulin syringe with a 27-gauge fitted needle and slowly injected into the tail vein.

2.2.8.2.6 Zoledronic acid injection

A 10mM stock solution of zoledronic acid ([1-hydroxy-2-(1H-imidazol-1-yl)ethylidene]bisphosphonic acid), supplied as the hydrated disodium salt was prepared in PBS, aliquoted and stored at -20°C. A 100µg/kg solution was made up immediately prior to injection. After filter sterilisation (32mm and 0.45µm membrane) of

the solution, 0.1ml was injected subcutaneously using a 1ml syringe and a 25-gauge needle.

2.2.8.2.7 PBS injection

PBS was injected to function as vehicle control. 0.1ml sterile PBS or filter sterilised (32mm and 0.45µm membrane) PBS was injected by the appropriate route using a 1ml syringe and a 25-gauge needle.

2.2.8.2.8 BrdU injection

BrdU (5-Bromo-2'-deoxyuridine) was dissolved in 2.6% DMSO in PBS; filter sterilised and was used at a final concentration of 400mg/kg. The solution was injected intraperitoneally three hours prior to sacrifice with 1ml syringe and a 25-gauge needle.

2.2.8.2.9 AlexaFluor-647 (AF647) and AF647-Risedronate (AF647-RIS) injection

A 400µg/kg solution AF647-RIS (kindly supplied by Professor M Rogers, University of Aberdeen, UK) and AF647 were prepared in sterile PBS prior to subcutaneous injection. AF647 has an excitation wavelength of 652nm and emission of 668 nm.

2.2.8.3 Exsanguination from the heart

Blood was collected at consistent time points for the course of each study and blood was removed after removal of food. Animals were injected intraperitoneally with 0.5ml pentabarbiturate. Each animal was monitored after injection and deep anaesthesia was confirmed by using the pinch reflex. A fresh 1ml syringe and 25-gauge needle was used to retrieve blood from the heart before cervical dislocation. Blood was immediately placed into a 1.5ml Eppendorf tube after removing the needle to reduce sheer stress. Blood was left to clot at ambient temperature and was stored on ice until further processing (section 2.2.9.1).

2.2.8.4 Collection of peritoneal macrophages

Animals were sacrificed according to schedule one procedures. Approximately 5ml of ice cold, sterile PBS was injected into the peritoneal cavity, massaged and the solution was then retrieved and placed into a fresh tube. Samples were kept on ice until further processing for flow cytometry and cytospins.

2.2.8.5 In vivo *imaging*

An Illumatool Lighting System was used to visualise GFP positive tumours in the hind legs. On day of sacrifice, hind legs were excised and stripped of muscle before

visualisation of the tumour using a Retiga EX-B camera with QCapture software (Version 2.70.0) and an exposure time of 104ms.

In some experiments the IVIS® Lumina II system and Living Image software was used for non-invasive *in vivo* imaging. Anaesthetised (isoflurane) animals were placed into a darkbox imaging chamber with a 12.5cm field of view (shelf position D) and focus on subject height. Gray-scale images were taken and animals were imaged for GFP (excitation filter: 465nm) and AF647 (excitation filter 640) using the auto-exposure setting of the software. For analysis, PBS injected mice were used as negative controls to adjust for background fluorescence. The relative fluorescence was visualised and overlaid with the gray-scale photographs using pseudo colours and Living Image software.

2.2.9 Sample processing

2.2.9.1 Blood samples

Blood samples were centrifuged at 10 000 rpm for 10 minutes at 4°C to separate serum and cellular components. The clear serum was then carefully removed and placed into fresh 1.5ml Eppendorf tubes. Serum samples were stored at -80°C.

2.2.9.2 Processing of tissue for RNA extraction

On day of sacrifice subcutaneous tumour tissue was removed, cut in half, immediately placed into RNA later and kept on ice until storing at -80°C. For osseous tumour tissue, long bones were placed into sterile petri dishes and tumour tissue was scraped out of the bone using sterile dissection tools before placing in ice cold RNA later. All samples were stored at -80°C until use.

2.2.9.3 Bone samples

2.2.9.3.1 Histology

Excised and stripped hind legs were placed in 4% PFA in PBS at 4°C and rotation for 48-72 hours. In some cases µCT was performed during this time. After fixation, the solution was exchanged to decalcifying solution (0.5% PFA, 0.5M EDTA in PBS, pH8), which was changed every two days for two weeks. Bone specimens were placed into histological cassettes and washed in PBS three times for 1 hour before being infiltrated with wax (carried out by the Bone Analysis Laboratory, University of Sheffield UK).

Processed bone specimens were embedded in paraffin wax and sectioned at a thickness of 3µm.

2.2.9.3.2 µCT and X-ray

Excised hind legs that were not used for histology were placed into 10% buffered formalin, and stored at ambient temperature until further use for either X-Ray or µCT analysis. Formalin solution was changed after a maximum of 3 months to 70% EtOH.

2.2.9.3.3 Multiphoton microscopy

On day of sacrifice

After excision, hind legs were stripped of muscle before wrapping each specimen in aluminium foil and placing it into liquid nitrogen. On return to the laboratory, samples were removed from the liquid N_2 and stored at -80°C.

Embedding

A hexane/methanol ice bath was used to ensure that samples would not defrost during the embedding process. Dry ice was used to cover the bottom of a polystyrene box. A large glass beaker was placed on top and filled to ¾ with dry ice as well as filling the spaces around the beaker. The glass beaker was slowly filled with methanol. A small metal container was carefully placed on top of the glass beaker before adding hexane to cover the bottom of the container. Metal chucks were placed into the hexane and left to cool. Moulds were filled with OCT embedding medium, placed on top of the metal chuck and left to freeze (Fig. 2.2). Frozen specimens were then wrapped in aluminium foil and stored at -80°C.

Sectioning

Each embedded bone sample was attached to a metal chuck with OCT and left to cool in the cryostat chamber. A microtome was used to expose the growth plate of both the tibia and the femur and were then stored at -80°C.

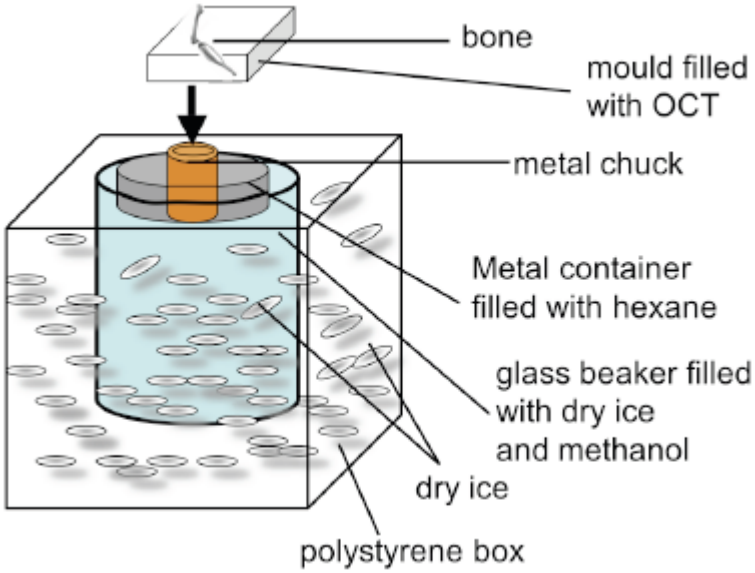

Figure 2.2 Cartoon of hexane/methanol ice bath used for embedding of bone samples prior to multiphoton microscopy

2.2.10 Microcomputed tomography imaging (µCT)

The analysis of bone by computerised tomography (CT) can be used to give valuable information of detailed bone structures. A high number of serial 2-D X-ray images are taken from the object while being rotated around a single axis. Apart from quantitative analysis of parameters like trabecular area/volume a three-dimensional image can be generated allowing invaluable insights into the structure of the bone. The Desktop X-ray microtomograph SkyScan 1172 was used for analysis of bone samples. Imaging was carried out at a voltage of 50kV and a currency of 200µA with a medium camera resolution of 2000x1024, an aluminium filter of 0.5 mm and pixel size was set to a dimension of 4.3µm. Scanning was initiated from the top of the proximal tibia or distal femur. For each sample, images were reconstructed using NRecon software. The CT_{AN} software was used to specify the volume of interest (VOI) on the raw X-ray images for trabecular bone. The reference line was defined as the break in the first bridge (Fig. 2.3). The offset for trabecular bone was set to 0.5mm away from the reference point. Quantitative analysis of bone volumes was measured for a height of 1.0mm for all samples and binary thresholds were typically set to a value of 75 and were consistant throughout a study.

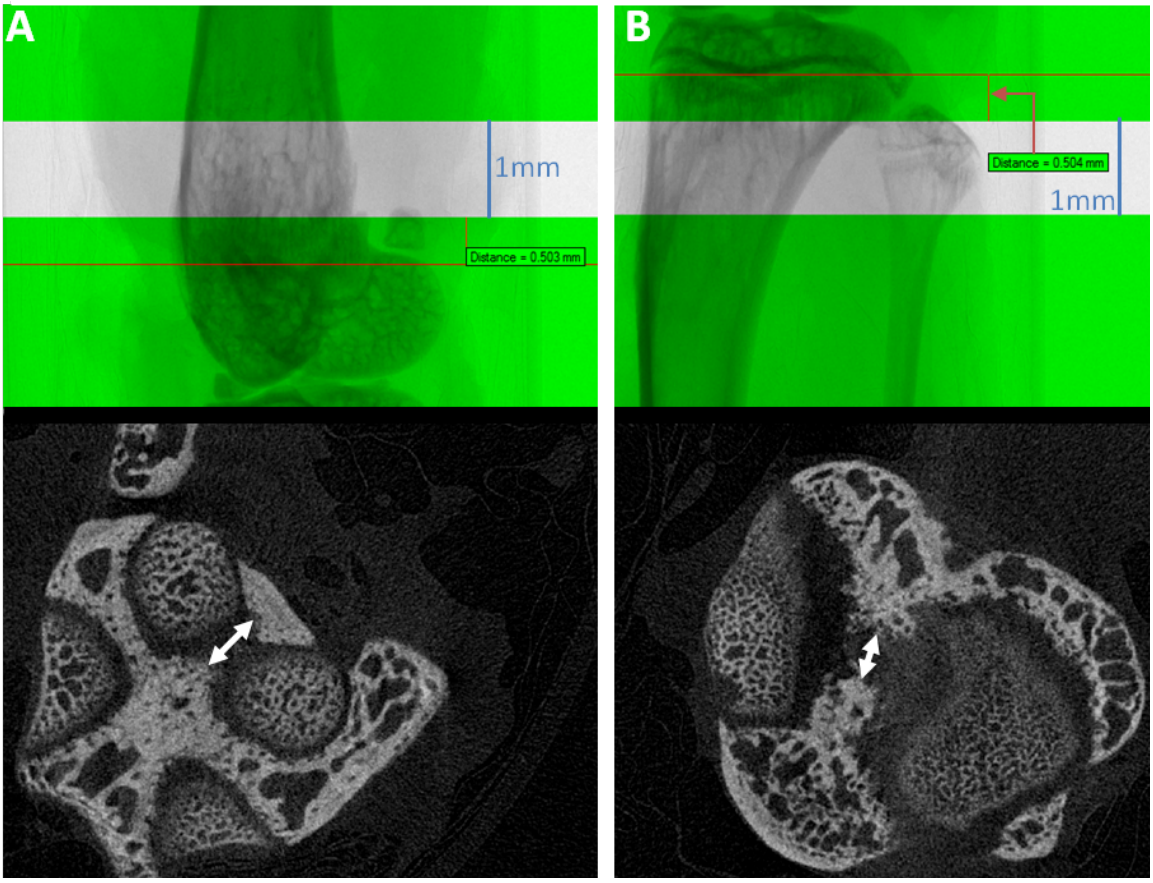

Figure 2.3 Example images of µCT reference points for trabecular bone analysis
Images depict the reference points (red horizontal line and cross sections), 0.5mm offset (red vertical line) and the selected 1mm area of analysis (blue vertical line) selected for A) femur and B) tibia using the CT_{AN} software. Cross sections depict typical reference points and show detection of a break in the first bridge (arrow).

2.2.11 X-Ray

X-ray analysis is commonly used in clinic and in preclinical studies to assess the effects of bone derived tumour growth on the skeleton. The electron dense bone matrix absorbs photons generated by the X-ray beam allowing analysis of bone integrity on a radiographic film. X-ray images were taken with a Faxitron-cabinet-X-Ray system and a mammography film. Tube voltage was set to 32kV and an exposure of 1 minute. Radiographs were then developed using a Curix60 developer and were scanned using the BIO-RAD GS-710 calibrated Imaging densitometer and Quantity One-4.5.1 software.

2.2.12 Immunohistochemistry

A range of staining procedures was used to identify cells and cell components on histological bone sections. Staining was carried out on a minimum of two non-serial bone sections (3µm) using the methods described below.

2.2.12.1 Dewaxing and dehydrating of paraffin embedded sections

Prior to use of paraffin embedded sections for staining procedures, slides were dewaxed in xylene (2x 5 min) and then taken through 99%, 99%, 95% and 70% ethanol (5 min each) to tap water. For dehydration prior to mounting of the stained samples, the slides were taken through 70% (10 sec) 95% (10 sec) 99%, 99% ethanol (30 sec each) and 2x xylene (1 and 3 minutes).

2.2.12.2 Haematoxylin and eosin staining (H&E)

H&E staining is widely used in histology, based on its ability to clearly demonstrate a number of different tissue structures. Haematoxylin stains cell nuclei blue with good intranuclear detail, while the eosin stains cell cytoplasm and most connective tissue fibres in various shades and intensities of pink, orange and red.

Slides were dewaxed before incubation in Gill's II haematoxylin for 90 seconds followed by washes in tap water for 5 minutes. Next, slides were incubated for 5 minutes in 1% aqueous eosin with 1% calcium carbonate, washed in tap water for 30 seconds and dehydrated before mounting.

2.2.12.3 TRAP (Tartrate-Resistant Acid-Phosphatase) staining

The tartrate resistant acid phosphatase expression in osteoclasts is commonly used in a TRAP staining method to identify the bone resorbing cells. Analysis of TRAP stained sections gives therefore insights into the location and number of osteoclasts in bone.

The following recipe is sufficient to stain 10 sections. To make the acetate-tartrate buffer, 5.44g sodium acetate trihydrate were dissolved in 200ml of distilled water and the pH was adjusted to 5.2 with 50ml of 1.2% acetic acid in dH_2O. 4.6g sodium tartrate were added to the solution and heated to 37°C. Other glassware was warmed to 37°C to ensure optimal conditions for the enzyme. Sections were dewaxed, placed in a coplin jar with warmed acetate-tartrate buffer and incubated at 37°C for 5 minutes. Next, sections were incubated in solution A for 30 minutes at 37°C (Solution A: 0.02g naphthol AS-BI phosphate and 1ml dimethylformamide mixed in a 50ml glass screw

cap bottle in a fume hood before adding 50ml of the warmed acetate-tartrate buffer). Solution B was prepared in a fume hood: 0.08g sodium nitrite was dissolved in 2 ml of distilled water. 2ml of a pararosaniline stock were mixed with the prepared 4% sodium nitrite solution to hexazotise the pararosaniline and was left to stand for 5 minutes. Just before use, 2.5ml of this solution was added to 50ml of pre-warmed acetate-tartrate buffer. Sections were then incubated in solution B for 15 minutes at 37°C and rinsed twice in running tap water before being counterstained for 20 seconds in haematoxylin and washes in running tap water, dehydration and mounting.

2.2.12.4 BrdU staining

BrdU is an analogue of thymidine and is often used for identification of proliferating cells in living tissues. The synthetic nucleoside is incorporated into newly synthesised DNA of every replicating cell exposed to BrdU. It is therefore possible to investigate the effects of treatment regimens on the growth of a wide range of cell types.

Slides were dewaxed before placing into PBS. Endogenous peroxidase was blocked with 3% H_2O_2 in methanol for 15min at ambient temperature before washing slides twice in PBS-T (PBS + 0.1% Tween 20) for 5 minutes. For antigen retrieval, slides were either microwaved at a high setting for 5 minutes in 10mM citric acid buffer (pH6) or using the pre-treatment antigen retrieval bath (Dako). Sections were then carefully washed in PBS-T (2x 5min) before blocking unspecific binding sites with a 1:10 casein/PBS solution for 30min at ambient temperature in a moist chamber. The primary antibody (mouse anti BrdU) was added at 1:175 in 5% casein in PBS and left to incubate over night at 4°C in a moist chamber. The next day, slides were washed in PBS-T (2x 5min) prior to adding the secondary antibody (anti-mouse biotin) at a dilution of 1:200 made up in 5% casein and incubation for 30 minutes at ambient temperature in a moist chamber. After washing in PBS-T (2x for 5 min) sections were incubated for 30 minutes at ambient temperature with ABC solution (avidin:biotin enzyme complex; the solution was made up at least 30 minutes prior to usage and according to manufacturer's description). Following two wash steps in PBS-T for 5 minutes, sections were incubated in DAB for approximately 5 minutes and transferred into water. Counterstaining of nuclei was performed by incubation in haematoxylin for 20-30 seconds and subsequent washes in water for 5 minutes. Sections were dehydrated before mounting in DePeX.

2.2.12.5 GFP staining

Apart from exciting GFP by using the *in vivo* imaging tool or by microscopy, anti-GFP antibodies can be used on sectioned bone specimens for tumour cell detection. An optimised protocol was kindly provided by Dr Michelle Lawson, University of Sheffield, UK.

Slides were dewaxed prior to blocking endogenous peroxidase in 3% H_2O_2 in PBS for 10 minutes. Subsequently slides were washed trice in distilled H_20 for 1 minute each before another wash step was carried out in 1x PBS (3x, 2 minutes each). To block unspecific binding, slides were incubated in 10% normal goat serum in PBS for 30 minutes. The primary antibody or isotype control was added at a 1:600 dilution in 5% normal goat serum (NGS) and incubated at 4°C over night. On the next day, sections were washed twice in PBS for 5 minutes each to remove excess primary antibody. Subsequently, sections were incubated with a 1:400 dilution (in PBS) of the secondary antibody (goat anit-rabbit HRP) for 45 minutes. Slides were then washed in PBS (2x 5 minutes) before detection with NovaRED Substrate Kit (made up to the manufacturers' instructions) for 5-15 minutes. After rinsing in distilled H_2O and washing in tap water for 5 minutes, nuclei were counterstained in Gill's Haematoxylin for 20 seconds before washing in running tap water for 3-5 minutes. Slides were dehydrated and mounted in DePeX.

2.2.12.6 ß-Galactosidase staining

Dr Alyson Gartland (University of Sheffield, UK) kindly provided an optimised protocol for ß-Gal immunohistochemistry. Paraffin bone sections were dewaxed before blocking endogenous peroxidase in 1% H_2O_2 in methanol for 30 minutes. After 3 wash steps in dH_2O (5 min each) and 3 wash steps in TBS (0.5M TRIS and 9% NaCl, 5 min each) unspecific binding sites were blocked by adding 5% normal goat serum diluted in TBS for 30 minutes. Primary antibody (rabbit anti-mouse ß-galactosidase) was added at a dilution of 1:1000 and slides were incubated over night at 4°C. The following day excess antibody was removed by 3 washes in TBS (5 min each) before incubation in secondary antibody (1:200, biotinylated goat anti-rabbit) for 30 minutes. Subsequently slides were washed in TBS (3x for 5 min) and detection was carried out using ABC solution and DAB as described for BrdU staining. Sections were counter stained with haematoxylin, dehydrated before mounting in DEPEX.

2.2.12.7 Immunohistochemistry staining for the human cytokeratin Cam5.2

Staining for the cytokeratin Cam5.2 was carried out by Sheffield Teaching Hospitals Foundation NHS Trust at the Department of Histopathology, Northern General Hospital or in a manual protocol preformed by Diane Lefley.

At Northern General Hospital, a Dako autostainer was used as well as antigen retrieval using the PT (pre-treatment) module and low pH retrieval solution for 20 minutes at 97°C. After dewaxing and antigen retrieval, slides were washed in Dako wash buffer diluted 1:20 and placed into the autostainer for the routine staining programme. Primary antibody dilution was 1:5 with 60 minutes incubation. Upon completion, the slides were washed in running tap water prior to counterstaining with haematoxylin, dehydration and mounting.

In the manual protocol the primary antibody was used at a serial dilution to test for the best staining/background results. Briefly, sections were incubated in 3% H_2O_2 in methanol before antigen retrieval in trisodium citrate buffer (pH6.5) for 10 minutes. After blocking in horse serum the primary antibody was added for 1 hour at ambient temperature. The secondary antibody (biotinylated horse anti-mouse at 1:200) was incubated for 1 hour at ambient temperature and detection was carried out using the ABC kit and DAB as described earlier.

2.2.12.8 Ki67 immunohistochemistry

Immunohistochemistry for the cell proliferation antigen Ki67 was carried out as previously described (Ottewell et al., 2008a) using a mouse monoclonal antibody specific for human Ki67, which is expressed by actively proliferating cells.

Slides were dewaxed prior to blocking endogenous peroxidase with 3% H_2O_2 in methanol for 10 minutes at ambient temperature followed by washes in PBS-T (PBS- and 0.1% Tween, 2x for 5 minutes). Antigens were retrieved by microwave (high for 5 minutes; low for 5 minutes) in 10mM Citric acid buffer (pH 6) and slides were washed in PBS-T (2x for 5 minutes). Unspecific binding sites were blocked in 1:10 casein/PBS for 30 minutes at ambient temperature followed by overnight incubation at 4°C in primary antibody (mouse anti-human Ki67) at a 1:125 dilution made up in 5% casein. Sections were then washed in PBS-T (2x for 5 minutes) before incubation for 30 minutes at ambient temperature in secondary antibody (anti mouse-biotin) at 1:200

made up in 5% casein. Slides were washed in PBS-T (2x for 5 minutes) prior to incubation in ABC solution (made up 30 minutes prior to use (2 drops of A; 2 drops of B; 5ml PBS)) for 30 minutes at ambient temperature and further washes and incubation in DAB for 3 minutes. Finally, slides were washed in H_2O, counterstained with haematoxylin for 30 seconds and dehydrated before mounting in DEPEX.

2.2.12.9 Caspase-3 immunohistochemistry

Immunohistochemistry for caspase-3 was carried out as previously described (Ottewell et al., 2008a) using the polyclonal anti-active caspase-3 antibody specific for human cleaved caspase-3.

Slides were dewaxed prior to blocking the endogenous peroxidase with 3% H_2O_2 in methanol for 10 minutes at ambient temperature. Sections were then washed in PBS-T (2x for 5 minutes) before antigen retrieval by microwaving (high for 5 minutes; low for 5 minutes) in 10nM Citric acid buffer (pH 6) and further washes in PBS-T (2x for 5 minutes). Unspecific binding sites were then blocked with 1:10 casein/PBS for 30 minutes at ambient temperature. Next, slides were incubated overnight at 4°C in the primary antibody (rabbit anti-human active caspase-3) at a dilution of 1:750 made up in 5% casein prior to thorough washes in PBS-T (2x for 5 minutes). Incubation in secondary antibody (anti rabbit-biotin) 1:200 made up in 5% casein was carried out for 30 minutes at ambient temperature before further washes in PBS-T (2x for 5 minutes). The slides were incubated in ABC solution (made up 30mins prior to use (2 drops of A; 2 drops of B; 5 ml PBS)) for 30 minutes at ambient temperature before washing in PBS-T (2x for 5 minutes) and incubation in DAB for 3 minutes. Finally, slides were washed in H_2O, counterstained with haematoxylin for 30 seconds and dehydrated before mounting in DEPEX.

2.2.12.10 Goldner's trichrome staining

The Goldner's trichrome method highlights specific structures like collagen and muscle in addition to allowing identification of bone marrow and tumour colonies. The basis of the staining is the difference in molecular size of the dyes used. Smaller particles penetrate the exposed tissue rapidly while larger ones require more time and can replace smaller molecules from the stained areas. Characteristics are: nuclei: blue/black, red blood cells: red, muscle and fibrin: pink, collagen: green. Staining was performed using a Masson-Goldner trichrome staining kit to the manufacturer's

instructions. Briefly, sections were dewaxed prior to adding Weigert's haematoxylin solution for 5 minutes and washing in running tap water 5 minutes. Sections were then rinsed in 1% acetic acid (30 seconds) before adding azophloxine solution for 10 minutes. After rinsing with 1% acetic acid, tungstophosphoric acid orange G solution was added for 2, 3, 4 or 5 minutes depending on the individual slides and rinsed with 1% acetic acid. Collagen of the bone should be colourless at this stage but muscle should be stained red. The section was covered with light green SF solution for 2, 3, 3.5, 4 or 5 minutes before a final wash with 1% acetic acid. Sections were then quickly dehydrated and mounted.

2.2.13 Scoring of histological slides

Two non-serial sections per tumour sample were stained for caspase-3, BrdU or Ki67 and the number positively stained cells per tumour area (mm^2) were scored using a Leica BMRB upright microscope with a 10x objective and Osteomeasure software.

Bone cell numbers were scored on TRAP stained sections and expressed as Ob or Oc number/mm trabecular bone surface or as the percentage of bone in contact with Ob or Oc (Fig. 2.4). Further details for criteria of osteoblast and osteoclast identification are described in Chapter 3, section 3.4.3.

For measurements of osteoclast size, Osteomeasure software and a Leica BMRB upright microscope with a 40x objective were used. The area of 40 osteoclasts per category (in contact and not in contact with tumour cells) was measured in randomly selected fields of view of TRAP stained sections. The data was expressed as the mean osteoclast size (mean osteoclast area/number of osteoclasts).

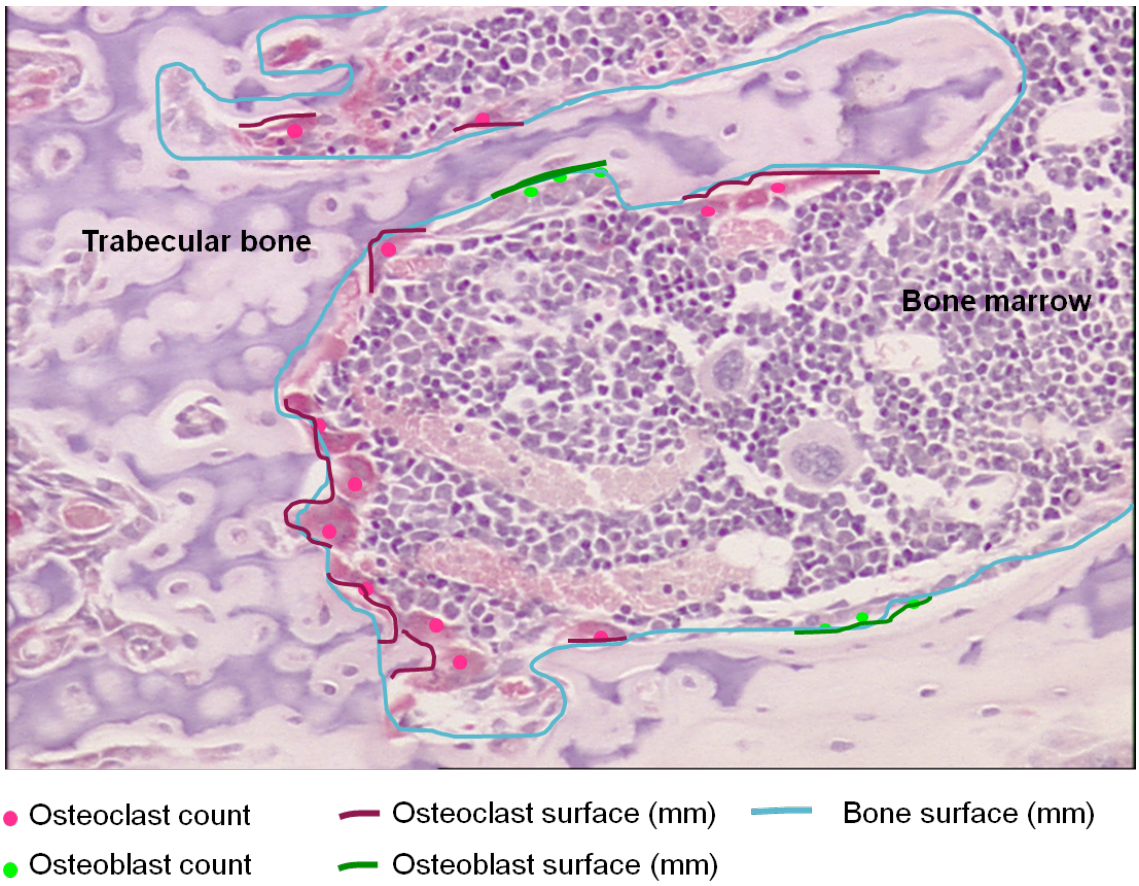

Figure 2.4 Example of osteoclast and osteoblast scoring on TRAP stained sections

2.2.14 Multiphoton microscopy

The use of GFP transfected breast tumour cells is an invaluable tool to identify tumour colonies within the chosen model system. However, because processing for histomorphometric analysis of tumours within bone requires various steps and sectioning of the bone, important information may be lost during these procedures. In addition, 2-D analysis of a 3-D object may not provide the best possible data in respect to location of single cells or colonies and their adjacent tissues. Multiphoton microscopy is able to by-pass these drawbacks as it allows visualisation of bone specimens up to a depth of approximately 500µm.

In some experiments, soft tissues and front legs were excised, wrapped in aluminium foil and snap frozen in liquid nitrogen prior to storage at -80°C and analysis using the Zeiss LSM510 NLO Inverted microscope. Bone samples were further embedded in OCT and sectioned as described in section 2.2.9.3.3. Bone specimens with exposed growth plates were washed in PBS before placing (with the growth plate facing downwards)

into a glass bottom dish. An inverted Multiphoton Confocal Microscope was used for analyses with a 20x objective (plan-apochromat 20x/0.8). The area of interest was found using the transmitted light setting on the microscope and tile scans were performed using the multiphoton chameleon laser at 900nm to detect collagen by second harmonic generation at 435-485nm and GFP at 525nm. In some cases GFP was visualised using a 488nm laser (BP 500-550 IR). AF647 was detected using a 633nm laser (excitation maximum at 652nm). Some areas of interest were chosen to perform a z-stack scans and images were taken with the LSM software.

2.2.15 BD™ Cytometric Bead Array

The BD™ Cytometric Bead Array (CBA) allows simultaneous quantification of multiple soluble proteins in less than 50µl serum. Each bead is labelled with a unique fluorescent intensity and is coated with the antibody of interest. The beads can then be clustered depending on their fluorescent signal and concentration of the protein of interest is calculated according to a standard curve generated for each bead. Mouse Flex Sets for IL-1α, IL-1β, IL-6, KC (murine IL-8) and MCP-1 were run to the manufacturer's instructions by the Flow cytometry Core Facility at the University of Sheffield using starved mouse serum samples. Species specificity for mouse cytokines only was tested by use of conditioned medium from MDA-MB-231-GFP cultures.

2.2.16 Serum measurements by ELISA

Protein quantification by ELISA was performed on serum samples. Food was removed on the night prior to sacrifice and blood was collected at a consistent time point (between 10 and 12am). All samples were stored at -80˚C until use.

2.2.16.1 Measurement of CTX in mouse serum

CTX, degradation products of the C-terminal telopeptides of type-I collagen which are released during bone matrix degradation, is commonly used as a bone resorption marker. The RatLaps™ EIA is an enzyme-linked immunosorbent assay for CTX quantification in mouse serum and was performed to the manufacturer's instructions. Briefly, 100µl of the biotinylated RatLaps antigen (biotinylated peptide, EKSQDGGR, a sequence specific to a part of rat type-I collagen) was added to the streptavidine coated microtitre wells and incubated at ambient temperature for 30 minutes. The plate was then washed three times by adding 300µl of wash buffer per well. Next,

20µl of standard, control (both supplied with the kit) and serum samples were added in duplicate as well as 100µl of the primary antibody solution per well. After overnight incubation at 4˚C, the plate was washed three times as described before. Then 100µl of the peroxidase conjugated secondary antibody were added per well and incubated at ambient temperature for 60 minutes prior to washing. Finally 100µl TMB (3,3',5,5'-tetramethylbenzidine) were pipetted into each well and incubated for 15 minutes prior to analysis on a plate reader at 450 and 850nm. A standard curve was created and the total CTX concentration was calculated and expressed in ng/ml.

2.2.16.2 Measurement of the bone formation marker PINP in serum

Bone formation requires the synthesis of type I collagen, a major organic part of the bone matrix. During collagen synthesis, amino- and carboxyterminal parts of propeptides are secreted into the circulation making them available for quantification in serum. The N-terminal propeptide of type I procollagen (PINP) was therefore used for determination of bone formation in mouse serum. The competitive enzymeimmunoassay (EIA) kit for mouse/rat PINP was used to the manufacturer's instructions. Briefly, 50µl of each calibrator or control were added in duplicate to the appropriate wells of the antibody coated 96-well-plate (polyclonal rabbit anti-PINP antibody). Next, 5µl of each sample and 45µl of Sample Diluent (BSA, 0.05% sodium azide in PBS) was pipetted into the appropriate wells in duplicate. Then, 50µl of biotinylated PINP was added to all wells prior incubation on a plate shaker at 600rpm at ambient temperature for 1 hour. The plate was then manually washed 3 times with 250µl of wash solution (PBS with Tween). Next, 150µl of the Enzyme Conjugate (avidin linked horseradish peroxidase in PBS) was pipette into all wells before incubation at ambient temperature for 30 minutes followed by washing as described before. Finally, 150µl TMB were added and incubated for 30 minutes at ambient temperature. In order to stop the reaction, 50µl of stop solution (0.5M hydrochloric acid) was added and the absorbance of each well was measured at 450 nm (reference 650 nm) using a plate reader 30 minutes after of addition of the Stop Solution. A standard curve was created and experimental sample concentrations were calculated and expressed in ng/ml.

2.2.16.3 Human sclerostin ELISA

Sclerostin is a negative regulator of the Wnt pathway and has been shown to inhibit osteoblastogenesis. The Sclerostin ELISA procedure was carried out as follows. 150µl of provided assay buffer was added into each well of the 96-well plate (coated with a polyclonal goat anti human Sclerostin antibody) before pipetting 20µl of the supplied standard and control solution as well as the experimental samples in duplicate into the assigned wells. Some wells were assigned as blank measurements. Next, 50µl biotinylated anti Sclerostin antibody was added into each well and the plate was incubated over night at ambient temperature in the dark. On the following day, the plate was washed 5x with 300µl diluted Wash buffer. 200µl of the Conjugate (streptavidin-horse radish peroxidase) were then added to each well and incubated for 1 hour at ambient temperature in the dark. After further washes (5x with 300µl diluted Wash buffer) 200µl Substrate (TMB solution) were pipetted into each well, incubated for 30 min (ambient temperature, dark) before adding 50µl Stop solution. Finally, the absorbance was measured immediately at 450nm with a reference wavelength of 630nm using a plate reader. Sclerostin concentrations were extrapolated from the standard curve and data were expressed in pmol/l.

2.2.16.4 Mouse RANKL ELISA

The RANKL immunoassay was performed by Alyson Evans. Briefly, 50ml of Assay Diluent was added to each well of the microplate coated with a polyclonal antibody specific for mouse RANKL followed by addition of 50mL of the supplied Standard and Control solution and the experimental samples and gentle tapping to mix. The plate was incubated for 2 hours at ambient temperature and was then washed with Wash Buffer (400ml/well). Next, 100ml of the Mouse TRANCEConjugate (polyclonal anti-mouse RANKL antibody conjugated to horseradish peroxidase) was pipetted into each well and incubation for 2 hours at ambient temperature. After washing the plate, 100mL of Substrate Solution (tetramethylbenzidine and were added to each well, incubated for 30 minutes at ambient temperature in the dark before adding 100mL Stop Solution (equal volumes of hydrogen peroxide and hydrochloric acid solution) and mixing (gentle tap). Finally, a plate reader was used to read the optical density of each well within 30 minutes at 450nm and a reference wavelength of 540nm. RANKL concentrations were extrapolated from the standard curve and data were expressed in pg/ml.

2.2.17 Tissue processing for analysis by flow cytometry

2.2.17.1 Tumour tissue

For preparation of single cell suspensions of subcutaneous tumour tissue was placed into ice cold PBS in a sterile petri dish prior to cutting the tissue into small pieces using a scalpel. Next, the tissue was washed twice in PBS before addition of 1ml of trypsin and incubation at 4°C for 1 hour followed by 1 hour at ambient temperature and 20 minutes at 37°C. 2ml of cell culture medium containing 10% FCS was added to the suspension to inhibit the enzyme. Cells were washed twice in PBS and were resuspended in 1% FCS in PBS before passing the suspension through a 70µm cell strainer into a Flow Cytometer tube. 200µl of same cell suspension was used for preparation of cytospins (section 2.2.25).

2.2.17.2 Bone marrow

Hind legs were excised and placed into ice cold PBS before flushing out the bone marrow using a 25-gauge needle and a 1ml syringe. Cell suspensions were washed twice in PBS before resuspension in 1% FCS in PBS and passing through a 70µm cell strainer into a Flow Cytometer tube. 200µl of same cell suspension was used for preparation of cytospins (section 2.2.25).

2.2.17.3 Peritoneal macrophages

Cells were collected as described in 2.2.8.4 and were spun down and washed twice in PBS prior to resuspending in 1% FCS in PBS and passing through a 70µm cell strainer into a Flow Cytometer tube. 200µl of same cell suspension was used for preparation of cytospins (section 2.2.25).

2.2.18 RNA extraction by TRI REAGENT™

Total RNA isolation from cell culture or *in vivo* samples was performed using the TRI REAGENT™ method, a single step extraction technique using an acid guanidinium thiocyanate-phenol-chloroform mixture. Cells were lysed by adding 1ml TRI REAGENT™ and passing the cell lysate several times through a pipette followed by incubation for 5min at ambient temperature. For *in vivo* tissue samples, RNAlater was removed and the tissue was washed twice using sterile PBS before adding 1ml TRI REAGENT™ and homogenising the tissue using a Bio Vortex. Next, 0.2ml chloroform was added to the solution which was manually inverted for 15sec prior to incubation at ambient temperature for 5min. This was followed by centrifugation of the sample at 12000rpm for 15min at 4°C in a bench top centrifuge. After centrifugation, two phases could be distinguished in the solution, with RNA remaining exclusively in the upper

aqueous phase. In order to precipitate the RNA, the upper aqueous phase was transferred to a fresh RNA-free Eppendorf tube followed by addition of 0.5ml 2-propanol and manual inverting. The sample was then incubated at ambient temperature for 5-10min and centrifuged once more at 12000rpm for 15min at 4°C. Once the supernatant had been removed carefully, the RNA pellet was washed by adding 1ml of 100% ice cold ethanol and mixing and centrifugation at 12000rpm for 5min at 4°C. Two more wash steps were carried out using freshly prepared 80% EtOH and centrifugation at 7500rpm for 5min at 4°C. In order to obtain the RNA, the supernatant was removed and the pellet was air-dried for 10min at ambient temperature. Finally, the RNA was dissolved in 30µl RNase-free DEPC-treated (diethyl pyrocarbonate, a nonspecific inhibitor of RNases) H_2O. All samples were further "cleaned" using the RNA Cleanup kit.

2.2.19 RNA Cleanup using the RNeasy Kit

The RNeasy Mini Kit was used to clean RNA that was previously isolated. The kit was used to the manufacturer's instructions. Briefly, the RNA sample volume was adjusted to 100µl with RNase-free water before adding 350µl RLT Buffer and rigorous mixing. Ethanol (250µl) was then added and mixed by pipetting and transfer of the sample to an RNeasy Mini spin column and a 2ml collection tube. Samples were centrifuged for 15 seconds at 10 000rpm and flow-through was discarded. Next, 500µl RPF buffer were added before centrifugation as in the previous step and discarding of the flow-through. The wash step was repeated, the columns were centrifuged for 2 minutes, the flow-through was discarded and the empty column was spun once more for 1 minute at maximum speed to eliminate any residual buffer from the RNA sample. Finally the column was placed into a new 1.5ml collection tube and 30µl of RNase-free water was added prior to centrifugation for 1 minute at 10 000rpm to elute the RNA. The concentration of each sample was then measured (section 2.2.20) and RNA quality was established (section 2.2.21) before samples were stored at -80°C.

2.2.20 Quantitative measurement of ribonucleic acid

The RNA concentration was determined in 1µl RNA solution using a NanoDrop. The absorbance was measured at a wavelength of 260nm (A260) and 280nm (A280) while also using a reference containing the appropriate solvent without ribonucleic acid. The ratio A260/A280 was analysed in order to assess the purity of a RNA sample. The ratio

1.8-2.0 is due to nucleic acids while a ratio less than 1.8 indicates that there may be proteins and/or other UV absorbers in the sample.

2.2.21 Qualitative measurement of ribonucleic acid

The Agilent 2100 Bioanalyzer was used to examine RNA integrity. RNA samples were diluted to a concentration of <500ng/µl in Depec H_2O and were analysed on a NanoChip by Dr P Heath from the Microarray Core Facility at the University of Sheffield, UK. Typical RIN (RNA Intergrity Number) values were between 9.9 and 7.3 for subcutaneous tumour tissue and *in vitro* samples. For RNA extracted from hind legs RIN values ranged from 7.0 to 5.1

2.2.22 Reverse transcription of RNA

First strand cDNA synthesis was performed using the SuperScript® III-Strand Synthesis SuperMix according to manufacturer's instructions. Reverse transriptases are enzymes that can synthesise a DNA strand using an RNA template and are commonly found in retroviruses enabling reverse transcription of their RNA genomes into DNA. In order to prime cDNA synthesis, 1µg of purified RNA were mixed with 1µl (50µM) oligo$(dT)_{20}$ primers, 1µl Annealing buffer and RNase-free (DEPC-treated) H_2O in a final volume of 8µl prior to incubation at 65˚C for 5 minutes followed by cooling at on ice for at least 1 minute. Next, 10µl of the 2x First-Strand Reaction Mix and 2µl SuperScript® III/RNaseOUT™ Enzyme Mix were added on ice before mixing and brief centrifugation. The mix was then incubated at 50°C for 50 minutes in order for cDNA synthesis to take place. The reaction was terminated by incubating the sample at 85˚C for 5min and then placing on ice. Exactly the same procedure as above, with the exception of the addition of reverse transcriptase was followed for a sample used as a control for DNA contamination of the RNA sample. cDNA samples were subsequently stored at -20˚C.

2.2.23 Quantitative Real Time Polymerase Chain Reaction (qRT-PCR)

qRT-PCR is commonly used for semi quantitative analysis of gene expression. Species-specific TaqMan® assays were used for analysis of selected genes. The specificity (all TaqMan® assays used were designed to detect human genes) and efficiency of each primer set had been previously assessed in the laboratory (see page 51). For each gene of interest the final reaction mix contained 5µl TaqMan® Universal PCR Mastermix, 3.5µl DEPC-treated water, 0.5µl TaqMan® assay and 1µl cDNA. Each cDNA sample was

loaded in duplicate. The tubes were mixed by centrifugation before loading onto a 384-well PCR plate and analysing using the ABI 7900HT platform and SDS 2.2.1 software. Exactly the same procedure as above, with the exception of the addition of cDNA (replaced by DEPC water) was followed for a sample used as a negative control. For every sample the house-keeping gene GapdH was run on the same plate for subsequent analysis of relative gene expression. After completion of the run, ΔCT values were calculated from the average CT value of each sample: $\Delta CT=CT_{Target\ gene}-CT_{GapdH}$. Furthermore the ΔCT values were averaged and ΔΔCT values were calculated: $\Delta\Delta CT=\Delta CT_{control}-\Delta CT_{sample}$. Finally, the fold change compared to control was calculated using 2^-(ΔΔCT).

2.2.24 Pre-amplification of cDNA prior to qRT-PCR

In some cases the TaqMan® Pre Amp Cells-to-CT™ Kit was used for pre-amplification of specific TaqMan® assays. The kit was used to the manufacturer's instructions.

Cell lysis

Tissue was washed in cold PBS and before adding 50µl Lysis Solution with DNase I (to remove genomic DNA) at 1:100 and homogenising the tissue. The lysis reaction was mixed by pipetting up and down five times followed by incubation at ambient temperature for 5 minutes. Next, 5µl of Stop Solution was added directly into each reaction and mixing as above. Samples were then incubated 2min at ambient temperature.

Reverse Transcription (RT)

A mastermix was prepared according to the number of samples and the table below, the mix was then placed on ice before pipetting 40µl of the RT mastermix into a PCR tube containing 10µl of the lysis reaction. Once assembled, reactions were centrifuged and incubated at 37° for 60 minutes, then at 95°C for 5 minutes to inactivate the enzyme before placing on ice.

Component	Amount per reaction
2x RT Buffer	25µL
20x RT Enzyme Mix	2.5µl
Nuclease-free Water	12.5µL

Preamplification

Equal volumes of each 20x TaqMan Gene Expression Assay were pooled in a microcentrifuge tube before dilution to a final concentration of 0.2x in 1x TE buffer.

For example: to pool 50 TaqMan assays, 10µl of each 20x assay were used and 500µl 1x TE buffer was added for a total volume of 1ml (0.2x). Next, 25µl of TaqMan PreAmp Master Mix, 12.5µl of pooled assay mix (0.2x) and 12.5µl of cDNA (from the completed RT reaction) were mixed in a PCR tube and placed in to a thermal cycler programmed as described in the table below. After run completion, the samples were placed on ice immediately and stored at -20°C. Before running the qRT-PCR reaction as described in section 2.2.23, the pre-amplified samples were diluted at 1:20 in 1x TE buffer.

	Stage	Repeats	Temperature	Time
Enzyme activation (hold)	1	1	95°C	10min
PCR (cycle)	2	14	95°C	15sec
			60°C	4min

2.2.25 Preparation of cytospins

Cell suspensions that were made up for flow cytometry (section 2.2.17) were used for cytospin preparations. 200µl of each cell suspension was added to the assembled cytospin slide (glass microscope slide, filter paper, funnel and metal holder) and centrifuged at medium speed for 5 minutes. The slides were then disassembled and coversliped using ProLong® Gold antifade mounting medium.

2.2.26 Statistical analysis

Statistical analysis was performed using GraphPad Prism software (Version 5.0a). Tests used for each study are indicated in the Materials and Methods section of each results chapter as well as in the respective figure legend. In all cases, a p-value of <0.05 was considered significant.

3. Establishing *in vivo* mouse models and methods for analyses of human breast tumour growth in bone

3.1 Summary

In vivo models of metastatic breast cancer are frequently used in preclinical studies and several techniques have been published using xenograft models of human cancer cells implanted in immunocompromised mice. The introduction of human cancer cells to bone via the systemic route are commonly applied in preclinical investigation of tumour growth and treatment. Once the *in vivo* experiment has been performed, comprehensive analysis of the bone and the tumour is possible by several techniques. A vast number of reports have been published assessing tumour growth in murine bone, however most studies have focussed on large tumour colonies and thus only little published information is available on how to analyse small (<1mm in diameter) tumours and surrounding bone cells appropriately. Osseous tumour growth is frequently measured by histology; but the majority of the published studies have been on end stage disease with large tumours filling almost the whole bone marrow cavity. Although these stages allow studies of the tumour, analysis of the bone microenvironment is greatly impeded due to the loss of bone, associated bone cells as well as the bone marrow.

This chapter summarises the establishment of two mouse models of human breast cancer growth in bone and the development of measurement of small cancer colonies as well as reproducible analysis methods of effects of tumour growth on the microenvironment.

3.2 Introduction

Metastatic bone disease affects approximately 70% of advanced breast cancer patients and outcome is generally poor. Clinical samples of metastatic breast foci are not obtained easily leading to a lack of studies investigating human metastatic bone disease. Animal models therefore enable preclinical studies to assess the different stages of the metastatic process and the effects of therapies on tumour growth and disease progression. Several xenograft models of mammary tumour growth in mouse bone have been published (Ottewell et al., 2006). In these models, human tumour cells are either introduced into the circulation (intracardiac or intraarterial), tumour tissue is transplanted orthotopically into the mammary fat pads followed by dissemination to visceral and osseous sites (Hoffman et al., 1999), or implanted directly into the bone marrow cavity of long bones of immunocompromised mice. The latter method is less representative of the metastatic process since the cells are directly placed into the metastatic site (bone), but can be used to study the late stages of the metastatic cascade. Moreover, the implantation requires surgical intervention in order to inject tumour cells directly into the medullary cavity of long bones. The technique may therefore make the separation of surgically induced tissue trauma and the tumour-induced effects on the microenvironment difficult.

Introducing cancer cells into the circulation may be a more representative method of the metastatic process compared to the orthotopic intraosseous model. Arguello et al. (1988) first described the formation of osseous tumours after B16 melanoma cell injection into the left cardiac ventricle of C57BL/6 mice. It was subsequently shown that intracardiac injection of the oestrogen receptor negative human breast cancer cell line MDA-MB-231 into nude mice resulted in aggressive tumour growth with a high preference to localise to bone (Yoneda et al., 1999). Although a large number of cells ($1x10^5$ to $5x10^5$ per mouse) are introduced into the circulation, only about 0.01% of the injected tumour cells have the potential to survive and form metastatic foci. The selectivity of the metastatic site (bone) is thought to depend on the site of injection, the involvement of chemoattractants, organ specific adhesion molecules and mechanical properties as for example vessel size (Arguello et al., 1988). Recent work has furthermore suggested that cancer cells with stem like properties colonise specific areas within the bone marrow, the metastatic niche (Psaila and Lyden, 2009).

The observed organ selectivity of cancer cells post intracardiac injection was further used to generate bone homing breast cancer cell lines. In summary, human breast carcinoma cells were introduced via the left heart ventricle and the resulting osseous tumour colony was harvested. After sequential intracardiac transplantation a bone specific cell line was generated with the characteristic of returning to the site at which it had been harvested (bone). The cells can then be introduced into the circulation via the intraarterial route (lateral tail artery) without losing the bone homing properties. The bone seeking MDA-MB-231/B02 cell line was first published by Peyruchaud et al. (2001) using the described method and is now frequently used in studies of metastatic breast tumour growth. It is important to note that the injection of the B02 cell line is to date reported as being an intravenous injection, however the introduction of tumour cells into the venous blood flow would lead to pulmonary metastases. For generation of bone metastases, intraarterial injection into the lateral tail artery with compression of the abdomen to impair blood flow is necessary and will lead to bone metastases in the posterior part of the skeleton. When comparing cancer-induced osteolytic bone disease in mice injected with B02 cells or the parental cell line MDA-MB-231, it was shown that B02 tumours caused an increase in osteolytic lesion number and area (Pecheur et al., 2002), underlining the bone specific properties of this cell line.

The described *in vivo* models are commonly used to study the processes involved in osseous tumour growth, as well as the effects of treatment, and several techniques are available for downstream analysis. Table 3.1 gives an overview of the published methods used to determine breast tumour burden in bone. Although the literature summarised in the table is by far not exhaustive, it demonstrates the variability of methods used between laboratories, and emphasises the high number of studies investigating end stage disease. Measurement of tumour burden in bone is often performed on histological sections but more recent imaging techniques (bioluminescence, PET (positron emission tomography), MRI (magnetic resonance imaging), PET μCT, optical μCT) are now commonly used. Bioluminescence, for example, has a great advantage over histological analysis because it is non-invasive and allows monitoring of tumour growth *in vivo*. Although the histomorphometric assessment of tumour size in bone is technically challenging and can only be performed *ex vivo*, the detailed information obtained is invaluable. The use of

histology enables the investigation of the cellular components of the tumour and the microenvironment in a 2-D relationship and provides the possibility to stain for a number of different molecules (tumour or host) on sections of the same sample.

Several, usually non-serial sections, should be analysed to get a good representation of a solid 3-D tumour, however, the number of sections analysed and whether these were adjacent to each other or not is often not mentioned in published manuscripts (Table 3.1).

Study details	Measurement of tumour burden by histology	Alternative method used to measure tumour burden
Sasaki et al., 1995 **Cells**: MDA-MB-231 **Injection** i.c. **Sacrifice**: day 28	**Analysed area:** Assessment of tumor volume by stereological technique (point grid) calculation of total tumour volume by using tumour area/section and the distance between sections (300 or 900 um). **Sections/samples analysed:** n.s.	None
Clohisy et al., 1996b **Cells:** MDA-MB-231, MDA-MB-435 **Injection:** intrafemural **Sacrifice:** week 7-10	None	Weight of hind limbs
Thomas et al., 1999 **Cells**: MCF7 **Injection** i.c. **Sacrifice**: week 9	**Analysed area:** histomorphometric analysis of total tumour area **Sections/samples analysed:** n.s.	None
Wetterwald et al., 2002 **Cells:** MDA-231-B/Luc+ **Injection:** i.c., i.v., intratibial **Sacrifice:** day 28-38		Bioluminescent Reporter Imaging (BRI), radiography, histology
Hiraga et al., 2003; Hiraga et al., 2004 **Cells**: 4T1/luc **Injection** mammary fat pad, will develop bone metastases **Sacrifice**: day 22	**Analysed area:** tumour area (mm^2) measured by imaging software and added together for tibia + femur. Data expressed as tumour area/mouse **Sections/samples analysed:** n.s.	None
van der Pluijm et al., 2005 **Cells**: MDA-231-B/luc+ **Injection** i.c. **Sacrifice**: day 46	**Analysed area:** Total tumor area, measured by image analysis software Differential analysis of intra- and extraosseous tumour area. **Sections/samples analysed:** n.s.	Bioluminescence imaging of whole body, expressed as relative light units
Phadke et al., 2006 **Cells**: MDA-MB-435-GFP **Injection** i.c. **Sacrifice**: Hours: 1, 2, 4, 8, 24, 48, 72. Weeks: 1, 2, 4, 6.	None	Differential analysis of tumour burden in distal/proximal femoral metaphyses/diaphyses by flow cytometry and quantitative real-time PCR

Table 3.1 Overview of published analysis techniques used to score osseous breast tumour burden

i.v.=intravenous, i.c. intracardiac, n.s.=not shown.

Detection of the tumour in bone is possible due to the morphological differences between human and host bone marrow cells. Solid tumour colonies can therefore be identified on for example haematoxylin and eosin stained sections. Difficulties can arise when analysing small tumour colonies because they are easily missed during the sectioning process and often only little material is available for subsequent analysis. The use of specific tumour cell markers should be considered in order to reliably identify colonies of less than about 100 cells and single cancer cells. Small numbers of tumour cells in bone are most commonly analysed using luciferase activity in bone marrow suspensions (Daubine et al., 2007) or by flow cytometry and quantitative real time PCR (Phadke et al., 2006), reflecting the difficulties associated with identification on histological sections.

The increased understanding of the relevance of the bone microenvironment in metastatic breast tumour growth lead to the decision to carry out detailed quantification of the static remodelling parameters like osteoblast and osteoclast number per mm bone surface in tumour bearing bones. A literature search of studies assessing osteoclasts and/or osteoblasts in tumour bearing bones demonstrated the large variability between studies of cancer-induced bone disease summarised in Table 3.2. While osteoclasts were frequently measured, the analysis of osteoblasts was less common and it was often not clear how the cells were identified and which bone areas were studied. Importantly, the lack of published studies assessing effects of tumour growth on bone cells other than at late stage disease highlighted the need to develop a protocol for the analysis of early (prior to development of extensive osteolysis) tumour growth in bone and the associated microenvironment during my PhD project. Apart from osteoblasts and osteoclasts, several other factors may play a role in the microenvironment-tumour cell interactions, including different cell types, soluble factors like cytokines and extracellular matrix proteins (Holen and Coleman, 2010).

This chapter describes the establishment of two *in vivo* xenograft models of breast tumour growth in bone and the development of a systematic approach for detection and analysis of small to large tumour colonies and associated bone disease.

Study details/model	Measurement of osteoblasts	Measurement of osteoclasts

Clohisy et al., 1996a **Cells:** 2472(sarcoma) G3.26 (melanoma) **Injection:** intrafemural **Sacrifice:** day 21	None	**Staining:** TRAP **Specimen:** femur **Other details:** area and Oc number/mm bone surface analysed in tumour bearing and corresponding sham control bones **Number of sections analysed:** 4/femur
Clohisy et al., 1996b **Cells:** MDA-MB-231, MDA-MB-435 **Injection:** intrafemural **Sacrifice:** week 7-10	None	**Staining:** TRAP **Specimen:** femur **Other details:** Oc defined as TRAP-positive cells in contact with bone surfaces, Oc/mm bone surface **Number of sections analysed:** 4/femur, at least 20 Oc/limb
Thomas et al., 1999 **Cells**: MCF7 **Injection:** i.c. **Sacrifice**: week 9	None	**Staining:** hematoxylin and eosin, orange G and phloxine **Specimen:** midsections of tibia/femur **Other details:** Oc number/mm of tumour-bone interface **Number of sections analysed:** n.s.
Corey et al., 2003 **Cells**: PC-3, LuCaP23.1 **Injection:** intratibial **Sacrifice**: week 4-9	**Staining:** Goldner's trichrome **Specimen:** proximal tibia **Other details:** Ob.S/BS (%) **Number of sections analysed:** n.s.	**Staining:** Goldner's trichrome **Specimen:** proximal tibia **Other details:** Oc.S/BS (%) **Number of sections analysed:** n.s.
Hiraga et al., 2004 **Cells**: 4T1/luc **Injection:** mammary fat pad, develops bone metastases **Sacrifice**: day 22	None	**Staining** TRAP, Mayers hematoxylin **Specimen:** tibia and femur **Other details:** proportion of 3mm corticoendosteal surface (0.5mm from the growth plate) in contact with TRACP positive Oc expressed as % of total bone surface **Number of sections analysed**: n.s.
van der Pluijm et al., 2005 **Cells**:MDA-231-B/luc+ **Injection:** i.c. **Sacrifice**: day 46	None	**Staining:** Goldner's trichrome or TRAP **Specimen:** tibia **Other details:** Oc number per millimeter of tumour/bone interface **Number of sections analysed:** n.s.

Study detail/model	Measurement of osteoblasts	Measurement of osteoclasts

Phadke et al., 2006 **Cells**: MDA-MB-435-GFP **Injection:** i.c. **Sacrifice**: Hours: 1, 2, 4, 8, 24, 48, 72. Weeks: 1, 2, 4, 6	**Staining** Goldner's trichrome, TRAP, alkaline phosphatase activity **Specimen:** distal femur (spongiosa) **Other details:** ratio of the alkaline phosphatise positive area mm^2/bone area in mm^2, Ob number/mm bone surface **Number of sections analysed**: Some decalcified femurs (alkaline phosphatase), n.s. for Ob number	**Staining:**TRAP **Specimen:** distal femur (spongiosa) **Other details:** Three images of the distal and proximal scored for the number of TRAP-positive cells **Number of sections analysed**: 2-8 sections from 2-4 bones per time point
Chantry et al., 2010 **Cells**: 5T2MM, MDA-MB-231-luc-D3H2LN **Injection:** i.v., i.c. **Sacrifice**: week 7 (MDAMB-231), and week 13 (5T2MM)	**Staining:** TRAP, hematoxylin **Specimen:** tibia **Other details:** analysis area of trabecular bone: 0.75mm^2 area 0.25mm from the growth plate. Analysis area of cortico-endosteal surface: 3mm starting 0.25mm from the growth plate. N.Ob/BS/mm and Ob.S/BS in % **Number of sections analysed**: n.s.	**Staining:** TRAP, hematoxylin **Specimen:** tibia **Other details:** analysis area of trabecular bone: 0.75mm^2 area 0.25mm from the growth plate. Analysis area of corticoendosteal surface: 3mm starting 0.25mm from the growth plate. N.Oc/BS/mm and Oc.S/BS in % **Number of sections analysed**: n.s.

Table 3.2 Overview of osteoblast and osteoclast histomorphometry carried out in studies of osseous tumour growth

i.v.=intravenous, i.c. intracardiac, TRAP=tartrate resistant acid phosphatase, OC=osteoclast, Ob=osteoblast, n.s.=not shown, Ob.S=osteoblast surface, BS=bone surface, N.Ob=number of osteoblast, N.Oc=number of osteoclast.

3.3 Aims

The main aims of this chapter were as follows:

- To establish a suitable *in vivo* model of metastatic breast cancer growth to bone for analysis of different stages of tumour growth and the effects of treatment.
- To develop methodology for reproducible analysis of bone cells (osteoblasts and osteoclasts) in tumour bearing and non-tumour bearing bones.
- To assess the suitability of a range of methods, including histomorphometry, immunohistochemistry and multiphoton microscopy, for the analysis of single tumour cells, small tumour foci (<1mm in diameter) and interactions between the tumour and the surrounding microenvironment.

3.4 Method development and results

3.4.1 Establishment of *in vivo* models of human breast tumour growth in bone

All *in vivo* experiments were carried out in accordance with local guidelines and with Home Office approval under project license 40/2972 held by Professor N.J. Brown, University of Sheffield, United Kingdom.

3.4.1.1 The intravenous model using B02 cells

The bone homing B02 cell line (Peyruchaud et al., 2001), derived from the parental human breast cancer cell line MDA-MB-231, was initially used to establish an *in vivo* model of human bone metastases. An experiment undertaken by Dr Ottewell (University of Sheffield, UK) in collaboration with and in the laboratory of Dr Philippe Clezardin (INSERM, Lyon, France) was successful in inducing osseous B02 tumour growth in balb/c nude mice (Ottewell et al., 2008a). Because the model had been shown to be effective (80-100% tumour take rate) the technique was used for initial *in vivo* experiments in this PhD project. B02-GFP/β-Gal (B02) cells (kindly received from Dr Clezardin) expressing green fluorescent protein (GFP), luciferase and beta-galactosidase (β-Gal) were cultured in 1640-RPMI supplemented with 10% FCS at 37˚C and 5% CO_2. Because it was not possible to perform bioluminescence imaging at the University of Sheffield animal facilities, monitoring tumour growth *in vivo* relied on GFP imaging. *In vivo* detection of a fluorochrome signal through the dense bone matrix and several layers of soft tissue require the tumour to reach a detectable size (approximately 2 weeks post injection of B02 cells (Peyruchaud et al., 2001) and a high number of GFP positive tumour cells on day of injection should be used. The percentage of GFP positive B02 cells was therefore analysed by flow cytometry prior to allocation of the cell batch for *in vivo* use. B02 cells and MDA-MB-231 cells (GFP negative) were analysed for GFP expression using the FACS Calibur flow cytometer. Cell suspensions suitable for *in vivo* experiments were defined as a GFP positive cell population of 85% or more. In case of a percentage lower than 85%, the cells were sorted for GFP (Fig. 3.1).

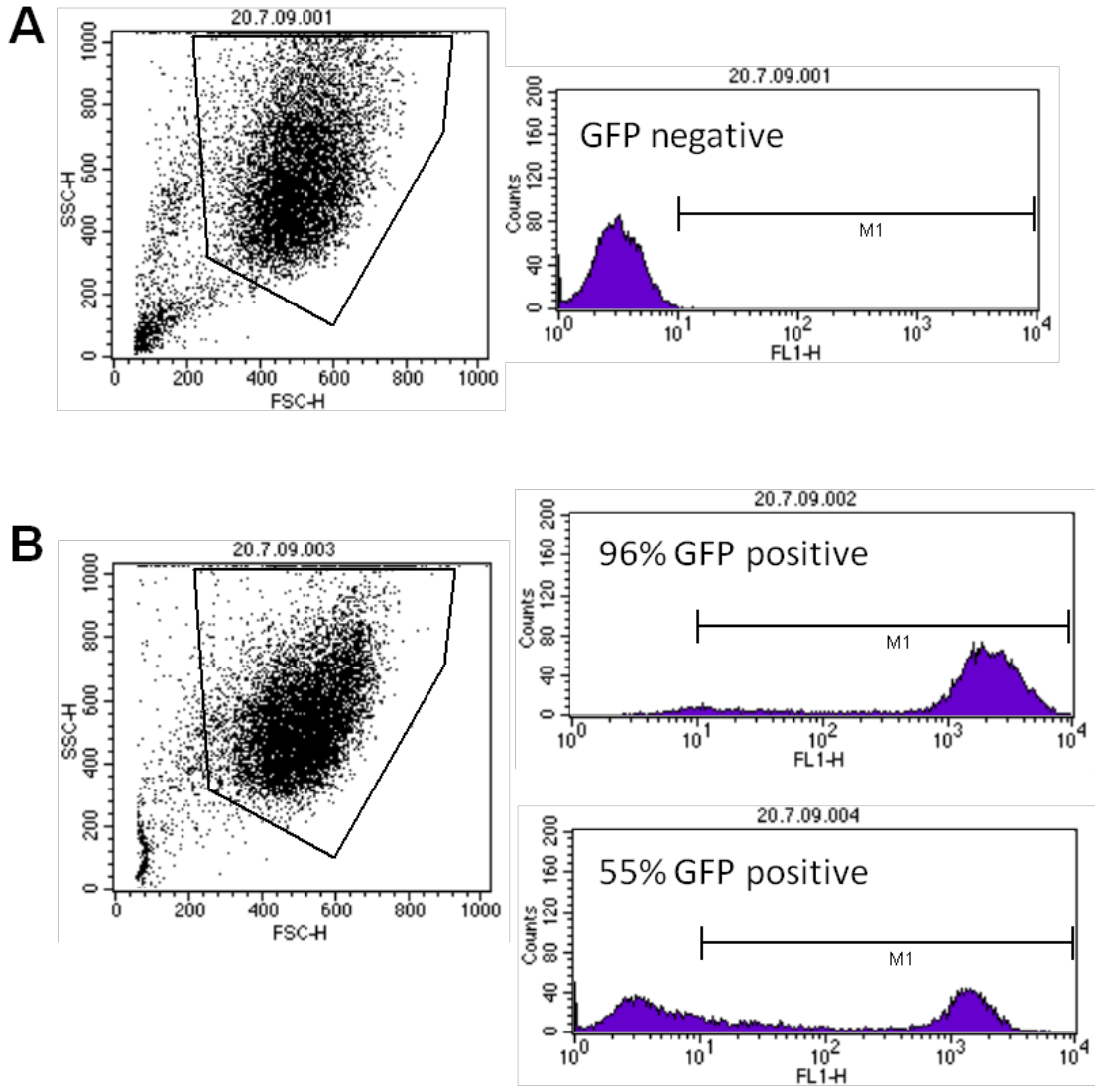

Figure 3.1 Example of FACS analysis of GFP expressing B02 cells
A) The MDA-MB-231 cell line and B) B02 cells were analysed for GFP (FL1-H) on the FACS Calibur system. B02 cells with a value of >85% were used for *in vivo* experiments while cell batches below were sorted for GFP before injection.

3.4.1.1.1 B02 injection procedure

All steps in the initial experiment, including cell and anaesthetic preparation, were carried out by me while Dr Ottewell injected the cells as described earlier (Ottewell et al., 2008a). Home office regulations require specialised training of the investigator prior to performing *in vivo* procedures, thus I was unable to perform the injections of the first experiment myself. Note that suppliers and further details to this procedure can be found in the general materials and methods section 2.2.8.2.2. On day of injection, a $1x10^6$ cells/ml suspension of GFP positive B02 was prepared. Cells were placed on ice and used for injection within approximately 1-hour post trypsinisation. Female, 6 week old balb/c nude mice (Charles River, UK) were injected with

ketamine/xylazine (56.5mg/kg ketamine and 5.5mg/kg xylazine) into the peritoneal cavity and placed into an incubator (33°C) to maintain body temperature and to ensure blood vessels are dilated to facilitate injection. Anaesthetised mice (tested by pinch reflex) were placed onto the bench top and a piece of autoclave tape was placed over the abdomen to act as tunicae. 0.1ml of the $1x10^6$cells/ml suspension ($1x10^5$ cells per mouse) was slowly injected into the lateral tail artery using a 1ml insulin syringe with a 27-gauge fitted needle. Animals were monitored closely directly post injection and then weekly by GFP imaging to assess tumour growth. Despite adopting the protocol of the original article (Ottewell et al., 2008a) and being performed or supervised by Dr Ottewell, experiments performed using the described method and the cell batch available in the laboratory resulted in very low numbers of osseous tumour growth detectable by GFP imaging (3% take rate, n=100). The extremely low tumour take rate could have been the result of a number of different parameters, listed in Table 3.3 and subsequent studies were performed to identify these.

Potential reason for lack of osseous B02 tumour growth	**Methodology**	**Section**
Loss of GFP expression *in vivo* could lead to detection difficulties of tumour foci	Analysis of osteolytic bone disease by x-ray and assessment of the presence of tumour colonies in H&E stained histological sections	3.4.1.1.2
Impeded B02 viability during injection	*In vitro* analysis of effects of needle gauge size on B02 cell viability	3.4.1.1.3
Too low cell number/mouse	*In vivo* experiment with increased cell number/mouse	3.4.1.1.4
Cells may lose their bone seeking properties *in vitro* if not continuously grown in selection medium	*In vivo* experiment with B02 cells grown in selection medium	3.4.1.1.4
B02 tumour growth could be impeded by the host (balb/c nude mice obtained in the UK)	Subcutaneous injection of B02 cells to investigate if cells are able to grow *in vivo*	3.4.1.1.4
Cell batch could have lost the bone homing properties during transport or sub-culturing	Use of different cell batches from different laboratories for *in vivo* work	3.4.1.1.4 3.4.1.1.5
Anaesthetic concentration varied from the literature	Increased concentration of ketamine and xylazine	3.4.1.1.5

Table 3.3 Summary of potential reasons for the lack of osseous B02 tumour growth
The table summarises the possible explanations of the low B02 take rate as well as the experiments performed to address this. The relevant sections describing each experiment can be found in the far right column.

3.4.1.1.2 Assessment of B02 tumour growth by means other than GFP imaging

One possibility for the lack of visible tumours by GFP imaging could be the loss of GFP expression *in vivo*. Therefore, radiographs were taken of hind legs on day of sacrifice to assess tumour-induced osteolytic bone disease. In addition, bones were processed for histology and a selection of samples was serial sectioned, stained for H&E and assessed for presence of tumour colonies. X-ray and histological investigation confirmed the lack of osseous tumour growth; no bone lesions were detected in any animal.

3.4.1.1.3 Investigation of needle gauge size on B02 cell viability

Because of concerns that the injection process itself could impair B02 cell viability; an *in vitro* experiment was performed investigating the effects of the needle gauge size on tumour cell growth. Briefly, 1ml/well of a $2x10^4$ B02 cells/ml suspension was seeded in triplicates into a 6-well-plate using either a 1ml syringe with a 27-gauge fitted needle, a 1ml syringe with a 25-gauge needle or a 1ml pipette tip. To mimic the injection process, the cells were passed through the syringe in 0.1ml steps. Cells were left to grow for 96 hours at 37˚C and 5% CO_2. Next, the medium of each well was carefully collected to assess non-viable cell numbers in the supernatant and the viable, adherent cells were trypsinised before resuspending in medium. Cell supernatants and adherent cell suspensions were counted using a haemocytometer. Figure 3.2 shows that there was no difference between viable adherent cell numbers or floating cells in the supernatant when comparing the use of needles (25- and 27-gauge size) to the 1ml pipette tip. The 27-gauge sized needle was used for all further *in vivo* experiments.

At this point, the negative data from the B02 experiments resulted in the decision to use an intracardiac breast tumour model with the parental human breast cancer cell line MDA-MB-231 for further experiments. The procedure of the intracardiac model is described in section 3.4.1.2. In parallel, further experiments using B02 cells were carried out in order to investigate the potential causes for the lack of tumour growth when using the intraarterial model.

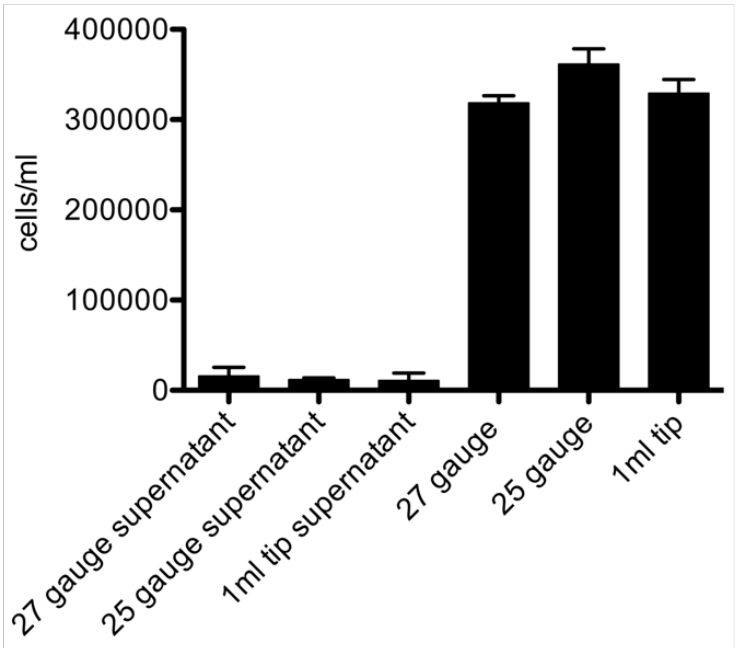

Figure 3.2 Investigation of needle gauge size on B02 cell viability
A total of 1ml/well of a $2x10^4$ B02 cells/ml suspension were seeded in triplicates into a 6-well-plate before quantification of floating (supernatant, non-viable) and adherent (viable) cells after 96 hours. Results are expressed as cells/ml. Mean ± SEM from triplicate samples in a single experiment.

3.4.1.1.4 Investigation of B02 tumour take rate after use of selection medium and injection of increased cell number

A literature search revealed that B02 cell numbers per mouse varied between studies with some using $5x10^5$ cells per mouse (Pecheur et al., 2002; Garcia et al., 2008) compared to $1x10^5$ (Peyruchaud et al., 2001; Ottewell et al., 2008a). In addition, two types of B02 selection media were prepared to select for GFP (RPMI-1640, 10% FCS, 1mg/ml Geneticin) and for GFP, luciferase and β-Gal guided by the recommendation of Mrs Deux B (RPMI-1640, 10% FCS, 1µg/ml puromycine, 500µg/µl hygromycine, 800µg/µl G418, email communication between Dr Ottewell PD, University of Sheffield and Mrs Deux B, INSERM, Lyon). B02 cells were grown either in selection media or the medium used in the previous experiments (RPMI-1640, 10% FCS). To ensure that predominantly GFP positive cells were injected under all three conditions, the cells grown in antibiotic-free medium were sorted for GFP prior to injection.

Firstly it was investigated whether increased cell number ($5x10^5$ vs. $1x10^5$) and culturing in GFP selection medium (RPMI-1640, 10% FCS, 1mg/ml Geneticin) would increase osseous tumour take (n=2). The supplier of animals was changed from Charles

River, (UK) to Harlan (UK) for subsequent experiments. Anaesthesia, preparation and injection of the cells were carried out as described in section 3.4.1.1.1. Furthermore, two mice were injected s.c. with $1x10^6$ B02 cells, in order to assess if the cells are capable of growing *in vivo* at a peripheral site. GFP images and x-rays taken at the end of the experiment (day 43) did not show GFP positive tumour growth in bone or osteolytic bone disease under either condition. However, the s.c. tumour of the mouse injected with cells grown in the antibiotic free medium was palpable approximately one week prior to sacrifice (day 43), suggesting that the cells grow, although slowly, at the subcutaneous site. Next, a new batch of cells (arrived November 2009) that had kindly been provided on request by the laboratory of Dr Clezardin in Lyon was tested for *in vivo* growth characteristics. In addition, the selection medium recommended by the Lyon team (RPMI-1640, 10% FCS, 1µg/ml puromycine, 500µg/µl hygromycine, 800µg/µl G418) in combination with the higher cell number ($5x10^5$) was used for tumour growth in 4 animals (Harlan, UK). Anaesthesia, preparation and injection of the cells were carried out as described in section 3.4.1.1.1. GFP images and x-rays taken at the end of the experiment (day 55) did not show GFP positive tumour growth or osteolytic bone disease.

Collectively the data from the experiments described here suggest that a higher cell number, addition of antibiotics and use if a new cell batch did not result in increased osseous tumour take rate. However, the cells did grow at the subcutaneous site in animals received from Harlan (UK) resulting in the decision that further experiments will be carried out using mice from this supplier.

3.4.1.1.5 Modification of B02 injection procedure

As I was unable to generate tumour growth in bone by using the described alterations to the original protocol, I arranged a visit to a collaboration laboratory (Galapagos SASU, Paris, France) that routinely and effectively uses the B02 model. I therefore was able to closely monitor the complete procedure from tumour cell culturing, preparation of cell suspensions prior to injection and *in vivo* administration. During the visit, a number of differences between the standard protocol used in Sheffield and the Galapagos SASU protocol were noticed and are summarised in Table 3.4.

	University of Sheffield	Galapagos SASU
Culture medium	RPMI 1640 + Glutamax 10% FCS	RPMI 1640 10% FCS 1% Glutamine 1% pen/strep
Cell preparation	Cells are prepared in PBS, immediately prior to injection ($1x10^6$cells/ml), placed on ice.	Cells are prepared in PBS immediately prior to injection ($4x10^6$cells/ml), no ice.
Time to injection	Injection take place within 1-1.5 hours (0.1ml/mouse) post trypsinisation	Injections take place within 20-25 minutes (0.1ml/mouse) post trypsinisation
Number of mice injected/flask	~20 mice are injected per prepared cell suspension	~5 mice are injected per T75 flask
Mice	Female, balb/c nu/nu, 6-7 weeks old at injection	Female, balb/c nu/nu 7-8 weeks old at injection
Anaesthetic	56.5 mg/kg ketamine 5.5 mg/kg xylazine in H_2O	116.0 mg/kg ketamine 7.3 mg/kg xylazine in NaCl
Cell number	100,000/mouse	400,000/mouse

Table 3.4 Comparison of B02 injection methods

The table summarises the steps involved in B02 cell preparation, injection and anaesthesia of animals used in Dr Holen's laboratory in Sheffield, UK and at Dr Pujuguet's laboratory at Galapagos SASU, Paris, France. Pen/strep = penicillin and streptomycin.

In addition to providing the opportunity to monitor the B02 model procedure, my injection technique was monitored and approved by Dr Pujuguets' experienced technical staff and a vial of B02 cells used at Galapagos was sent to Sheffield. On arrival, the cells were thawed and cultured in 1640-RPMI supplemented with 10% FCS and 1% penicillin/streptomycin. On day of injection, the cells were prepared as described in Table 3.4 (Galapagos). A total of 10 mice (Harlan, UK) were injected in two batches. One T75 flask was used for 5 mice and cells were prepared fresh in between to minimise the time the cells were kept in PBS. Mice were anaesthetised with a higher dose than used previously (116.0mg/kg ketamine, 7.3mg/kg xylazine, in NaCl compared to 56.5mg/kg ketamine, 5.5mg/kg xylazine, in H_2O) and animals were injected with B02 cells as described earlier. All animals were monitored weekly by non-invasive GFP imaging. Two weeks post injection, the first animals showed detectable tumour growth in the hind legs. The experiment was terminated once first signs of morbidity were visible (between day 30 and day 36). A 90% tumour take rate was achieved in this experiment and example GFP images are shown in Figure 3.3.

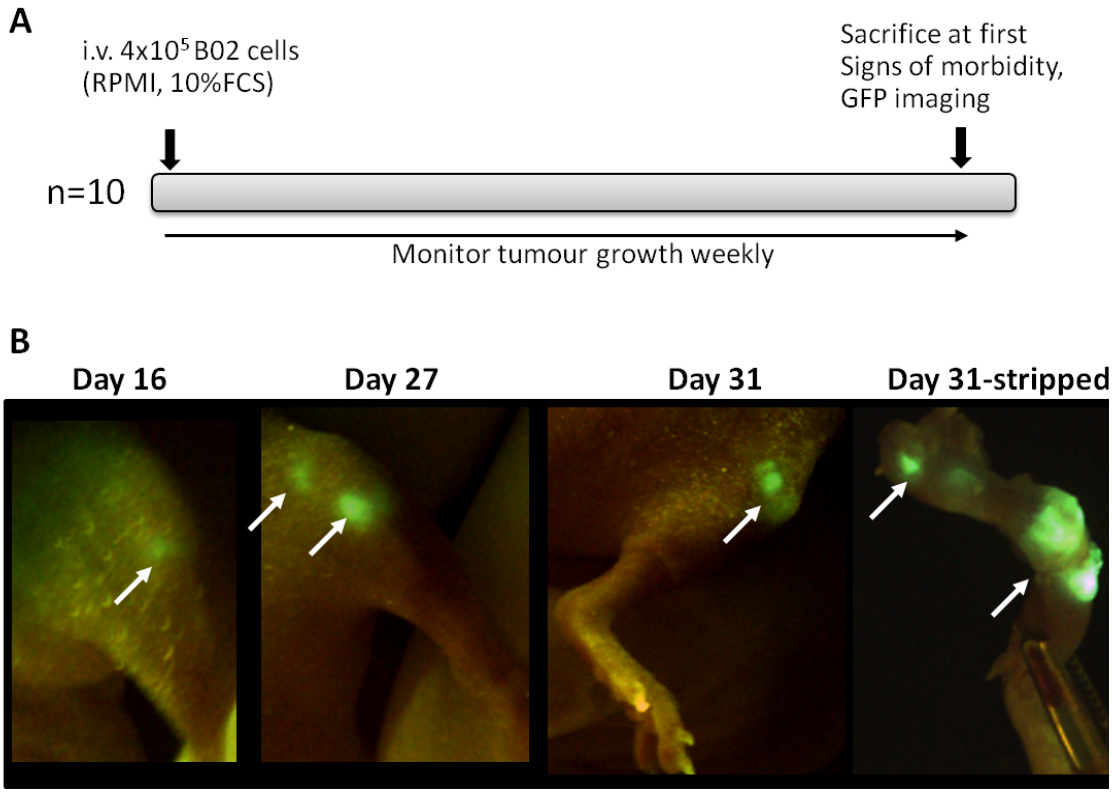

Figure 3.3 *In vivo* outline of B02 experiment using the Galapagos method
A) Outline of *in vivo* experiment. Female, 6 week old balb/c nude mice (n=10) were injected with $4x10^5$ B02 cells grown in RPMI-1640, 10% FCS, 1% pen/strep. Animals were anaesthetised with 116.0mg/kg ketamine, 7.3mg/kg xylazine, in NaCl. B) Example images taken post sacrifice (day 30-36, GFP, white arrow) showing osseous tumour growth.

Collectively, the *in vivo* experiments carried out to optimise the B02 model showed that the cell number, anaesthesia and possibly the cell batch and animal supplier were important for successful tumour take. Since I was able to optimise the B02 model successfully, further experiments in our unit will be using the method described in section 3.4.1.1.5. Table 3.5 summarises the different conditions and results of experiments undertaken during the optimisation process. The material collected from all B02 experiments was used either for analysis (Chapter 4) and/or for the familiarisation and optimisation of analysis techniques such as tissue fixation, decalcification, processing, µCT analysis, histological staining procedures, histological analysis of bone cells and multiphoton microscopy.

B02 cell number/mouse & cell batch origin	Medium	Anaesthetic	Animal supplier	Take rate (n)
$1x10^5$cells/mouse; original cell batch obtained from Dr Clezardin, Lyon	RPMI-1640, 10% FCS,	56.5mg/kg ketamine 5.5mg/kg xylazine in H_2O	Charles River, UK	3% (100)
$5x10^5$cells/mouse; second cell batch obtained from Dr Clezardin, Lyon	RPMI-1640, 10% FCS, +/- 1mg/ml Geneticin	56.5mg/kg ketamine 5.5mg/kg xylazine in H_2O	Harlan, UK	0% (2)
$5x10^5$cells/mouse; second cell batch obtained from Dr Clezardin, Lyon	RPMI-1640, 10% FCS, 800mg/ml Geneticin, 1µg/ml puromycine, 500µg/µl hygromycine	56.5mg/kg ketamine 5.5mg/kg xylazine in H_2O	Harlan, UK	0% (4)
$4x10^5$cells/mouse; Cell batch obtained from Dr Pujuguet, Paris	RPMI-1640, 10% FCS, 1% Pen/Strep	116.0mg/kg ketamine, 7.3mg/kg xylazine, in NaCl	Harlan, UK	90% (10)

Table 3.5 Summary of B02 experiments
The table summarises the origin of the cell batch, the number of cells used per mouse, the medium used to grow the cells *in vitro*, the anaesthesia used and the resulting take rate.

3.4.1.2 The intracardiac model using MDA-MB-231-GFP cells

After having performed several experiments with very low tumour take rate, it was decided that a different tumour model should be used in the PhD project to ensure tumour growth. MDA-MB-231 cells had been previously transfected with GFP (provided by Dr Ottewell, University of Sheffield) enabling imaging of GFP positive tumours *in vivo*. MDA-MB-231-GFP cells were thawed, cultured and the percentage of GFP positive cells was assessed by flow cytometry. A T75 flask of GFP positive MDA-MB-231 cells was used to prepare a $1x10^6$ cells/ml suspension in PBS and placed on ice. Female balb/c nude mice (6 weeks of age at day of injection, Harlan, UK) were anaesthetised with 56.5mg/kg ketamine, 5.5mg/kg xylazine, in H_2O and 0.1ml of the cell suspension was injected into the left heart ventricle. Successful injections were judged by the bright red colour of the oxygenated blood, which was drawn into the bevel of the needle prior to injection. Dr PD Ottewell performed the intracardiac injections in the first experiment. A 44% (n=30) take rate was achieved in this experiment and thus all further bone metastasis studies shown in this PhD thesis were carried out using the intracardiac model. After receiving the required training and

being authorised to perform the technically challenging intracardiac injections myself, the take rate increased during the course of my PhD up to 88%. Weekly live imaging showed that tumours were visible by GFP from 2 weeks post injection or from 10 days when imaging muscle free hind legs on day of sacrifice.

In summary, the intracardiac model using MDA-MB-231 cells was successful in generating osseous tumour growth in the first performed experiment and was therefore used for all further *in vivo* studies of osseous tumour growth performed during my PhD.

3.4.2 Development of detection and measurement of tumour growth in bone *ex vivo*

One of the aims of the PhD project was to analyse small (<1mm diameter) breast tumour colonies in bone in order to determine tumour-induced (Chapter 4) and treatment-induced changes (Chapter 5) to the bone microenvironment. Although the initiating phases of bone metastases are of interest to many researchers, there is only little published data available. This section summarises the development of methods for analysis of small tumour colonies in bone. Size differences, depending on the study protocol, between GFP positive osseous tumour colonies were visible when imaging hind legs on day of sacrifice. Small colonies were therefore defined as GFP positive areas in bone with less than 1mm in diameter, medium sized tumours as GFP areas with a diameter between 1 and 2mm and large tumour colonies had an approximate diameter of over 2mm. The terminology of small, medium and large tumours will be used from now on.

3.4.2.1 Histological detection and identification of small breast tumour colonies in bone

In order to detect tumour colonies of approximately 1mm in diameter, a method had to be developed to localise and identify the cancer focus on histological sections. In addition, several techniques were tested for tumour cell identification in bone, including immunohistochemistry for GFP, beta-galactosidase (β-Gal) and the human cytokeratin Cam5.2 as well as multiphoton microscopy.

3.4.2.1.1 Localisation of the tumour in the bone specimen

Histological analysis of bone specimens is currently irreplaceable in gaining detailed information of the complex cellular components of the bone. However, in order to comprehensively analyse small tumour colonies and the directly surrounding cells, histological detection of the tumour is required. To my knowledge, there is currently no standard protocol available on how to process and section histological bone specimens with small tumour colonies. Indeed, this was proven to be challenging since small colonies were often missed during the sectioning process. Although tumour colonies were detectable by GFP imaging, tumours could not be identified on histological sections 10 days and sometimes even 15 days post tumour cell injection. This was further shown to be partly due to the orientation of the bone during embedding. For standard bone histology, all bone specimens in one study are orientated in the same way to ensure the analysis of comparable areas. Because the location of small tumour colonies was shown to be highly variable within the metaphysis region (medial or lateral, posterior or anterior), the standard embedding procedure was found to be unsuitable. In order to surpass these problems, a system was developed increasing the detection of small tumours on histological bone sections (Fig. 3.4). Detailed GFP images were taken of the stripped hind legs on day of sacrifice including posterior, anterior, medial and lateral view of the hind legs (Fig. 3.4A). The images were used to orientate the bones accordingly during embedding, placing the side with the tumour towards the sectioning surface (Fig. 3.4B).

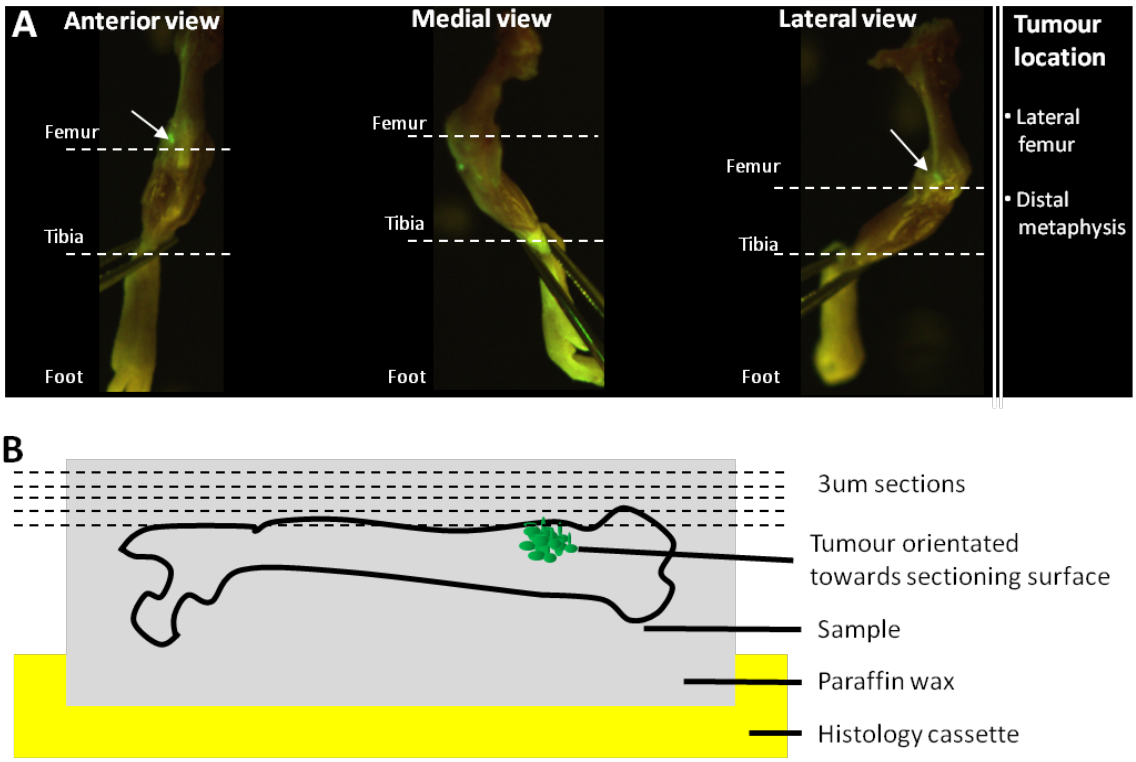

Figure 3.4 GFP images and embedding procedure for sectioning of hind legs with small tumour colonies

A) Example images of right hind leg with a small (<1mm in diameter) tumour colony. GFP images are shown for anterior, medial and lateral surfaces to locate the tumour (GFP, arrow). B) Schematic, sagittal view through a histology block to visualise orientation of the femur in A) during embedding with the tumour colony facing towards the sectioning plane.

The block was sectioned until tissue (bone associated soft tissue and/or bone) was visible and some sections were stained for H&E and assessed for tumour growth. If tumour was detected, approximately 20 sections were collected and stored at 4°C for analysis. If no tumour was identified further sections were cut and the whole process was repeated (Fig. 3.5). By using this method fewer rounds of sectioning and staining had to be performed, ultimately saving time as well as increasing the number of detected tumours. The gap in between different tumour levels was kept at a minimal depth for the detection of small tumours. The actual size of the gap was therefore partly dependent on the person using the microtome (sections used in this PhD were either cut by Mrs A Evans or staff of the Bone Analysis Laboratory, University of Sheffield). For medium to large tumour colonies, a similar process was carried out as described above with the alteration that defined gaps (>20µm) were cut in before collection of 10-20 sections to ensure good representation of the three dimensional tumour.

During analysis of tumour size, MDA-MB-231 tumour colonies as small as 0.15mm^2 (10 days post tumour cell injection) could be detected by morphology alone. However, detection of smaller tumour colonies (for example 5 days post injection) or even single tumour cells, as would be required if the very early, initiating stages of the metastatic tumour growth in bone were to be assessed, would greatly benefit from a tumour cell specific staining method to aid identification. Several markers were therefore tested for their suitability. In addition, the option of using multiphoton microscopy (a technique enabling 3-D imaging with great tissue depth) to detect single tumour cells was evaluated.

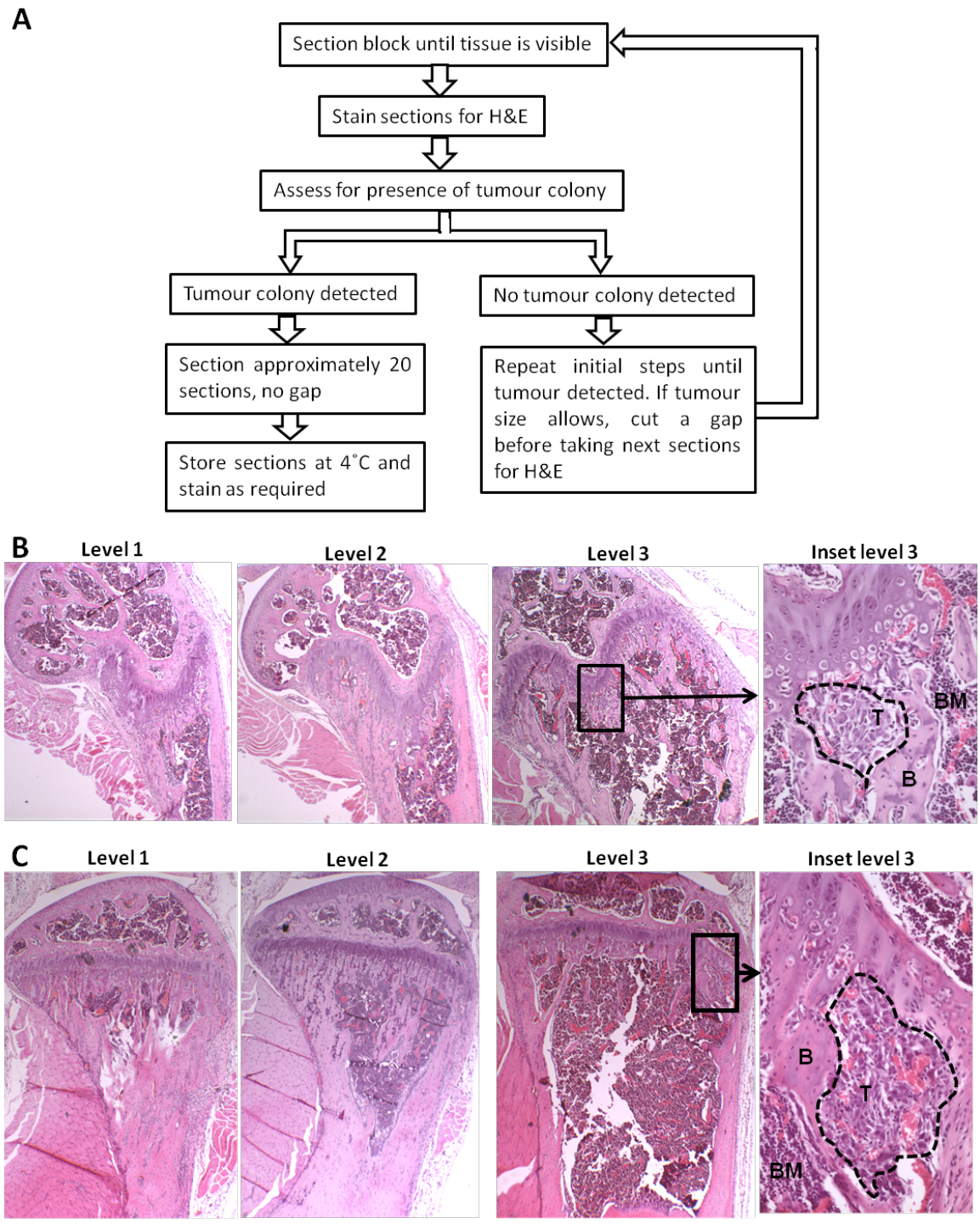

Figure 3.5 Overview of workflow for sectioning of hind legs with small tumour colonies

A) Overview of sectioning process of small tumour colonies. Example H&E images of B) femur and C) tibia illustrating the necessity of repeated sectioning and staining to locate a tumour colony. Both tibia and femur show tumour colonies 15 days post tumour cell inoculation. Note that no tumour cells are visible in level 1 or 2. White dotted line=tumour circumference, T=tumour, BM=bone marrow, B=bone, white box=area of magnification. Level 1-3: 1.6x objective, inset level 3: 20x objective.

3.4.2.1.2 Assessment of GFP, β-Gal or cytokeratin staining for tumour cell identification in bone

The use of GFP expressing human breast cancer cells provides the opportunity to track small cancer colonies by histological means. GFP and β-Gal staining was performed on B02 tumour-bearing bone sections (kindly provided by Dr Ottewell, University of Sheffield) as well as tumour-free sections to assess background staining. Negative controls (isotype control) were added to each staining run. Optimised immunohistochemistry protocols were kindly provided by Dr Shelly Lawson (GFP) and Dr Alyson Gartland (β-Gal), University of Sheffield. When analysing the GFP stained sections, it was noticed that only a fraction of the tumour cells were GFP positive suggesting that a number of B02 cells have lost their GFP expression *in vivo* (Fig. 3.6A), while β-Gal staining appeared to detect more B02 cells when compared to GFP (Fig. 3.6B). However not all cancer cells were stained and tumour-free sections used as an additional negative control showed background staining of murine bone cells.

Although β-Gal staining showed promising results, it could not be carried out on the majority of the present studies because these were performed using MDA-MB-231-GFP cells (not expressing β-Gal). GFP staining was found to be unreliable as a marker for breast tumour growth in bone.

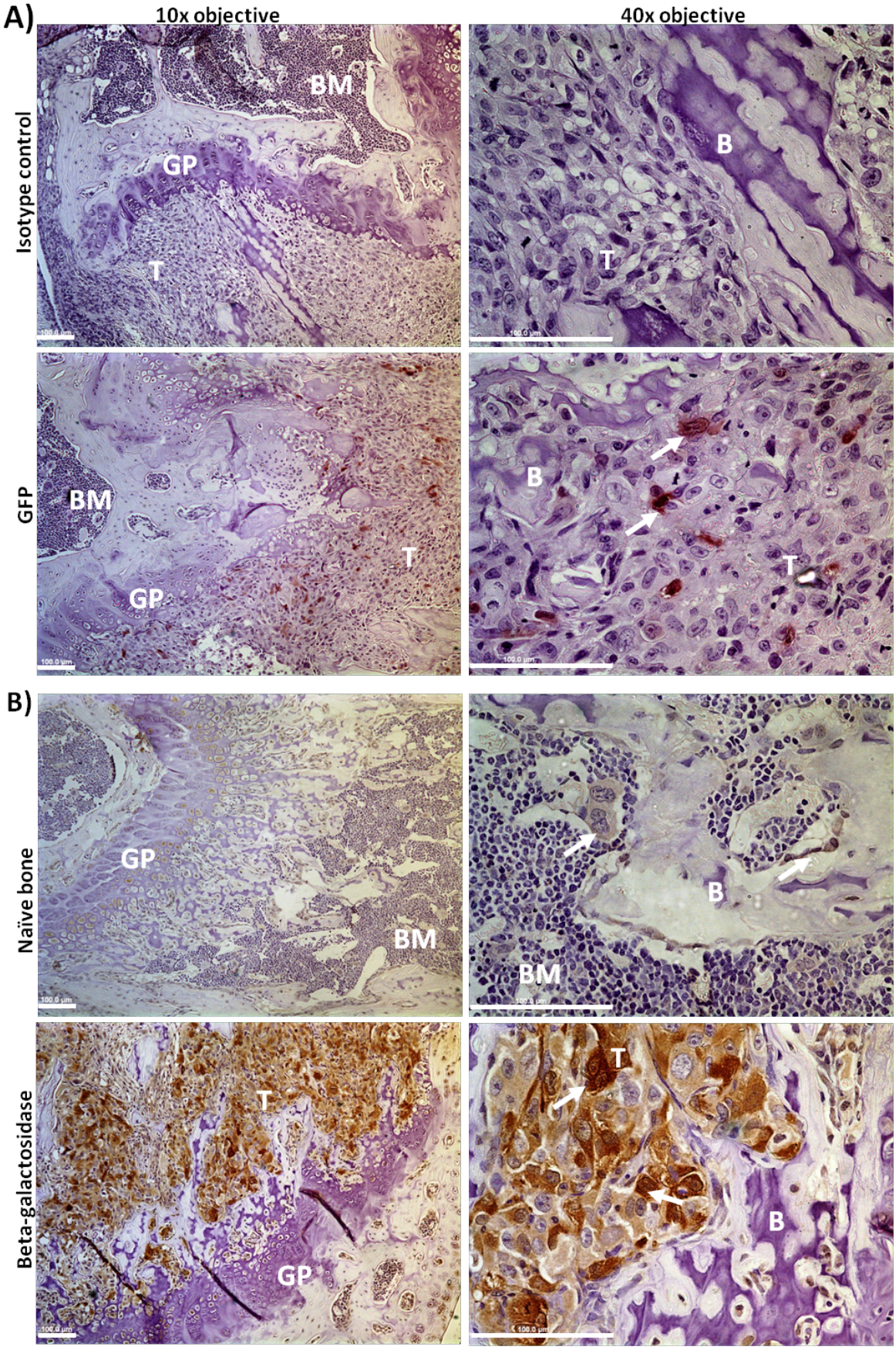
A)
10x objective
40x objective
Isotype control
GFP
BM
GP
T
B
B)
Naïve bone
Beta-galactosidase

Figure 3.6 Comparison of GFP and β-Gal immunohistochemistry (page 101)
Histological bone sections with B02 tumour colonies were stained for A) GFP and B) β-Gal. Isotype control staining was carried out on tumour bearing bones and the normal staining protocol was performed on tumour free sections to visualise the background staining and thus the specificity to potentially detect single tumour cells in bone. Note that in both GFP and β-Gal stained sections not all tumour cells were stained. T=tumour, BM=bone marrow, B=bone, GP=growth plate, solid arrowhead=positive tumour cells. Scale bar=100μm, left panel: 10x objective, right panel: 40x objective.

Immunohistochemical analysis following staining with antibodies specific for the human cytokeratin Cam5.2 were also tested for identification of human breast cancer cells (B02 and MDA-MB-231) in mouse bone. Staining was carried out using an automated stainer (performed by the NHS diagnostics laboratory at Northern General Hospital, Sheffield) using antibody A (BD Biosciences, order reference 345779) for B02 cells. At a later stage, antibody B (BD Biosciences, order reference 349205) was used in a manual protocol for MDA-MB-231 detection (Fig. 3.7). The use of different primary antibodies was due to discontinuation of antibody A. In the manual protocol several dilutions of the primary antibody were tested (neat, 1:2, 1:5 in 5% serum; performed by Mrs D Lefley). The marker Cam5.2 did not appear to be specific as strong staining of bone cells was present in both protocols.

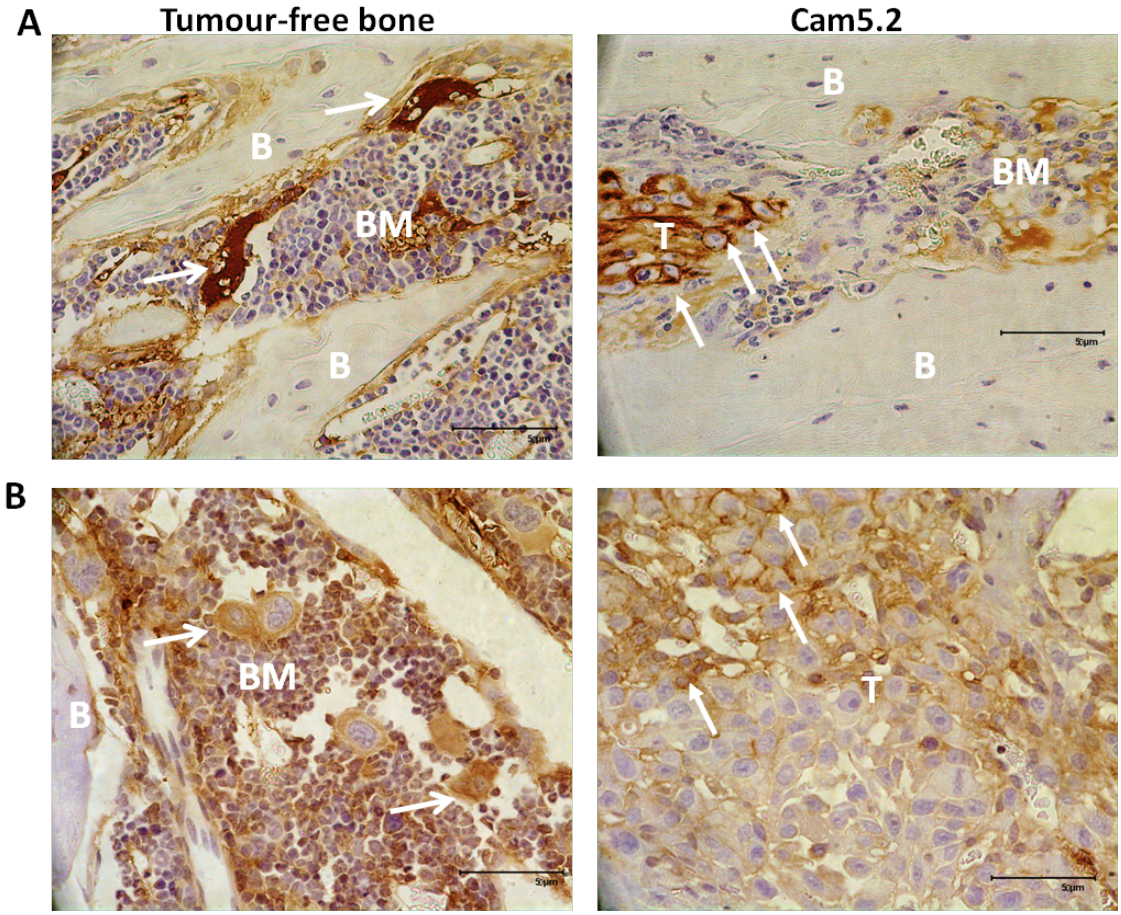

Figure 3.7 Cam5.2 staining of osseous bone tumours
A) B02 tumour bearing sections were stained for Cam5.2 using an automated stainer. B) Cam5.2 staining on MDA-MB-231 cells in bone using a manual staining procedure (primary antibody at 1:2). Tumour-free bone sections were used to test for staining of bone cells. T=tumour, BM=bone marrow, B=bone, open arrowhead=background staining in tumour-free bone, solid arrowhead=positive tumour cells. Scale bar=50µm, 20x objective.

In conclusion, it was not possible to identify a specific immunohistochemical antigen for detection of breast cancer cells in mouse bone. Although histological detection of tumour colonies prior to day 10 is possible by morphology, the process is laborious and therefore too time consuming for routine use.

3.4.2.1.3 Assessment of multiphoton microscopy for the detection of single tumour cells

The use of GFP transfected breast tumour cells is an invaluable tool to identify tumour colonies within any chosen model system. However, 2-D analysis of a 3-D object may not provide the best possible data in respect to the location of single cells or colonies to bone surfaces. Multiphoton microscopy is able to by-pass this problem as it allows visualisation of bone specimens up to a depth of 500µm in a 3-D manner. The technique is therefore useful for detection of small tumour colonies and single tumour cells within the bone marrow cavity.

Appropriately processed bone specimens (Materials and Methods section 2.2.9.3.3) were imaged using a Multiphoton Confocal Microscope (Zeiss LSM510 NLO Inverted). Tile scans of the metaphysis area were performed using the multiphoton chameleon laser at 900nm to detect collagen by second harmonic generation and GFP. Multiphoton images of a sample known to carry a GFP positive tumour in the femur is depicted in Figure 3.8A, demonstrating the detection of the GFP positive colony. Some samples obtained from experiments investigating early stages of tumour growth were analysed using the same protocol in order to assess the detection of single tumour cells. Areas showing GFP positive objects were chosen to perform z-stack scans for further analysis. The detection of single GFP-positive tumour cells (identified by size, Fig. 3.8B) and a green object, which was characterised as background staining is shown in Figure 3.8C. Sample processing may cause debris, which can be picked up by the laser and therefore give false positive results. In conclusion, the method of using the multiphoton microscope as a mean to identify single tumour cells in bone is possible, however, the method cannot be used to analyse the cells of the microenvironment. In addition, a large amount of the sample is lost during processing and re-use of the imaged bone is not possible.

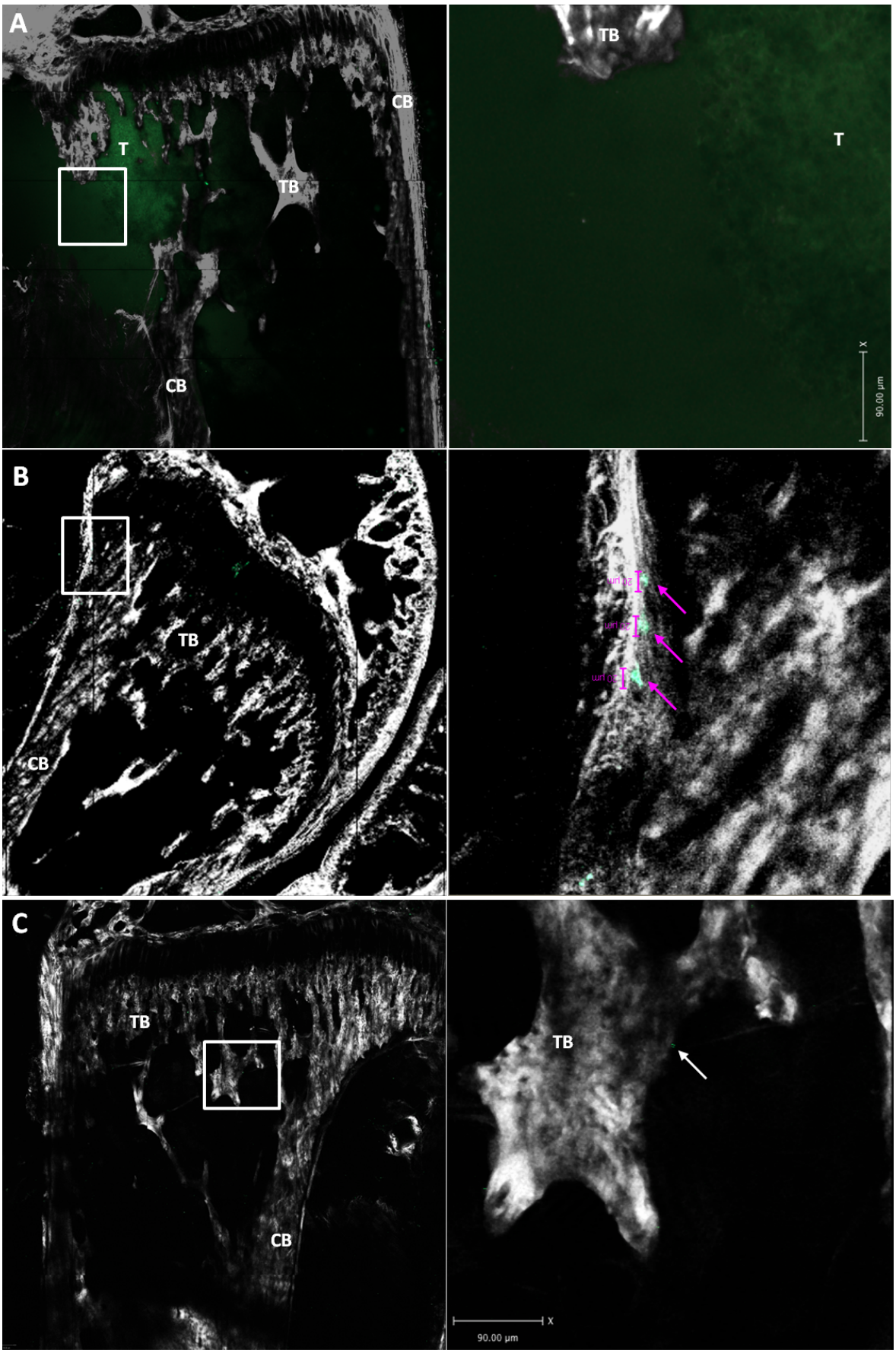
A
CB
T
TB
CB
TB
T
90.00 µm
B
TB
CB
C
TB
CB
TB
90.00 µm

Figure 3.8 Multiphoton images of B02 tumour cells in bone (page 105)
A) Tumour-bearing femur, B) femur with GFP positive tumour cells (arrows, 20µm scale bars) and C) tibia without detectable tumour growth (green object indicated by white arrow is too small). White-grey: bone, visualised by second harmonic generation; green: GFP, TB=trabecular bone, CB=cortical bone, T=tumour.

3.4.3 Optimisation of bone cell analysis

One aim of the histological analysis in this PhD project was to analyse the effect of tumour presence and anti-cancer therapy on the bone microenvironment, in particular the osteoclast and osteoblast populations. Most studies carried out in our unit have so far either analysed non-tumour bearing bones or samples with large tumours filling most of the marrow cavity. Since initial analysis of H&E stained samples showed that most tumours around 15 days post tumour cell injection are localised around trabecular spicules, it was decided to focus on this area for bone cell analysis, and cortical bone surfaces were excluded. It was necessary to address a number of questions prior to scoring the study material.

- Which parameters should be set for analysis of osteoclast and osteoblast identification? Due to the lack of published studies investigating osteoblasts in tumour bearing bones (Table 3.2), a set of criteria was established for identification of osteoblasts and osteoclasts.
- Is the distribution of bone cells along the trabecular bone surface even and do numbers differ between tibia and femur?
- Does tumour size vary between tibia and femur? It was necessary to establish whether tumour growth was predominantly in one part of the long bone to determine if the tibia, the femur or both should be analysed.

3.4.3.1 Criteria for osteoblast and osteoclast identification

Bone histomorphometry and analysis of bone cells has been performed frequently and guidelines and nomenclature have been published by Parfitt et al. (1988). Tartrate-resistant acid phosphatase (TRAP) staining of histological sections enables the identification of osteoclasts as TRAP positive cells in direct contact with bone surfaces (Fig. 3.9). The identification of osteoblasts is, however, more difficult. The use of undecalcified, plastic (methyl-methacrylate) embedded sections stained for Goldner's trichrome is often used for the detection of osteoid and thus the cells adjacent to the matrix are identified as osteoblasts. A downside of the plastic embedded sections is the loss of immunereactivity for immunohistochemical procedures. Because I wanted to be able to perform several staining procedures on the histological material obtained from the *in vivo* studies, all bone samples were decalcified and paraffin embedded. The Mellanby Centre for Bone Research at the University of Sheffield has long standing expertise in histomorphometric analysis and within the centre, osteoblasts are commonly identified by their distinct morphological features on TRAP or H&E stained sections (Corey et al., 2003; Deleu et al., 2009; Heath et al., 2009; Chantry et al., 2010; Mohanty et al., 2010). I therefore received detailed training by experienced staff members of the Mellanby Centre. Figure 3.9 gives an overview over criteria used for bone cell identification and example images of cells identified as osteoblasts and osteoclasts covering all animal ages used in this PhD thesis.

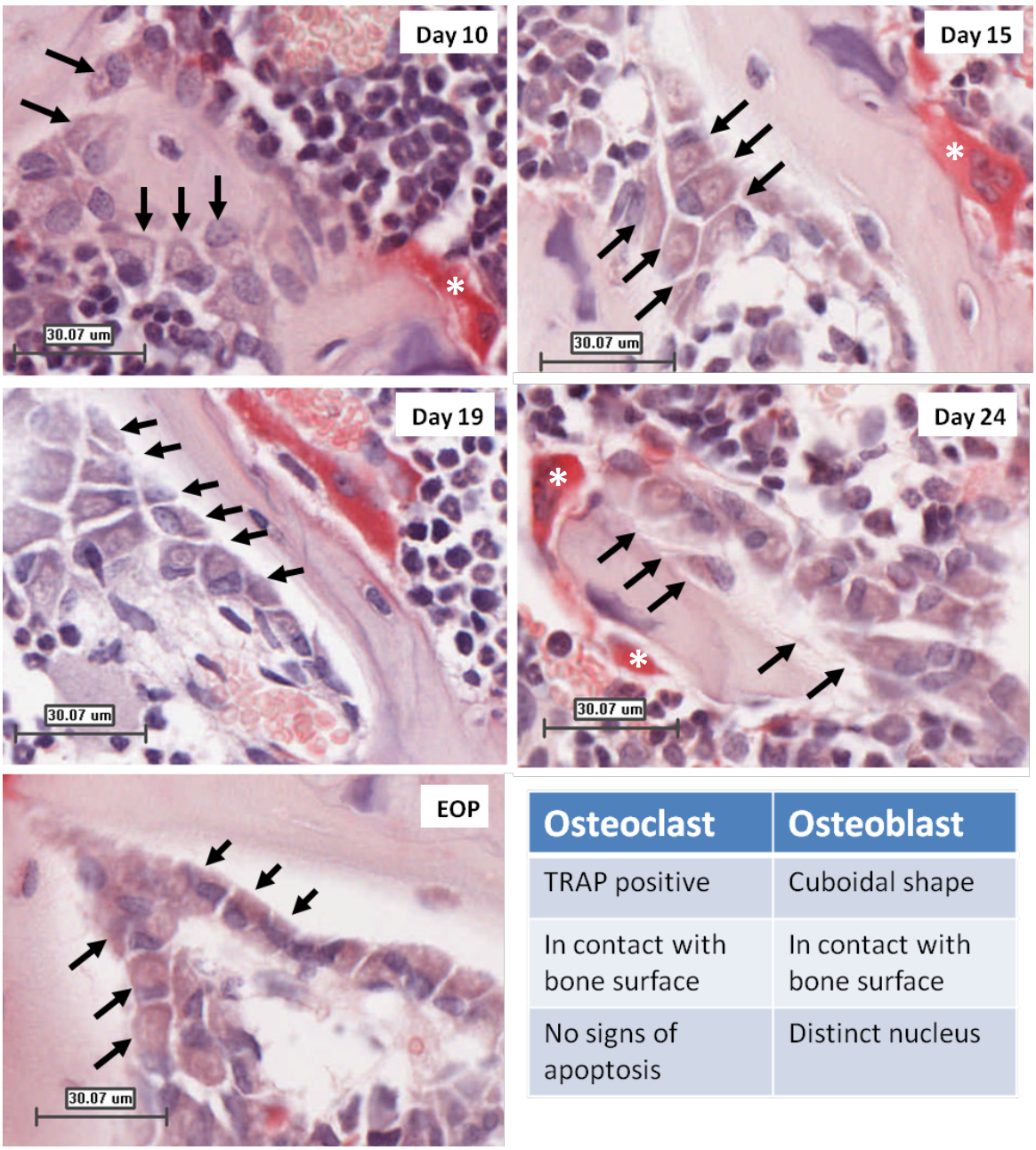

Figure 3.9 Guide for identification of osteoblasts and osteoclasts
Images depict TRAP stained sections taken from paraffin embedded mouse hind legs. Osteoclasts are stained red (white star). Arrows indicate cuboidal osteoblasts on trabecular bone. Mice were 6-7 weeks of age at beginning of the experiment and samples were collected at on the day indicated in each image. EOP = end of procedure = day 28-33.

3.4.3.2 Identification of bone area used for osteoblast and osteoclast analysis

In order to assess bone cell numbers reproducibly, analysis of osteoclasts and osteoblasts on trabecular bone from tumour free (naïve) animals sacrificed at day 10, 15, 19, 24 and 33 post start of the experiment (Chapter 4) was initially carried out by two methods: 1) using a predefined area of the metaphysis of long bones and 2)

scoring all trabecular bone surfaces (Fig. 3.10A). The comparison of the osteoblast to osteoclast ratio (Ob/Oc) obtained from naïve samples using the pre-defined area compared to the entire trabecular bone did not show a significant difference at any time point (Fig. 3.10B), indicating that bone cells in a naïve setting are evenly distributed along trabecular bone surfaces. More detailed analysis of osteoblast and osteoclast numbers per mm trabecular bone surface by both methods showed that osteoblast numbers were unchanged but osteoclast numbers were increased in the pre-defined area compared to the total trabecular bone surface. This suggests that the density of osteoclasts in this particular area of the metaphysis is higher compared to a setting in which all trabecular bone surfaces are taken into account.

When I later assessed bone cell numbers in tumour bearing samples it was noticed that the tumour and surrounding bone were often located outside the pre-defined section due to highly variable location of the tumour within the metaphysis. Since one of the aims of Chapter 4 was to assess the tumour-induced changes on the microenvironment it was important to analyse areas of bone that were in close proximity to a tumour colony. A better representation of bone cell numbers in tumour bearing versus naïve samples was therefore given when analysing the entire trabecular bone surface (Fig. 3.11).

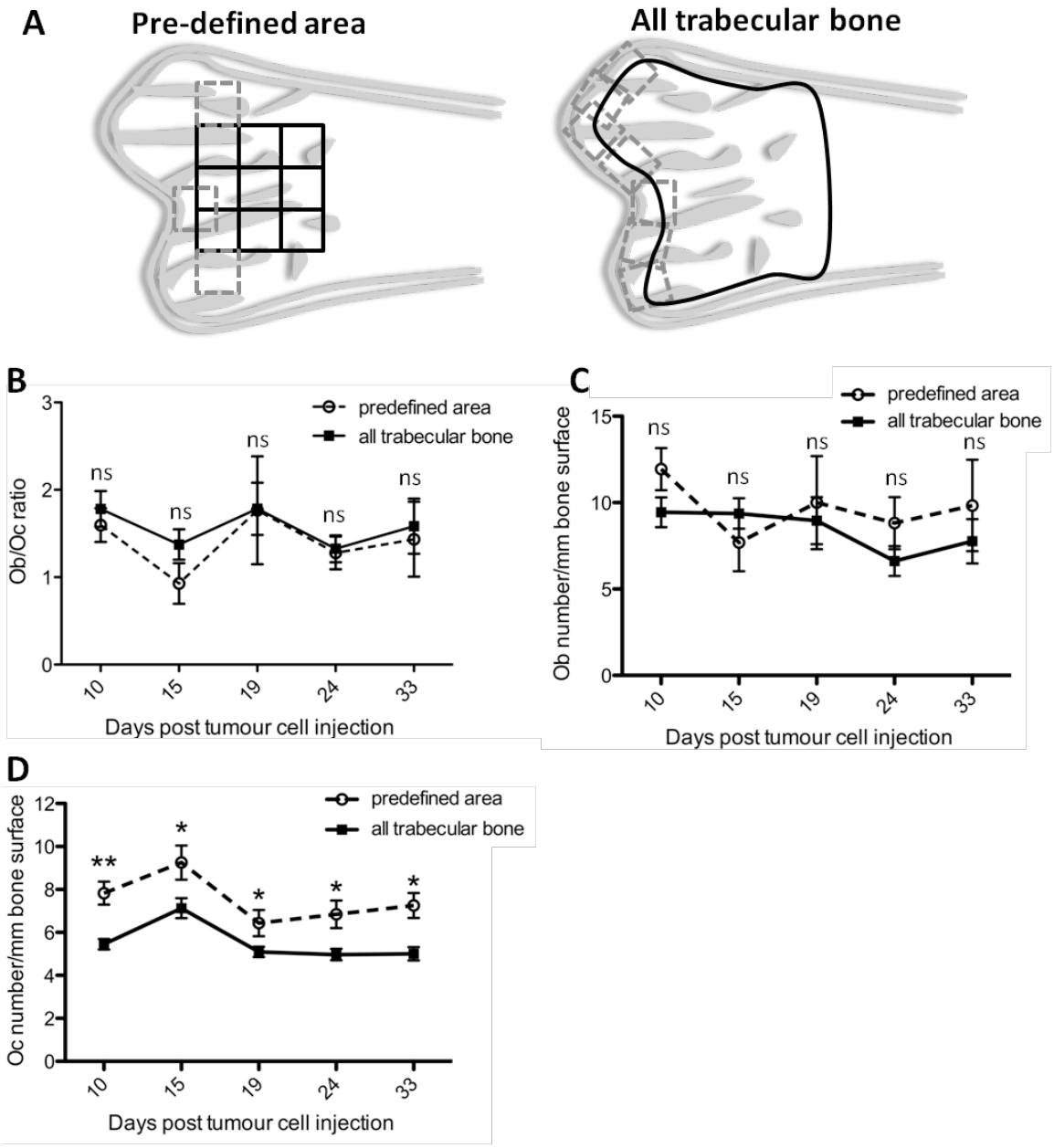

Figure 3.10 Comparison of analysis of a predefined area of trabecular bone compared to all trabecular bone surfaces in samples from naïve mice

A) Schematic overview of the analysed areas in a predefined area (3x3 squares of 250µmx250µm, 125µm away from the growth plate and 250µm away from cortical surfaces) and the whole trabecular bone area (all trabecular bone surfaces were scored except bone closer to the growth plate than 125µm). B) Quantitative analysis of Ob/Oc ratio, C) Ob number/mm bone surface and D) Oc number/mm bone surface in both settings. Two non-serial sections of 2 tibias and 2 femurs (n=2 tumour-free mice) were scored per time point. T-test for each time point separately, ** is $p<0.01$, * is $p<0.05$, ns=not significant.

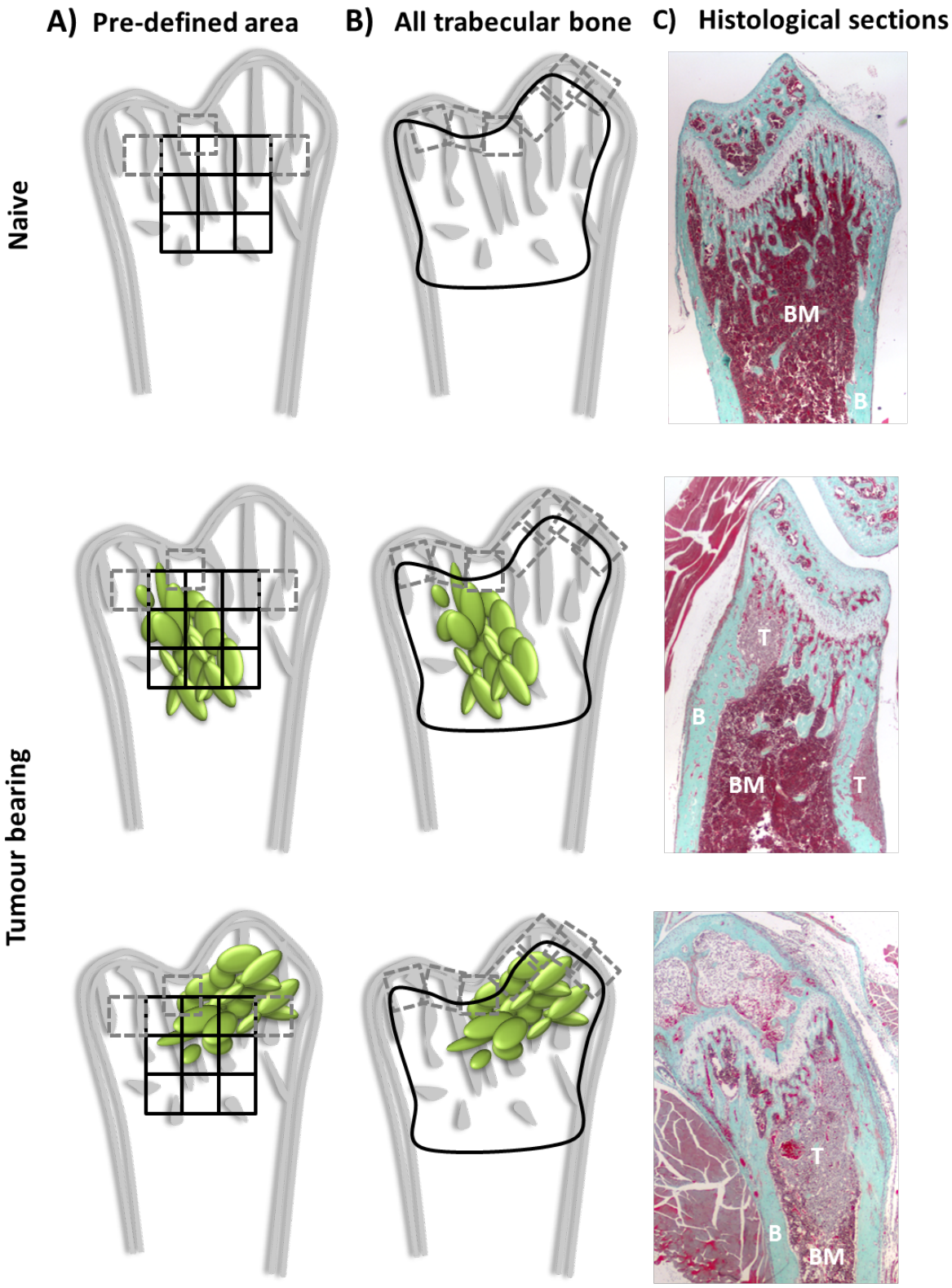

Figure 3.11 Comparison of trabecular bone areas in naïve and tumour bearing mice

A) Predefined area (3x3 squares of 250µmx250µm, 125µm away from the growth plate and 250µm away from cortical surfaces) in a naïve situation and examples of MDA-MB-231-GFP tumour bearing bones. B) Inclusion of all trabecular bone surfaces in naïve and tumour bearing mice represents the entire area of bone in contact and not in contact with tumour. C) Histological examples stained for Goldner's trichrome. From top to bottom: femur, tibia, femur. T=tumour, B=bone, BM=bone marrow, 1.6x objective.

3.4.3.3 Investigation of predilection of tumour growth between tibia and femur

I furthermore assessed whether the model used in the present study had a preference for a specific site within the long bone. The size of the tumour colonies in tibia or femur did not differ in bones taken 10 or 33 days after intracardiac tumour cell injection (Chapter 4), suggesting that both sites were equally susceptible to tumour growth (Fig. 3.12A). Furthermore, assessment in trabecular bone cell number in tibias and femurs showed no significant difference when comparing the two sites (Fig. 3.12B). It was therefore decided to use the entire trabeculum in both the femur and tibia for the entire thesis, increasing sample size considerably.

Based on these results I decided to use the tibia and femur as well as the whole trabecular area for scoring of bone cell numbers in the studies described in Chapters 4 and 5.

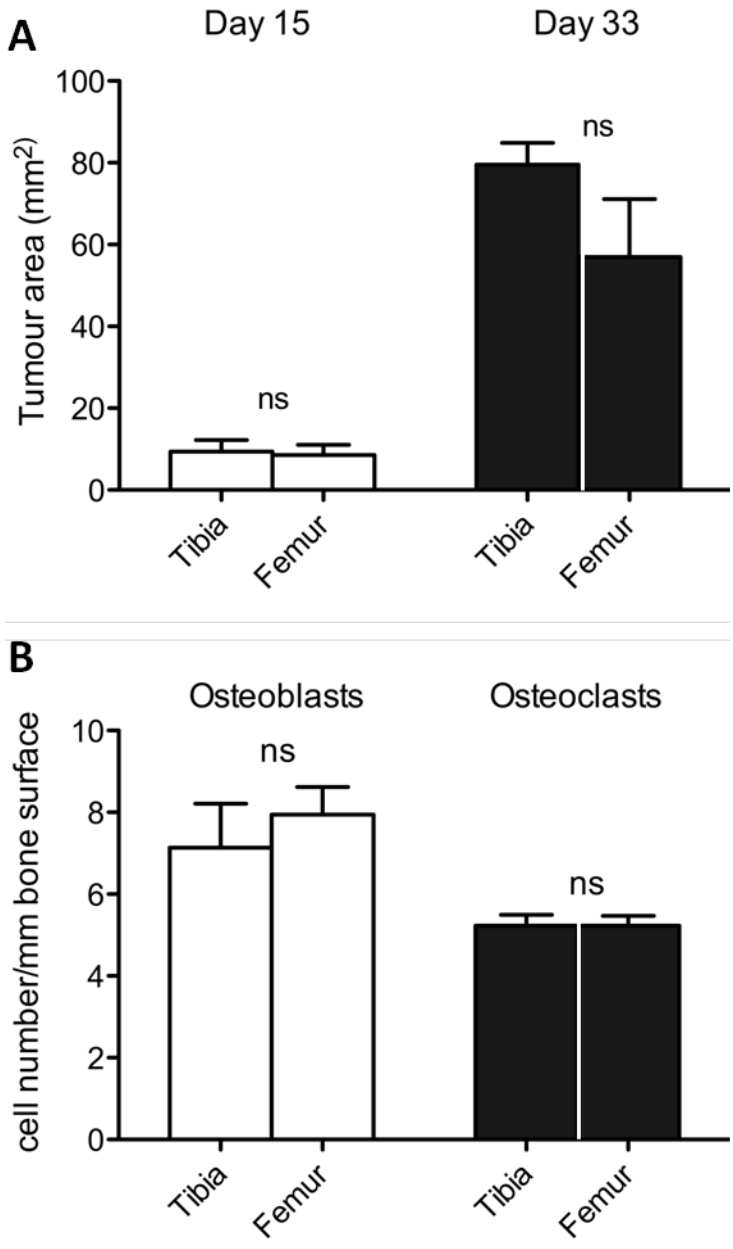

Figure 3.12 Distribution of tumour colonies and bone cell numbers in tibia and femur

A) Tumour area was scored in H&E stained sections in tibias and femurs of animals sacrificed 10 or 33 days after MDA-MB-231-GFP tumour cell injection. B) Osteoblasts and osteoclasts were scored in tumour-free tibias and femurs (n=5). T-test, ns=not significant ($p>0.05$).

3.5 Discussion

This chapter described the establishment of two *in vivo* models of human breast cancer metastases to bone and the optimisation of histological processing and analysis methods used in this PhD study.

The ideal preclinical model of breast cancer metastases to bone would mimic shedding of cancer cells from a primary tumour, vascular invasion and spread to metastatic sites, followed by microenvironment-dependent proliferation and finally independent tumour growth. Many *in vivo* models are able to reproduce parts of these processes but at present, there is no single model of breast cancer metastases that is able to mimic the entire human disease process. Despite this, the preclinical models are irreplaceable for studies aiming to unravel the steps involved in induction of metastatic tumour growth and progression as well as the mechanisms of action and efficacy of therapies. Spontaneous tumour models such as the PyMT mouse model involve the development of spontaneous mammary tumours and have been shown to lead to secondary tumour growth at skeletal and visceral sites. However, spontaneous preclinical systems as well as the 4T1 model (syngeneic mouse model where 4T1 cells are injected into mammy fat pads which will develop secondary disease at sites including bone) may require the removal of the primary tumour, bone metastases are infrequent and experiments are lengthy (several months). In the present study a model of bone metastases was required, with the possibility to detect osseous tumour growth as well as having a reasonable time frame between tumour cell injection and the end stage of the disease (approximately 4 weeks).

Initial experiments were therefore carried out using the B02 model, in which the cancer cells are introduced into the circulation via the lateral tail artery and osseous tumour growth can be detected approximately 15 days post cell implantation (Peyruchaud et al., 2001). When reproducing the protocol used in a published study by Ottewell et al. (2008a) and using the available cell batch, members of the laboratory and me were not able to induce osseous tumour growth. In addition, several changes to the protocol did not lead to tumour growth in bone. In a final experiment that was carried out after a visit to Galapagos SASU and in which the company's protocol was followed stringently; a 90% tumour take rate was achieved. It is not possible to pinpoint the reasons for the lack of tumour growth on any of the investigated factors.

Another possibility for the inability of some cell batches to form osseous tumours could be a change in gene expression possibly taking place during *in vitro* culturing. A study carried out by Garcia et al. (2008) compared the *in vitro* transcriptome of the bone seeking B02 cells to the parental MDA-MB-231 cells. The group showed that B02 cells had 114 upregulated and 247 downregulated genes compared to the parental cells line, underlining the changes acquired during *in vivo* passaging. Although gene expression analysis of the B02 cell batches used in the present PhD thesis may have helped to explain the inability of some cell batches to form tumours, this was not within the scope of this PhD project and was therefore not performed.

Despite having successfully optimised the B02 model, I have carried out all *in vivo* experiments presented in this PhD thesis using the intracardiac model (MDA-MB-231-GFP cells injected i.c.). Disadvantages of both models are that the high cell number injected into the vasculature does not reflect the metastatic process; the models therefore only allow investigation of the later steps of metastasis. Moreover, young mice (around 6 weeks of age) are commonly used in the described models Peyruchaud et al., 2001; Garcia et al., 2008; Ottewell et al., 2008a). At this age, active bone turnover takes place in the metaphyses of the long bones, which is the main site of tumour growth in this model. The active bone remodelling and blood flow characteristics in these areas could possibly determine the sites as preferential for experimental tumour cell homing. Homing of cancer cells to metastatic niches is an area of active research and the presence of metastatic niches has been suggested, including the vascular and the osteoblastic niche. A recent report showed that HSPCs (hematopoietic stem/progenitor cells) homed preferentially to the metaphsyseal region post injection and it was proposed that the cells are localised within an endosteal niche. The niche was further characterised as being in close proximity to trabecular bone and the associated vasculature (Ellis et al., 2011). It may therefore be possible that the endothelium, as well as other cells within the trabeculum, express specific molecules involved in tumour cell adhesion, supporting the initial steps of tumour cell homing to bone. The requirement of young animals may be due to an increased repertoire in the factors present in a metastatic niche.

There is strong evidence that cells of the tumour microenvironment, including tissue specific cells, stromal cells, vasculature and immune cells, play an important role in

tumour growth. One aim of my PhD thesis was to determine the effect of tumour growth in bone following therapeutic targeting of the bone microenvironment. In the first *in vivo* experiments using the intracardiac route (Chapter 4), the presence of small tumour colonies (GFP areas <1mm in diameter) was frequent. The analysis of these colonies required a specific series of steps (comprehensive GFP imaging, embedding, sectioning and examination of H&E test slides) to detect the tumour cells on subsequent histological sections. Moreover, it was determined that the initiating steps of tumour growth in bone (<10 days post tumour cell injection) were difficult to investigate without a specific marker for tumour cell identification. GFP (MDA-MB-231-GFP and B02), β-galactosidase (B02 only) and cytokeratin staining were therefore used to investigate their specificity and reliability in detecting tumour cells on histological bone sections. While β-Gal was found to detect tumour cells reliably problems with the detection of single cells can arise because of the endogenous β-Gal expression found in bone (Kopp et al., 2007). It is possible that the GFP and β-Gal expression is more reliable in early tumour growth studies than in the large tumours used for optimisation of the technique but the background staining for each maker is a concern. Although multiphoton microscopy is a valuable tool to investigate a three-dimensional relation between tumour cells and the surrounding bone matrix, the usefulness of the technique is limited as it relies on fluorescent markers for detection of the cell/tissue of interest. In this respect it was decided that the method would not provide additional information to that obtained by histology when assessing the tumour-induced changes to the bone microenvironment.

One aim of this thesis was to investigate the effects of different tumour sizes and therapy on bone cells and thus a method for comprehensive analysis of these areas was required. The preferred method was found to include the analysis of all trabecular bone surfaces in tibias and fermurs due to the high variability in tumour location within the metaphysis. Furthermore, very limited published data are available on the quantification of osteoblasts in solid tumour bearing bones and the analysis methods in the few studies assessing changes in osteoblasts have used different techniques (Corey et al., 2003; Phadke et al., 2006). Table 3.2 gives an insight into the variability and lack of consistency between published studies in the same field, making comparison of the results very difficult. Groups within the Mellanby Centre of Bone

Research at the University of Sheffield (Deleu et al., 2009; Heath et al., 2009; Chantry et al., 2010; Mohanty et al., 2010) have carried out osteoblast analysis predominantly in multiple myeloma bearing animals and I have successfully optimised the existing criteria for use in osseous breast cancer growth in nude mice.

In summary, although the optimisation of the B02 model was successful after multiple attempts, the intracardiac model of MDA-MB-231-GFP tumour growth in bone was taken forward for the rest of this study due to time constraints. In addition, a workflow for the identification of small tumour colonies in bone was established and analysis of bone cells was optimised. The work described in this Chapter supports the subsequent studies, ensuring consistent, reproducible assessment of tumour growth and the associated bone disease.

4. Location matters – osteoblast and osteoclast distribution is modified by the presence and proximity to breast cancer cells *in vivo*

4.1 Summary

Bone metastasis is a common complication of advanced breast cancer and remains incurable. Improvement of therapies relies on increased understanding of the cellular and molecular mechanisms underlying bone metastasis formation. However, the majority of preclinical studies have focused on end-stage disease and little is known about the events taking place following initial colonisation of bone.

I performed a longitudinal study with 5 time points to characterise osseous tumour progression and the effects on bone integrity following intracardiac inoculation of MDA-MB-231-GFP breast cancer cells in immunocompromised mice. Comprehensive analysis of the number and distribution of osteoclasts and osteoblasts were performed, differentiating between areas in direct contact with the tumour and areas distal (not in direct contact with the tumour but within the same bone compartment) to the cancer cells. Tumour colonies in bone were detected from day 10 while reduced trabecular bone volume was apparent from day 19 onwards. Compared to that of naïve control animals, areas of bone in direct contact with the tumour had significantly reduced osteoblast but increased osteoclast numbers. Conversely, in areas away from the tumour, numbers of osteoblasts were increased and osteoclast levels remained comparable to those of naïve mice. Analysis of systemic changes in serum bone turnover markers (PINP, CTX), RANKL, sclerostin, IL-1, IL-6, KC (murine IL-8) and MCP-1 levels were in line with the observation that changes to the bone microenvironment where spatially confined to the tumour bearing bone. This is the first longitudinal study reporting the detailed spatial and temporal relationship between bone and cancer cells. These data reveal that the dynamic between cancer cells and bone cells is more complex than previously described, and suggest that therapeutic targeting of the early steps in this process may be required to eradicate bone metastasis.

4.2 Introduction

Bone metastasis is a frequent feature of late stage breast cancer and currently patients mainly receive palliative treatment, as the disease is considered incurable. In breast cancer, bone metastases are associated with lytic bone lesions caused by tumour cells disrupting the fine-tuned balance between bone resorption (mediated by osteoclasts) and bone formation (mediated by osteoblasts) that exists during normal bone turnover (Mundy et al., 1997). The resulting osteolytic lesions are the main cause of morbidity and mortality and are a major clinical feature in this group of patients. Understanding the underlying cellular and molecular mechanisms throughout tumour progression in bone is key to the development of new and improved treatment strategies. To date, most studies have focused on end stage disease, with only little information on how and when small but established breast cancer colonies induce changes in bone cell number and distribution, ultimately leading to overt bone destruction. For example, Clohisy et al. (1996) reported that intrafemoral injection of MDA-MB-231 human breast cancer cells into balb/c nu/nu mice resulted in osteolytic bone disease, and a significant increase in osteoclast number, compared to sham-injected femurs after 7-10 weeks.

It is currently not possible to predict which patients will relapse after their initial treatment and subsequently develop bone metastases. Due to the lack of biological markers that can be applied in routine diagnosis, bone metastases are detected once the tumour is established. Although there are effective therapies available to treat the resulting cancer-induced bone disease, it is currently not possible to prevent the development of bone metastases. The standard approved therapy for tumour-induced osteolysis is zoledronic acid, a nitrogen-containing bisphosphonate (NBP). The drug acts by reducing osteoclast activity via inhibition of the mevalonate pathway thus counteracting the osteolytic effects induced by the tumour (van Beek et al., 1999; Coxon et al., 2000; Dunford et al., 2001). In addition, NBPs have been shown to exhibit direct and/or indirect anti-cancer effects both in *in vitro* (Fromigue et al., 2000) and in *in vivo* studies (Sasaki et al., 1995; Yoneda et al., 2000; Hiraga et al., 2004). Despite the strong bone-sparing effects demonstrated in several *in vivo* studies, use of NBPs alone is not sufficient to eradicate tumour growth in bone in models of multiple myeloma (Croucher et al., 2003), breast cancer (Michigami et al., 2002; van der Pluijm et al.,

2005; Daubine et al., 2007) or prostate cancer (Corey et al., 2003). In order to develop successful therapeutic strategies for prevention of bone metastasis, a better understanding of the early stages of secondary tumour growth in bone is required. In particular, the initiating stages of the interaction between cancer cells and bone cells, prior to the reduction of trabecular bone and the formation of osteolytic lesions, are of interest. Analysis of these events is largely limited to the study reported by Phadke and colleagues (Phadke et al., 2006), showing that the presence of cancer cells in bone results in reduced overall numbers of both osteoblasts and osteoclasts 4 weeks following intracardiac tumour cell implantation, but not at earlier time points. To my knowledge, no comprehensive histological analysis has been carried out charting changes in osteoblast and osteoclast numbers associated with breast tumour progression in bone. I have performed a detailed study of the spatial and temporal changes of both tumour cells and bone cells, including time points prior to the appearance of osteolytic bone disease. The development of human breast cancer growth and the resulting cancer-induced bone disease from early (day 10 and 15), intermediate (day 19 and 24) to late (day 28-33) stage disease was characterised and changes in bone cell numbers were determined in detail. The new information presented in this chapter gives insight into the early interactions between tumour cells and the bone microenvironment and may have implications for treatment optimisation, in particular when to initiate therapy.

4.3 Aims

In order to investigate the longitudinal tumour-induced changes on the bone-microenvironment and the bone matrix, the following research questions were asked:

- Can MDA-MB-231-GFP growth in the hind legs of mice be characterised regarding location and viability of the tumour tissue? At which time point can the first tumour foci be readily detected and analysed in bone?
- At which point does the osseous tumour cause measurable bone disease and can peripheral tumours cause osteolysis? Is there a systemic effect of breast tumour growth on bone?
- Does the osseous tumour colony induce changes to osteoblast and osteoclast numbers and are the changes dependent on tumour cell contact?
- Does the tumour colony induce changes to systemic markers of bone remodelling and/or cytokines involved in osteoclast activity?
- Do changes of bone related gene expression by the tumour occur depending on the site of tumour growth *in vivo*?
- Does the presence of breast cancer at a peripheral site induce similar effects on bone (bone integrity, serum cytokines, tumour gene expression) or are the osseous effects defined to tumour growth inside bone?

4.4 Materials and methods

Detailed information can be found in the main Materials and Methods Chapter 2.

4.4.1 Tumour models and study protocols

All experiments were carried out in accordance with local guidelines and with Home Office approval under project license 40/2972 held by Professor N.J. Brown, University of Sheffield, United Kingdom.

In order to generate bone tumours, MDA-MB-231-GFP cells ($1x10^5$) were injected directly into the left heart ventricle of 6-week-old female balb/c nu/nu mice under general anaesthesia (56.5mg/kg ketamine, 5.5mg/kg xylazine, in H_2O). Animals were randomly grouped into each of the 5 sequential time points (n=12 + 5 naïve/time point) covering early (day 10 and 15), intermediate (day 19 and 24) and late stage disease (end of protocol (EOP) including days 28-33). The range of days in the last time point was due to Project License regulations stipulating sacrifice at first signs of morbidity (Fig. 4.1A). Only animals with detectable bone tumours were entered into subsequent analysis. On the day of sacrifice, food supply was removed for 6 hours and blood was collected by intracardiac puncture under deep non-recovery anaesthesia. Serum was stored at -80˚C and hind legs were fixed in 4% PFA for 72 hours and scanned by µCT. Subsequently, the bones were decalcified before embedding in paraffin wax.

In the subcutaneous tumour study, MDA-MB-231-GFP cells ($5x10^5$) were injected into the right flank of female balb/c nude mice (6 weeks). Tumour bearing mice (n=3 per time point) and naïve mice (n=2 per time point) were sacrificed on days comparable to the bone experiment including days 15, 24 and 33 post tumour cell injection (Fig. 4.1B). On day of sacrifice, hind legs were fixed in 10% buffered formalin for subsequent µCT analysis, subcutaneous tumour tissue was excised, placed in RNA later and was stored together with the serum at -80˚C.

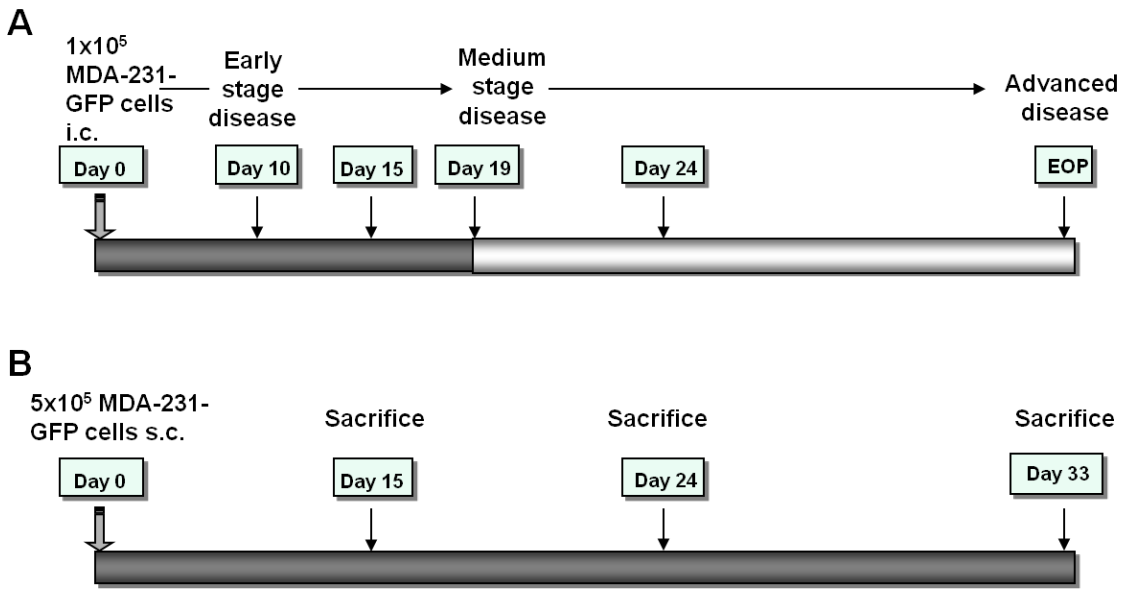

Figure 4.1 Study outline investigating bone associated tumour growth
A) Longitudinal study of bone associated tumour growth. Following i.c. inoculation of 1×10^5 MDA-MB-231-GFP tumour cells on day 0, animals were randomly divided into 5 groups to cover different stages of tumour progression at day 10, 15, 19, 24 and EOP (depending on morbidity including days 28-33). Twelve tumour-bearing and five naive animals were sacrificed per time point. B) Subcutaneous tumour growth experiment. Following s.c. injection of 5×10^5 MDA-MB-231-GFP tumour cells on day 0, animals were randomly divided into three groups to cover different stages of tumour progression comparable to the bone study at day 15, 24 and 33 (EOP). Three tumour-bearing and two naive animals were sacrificed per time point.

4.4.2 Measurement of tumour size

Histological sections (3µm) of decalcified hind legs were stained with H&E and analysis was carried out using a Leica BMRB upright microscope with a 4x objective and Osteomeasure software. Tumour area (expressed as % intraosseous tumour area of metaphyseal bone area) was measured by drawing around the inner surface of the bone marrow cavity in the metaphysis (defined as a maximum of 4x4 fields of view from the top of the growth plate towards the diaphysis) as well as the tumour area in this region. 2-3 non-serial histological sections per sample were scored.

For measurement of subcutaneous MDA-MB-231 tumours, the diameter was measured twice using callipers. Tumour volume was expressed as cm^3 by calculating the volume of a sphere using: $4/3 \times \pi \times r^3$.

4.4.3 Analysis of bone cells

To allow quantification of Ob (osteoblast) and Oc (osteoclast) numbers in the same sample, both cell types were scored on Tartrate-resistant acid phosphatase stained (TRAP, osteoclast specific) sections. The number of TRAP positive osteoclasts per millimetre trabecular bone surface was scored using a Leica RMRB upright microscope with a 10x objective and Osteomeasure software. In the same sections, osteoblasts (detected by morphology) were scored as described above. In detail, we analysed the following: a) total number of Oc and Ob per mm bone surface on the entire trabecular bone, b) the number of Oc and Ob per mm trabecular bone surface where the bone cells were in direct contact with tumour tissue (Category 1, Fig. 4.2) and c) the number of Oc and Ob per mm trabecular bone that were not in direct contact with tumour cells (Category 2, Fig. 4.2). At least two non-serial sections were analysed per sample. For naïve mice all trabecular bone surfaces were analysed for Ob and Oc numbers.

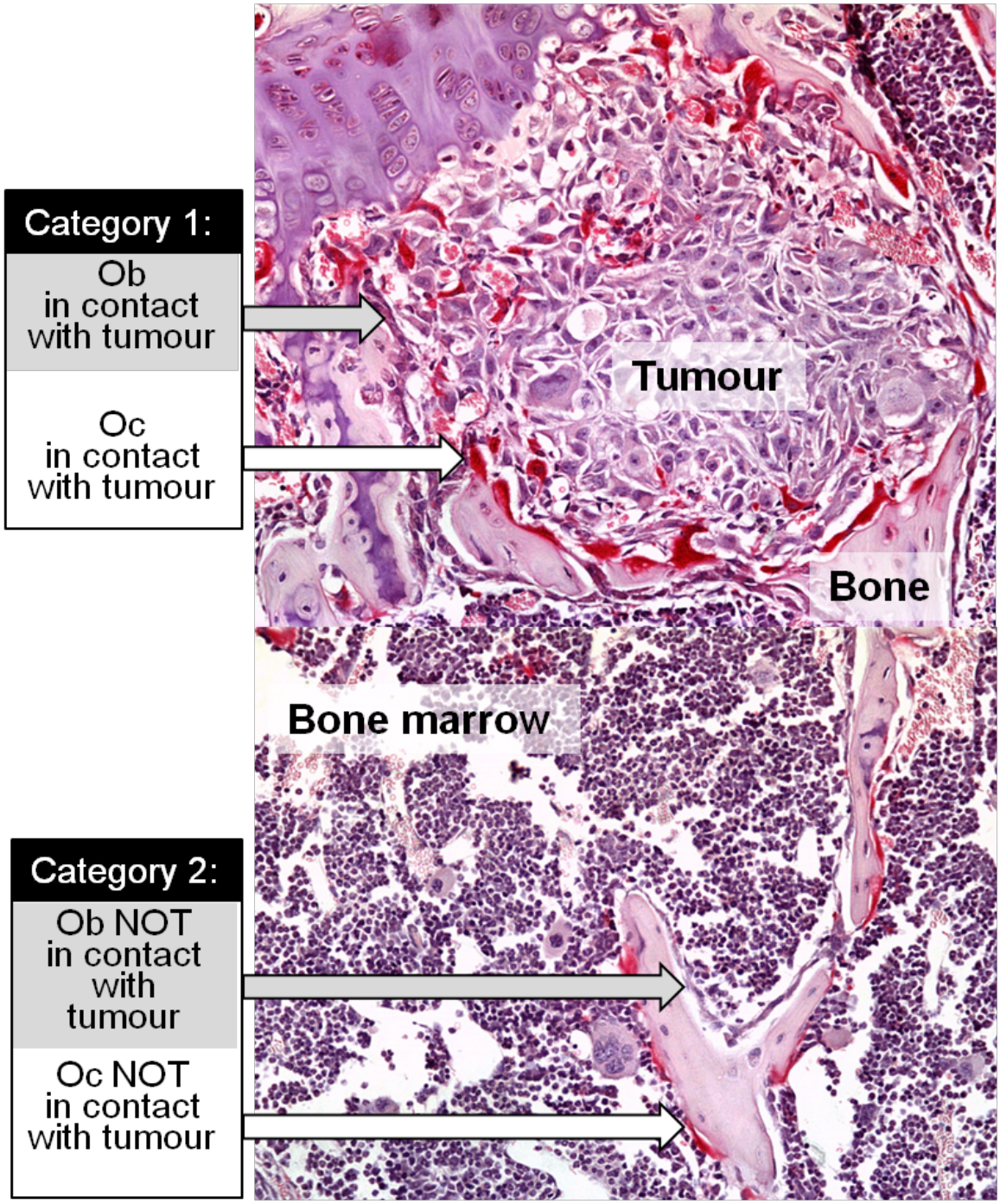

Figure 4.2 Schematic outline of location dependent analysis of bone cells
Example TRAP section showing an overview of the two location-dependent categories used for scoring of osteoclasts (Oc) and osteoblasts (Ob): category 1) Oc and Ob in direct contact with cancer cells and category 2) Oc and Ob not in direct contact with cancer cells but in the same bone compartment. Analysis was carried out on at least 2 non-serial TRAP stained sections from one bone.

4.4.4 Analysis of serum markers by ELISA and cytokine bead array (CBA)

A range of serum markers was used to analyse effects of osseous tumour growth. The murine bone remodelling markers CTX and PINP were measured as well as human sclerostin and mouse RANKL levels. Details on suppliers and methods can be found in the general Materials and Methods section 2.2.1.6. Serum was also used for CBA analysis of murine IL-1α, IL-1β, IL-6, KC (IL-8) and MCP-1. The CBA protocol was carried out by the Flow Cytometry Core Facility, University of Sheffield and to the manufacturer's instructions. The RANKL ELISA was performed by Mrs A Evans.

4.4.5 Quantitative real time PCR (qRT-PCR) analysis

Total RNA was extracted from *in vitro* and *in vivo* samples and cDNA was prepared as described earlier. qRT-PCR was performed on individual gene products using the ABI Prism 7900HT Sequence Detection System and FAM labelled probes (species specific TaqMan® assays, page 50).

4.4.6 Statistical analysis

Prism GraphPad (Version 5.0a) was used for all statistical analysis. Analysis was by Mann-Whitney or Kruskal-Wallis with Dunns post test. The applied test is indicated in each Figure legend. Data are presented as mean +/- SEM and have been interpreted differences as being significant at $p \leq 0.05$.

4.5 Results

I performed a comprehensive study of breast tumour growth in bone investigating tumour cell-bone cell interactions from early (day 10-15 following tumour cell injection) to intermediate (day 19 and 24) and end-stage disease (day 28-33=EOP, n=12 mice per time point). All time points included 5 naïve mice in order to compare tumour bearing to non-tumour bearing bone and to be able to distinguish between tumour-induced and age-related changes to the skeleton. A range of techniques was used to assess bone integrity, tumour area, bone-tumour cell interactions, and serum markers of bone turnover and cytokines at each time point. In addition to characterising the effects on osteoclasts, I focused on the analysis of osteoblasts due to the lack of information regarding their role in breast cancer-induced bone disease from *in vivo* studies. The subcutaneous *in vivo* experiment was set up in order to assess the effects of peripheral tumours on systemic bone turnover. In addition, the study allowed comparison between changes in systemic cytokine levels and gene expression in animals with tumour growth at different sites (*in vitro* compared to *in vivo,* including subcutaneous and bone). This results section will firstly focus on the analysis of osseous tumours, followed by the effect of subcutaneous tumour growth on bone and will close with the comparison in gene expression between tumours implanted at the two sites.

4.5.1 Determination of the spatial and temporal changes in bone remodelling during different stages of osseous breast cancer growth

4.5.1.1 Characterisation of osseous tumour burden

MDA-MB-231-GFP cell growth in long bones was identified by GFP imaging on day of sacrifice (Fig. 4.3A) and examples of tumour foci in bone are depicted on images of Goldner's trichrome stained sections (Fig. 4.3B). When analysing the distribution of breast tumour foci detected by GFP between femurs and tibias of tumour bearing mice, no preference between the two sites was apparent at any time point (Fig. 4.4). However, it appeared that the number of tumour positive tibias and femurs increased with time, as the percentage of tumour free bones was reduced from around 40% on day 10-19 to 8% at EOP. The data suggest that tumour cells seed to both the tibia and the femur but that initiation of tumour growth between the two sites is independent.

Quantification of tumour area in the metaphysis was performed on histological sections of tibias and femurs in which tumour growth had been confirmed by GFP. In specimens taken from day 10 to EOP, the percentage of the bone marrow cavity occupied by tumour tissue increased steadily with time (Fig. 4.5A). In order to investigate tumour viability at each point I performed Ki67 immunohistochemistry, which allows the quantification of actively proliferating cells (Fig. 4.5B). The number of Ki67 positive cells remained near constant throughout the different stages of tumour progression. It was not possible to perform comprehensive analysis on the day 10 tumours due to the limited tumour material available at this early time point.

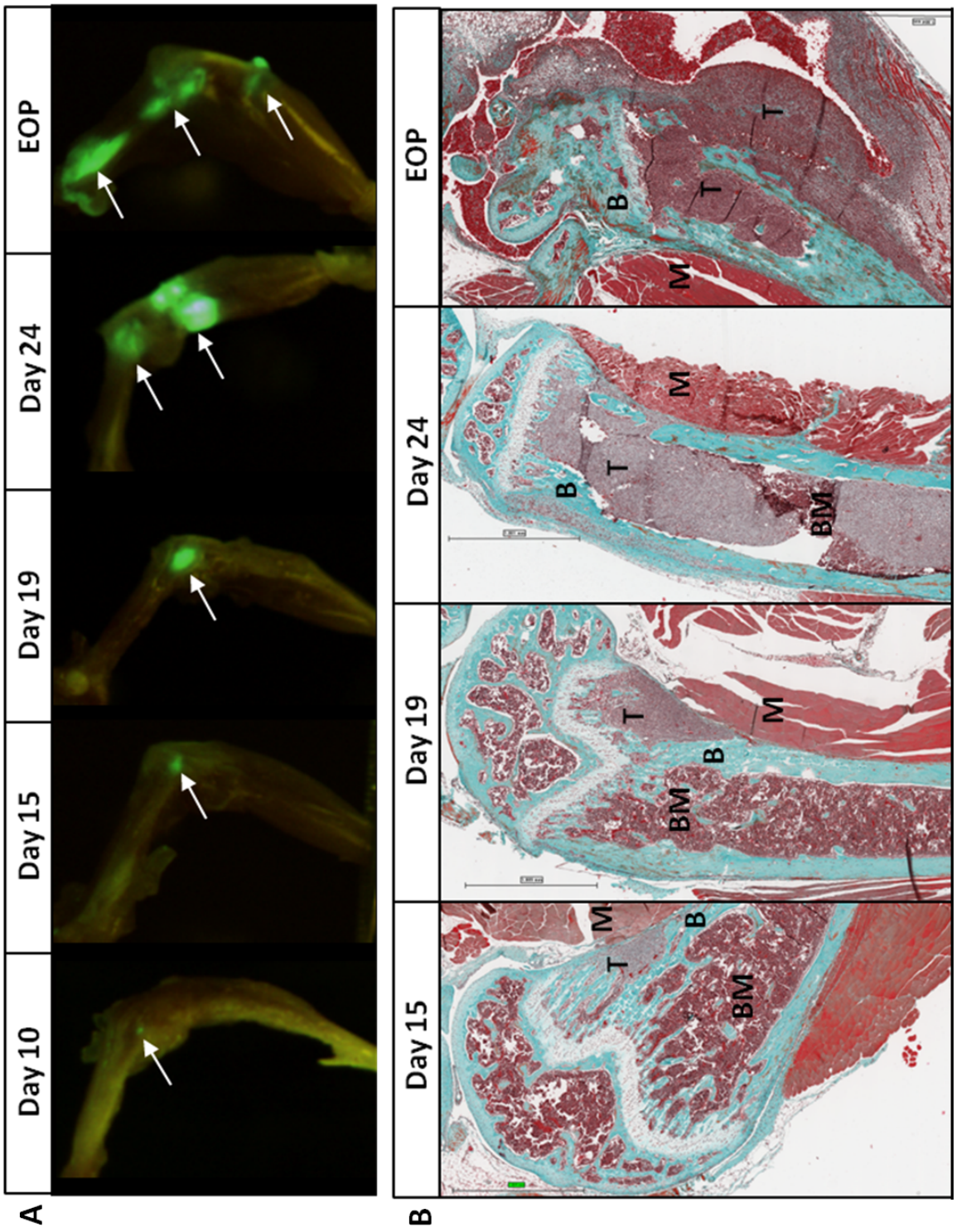

Figure 4.3 Imaging of longitudinal breast tumour growth in bone

A) *In vivo* GFP imaging of skin and muscle stripped hind legs confirmed tumour growth in all groups at day of sacrifice. Arrows indicate tumour foci (green). B) Visualisation of tumour growth in tibias and femurs for time points 15 to EOP by Goldner's trichrome stain. T=tumour, BM=bone marrow, B=bone, M=muscle, scale bar: 1mm.

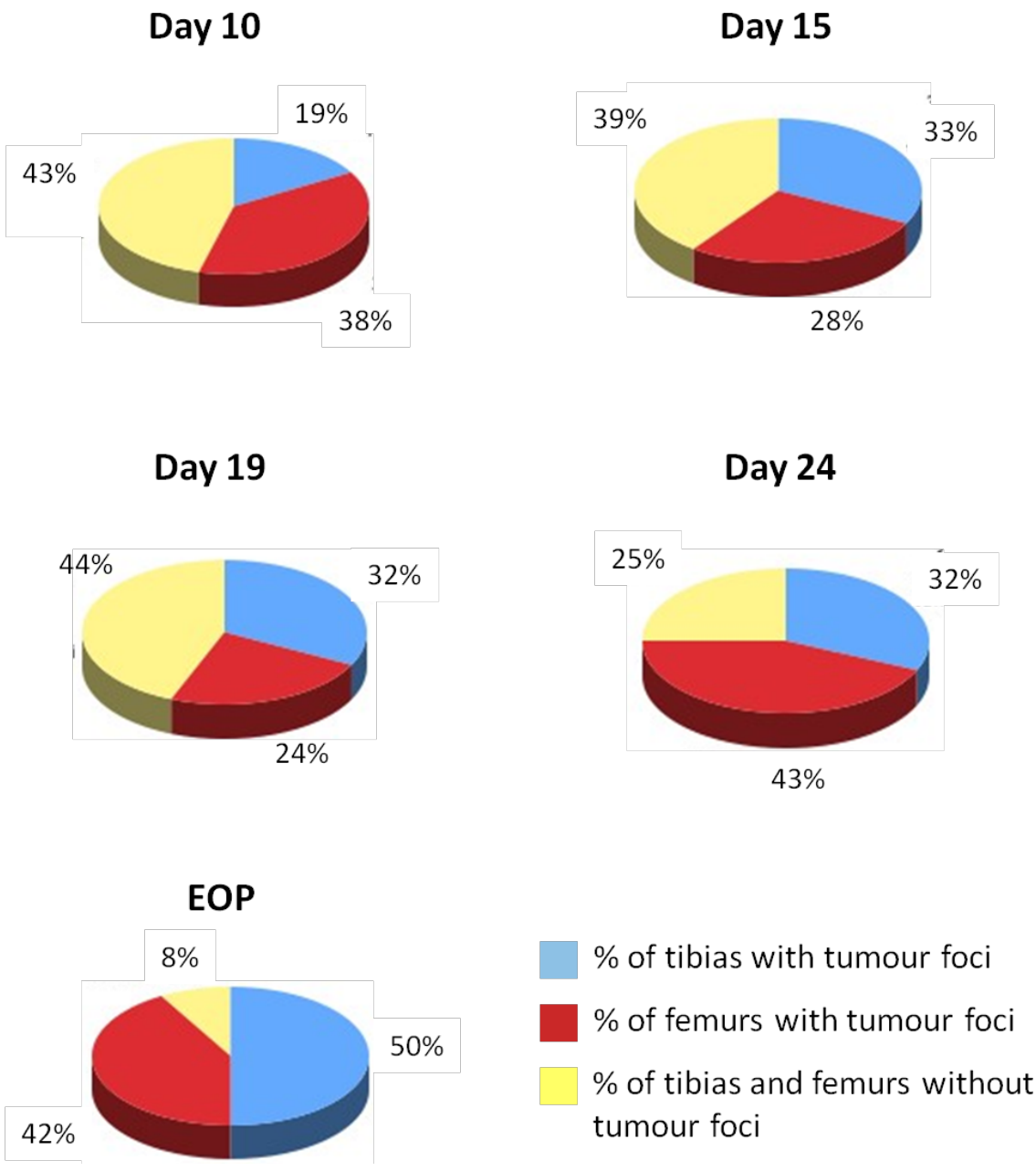

Figure 4.4 Distribution of tumour foci in tibias and femurs

GFP images taken at day of sacrifice were used to assess the percentage of tumour bearing bones (tibias or femurs). The data are expressed as the % of total tibias and femurs in tumour bearing long bones.

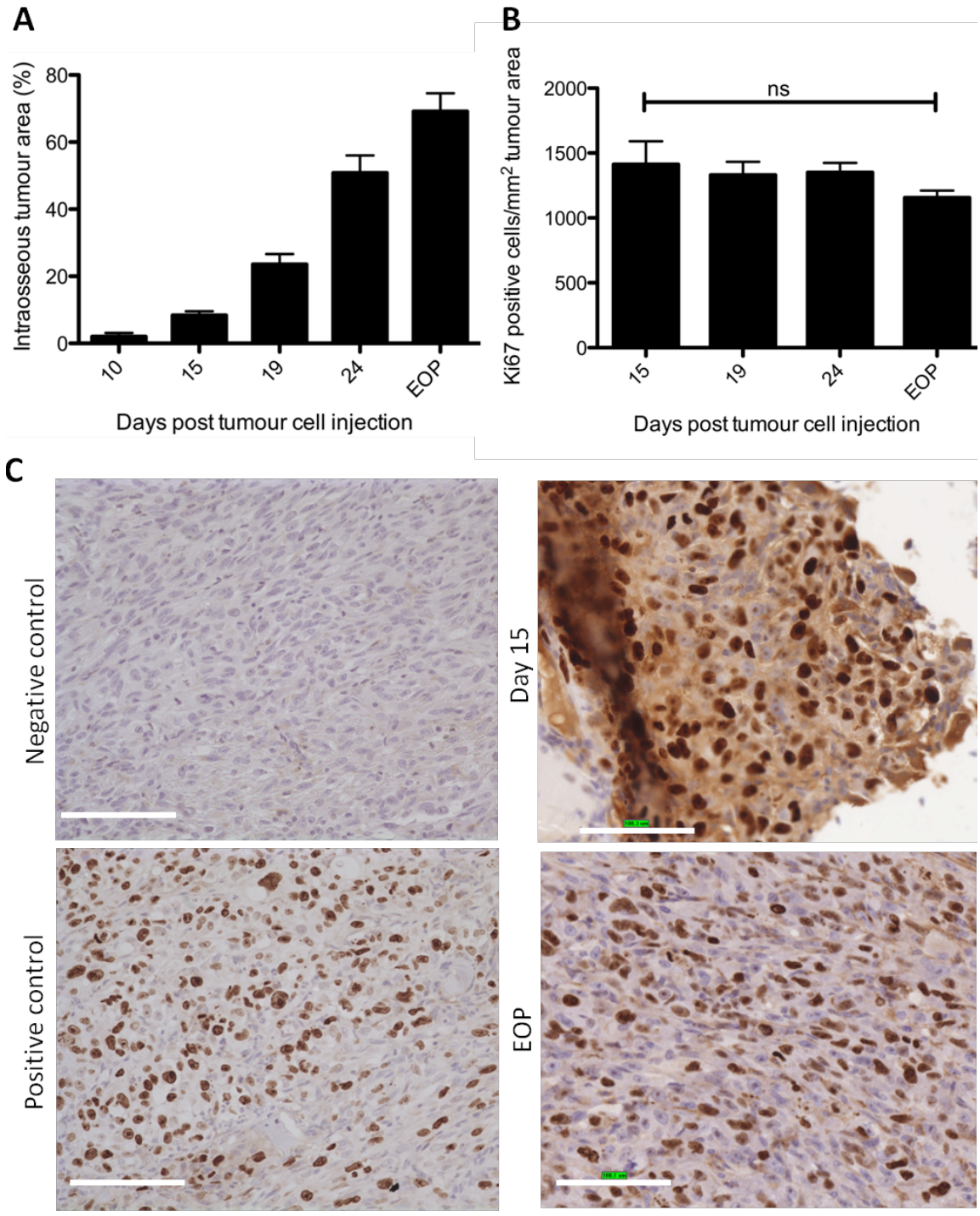

Figure 4.5 Quantification of intraosseous tumour burden and proliferation

A) Histological analysis of tumour area in hind legs (presented as % intraosseous tumour area of metaphyseal bone area) on H&E stained sections. Day 10 n= 4, day 15 n=7, day 19 n=8, day 24 n=9, EOP n=6. A minimum of 2 non-serial sections per sample was analysed. B) Quantification of Ki67 positive (proliferating) tumour cells. A minimum of 2 non-serial sections were analysed per sample. Kruskal-Wallis and Dunn's post-test, ns=not significant. C) Example images of negative (no primary antibody) and positive (bone section with tumour known to stain for Ki67) control as well as small tumour colonies (day 15) and end stage disease (EOP) stained for Ki67 (20x objective, scale bar=100µm).

4.5.1.2 Development of osteolytic bone disease

While it is well known that breast cancer metastases to bone are the cause of osteolytic bone disease, it may be important to identify the exact stage at which cancer cells initiate bone destruction in order to successfully treat and ultimately prevent it. When analysing µCT cross sections of hind legs, overt osteolytic lesions were apparent in 100% of tumour bearing mice from day 19 onwards. Example images of µCT radiographs and cross sections are shown in Figure 4.6. The presence of osteolytic lesions is currently used as a clinical indication for metastatic bone disease. However, tumour cells may lodge onto or close to trabecular bone surfaces and establish here before affecting the cortical bone area. In order to analyse the more detailed effect of longitudinal breast cancer growth on trabecular bone destruction, µCT analysis of trabecular bone in the proximal femur and distal tibia was performed. MDA-MB-231-GFP tumour cell growth reduced trabecular bone volume (bone volume/tissue volume, % BV/TV) from day 19 onwards compared to the bone volume in naïve mice, with a significant reduction on day 24 (5.51% vs. 11.67%, $p<0.001$) and at EOP (3.41% vs. 12.1%, $p<0.001$., Fig. 4.7). The data indicate that smaller tumour colonies (day 10 and 15) do not induce a detectable reduction in trabecular bone volume when compared to age-matched naïve bones. Further µCT analysis suggested that decreased trabecular number, rather than thickness, appeared to be responsible for the reduction in % BV/TV in tumour bearing mice from day 19 to EOP (Fig. 4.7C and D).

The animal model used in this study induces metastatic tumour growth in hind legs but, especially in early disease, the tumour foci are not always present in both femurs and both tibias. I therefore investigated if local tumour colonies in bone have an effect on distal bone turnover in those tibias and femurs not affected by tumour growth. As shown in Figure 4.7B there was no change in trabecular bone volume in non-tumour bearing (opposite) legs compared to naïve mice at any time point. Together the µCT data suggest that MDA-MB-231-GFP cells do not induce a systemic effect on bone turnover and that the lesions are caused by localised effects within affected bones.

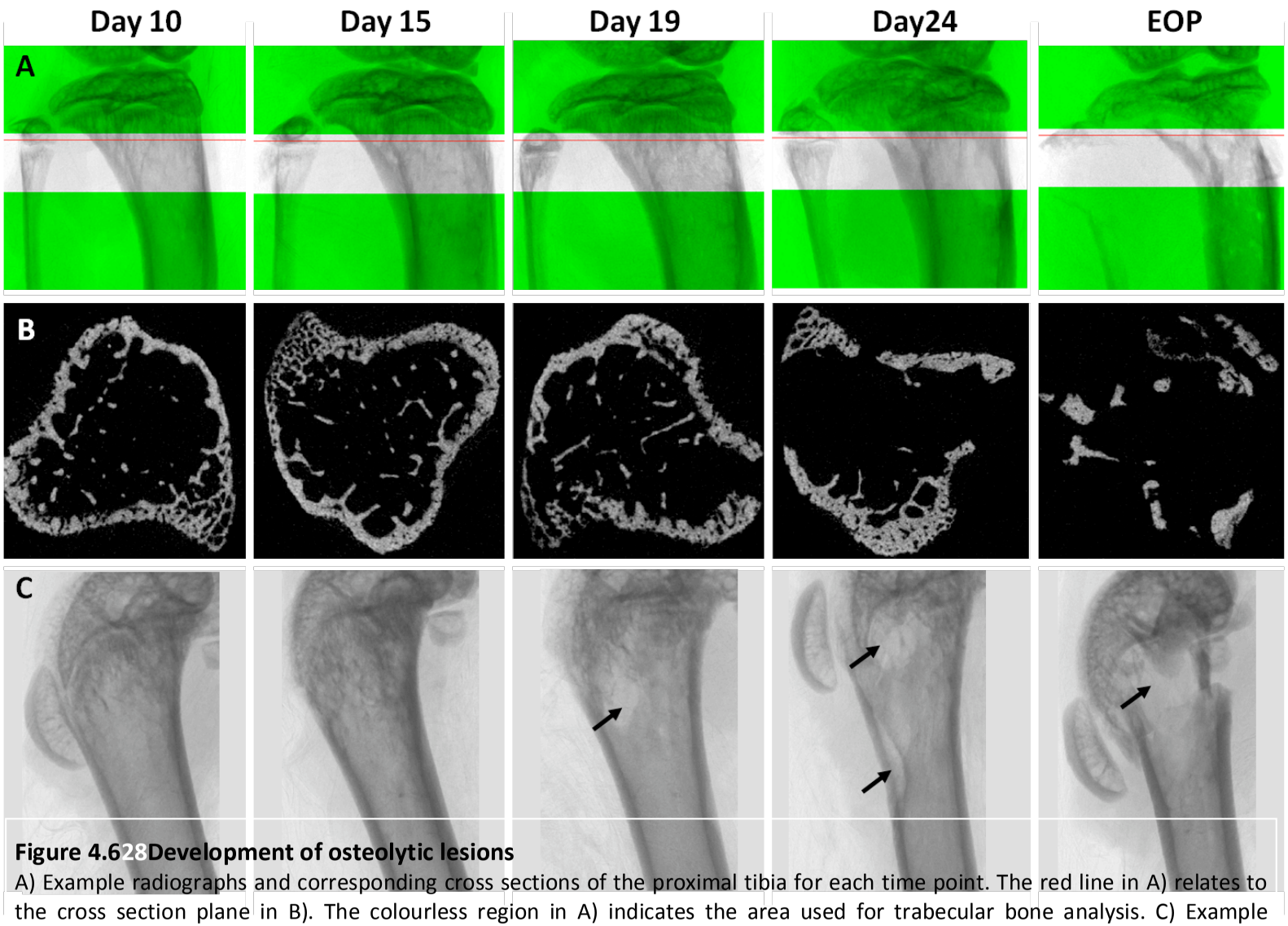

Figure 4.628Development of osteolytic lesions
A) Example radiographs and corresponding cross sections of the proximal tibia for each time point. The red line in A) relates to the cross section plane in B). The colourless region in A) indicates the area used for trabecular bone analysis. C) Example radiographs of the distal femur visualising osteolytic lesions (arrows).

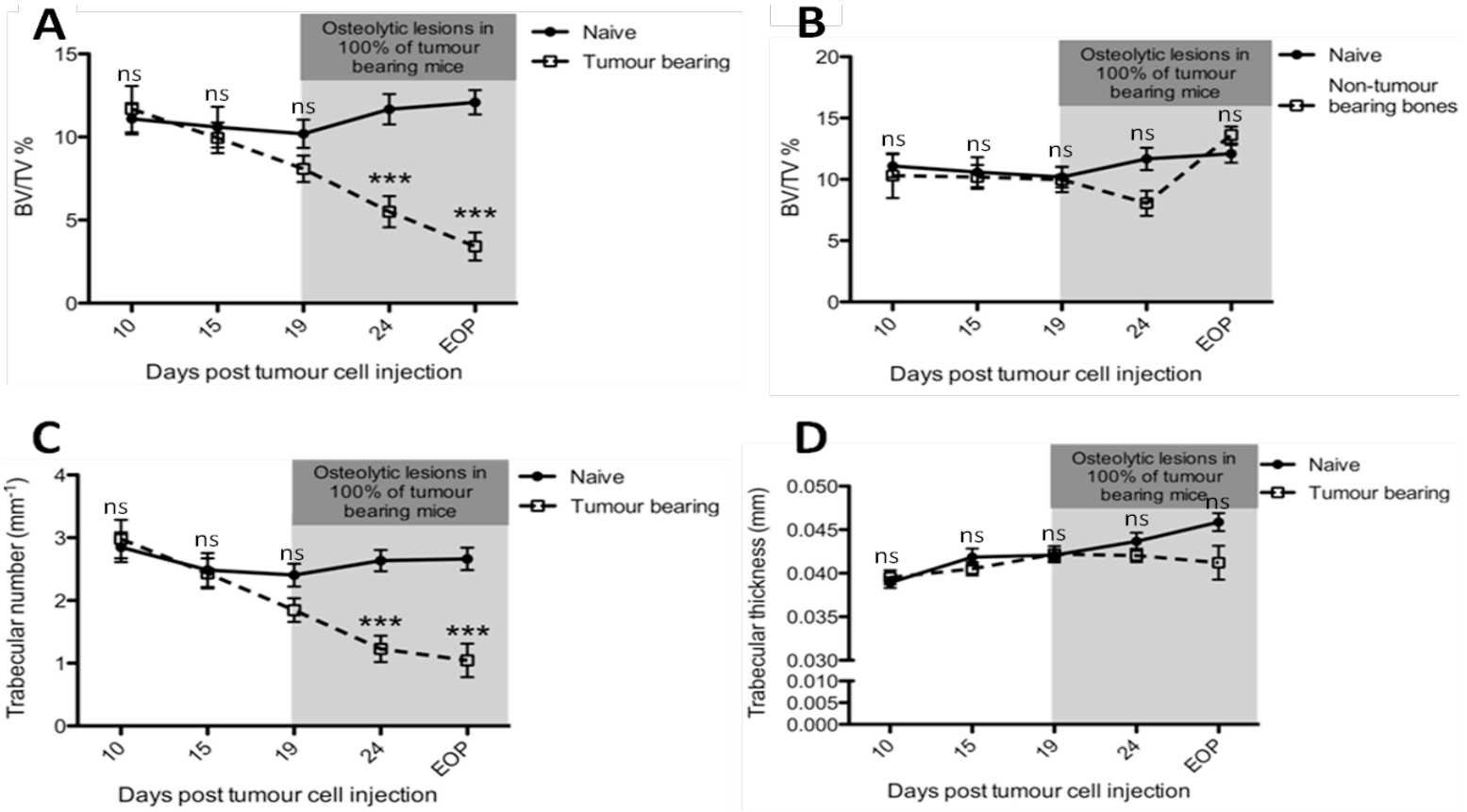

Figure 4.7 Quantification of trabecular bone parameters by µCT

All measurements were carried out for the proximal tibia and distal femur. A) Analysis of trabecular bone volume is depicted as %BV/TV (bone volume/tissue volume) and was performed for tumour bearing vs. naive bones. B) Quantification of %BV/TV in non-tumour bearing vs. naïve tibias and femurs. C) Analysis of trabecular number and D) trabecular thickness for tibia and femur of tumour bearing vs. naïve mice. Mann-Whitney test was carried out for each time point separately, *** is $p<0.001$, ns=not significant. Day 10 n=5 T (tibia) and n=8 F (femur), day 15 n=10 T and n=8 F, day 19 n=11 T and n=6 F, day 24 n=13 T and n=17 F, EOP n=9 T and n=6 F. Naïve: n=7-8 T and 7-8 F/time point.

4.5.1.3 Bone cell distribution changes with increasing tumour burden

After having established the time frame in which tumour cells induce a detectable reduction in trabecular bone volume I next carried out comprehensive analysis of the effects of small, intermediate and large tumour colonies on osteoclasts (Oc) and osteoblasts (Ob). I first assessed the differences between total Oc and Ob numbers in tumour bearing compared to naïve (non-tumour bearing) mice.

In agreement with other studies, I found a significant increase in the total number of osteoclasts in trabecular bone from breast cancer bearing compared to naïve mice. Interestingly, the total number of resorbing cells increased from day 19 onwards, in line with the reduction in trabecular bone volume detected by µCT. Osteoclast numbers were significantly higher than in naïve controls on day 19 (5.8 vs. 4.98, $p<0.05$) and on day 24 (4.48 vs. 6.02, $p<0.01$, Fig. 4.8A). When analysing the effects of the tumour on the total number of osteoblasts, the most profound changes were shown to be taking place before trabecular bone destruction was apparent, with a significant increase in total osteoblast numbers per mm bone surface compared to non-tumour bearing mice on day 15 (13.48 vs. 7.39, $p<0.001$, Fig. 4.8B). At earlier stages of disease (10 days post tumour inoculation) there was no significant difference in osteoclast or osteoblast numbers between naïve and tumour bearing animals. In contrast to osteoclasts, osteoblast numbers of tumour-bearing mice were dramatically reduced with the onset of detectable bone disease, dropping below the levels found in naïve animals at EOP (2.19 vs. 6.75, $p<0.001$).

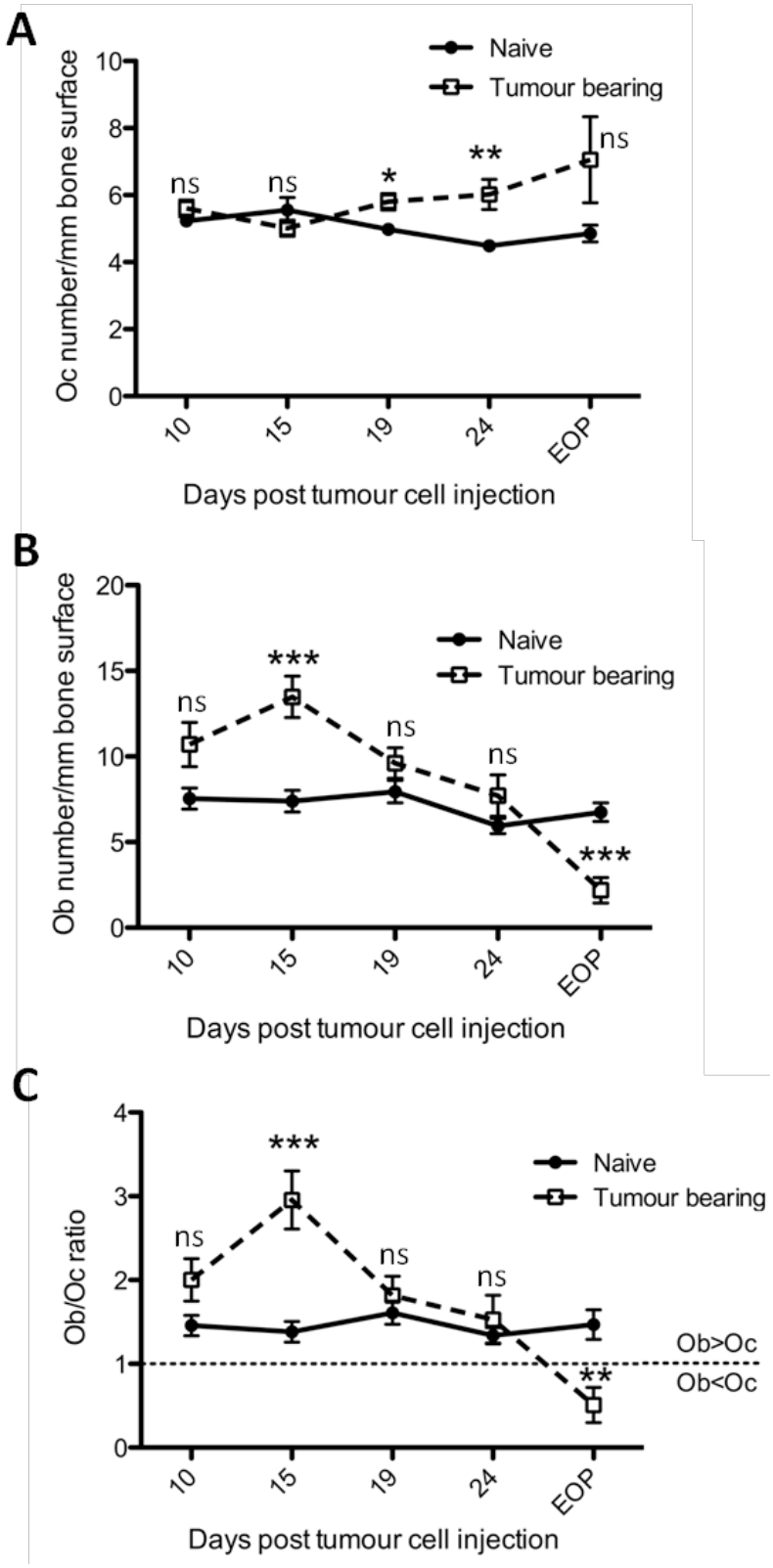

Figure 4.8 Effects of increased tumour burden on bone cell distribution

Total osteoclast A) and osteoblast B) numbers per mm trabecular bone surface in the proximal tibia and distal femur were assessed on TRAP stained histological bone sections. 2 non-serial sections per sample were analysed. C) Osteoblast/osteoclast ratio of total bone cell numbers. The following numbers of mice were used for TRAP analysis: day 10 n=5, day 15 n=6, day 19 n=8, day 24 n=9, EOP n=6. Mann-Whitney test was carried out for each time point separately, * is $p<0.05$, ** is $p<0.01$ and *** is $p<0.001$, ns=not significant.

Analysis of the ratio between osteoblasts and osteoclasts in non-tumour bearing mice showed that the cell populations were maintained at a constant level (ranging from 1.38 to 1.61) throughout the duration of the experiment. In early stages the Ob/Oc ratio of tumour bearing animals was higher compared to naïve mice with a significant increase on day 15 (2.96 vs. 1.38, $p<0.001$, Fig. 4.8C). As expected, corresponding with the onset of osteolytic bone disease the Ob/Oc ratio dropped at the end of the protocol below that of naïve mice (0.51 vs. 1.47, $p<0.01$), mainly driven by a substantial reduction in osteoblast numbers.

Taken together, the results show that breast tumour foci in bone have a substantial effect on total osteoblast numbers 15 days after tumour cell injection, before the entire osteoclast population on trabecular bone increases and osteolytic bone disease is detected by µCT.

4.5.1.4 Analysis of serum bone remodelling markers PINP and CTX

To determine whether the changes in osteoblast number were reflected by corresponding changes in levels of biochemical markers of bone formation, I measured pro-collagen type I N-terminal pro-peptide (PINP) as an indicator of osteoblast activity. PINP levels in naïve mice were constant and ranged from 41.01 ng/ml (day 10) to 49.6 ng/ml (day 15), 42.26 ng/ml (day 19) and 40.01 ng/ml (day 24) followed by a drop at EOP to 23.36 ng/ml (Fig. 4.9A). When comparing PINP serum concentrations of naïve to tumour bearing animals no difference was detected. The data do not reflect the elevated Ob numbers found at day 15 or the sharp reduction at the end of the protocol. In addition, I performed quantitative analysis on CTX (carboxy-terminal collagen crosslinks) serum levels, a marker for bone resorption, on a subset of samples from the study. Although overt formation of osteolytic lesions and reduction of trabecular bone volume could be detected at the later stages of this study, I could not observe any changes in CTX levels (Fig. 4.9B), leading to exclusion of the assay for further samples in the study.

The data therefore suggest that systemic measurements of serum markers may not be sensitive enough to detect local (in the tumour affected bone) changes of bone cell activity or, that in the case of PINP the osteoblasts are inactive. A better representation of the temporal changes in bone turnover would be to bleed mice

repeatedly from the start of the experiment. Although this was attempted, it was not possible to collect sufficient volumes of blood for repeated analyses.

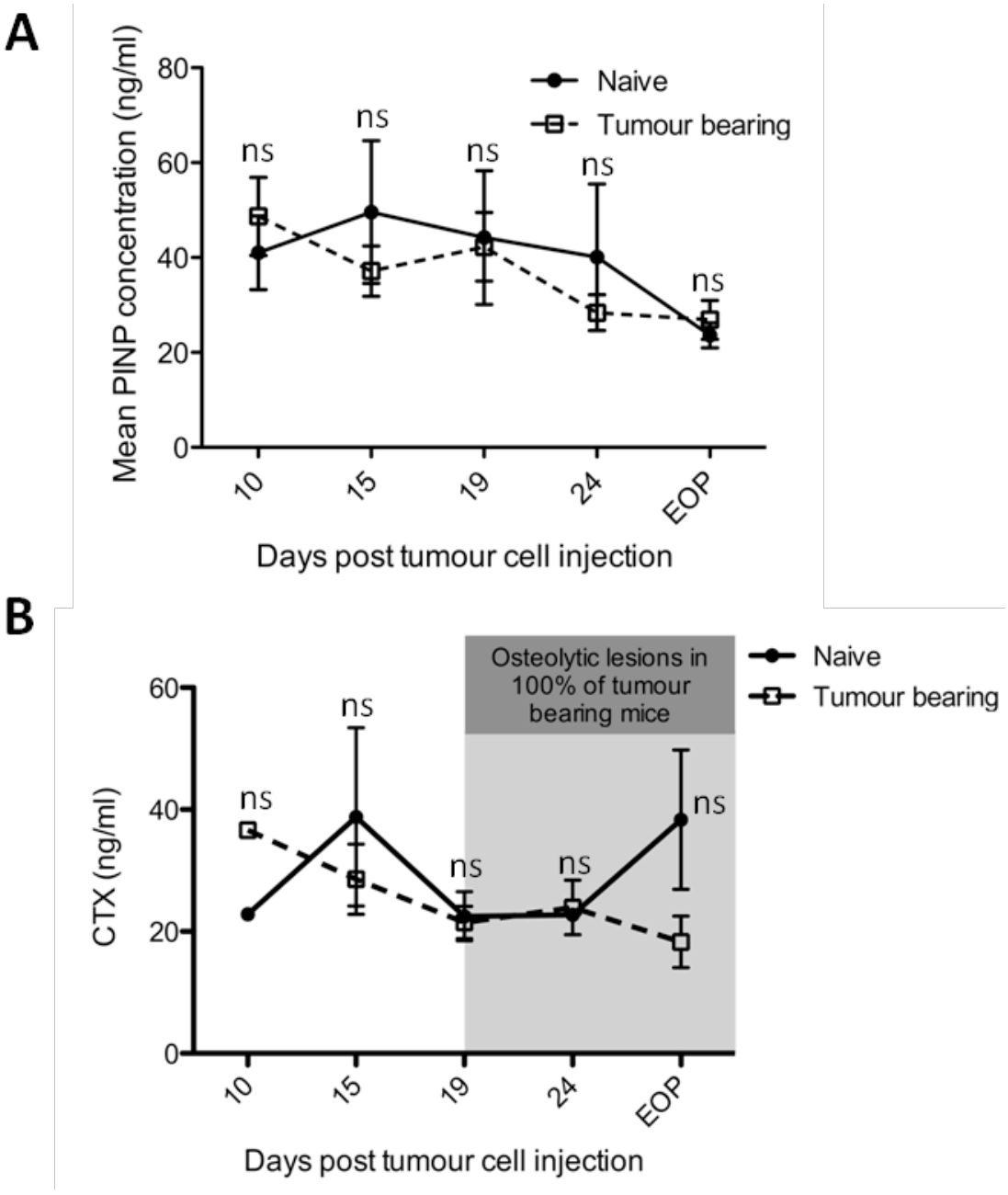

Figure 4.9 Serum levels of bone formation markers PINP and CTX

A) PINP serum levels were measured by ELISA on animals of the entire study with n=6 day 10, n=9 day 15, n=8 day 19, n=10 day 24 and n=6 EOP. Five naïve mice per time point were included. Mann-Whitney test for each time point separately, no significant differences were detected. B) CTX serum levels were measured by ELISA on a subset of animals from the study. Day 10 n=1, day 15 n=3, day 19 n=2, day 24 n=3, EOP n=2. Two naïve animals per group were used for analysis.

4.5.1.5 Osteoblast and osteoclast numbers change according to their proximity to the tumour

As the µCT analysis indicated that the tumour initiated local (in the tumour bearing bone) bone destruction; I further investigated whether or not the changes in osteoblast and osteoclast numbers were dependent on direct cancer cell-bone cell contact. To do this, two location-dependent categories of bone cells in tumour bearing bones were scored: **Category 1)** osteoclasts or osteoblasts in direct contact with tumour cells, and **category 2)** osteoclasts or osteoblasts not in direct contact with the tumour (Fig. 4.2). Quantification of osteoclast numbers in these two categories revealed a clear differential effect of the tumour depending on the proximity to the cancer cells. Osteoclast numbers in direct contact with tumour cells (category 1) where significantly increased compared to those osteoclasts away from the tumour colony (category 2). In fact, those cells distal to the cancer cells remained at a level similar to naïve animals throughout the whole experiment. This differential effect was detected at all time points, with significantly different osteoclast numbers/mm bone surface on day 10, 15, 19, 24 and at EOP (day 10: 18.7 vs. 5.26, $p<0.001$; day 15: 13.67 vs. 4.12, $p<0.001$, day 19: 11.41 vs. 3.87, $p<0.001$; day 24: 11.7 vs. 2.92, $p<0.001$ and EOP: 9.79 vs. 3.15, $p< 0.01$, Fig. 4.10A).

Intriguingly, analysis showed that the presence of tumour colonies had the exact opposite effect on the two location dependent categories of bone forming osteoblasts. The osteoblast population away from the tumour colony was significantly increased 15, 19 and 24 days post tumour cell injection compared to those in direct contact with the tumour ($p<0.001$ with 16.04 vs. 3.44 on day 15, $p<0.001$ with 13.15 vs. 2.84 on day 19, $p<0.001$ with 14.62 vs. 1.06 on day 24 and $p<0.05$ with 4.14 vs. 0.43 at EOP, Fig. 4.10B). From day 10 onwards a reduction in osteoblast numbers of category 2) was found while osteoblasts in category 1) decreased from day 24 onwards. Figure 4.11 shows example images of TRAP stained sections used for analysis.

The data show that the presence of breast cancer in bone has a differential effect on both osteoclasts and osteoblasts depending on their proximity to the tumour and that the development of cancer-induced bone disease involves changes to both cell types.

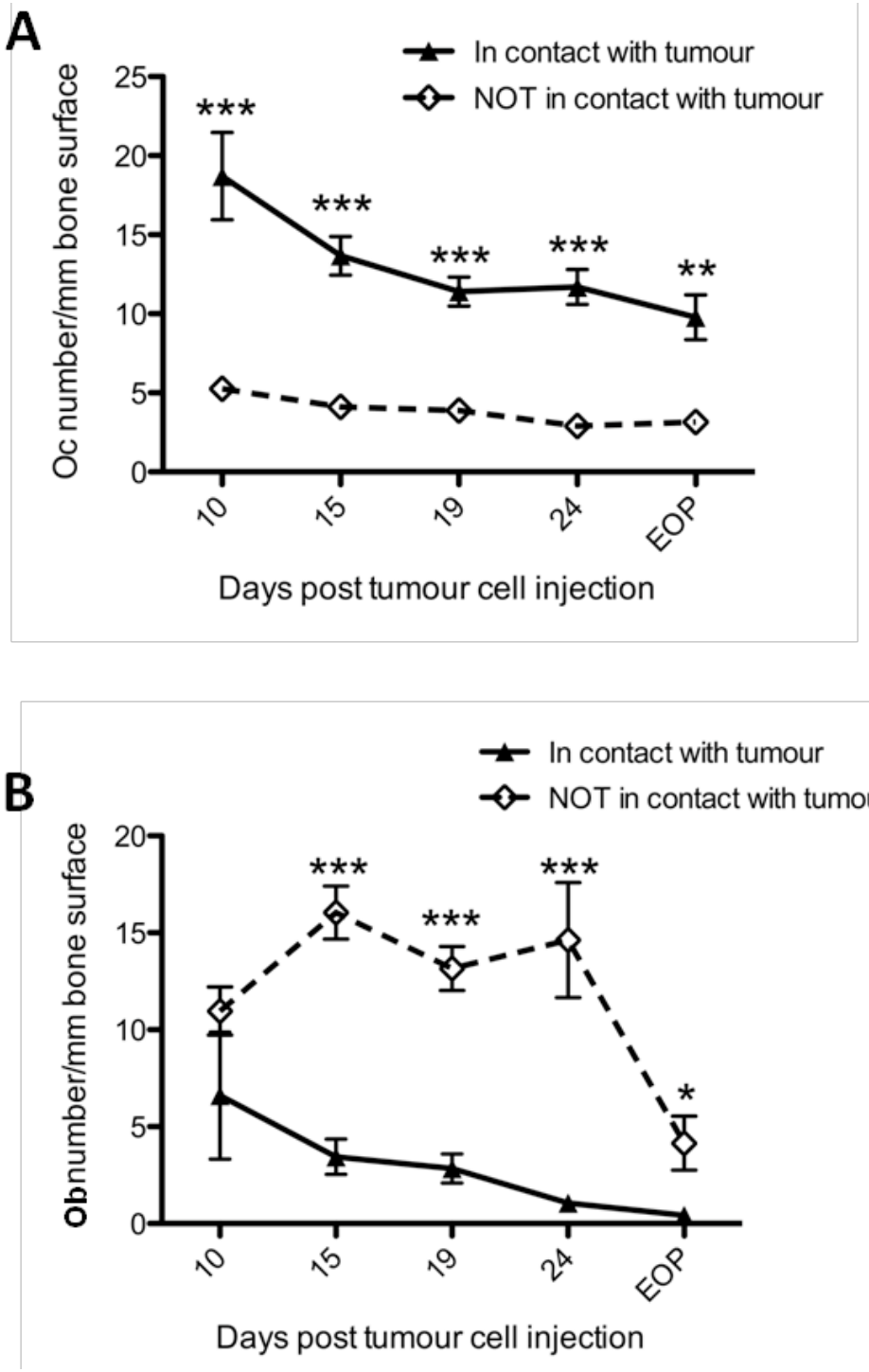

Figure 4.10 The proximity to tumour cells determines changes in osteoblast and osteoclast numbers

Quantitative results for location dependent A) osteoclast and B) osteoblast numbers in tumour bearing mice. The following number of tumour bearing animals was included for each time point: day 10 n=5, day 15 n=6, day 19 n=8, day 24 n=9, EOP n=6. Mann-Whitney test for each time point separately, * $p<0.05$, ** $p<0.01$, *** $p<0.001$.

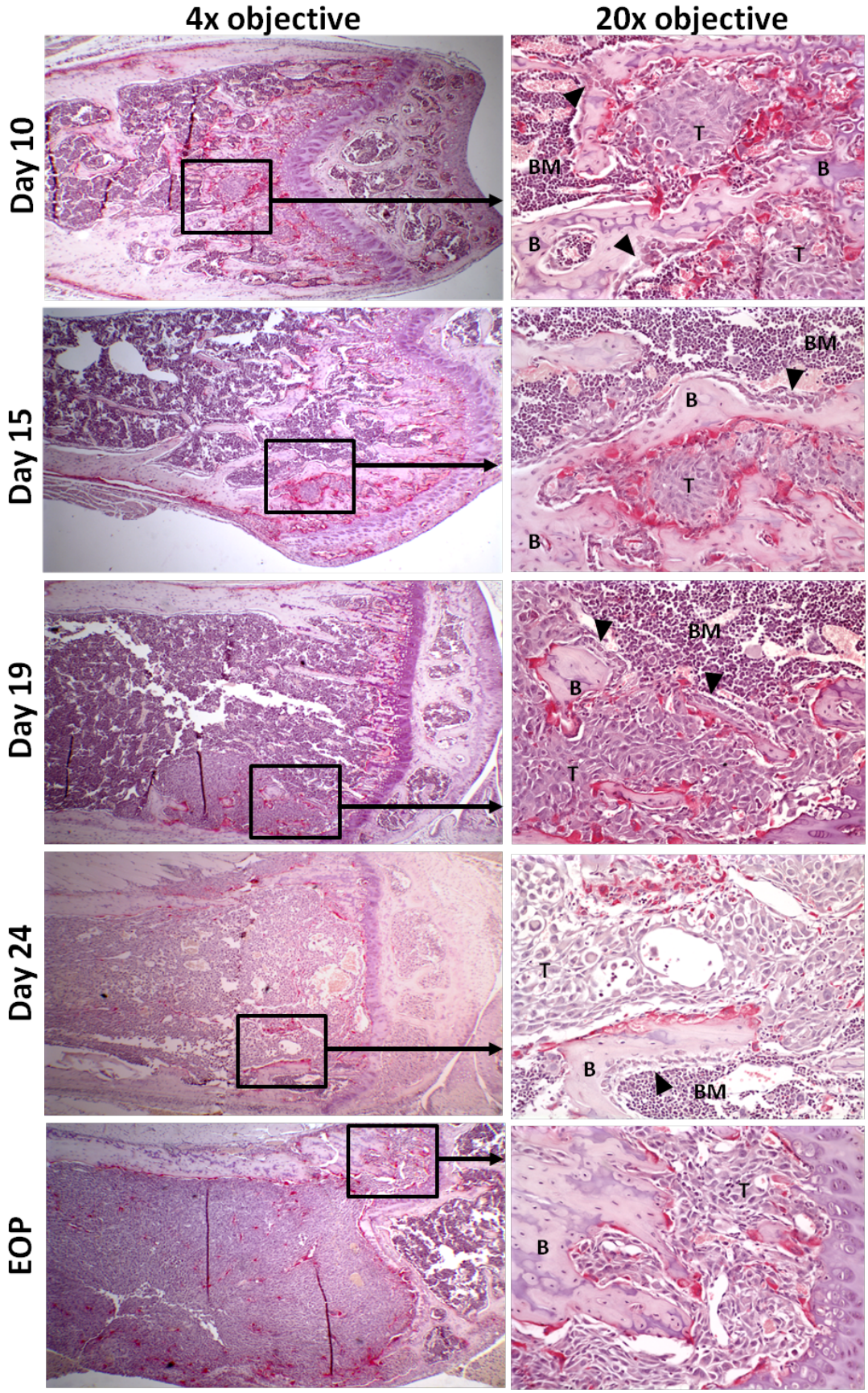

Figure 4.11 Example images of TRAP stained sections

Images of TRAP stained sections showing examples of sections used for analysis of bone cells. Arrow heads indicate presence of osteoblasts. Osteoclasts are stained red, B=bone, T=tumour, BM=bone marrow. Black box indicates area of magnification.

4.5.2 Assessment of soluble molecules possibly involved in tumour-induced changes of bone cell numbers including RANKL, sclerostin and proinflammatory cytokines

4.5.2.1 Investigation of changes in serum RANKL and sclerostin levels

Osteoclastogenesis and activity is greatly regulated through the RANK, RANKL and OPG pathway. The increase in osteoclast numbers detected at day 19 may therefore be connected to the earlier increase in osteoblast numbers on day 15. The activity of the bone forming cells was therefore investigated by serum RANKL measurements, an osteoblast-derived factor known to increase osteoclastogenesis. Surprisingly, RANKL levels were found to be lower in tumour bearing compared to naïve animals at all time points (Fig. 4.12) with a significant reduction on day 10 (50.55pg/ml vs. 212.41pg/ml, $p<0.05$). Note that the concentration of the RANKL decoy receptor OPG should also be measured in order to acquire a complete picture on the osteoclast activating potential of RANKL.

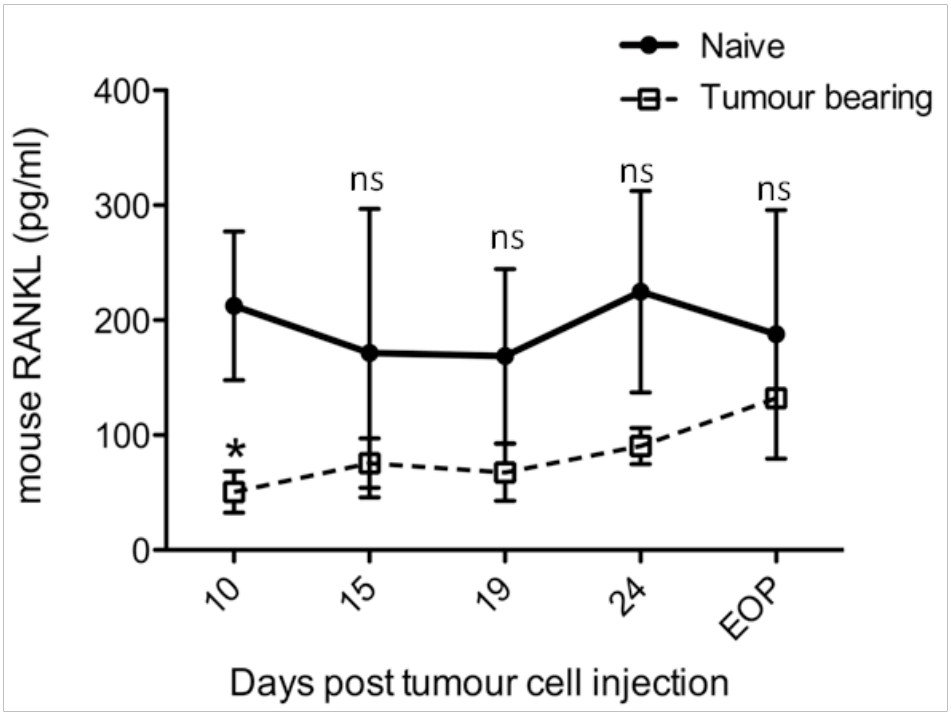

Figure 4.12 Detection of mouse RANKL in serum

Mouse RANKL serum levels were measured by ELISA on tumour bearing animals with n=4 at day 10, n=7 at day 15, n=5 at day 19, n=6 at day 24 and n=3 at EOP (dotted line). Serum from three naïve mice per time point was included (solid line). Mann-Whitney test for all time points separately, * is $p<0.05$, ns=not significant.

I further investigated if the biphasic nature of the changes observed in total (Fig. 4.8B) and location-dependent osteoblast numbers (Fig. 4.10B) could be induced by a change in the concentration of molecules acting on osteoblast differentiation. Because of the importance of the Wnt-pathway on osteoblast differentiation I aimed to investigate the serum levels of the Wnt-inhibitor sclerostin, a molecule known to inhibit osteoblast formation. Mendoza-Villanueva et al. (2011) have shown that MDA-MB-231 cells produce sclerostin *in vitro* leading to inhibition of osteoblast differentiation. As the changes in bone cell numbers were induced by the presence of tumour cells, I measured tumour cell-derived sclerostin levels in mouse serum by ELISA specific to human sclerostin. No difference in sclerostin levels were detected throughout the study, suggesting that cancer cell derived sclerostin is not responsible for the changes in Ob numbers (Fig. 4.13) or that human derived sclerostin only has a localised effect.

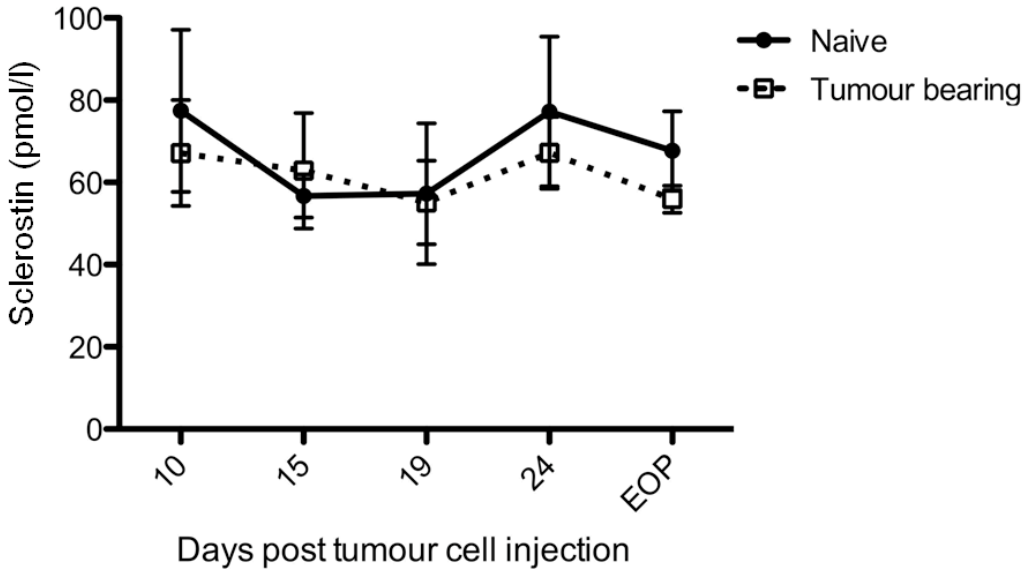

Figure 4.13 Detection of human sclerostin in mouse serum
Sclerostin serum levels were measured by ELISA on animals of the entire study with n=4 at day 10, n=5 at day 15, n=5 at day 19, n=6 at day 24 and n=3 at EOP (dotted line). Serum from three naïve mice per time point was included (solid line). No significant difference was detected by Mann-Whitney test for all time points (ns=not significant).

The systemic measurement in murine RANKL and human sclerostin levels show that concentrations of these molecules do not change in the circulation of tumour bearing vs. naïve mice. The data therefore suggest that cell-cell contact and local changes (in the tumour bearing bone) to the microenvironment are more important for the changes seen in bone cell numbers. The results agree with the µCT and histomorphometry data showing that the tumour has no effect on, for example the opposite, tumour-free leg.

4.5.2.2 Investigation of tumour-induced changes on host cytokine levels (species specific)

Several cytokines were shown to be involved in the induction of osteoclastogenesis and activity including the osteoblast and stromal cell derived murine cytokines IL-1α, IL-1β, IL-6, KC (mouse IL-8) and MCP-1. In order to investigate if the increase in osteoblast numbers at day 15 and 19 was linked to an increase in osteoclast activating cytokines released by the host stroma, serum levels were analysed by cytometric bead array. Measurements of IL-1α and IL-1β were below detection level (below 10pg/ml) and showed no difference between naïve and tumour bearing bones (Fig. 4.14A and B). Although the detection of IL-6 was too low to draw meaningful conclusions, tumour-bearing animals appeared to express more IL-6 compared to naïve animals from day 19 onwards (Fig. 4.14C). No significant changes between tumour bearing and naïve animals could be detected when analysing serum KC levels but concentrations were generally lower in tumour bearing animals sacrificed on day 10 and 15 compared to the age matched naïve controls. MCP-1 levels increased in tumour bearing mice on day 19 and remained level with the concentration found in tumour-free mice on day 24 and at EOP, although no significant differences could be detected at any time (Fig. 4.14D and E). Together the data indicate that systemic measurement of cytokine levels does not change significantly in animals bearing osseous tumours compared to the age matched tumour-free mice.

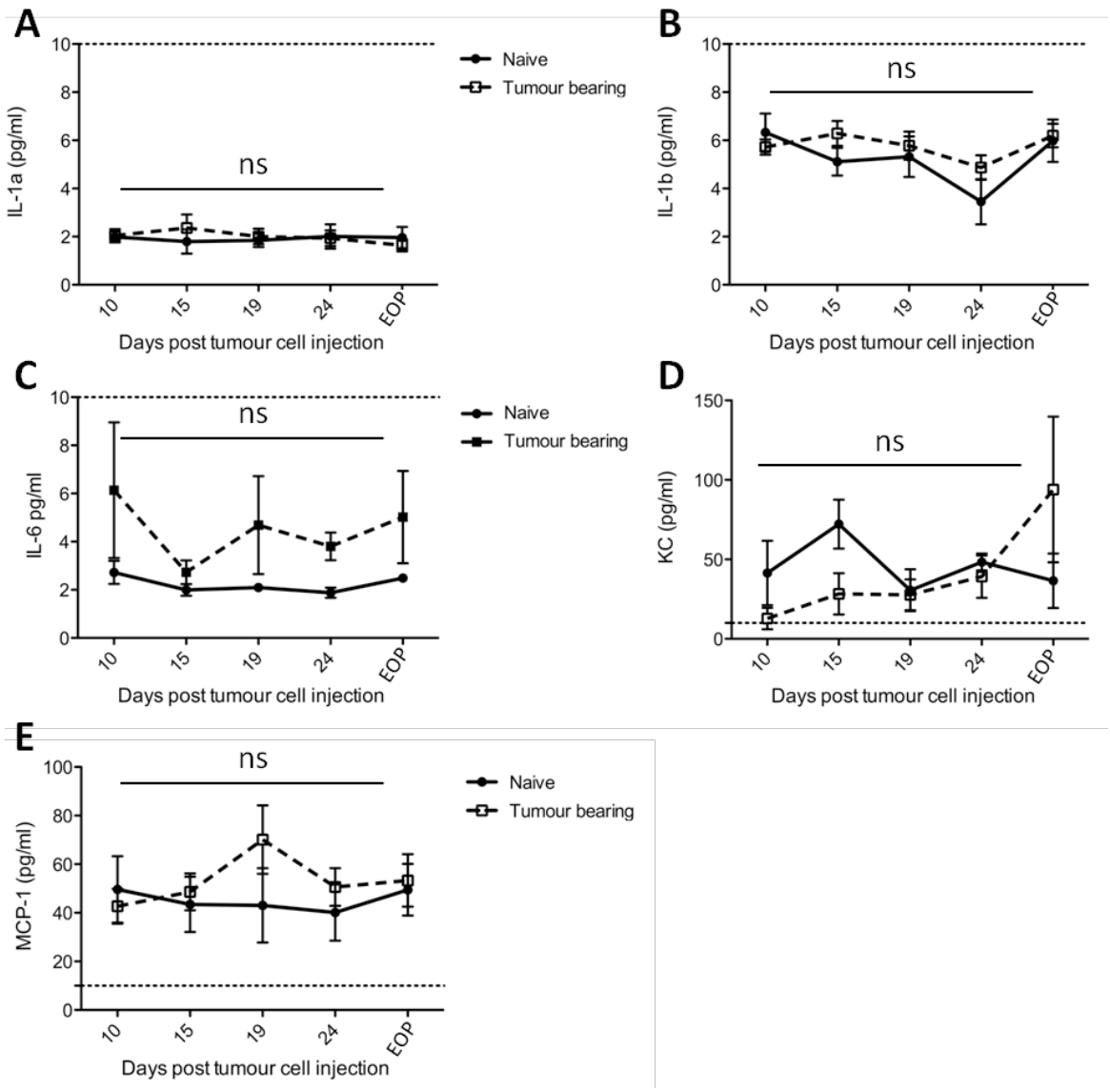

Figure 4.14 Measurement of host serum cytokine levels by CBA in animals with osseous tumour growth

The serum concentrations of mouse IL-1α IL-1β, IL-6, KC (IL-8) and MCP-1 were analysed by cytometric bead array to the manufacturer's instructions. Lower detection limit of all cytokines was 10pg/ml (indicated by the dotted line). Mann-Whitney test for each time point separately, graphs show mean ± SEM, no significant differences were detected, ns=not significant.

4.5.3 Investigation of locally induced changes on bone cells and tumour cell gene expression

4.5.3.1 Direct tumour cell contact increases osteoclast size

Because of the clear location-dependent effect of the tumour on bone cell numbers, I investigated if direct contact induced changes in osteoclast size. It has been proposed that cultures of large osteoclasts (>10 nuclei) are more likely to be actively resorbing than small osteoclasts (<5 nuclei) (Trebec et al., 2007). Since the quantification of nuclei on histological sections is difficult, I compared mean osteoclast area (measured in mm^2) of tumour bearing mice to the cell size of naïve animals. Two time points were chosen for analysis, day 15 and 19, due to the first detectable changes in bone cell numbers and μCT results on these days. In line with the decrease in trabecular bone detected by μCT (Fig. 4.7) it was found that tumour-bearing animals had larger osteoclasts compared to naïve mice (day 15 $1.8x10^{-4}mm^2$ vs. $1.4x10^{-4}mm^2$, $p<0.05$ and day 19 $2.1x10^{-4}mm^2$ vs. $1.4x10^{-4}mm^2$, $p<0.001$, Fig. 4.15A). I then performed location-dependent analysis and counted the number of osteoclasts in direct contact and not in direct contact with cancer cells. This revealed that the increase in osteoclast size in tumour bearing mice was due to large osteoclasts in direct contact with the tumour cells (Fig. 4.15B). Osteoclasts in contact with tumour had a mean size of $3.3x10^{-4}mm^2$ compared to those distal to the tumour with $1.3x10^{-4}mm^2$ on day 15 ($p<0.001$) and $3.3x10^{-4}mm^2$ compared to $1.5x10^{-4}mm^2$ on day 19 ($p<0.001$). The TRAP positive cells away from the tumour were shown to be of a similar size as in naïve animals. The data strongly suggest that cell-cell contact is required for the tumour-induced changes in osteoclast size possibly indicating an increase in their osteolytic activity.

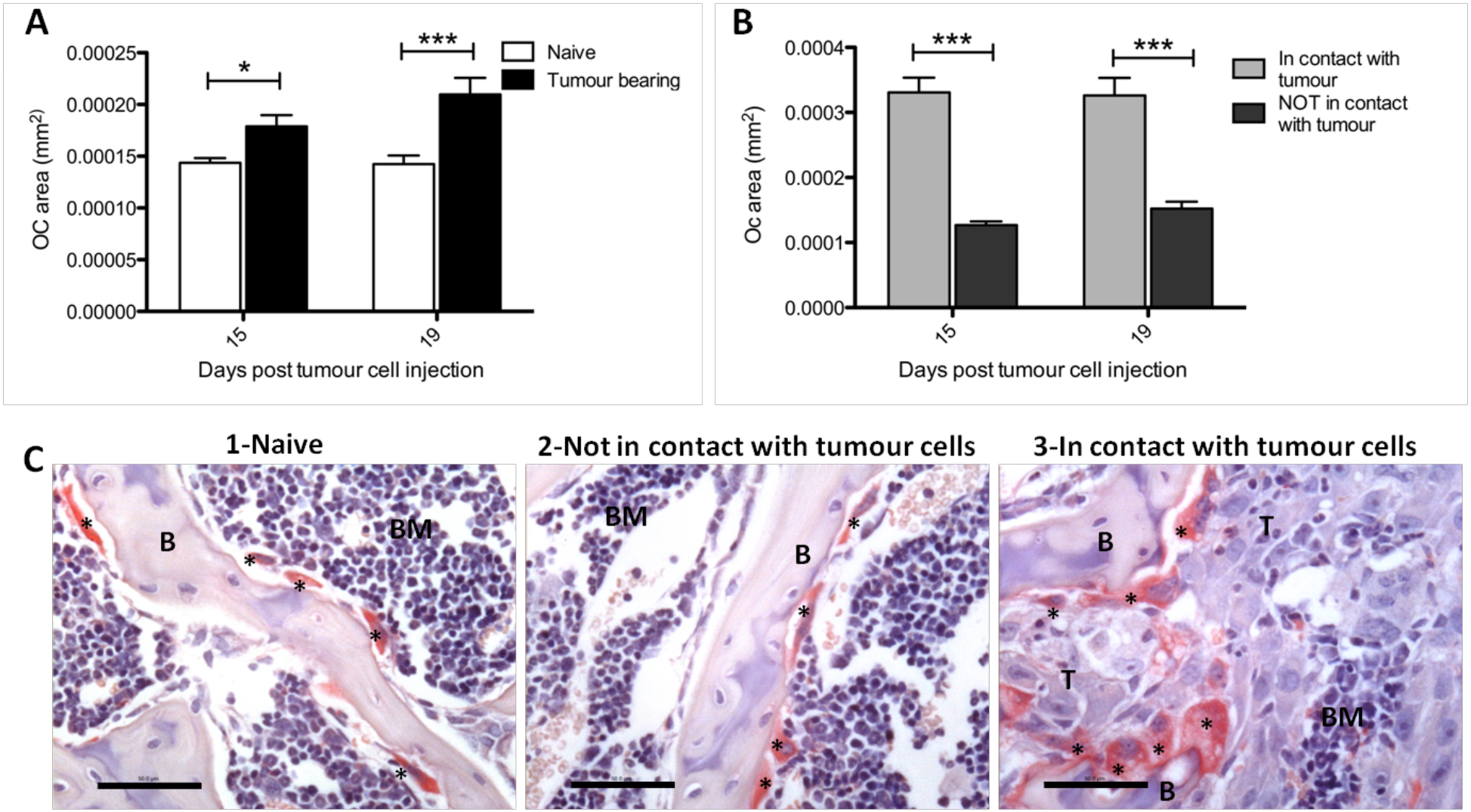
A
0.00025
0.00020
0.00015
0.00010
0.00005
0.00000
OC area (mm2)
*
***
Naive
Tumour bearing
15
19
Days post tumour cell injection
B
0.0004
0.0003
0.0002
0.0001
0.0000
Oc area (mm2)
***
***
In contact with tumour
NOT in contact with tumour
15
19
Days post tumour cell injection
C
1-Naive
2-Not in contact with tumour cells
3-In contact with tumour cells
B
BM
T

Figure 4.15 Osteoclast size (page 148)

Osteoclast size (area in mm^2) was quantified on TRAP stained sections (20x objective). A) Mean osteoclast area in naïve vs. tumour bearing mice. B) Mean osteoclast area in tumour bearing animals differentiating between Ocs in direct contact with tumour cells and NOT in direct contact with the tumour. Mann-Whitney test for each time point separately, * $p<0.05$, *** $p<0.001$. C) Example images of TRAP sections for 1) naïve mice, 2) not in contact and 3) in contact with tumour (20x objective, * Oc (red), B=bone, BM=bone marrow, T=tumour, scale bar=50µm.

4.5.3.2 Analysis of tumour gene expression (species specific analysis to human genes)

The complexity of the tumour and the surrounding microenvironment is partly shown in the analysis so far described in this chapter. In order to further decipher the effects tumour cells may have on the microenvironment, I have assessed changes in gene expression of a number of bone-related genes of MDA-MB-231-GFP cells grown *in vitro* and *in vivo* at a subcutaneous site (Fig. 4.1B) and of tumours growing in bone post intracardiac injection (sacrificed 23 days post tumour cell injection). The aim of the gene expression analysis was to assess whether the tumour produces bone related molecules, possibly explaining the tumour-induced changes in bone cells. Species specificity of the used TaqMan® assays to human genes only has previously been assessed in the laboratory (page 50). Genes of interest were the inhibitors of osteoblast differentiation DKK1, DKK2 and SFRP1; the RANKL decoy-receptor OPG (a negative regulator of bone resorption); the osteoclast enhancing proteins RANKL, RANK and GMCSF as well as the tumour suppressor DKK3 (Table 4.1). When assessing the gene expression pattern of subcutaneous tumours taken on different time points post tumour cell injection including day 15, 23 and 33 no significant changes were detected (Table 4.2). SFRP2, SDF1 and CXCR4 were not detectable at any investigated time point. Further analysis of site comparison was therefore carried out on pooled subcutaneous samples.

DKK1	Inhibits osteoblast differentiation by binding to LRP5/6 and leads to inhibition of the Wnt-pathway
DKK2	Inhibits osteoblast differentiation by binding to LRP5/6 and leads to inhibition of the Wnt-pathway
DKK3	Tumour suppressor, downregulated in a variety of cancers
SFRP1	Wnt-decoy receptor, leads to inhibition of Wnt-pathway and osteoblast formation
OPG	Negative regulator of bone resorption, decoy receptor to RANKL
RANK	Essential for osteoclastogenesis
RANKL	Essential for osteoclastogenesis
GMCSF	Essential for osteoclastogenesis

Table 4.1 Function of gene-products
Overview of the genes investigated by qRT-PCR and the reported function.

Gene	ΔCT day 15	ΔCT day 23	ΔCT EOP (day 33)	P value
DKK1	7.66 ± 0.16	7.94 ± 0.11	8.00 ± 0.14	0.3340
DKK2	13.69 ± 0.41	13.96 ± 0.53	14.95 ± 0.69	0.3119
DKK3	19.97± 0.24	19.54 ± 0.76	19.78 ± 0.74	0.8501
SFRP1	15.75± 0.56	16.21 ± 0.91	16.12 ± 1.21	0.9147
OPG	7.39± 0.46	6.79 ± 0.13	7.26 ± 0.34	0.5940
RANK	11.25± 0.35	11.65 ± 0.11	11.33 ± 0.08	0.5597
GMCSF	6.55± 0.16	6.69 ± 0.24	6.57 ± 0.53	0.9710

Table 4.2 Gene expression of bone related genes in subcutaneous tumours
MDA-MB-231-GFP cells were grown subcutaneously in balb/c nude mice for 15, 23 and 33 days. Quantitative real time gene expression analysis for bone related genes was performed. Data are expressed as the CT (cycle threshold) values relative to GapdH ($\Delta CT = CT_{gene\ of\ interest} - CT_{GapdH}$). Mean±SEM, Kruskal Wallis test, a p value of <0.05 was considered significant, ND=not detectable.

Next, MDA-MB-231-GFP cells grown *in vitro* as well as osseous and subcutaneous tumours were analysed for changes in gene expression to assess whether the site-specific environment alters tumour gene expression. Analysis of DKK2 and RANK showed no significant change when comparing the *in vitro* to the *in vivo* samples (Fig. 4.16). Furthermore, OPG and GMCSF were significantly increased in both the subcutaneous and the osseous tumour samples compared to cell culture conditions. However, no differences were found between the two *in vivo* sites. When analysing the Wnt-pathway antagonists DKK1 and SFRP1, a significant increase in gene expression relative to GapdH was detected in bone compared to subcutaneous tumours (DKK1: 4.31 vs. 1.38, $p<0.001$ and SFRP1: 10.74 vs. 3.40, $p<0.01$). Furthermore, DKK3 was undetectable in the bone sample while *in vitro* and s.c. grown

cells were expressed similarly, suggesting site-specific downregulation of the proposed tumour suppressor gene in osseous tumours. The highest change was detectable when assessing RANKL expression with a 128 fold upregulation in the osseous tumour compared to the *in vitro* and subcutaneous samples (p<0.001).

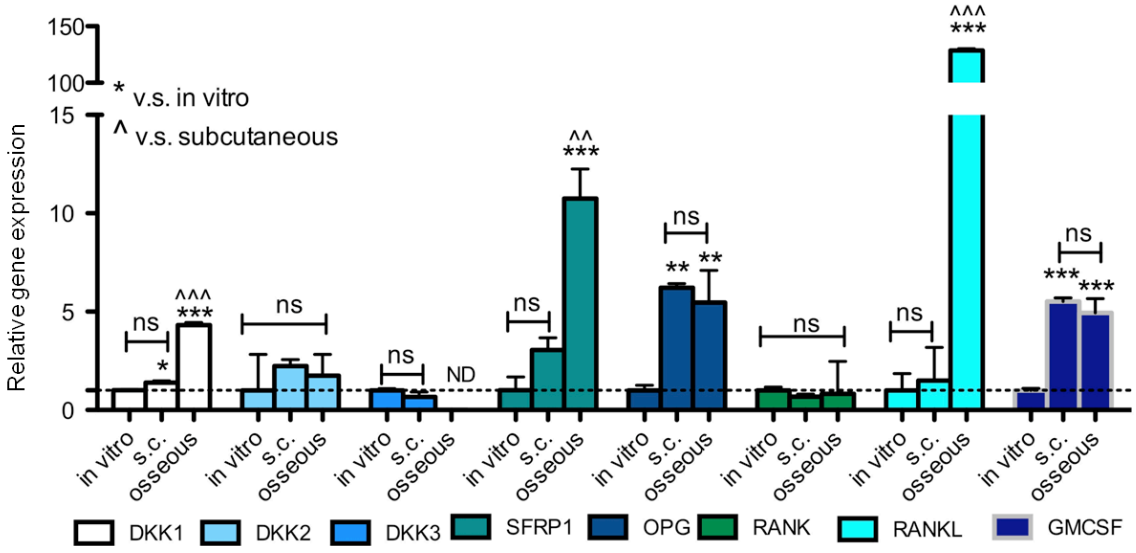

Figure 4.16 MDA-MB-231-GFP gene expression in *in vitro* and *in vivo* samples
MDA-MB-231-GFP cells were grown either *in vitro*, *in vivo* at a s.c or osseous site. Quantitative real time PCR analysis was performed using TaqMan® assays. Data are expressed as the relative expression of the gene of interest to GapdH (2^-(ΔΔCT) with $\Delta\Delta CT=\Delta CT_{in\ vivo} - \Delta CT_{in\ vitro}$). Mean±SEM, one way ANOVA and Tuckey post test, * = vs. *in vitro*, ^ = vs. s.c., ND = not detectable. * is p<0.05,** is p<0.01, *** is p<0.001, ns = not significant. All genes presented are species specific except for RANKL.

Collectively the data suggest that the *in vivo* microenvironment (s.c. or bone) induces significant changes to bone related gene expression patterns of MDA-MB-231-GFP cells. Importantly, the site-specific increase in gene expression of the osteoblast inhibitors DKK1 and SFRP1 and osteoclast activator RANKL in bone tumours (day 23) could help explain the reduction in osteoblasts and the local increase of osteoclasts seen at this stage of tumour growth and thus increasing the osteolytic potential of the cancer cells.

4.5.4 Effects of peripheral tumour growth on bone integrity and cytokine expression

It is well established that breast tumour growth in bone severely affects bone remodelling; however, it is unclear whether the same tumour cells are able to induce changes to the bone when located at a peripheral site. I therefore investigated the effects of subcutaneous MDA-MB-231 tumour growth on bone integrity and serum cytokine levels. The sizes of the subcutaneous tumours used in this experiment (day 23-33) were comparable to the ones found in bone at EOP.

4.5.4.1 Bone integrity is not affected by peripheral breast tumour colonies

MDA-MB-231-GFP cells were implanted subcutaneously into nude mice and animals were sacrificed at three time points comparable to those in the bone study. Eight out of nine animals developed subcutaneous tumours and size (cm^3) increased from day 15 to day 33 (Fig. 4.17A).

Analysis of the proximal tibia and distal femur by µCT showed that trabecular bone volume per tissue volume, trabecular number and thickness were all unchanged when comparing bones from tumour bearing mice to those of age matched naïve control mice (Fig. 4.17B-D). The data strongly suggest that the presence of a tumour at a peripheral site does not interfere with normal bone remodelling as shown by µCT measurements, supporting the previous findings that cancer-induced bone disease are a result of tumour cell-bone cell interactions and not due to systemic effects.

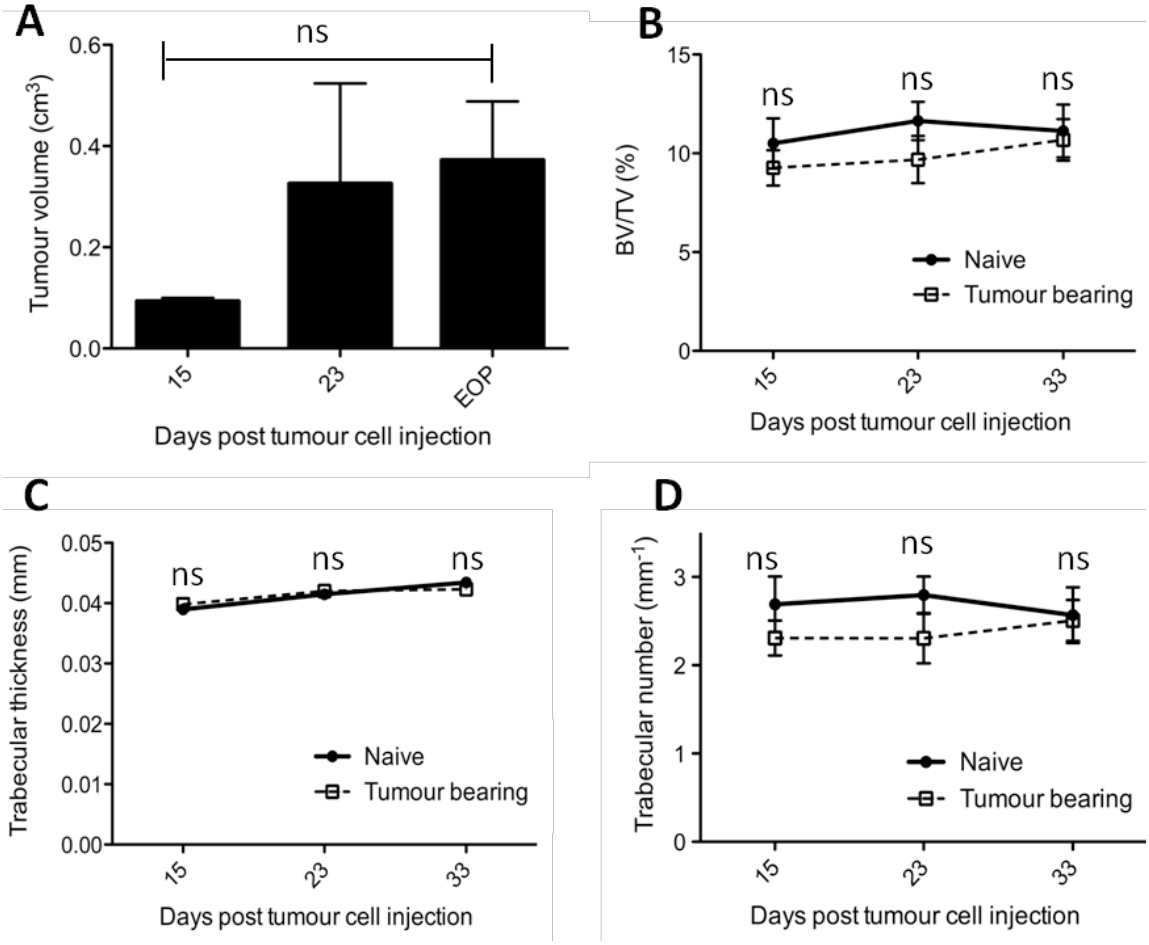

Figure 4.17 Effects of subcutaneous breast tumour growth on bone integrity

A) Subcutaneous MDA-MB-231-GFP tumours were measured by calliper. Analysis of left and right tibias and femurs from tumour bearing and naïve mice was performed by µCT for B) BV/TV, C) trabecular thickness and D) trabecular number. (n=2 naïve mice; n=3 on day 15, n=2 on day 24 and n=3 on day 33 tumour-bearing mice). Mann-Whitney test for each time point separately or Kruskal-Wallis test, ns=not significant.

4.5.4.2 Effects of peripheral breast tumour growth on serum host cytokine levels (species specific to mouse)

In order to investigate if the presence of a peripheral tumour induces changes in serum cytokine levels and to further underline the focal nature of osteolysis in this model, the serum concentration of murine IL-1α, IL-1β, IL-6, KC (IL-8) and MCP-1 were measured. The concentration of IL-1α, IL-1β and IL-6 were found to be below detection level as seen in the measurements taken from mice with bone metastases and no difference was seen between tumour bearing and tumour-free mice (Fig. 4.18A-C). In addition, no change was detected between the two groups when analysing KC levels (Fig. 4.18D). Investigation of serum MCP-1 showed lower levels in mice bearing a subcutaneous tumour for 24 days compared to the control mice at this time point and a significant decrease was visible at EOP (67.42pg/ml vs. 88.54pg/ml, $p<0.05$).

The data suggest that subcutaneous tumour growth does reduce the serum level of MCP-1 compared to tumour-free mice significantly but has little effect on other pro-inflammatory cytokines. These data require further confirmation due to the small sample number available for analysis.

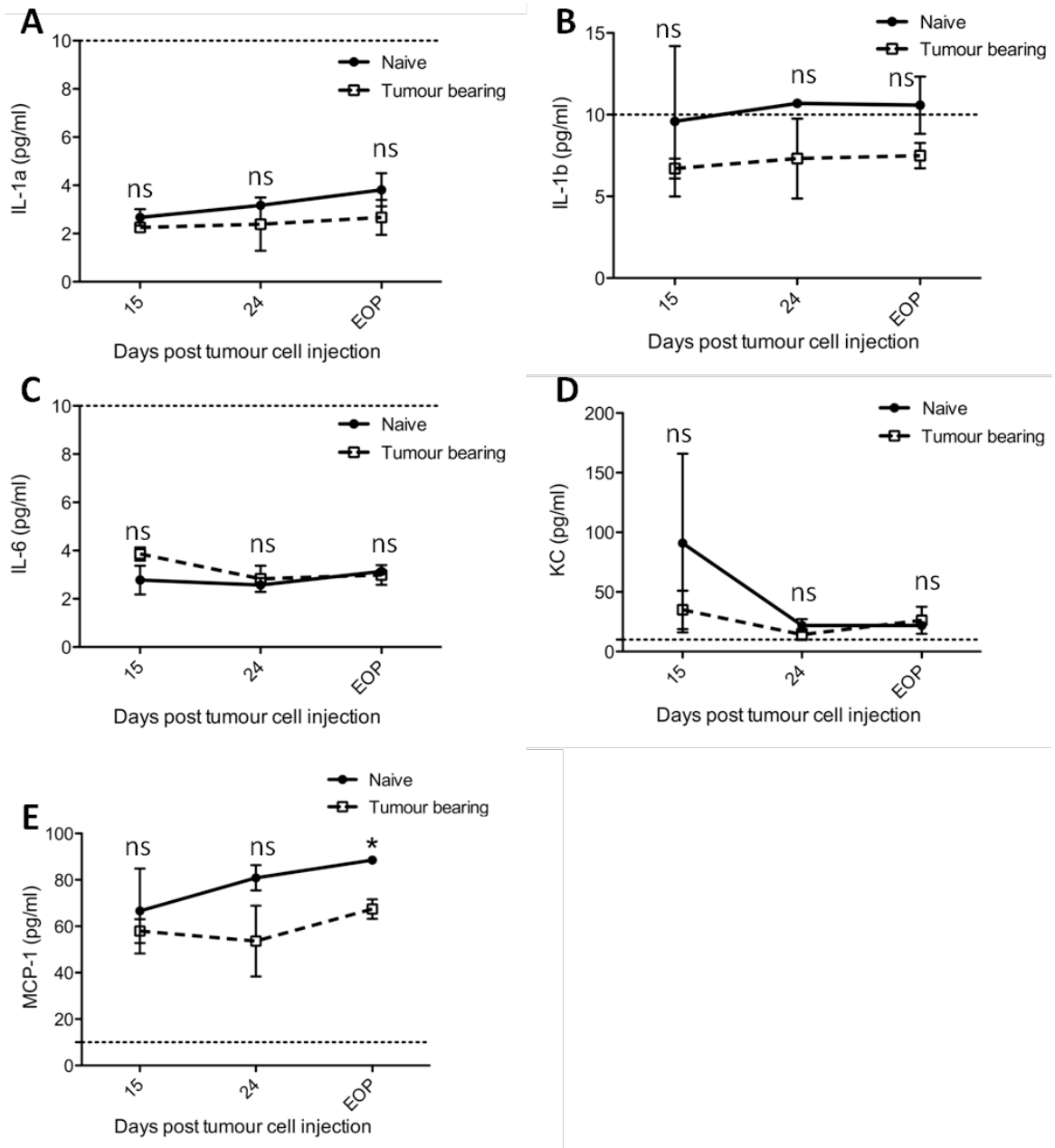

Figure 4.18 Quantification of mouse cytokines in animals bearing subcutaneous breast tumours

The serum concentrations of murine IL-1α IL-1β, IL-6, KC (IL-8) and MCP-1 were analysed by cytometric bead array. Two tumour-free animals (naïve) were analysed per time point and the number of tumour bearing mice was n=3 on day 15, n=2 on day 24 and n=3 at EOP. Lower detection limit of all cytokines was 10pg/ml (indicated by the dotted line). Mann-Whitney test for each time point separately, graphs show the mean ± SEM, * is $p<0.05$, ns=not significant.

4.6 Discussion

The main part of this study aimed to characterise the cellular interactions associated with different stages of bone metastasis, investigating the temporal and spatial relationship between breast cancer cells, osteoblasts and osteoclasts in the bone microenvironment. The increase in tumour burden from day 10 until day 28-33 was accompanied by a statistically significant decrease in trabecular bone volume from day 19 onwards, suggesting that the tumour establishes in the bone microenvironment prior to initiating extensive bone destruction. However, it is possible that there is a lag-phase between the growth of the tumour and the cancer-induced bone loss or that the changes at early time points are not detectable by μCT. Further analysis suggested that cancer-induced bone destruction is a localised process mainly affecting trabeculae in direct contact or in close proximity (in the tumour bearing bone) to the tumour colony. This is in agreement with a study undertaken by Clohisy et al. (1996b), where breast cancer-induced bone disease was shown to form focal lesions rather than systemic bone disease.

Detailed analysis of total osteoclast numbers (regardless of their proximity to the tumour) showed a significant increase from day 19 onwards compared to tumour-free bones, the same time point at which trabecular bone was reduced and osteolytic lesions were detected in 100% of tumour bearing mice. Analysis of earlier time points (day 10 and 15) revealed that there was no change in total osteoclast numbers, suggesting that small tumour colonies have no significant effect on the total number of osteoclasts. Clohisy et al. (1996a) have investigated the changes in osteoclast numbers after intrafemural injection of the osteosarcoma cell line 2472 into C3H/He mice, showing that osteoclast numbers increased from 6 to 9 days post tumour cell injection compared to sham injected bones. However, osteoclast numbers dropped at a later time point (day 12) whereas detection of osteolysis was significant from day 9 onwards. It is important to mention that osteosarcoma is a primary bone tumour and is likely to be more aggressive than bone metastases from solid tumours such as breast cancer.

In contrast to the current perception of breast cancer-induced bone disease, the presence of cancer colonies also had a dramatic effect on the total number of bone forming osteoblasts. The changes in osteoblast number were of a biphasic nature with

a sharp increase at day 15, at a time when tumour burden is moderate, followed by a substantial reduction by day 19. Bone remodelling in healthy individuals is a well-controlled process with coupled cycles of bone resorption followed by bone formation (Mundy et al., 1997). Our data suggest that these interactions are disrupted during the early tumour growth stages (day 15) prior to detection of excessive bone resorption. The Ob/Oc ratio was disrupted at this early time point, and when overt osteolysis was present (EOP). Interestingly it has been shown that a co-culture of the human breast cancer cell line MCF-7 with mouse marrow cells is only capable of inducing osteoclastogenesis when osteoblasts were present (Thomas et al., 1999). Although I could detect major changes in the numbers and ratios of bone cells during tumour progression, the bone forming or resorbing activity of these cells is ultimately key to determining the downstream biological effect. Measurements of PINP indicated that the increase in osteoblast numbers on day 15 did not induce increased bone formation. This suggests either that some of the osteoblasts at day 15 are inactive, or less active than in a healthy setting. However, it is unclear if the detection of systemic PINP can reflect the locally (in the tumour bearing bone) induced changes in bone cell numbers.

Since breast cancer colonies in bone had a significant effect on total bone cell numbers, I next investigated if direct contact between bone and tumour cells was required to initiate these changes. In this respect it is noteworthy that the spatial relationship between different cell types is not often taken into account, and it is unclear how far secreted molecules can diffuse in bone *in vivo* at a concentration high enough to induce cellular changes. I therefore analysed the changes of osteoblasts and osteoclasts in two categories: 1) Oc and Ob numbers in direct contact with cancer cells and 2) Oc and Ob numbers not in direct contact with the tumour colony. Direct cell-cell contact was found to be required to increase osteoclast numbers, possibly explaining the focal induction of osteolytic bone disease. In published studies this local tumour-effect is not taken into consideration and only the overall number of osteoclasts is investigated (Phadke et al., 2006; Chantry et al., 2010). Based on the present results it may therefore be important to distinguish between the proximity of bone cells to tumour cells, especially in the increasingly relevant studies of early metastatic events. Surprisingly, the presence of tumour cells had the opposite effect on osteoblast

numbers when analysed depending on tumour cell contact, with significantly increased osteoblast numbers present in bone away from the tumour. The tumour therefore appears to have a localised effect but also modifies more distal areas of the same tumour bearing bone, indicating the involvement of soluble as well as surface molecules. However, it is not clear if these changes occurred due to tumour-mediated factors or if they are initiated as a downstream effect of the local cancer-induced changes in bone turnover. The differential expression of anti-osteoblastic molecules, including DKK-1 and noggin, by osteolytic but not osteoblastic cancer cell lines has been reported by Schwaninger et al. (2007) indicating that tumour cells can also affect osteoblasts directly, thus enhancing the bone destructive nature of the tumour.

I further aimed to assess this question by analysing selected soluble murine and human molecules as well as more local effects of the tumour on the microenvironment. When aiming to investigate whether soluble factors (RANKL, sclerostin) on a systemic level could be responsible for the changes in bone cell number, the data was in agreement with the μCT data showing that the tumour has a localised, not a systemic effect. *In vitro* studies have investigated the molecular pathways involved in cancer cell-bone cell interactions by measuring effects on secreted molecules. Kinder et al. (2008) assessed whether osteoblasts produce a specific range of osteoclast activating cytokines after stimulation with MDA-MB-231 breast cancer cells. When osteoblast cultures were treated with conditioned medium taken from MDA-MB-231 cells or when co-cultured with the breast cancer cell line, an inflammatory stress response of the osteoblasts was detected. MDA-MB-231 cells induced an increased expression of osteoblastic IL-6, IL-8 and MCP-1, molecules that have been previously shown to activate osteoclasts. I have therefore analysed the effect of osseous tumour growth on the murine cytokines IL-1α, IL-1β, IL-6, KC and MCP-1, but no statistically significant differences were found.

Since none of the above discussed soluble factors appeared to be responsible for the changes seen in Ob and Oc numbers, I further analysed the more local effect of the tumour colony on the microenvironment. Initially, Oc size was measured since it has been reported to be an in indicator of osteoclast activity (Trebec et al., 2007). Indeed, osteoclasts in direct contact with cancer cells were significantly larger than those away from the tumour, suggesting direct effects of the tumour on the osteoclasts. In

addition, gene expression levels of bone related genes were analysed in osseous tumours, which were compared to subcutaneous and *in vitro* samples. The elevated DKK1 and SFRP1 levels in the osseous tumour samples could explain the decrease in osteoblast number and the associated increase in osteolytic bone disease at day 23. The data support a recent finding by Secondini et al. (2011) who reported a reduction in bone formation as well as resorption after intraosseous implantation of the osteolytic prostate cancer cell line PC3. Interestingly, the anti-osteoblastic effect could be inhibited when noggin-silenced cells were used. SFRP1 is a soluble antagonist of the Wnt pathway and has recently been associated with reduced bone formation *in vivo* (Yao et al., 2010). MDA-MB-231-GFP cells growing in bone may therefore have the ability to further deregulate normal bone remodelling processes. In addition, the sharp upregulation of tumour RANKL could explain the local effect on osteoclast numbers but should be investigated in more detail.

Together the data investigating systemic changes in molecules affecting bone cells (RANKL, sclerostin, cytokines), the analysis of bone turnover markers (PINP) and more local tumour gene expression studies strongly suggest that the alteration in osteoclast and osteoblast numbers are due to spatially defined changes possibly only taking place within the tumour bearing bone compartment. In agreement with the present work is a study published in 2006 analysing the kinetics of bone colonisation of human breast cancer cells following intra-cardiac injection (Phadke et al., 2006). Although MDA-MB-435 cells were used, the precise origin of which has been the subject of conflicting reports (Chambers et al., 2009), the results agree with my findings in several ways. Histological changes of osteoblasts and osteoclasts at 0, 2 and 4 weeks post tumour cell injection were analysed and tumour colonies found to localise to the metaphysis of both femur and tibia. However, whether bone cells changed differentially according to the degree of direct contact to the tumour was not determined. Oc and Ob numbers were unchanged 2 weeks post cancer cell injection compared to day 0, but no age-matched naïve animals were used for comparison. In line with my study, further growth of the tumour up to 4 weeks reduced Ob numbers dramatically ($p<0.001$ vs. day 0 control). Interestingly, a significant increase in apoptotic osteoblasts was detected 6 weeks after MDA-MB-231-GFP cell injection, possibly contributing further to the osteolytic potential of the tumour (Phadke et al., 2006).

The second part of this chapter investigated whether peripheral tumour growth is able to affect bone turnover. Taken together, the data obtained from the subcutaneous tumour study supported the results obtained from the bone study suggesting that only tumour cells within a bone compartment are able to cause detectable changes to factors relevant to bone health.

In summary, this is the first demonstration that a pronounced tumour-mediated effect on osteoblasts and osteoclasts takes place prior to the formation of overt osteolytic bone disease, and that the extent of these depend on the degree of contact between bone and tumour cells. In support of this was the finding that bone integrity was unaffected by tumour growth in the opposite leg or at a peripheral site. Our data therefore suggest that the effects on bone cells are of a localised nature and that therapeutic targeting of the early steps in this process is likely to be required to eradicate bone metastasis.

5. Early administration of a single dose of combination therapy induces sustained inhibition of metastatic breast tumour growth in bone *in vivo*

5.1 Summary

Cancer-induced bone disease is associated with poor outcome and patients will often receive palliative treatment with bone sparing drugs like bisphosphonates in addition to the standard anti-cancer therapy. *In vitro* and *in vivo* studies have reported synergistic anti-tumour effects after administration of the chemotherapeutic agent doxorubicin followed 24 hours later by the bisphosphonate zoledronic acid. However, the effects of the sequence- and schedule-dependent combination treatment administered during early stages of breast tumour growth in bone, as well as the effects on the bone microenvironment, remain to be elucidated.

The aim of this study was to investigate the anti-tumour effects of a clinically relevant single administration of doxorubicin (2 days post MDA-231-GFP inoculation) followed 24 hours later by zoledronic acid, in a mouse model of breast cancer metastases to bone. Tumour size and bone integrity were investigated at two separate time points, 15 and 23 days after tumour cell injection. Direct effects on the tumour were assessed by quantification of apoptotic and proliferating cells and changes in expression of genes implicated in apoptosis, proliferation and bone turnover. Effects on the bone microenvironment were investigated by histomorphometry and analysis of soluble bone-derived molecules in serum.

Results from this study are the first to show sustained inhibition of tumour growth and bone protection after early administration of a single dose of dox then zol compared to single agents and PBS control. The combination treatment induced an increase in apoptotic tumour cells as well as substantial changes in osteoblast and osteoclast numbers. Importantly, tumour-induced changes in bone cell numbers were inhibited by combination treatment with a significant decrease in both cell types compared to tumour bearing controls.

The data suggest that a single dose of dox then zol significantly protects bone integrity and reduces tumour growth in bone, but that even early administration of combination therapy is not sufficient to eliminate bone metastases.

5.2 Introduction

Metastatic breast cancer is currently incurable and patients with diagnosed bone metastases often only receive palliative treatment like radiation therapy and bisphosphonates (BPs). In addition to their well-established anti-resorptive activities data is emerging that especially amino-bisphosphonates (NBPs) exhibit anti-cancer effect. There is an ongoing debate, however, whether the anti-tumour effects are of a direct or indirect nature and it is often argued that the local concentration of free NBPs is too low to affect cells other than the bone resorbing osteoclasts. In theory, NBPs can affect every cell type through the inhibition of the ubiquitous mevalonate pathway ultimately leading to apoptosis. Several *in vitro* (Neville-Webbe et al., 2002) and *in vivo* (Brown et al., 2009) studies have shown beneficial effects of BPs alone or in addition to standard therapy, of a variety of tumours in and outside bone. A comprehensive comparison of the bone studies suggests that improved outcome could be obtained with an earlier BP treatment schedule than that currently in place for metastatic bone disease (Brown et al., 2009). The results from Chapter 4 are in line with this observation, showing that even small tumour colonies induce major changes to the microenvironment before overt osteolysis is detected. Early intervention may therefore be necessary to inhibit homing and growth of the tumour cells at the metastatic site.

The clinical relevance of bisphosphonates as anti-cancer agents has been subject to considerable debate and results relating to anti-tumour effects from clinical trials of bisphosphonates have been conflicting with some reporting direct anti-tumour effects (Diel et al., 1998; Diel et al., 2008) and some not (Saarto et al., 2001). The clinical trials data reflect the variable responses to bisphosphonates reported in *in vivo* studies, with the majority of reports observing anti-tumour effects and few reporting either no effect or increased cancer cell growth. Despite the inconsistent reports of the benefits of bisphosphonate treatment alone, most studies using BPs in combination with standard therapies have shown beneficial effects of bisphosphonate co-administration Brown et al., 2009).

In order to treat metastatic bone disease effectively it may therefore be important to target both the tumour, for example with cytotoxic drugs, and the bone microenvironment, for example with bisphosphonates or denosumab. In this respect,

several *in vivo* studies have investigated the activity of the sequence- and schedule-dependent treatment of doxorubicin followed 24 hours later with zoledronic acid. A dosing regimen of weekly injections for a total of 6 weeks induced significant reduction in s.c. MDA-MB-436 xenografts (Ottewell et al., 2008b; Ottewell et al., 2010), osseous breast tumours (Ottewell et al., 2009) and inhibited spontaneous development of mouse mammary tumours (Ottewell et al., 2011). However, the clinical relevance of these studies is debatable since patients currently receive zoledronic acid only once every 3-4 weeks compared to the 6 weekly doses and agents are given on the same day rather than in a 24-hour schedule. The here presented study and one report by Ottewell et al. (2008a), who investigated the effect of doxorubicin (weekly for 2 weeks) and a single injection of zoledronic acid (24 hours after the first doxorubicin injection) on advanced breast tumours in bone are therefore more clinically relevant. A detailed overview of the previously performed studies using the sequence- and schedule-dependent combination therapy is shown in Table 5.1. Despite the comprehensive analysis undertaken in these studies, only little is known about the treatment-induced changes associated with early stages of tumour growth in bone and the effects on the bone microenvironment.

	Effects of combination therapy on the tumour			Effects of combination therapy on bone		
***In vivo* model**	**Size**	**Proliferation**	**Apoptosis**	**Trabecular bone volume**	**Oc number**	**Ob number**
B02 lesions in bone (Ottewell et al., 2008a)	↓ intraosseous No effect on extraosseous	↓ intraosseous No effect on extraosseous	↑ intraosseous ↑ extraosseous	↑	n.a.	n.a.
MDA-MB-436 intratibial (Ottewell et al., 2009)	↓ intraosseous	↓ intraosseous	↑ intraosseous	n.a.	↓	n.a.
MDA-MB-436 s.c. (Ottewell et al., 2008b)	↓	↓	↑	↑	n.a.	n.a.
MDA-MB-436 s.c. (Ottewell et al., 2010)	↓	↓	↑	n.a.	↓	n.a.
PyMT mammary fat pad (Ottewell et al., 2011)	↓	↓	↓	↑	n.a.	n.a.

Table 5.1 Overview of *in vivo* studies using combination therapy with doxorubicin followed by zoledronic acid

The table summarises the effects of combination therapy compared to vehicle control on tumour (size, proliferation, apoptosis) and bone (bone volume, osteoclast (Oc) and osteoblast (Ob) number on trabecular bone) for each study. Note the lack of investigation into the indirect treatment effects on bone cell (n.a=not analysed).

The here presented study investigated whether early administration of a single, clinically achievable dose of zoledronic acid in combination with doxorubicin is sufficient to reduce breast tumour growth inside and outside the bone marrow cavity of immunocompromised mice. Treatment-induced effects on tumour and bone cells were analysed in detail. To do this, the experiment was terminated at day 15 and 23, time points at which major tumour-induced changes to bone cell numbers were detected (Chapter 4)

5.3 Aims

The main aims of the here presented chapter were as follows:

- Does a clinically relevant dosing regimen of a single dose of combination therapy reduce osseous tumour burden and improve bone integrity compared to single agents and PBS control when administered early (day 2)?
- Can the anti-tumour effects be attributed to effects on the bone environment (osteoblasts and osteoclasts) and/or is the tumour affected (apoptosis, proliferation) at the assessed time points?
- Are systemic changes in pro-inflammatory cytokine levels affected by the treatment and are these connected to any changes in tumour growth and bone cell numbers?
- Can tumour colonies in bones of treated mice be used for gene expression analysis and are changes in gene expression still detectable 21 days after treatment?

5.4 Materials and Methods

Detailed information can be found in the Materials and Methods section (Chapter 2).

5.4.1 Tumour model and study protocol

All experiments were carried out in accordance with local guidelines and with Home Office approval under project license 40/2972 held by Professor N.J. Brown, University of Sheffield, United Kingdom.

To assess the effects of treatment on bone cell numbers in a non-tumour bearing environment, animals that had not developed tumours following injection with B02 cells (Chapter 3) were used. A total number of 24 non-tumour bearing animals (n=3/treatment group) that had received 1) PBS, 2) doxorubicin (2mg/kg i.v.), 3) zoledronic acid (100µg/kg s.c.) and 4) doxorubicin followed 24 hours later with zoledronic acid at day 2 were sacrificed on day 10 or 15. Hind legs were collected and processed for histology. An overview of the experiment outline is shown in Figure 5.1. Note that 'doxorubicin followed 24 hours later with zoledronic acid' treatment will further be abbreviated to 'combination' treatment.

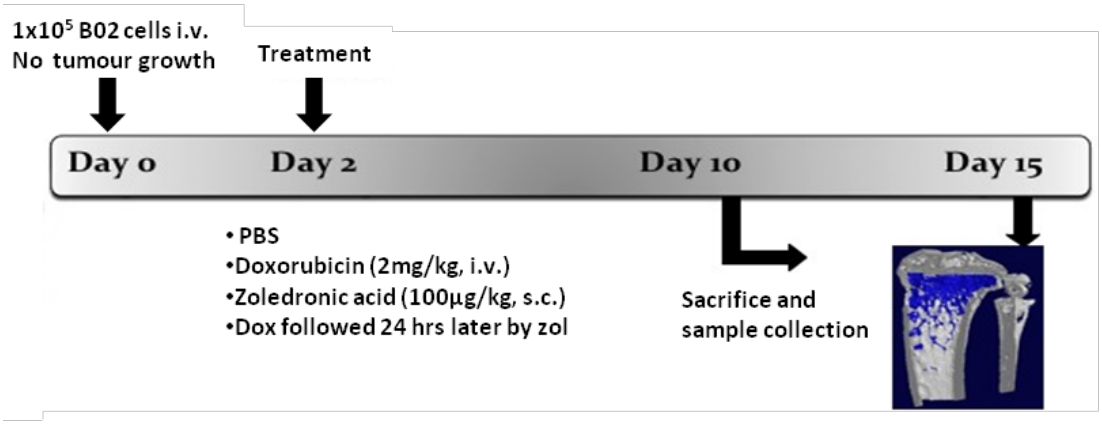

Figure 5.1 Schematic study protocol of experiments assessing treatment-effects on non-tumour bearing bones

Balb/c nude mice (female, 6 weeks) were injected with B02 cells (i.v.) on day 0. None of the mice developed tumours. Treatment was initiated on day 2 and animals were sacrificed on day 10 or 15.

In the main part of the study, the effects of treatment on tumour bearing bones were investigated using a total of 100 mice with n=15 per treatment group on day 15 and n=10 per treatment group on day 23. MDA-MB-231-GFP cells ($1x10^5$) were injected directly into the left heart ventricle of 6-week-old female balb/c nu/nu mice under general anaesthesia. Animals were randomly grouped into 4 treatment groups: 1) PBS, 2) doxorubicin (2mg/kg i.v.), 3) zoledronic acid (100µg/kg s.c.) and 4) doxorubicin followed 24 hours later with zoledronic acid. Treatment was initiated 2 days post tumour cell injection (Fig. 5.2). Food was removed on day of sacrifice for at least 6 hours and blood was collected under deep non-recovery anaesthesia. For mice sacrificed on day 15, hind legs were scanned by µCT and then processed for histology. On day 23, right hind legs were processed as above while bone marrow and tumours of left hind legs were used for gene expression analysis. Table 5.2 summarises the number of animals included for each analysis method.

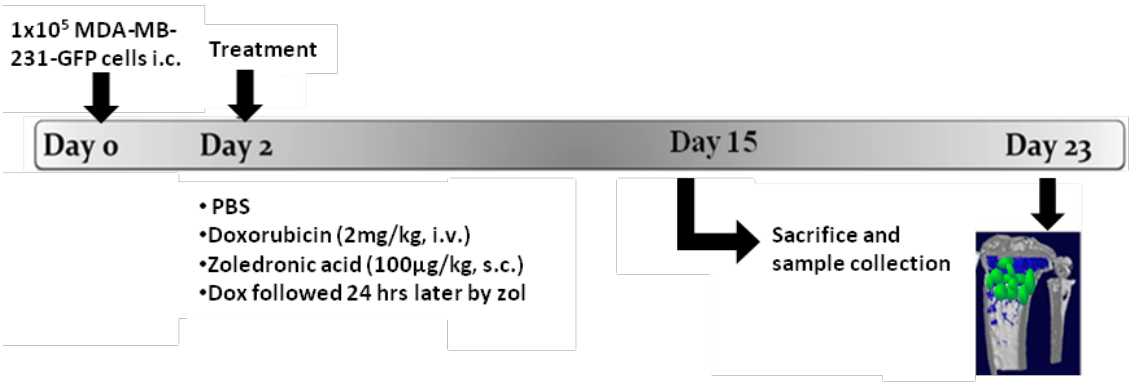

Figure 5.2 Study protocol of experiments assessing treatment-effects on tumour bearing bones

Balb/c nude mice (female, 6 weeks) were injected with MDA-MB-231-GFP cells on day 0. Treatment was initiated on day 2 and animals were sacrificed on day 15 or 23.

Day 15	Osseous tumour detection (GFP)	Bone integrity (µCT)	Tumour area (H&E)	Bone cell number (TRAP)	Apoptosis and proliferation (Casp3, Ki67, BrdU)	Bone resorption (CTX)	Bone formation (PINP)	CBA
PBS	8	6	7	7	7	7	3	8
Dox	6	6	5	5	5	6	3	6
Zol	8	6	8	8	8	7	3	8
Dox/Zol	8	7	4	4	3	8	3	8

Day 23	Osseous tumour detection (GFP)	Bone integrity (µCT)	Tumour area (H&E)	Bone cell number (TRAP)	Apoptosis and proliferation (Casp3, Ki67, BrdU)	Bone resorption (CTX)	Bone formation (PINP)	CBA
PBS	7	3	7	6	7	6	7	7
Dox	5	3	5	3	3	3	5	5
Zol	5	3	5	5	5	5	5	5
Dox/Zol	6	3	6	6	6	5	6	6

Table 5.2 Summary of the number of mice included in analyses
The table shows the number of animals with detectable GFP positive bone tumours on day of sacrifice (day 15 or 23) and the number of animals included in analyses. CBA=cytometric bead array.

5.4.2 Measurement of tumour area

Histological sections (3µm) of decalcified hind legs were stained with H&E and analysis was carried out using Osteomeasure software. Tumour area (mm^2) was measured on 2-3 non-serial sections per sample by drawing around all visible tumour foci. Intra- and extraosseous tumour areas were scored separately.

5.4.3 Immunohistochemistry

For immunohistochemical analysis of tumour cell apoptosis and proliferation, two non-serial sections per tumour sample were stained for BrdU (day 15), Ki67 (day 23) and caspase-3 (day 15 and 23). The number of DAB positive cells per mm^2 tumour area was scored using a Leica BMRB upright microscope and Osteomeasure software with a 10x objective. Intra- and extraosseous tumour areas were scored separately. Note that different markers for tumour cell proliferation were used on day 15 and 23 due to changes in project licence regulations.

Osteoclast and osteoblast numbers on trabecular bone surfaces were scored on TRAP stained sections as described earlier. At least two non-serial sections were analysed per sample.

5.4.4 Determination of serum bone remodelling markers by ELISA and cytokine levels by cytometric bead array (CBA)

The bone remodelling markers CTX and PINP were measured in serum collected from mice following 6 hours of fasting. CBA analysis of murine IL-1α, IL-1β, IL-6, KC (IL-8) and MCP-1 was also carried out. The CBA protocol was carried out by the Flow Cytometry Core Facility, University of Sheffield and to the manufacturer's instructions and the assay was shown to be species specific for detection of mouse cytokines.

5.4.5 Gene expression analysis by qRT-PCR

The TaqMan® PreAmp Cells-to-CT™ Kit (Applied Biosystems) was used for sample preparation prior to qRT-PCR analysis on individual gene products using the ABI Prism 7900HT Sequence Detection System and FAM labelled probes (species specific TaqMan® assays, Chapter 2). The human TaqMan® assays used in this study have previously been shown to not cross-react with corresponding mouse genes (tested by Dr JK Woodward and in Ottewell et al., 2009).

5.4.6 Statistical analysis

Prism GraphPad (Version 5.0a) was used for all statistical analysis. Analysis was by t-test or one-way ANOVA followed by Tuckey post-test. The applied test is indicated in each Figure legend. All data are shown as mean±SEM and differences have been interpreted as being significant at $p \leq 0.05$.

5.5 Results

The present study investigated the effect of a clinically relevant dose of doxorubicin administered 24 hours before zoledronic acid on breast tumour growth in bone. In addition to the assessment of tumour size and bone integrity, the effects of the treatment on the bone microenvironment (Ob and Oc) and measurement of bone remodelling markers and cytokines in serum were investigated.

5.5.1 A single administration of zoledronic acid is sufficient to protect bone

Following sacrifice, the location and number of tumours was assessed. Hind legs were excised and stripped of muscle before visualising the GFP positive tumour colonies. Tumour growth was detected in hind legs of mice from all treatment groups suggesting that none of the treatments completely prevented tumour growth. Foci were generally located around the knee joint in the proximal tibia and/or distal femur (Fig. 5.3).

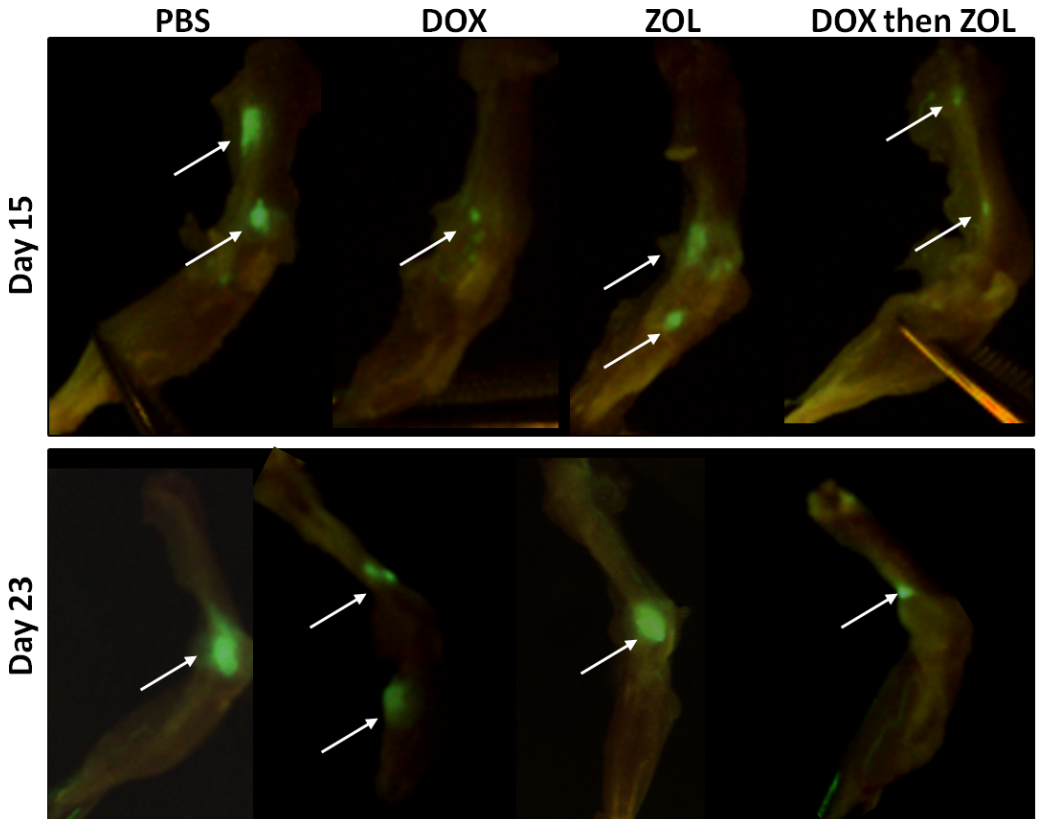

Figure 5.3 Visualisation of tumour growth in bone by GFP
Example images of hind legs with confirmed tumour growth (green, arrow).

µCT analysis revealed that a single dose of zoledronic acid administered two days post tumour cell injection significantly increased trabecular bone volume at both investigated time points when compared to PBS or single agents (zol 29.24% and dox then zol 22.43% vs. PBS 8.4%, both $p<0.001$ on day 15; zol 28.09% and dox then zol 32.39% vs. PBS 6.1%, both $p<0.001$ on day 23, Fig. 5.4A). It was furthermore shown that doxorubicin did not reduce trabecular bone volume when compared to PBS control animals at any time point. Further analysis also showed increased trabecular number (Fig. 5.4B) in the zol only and combination treatment group when compared to animals receiving dox or PBS. Only small changes in trabecular thickness (Fig. 5.4C) were detected. Example radiographs and cross sections are depicted in Figure 5.5.

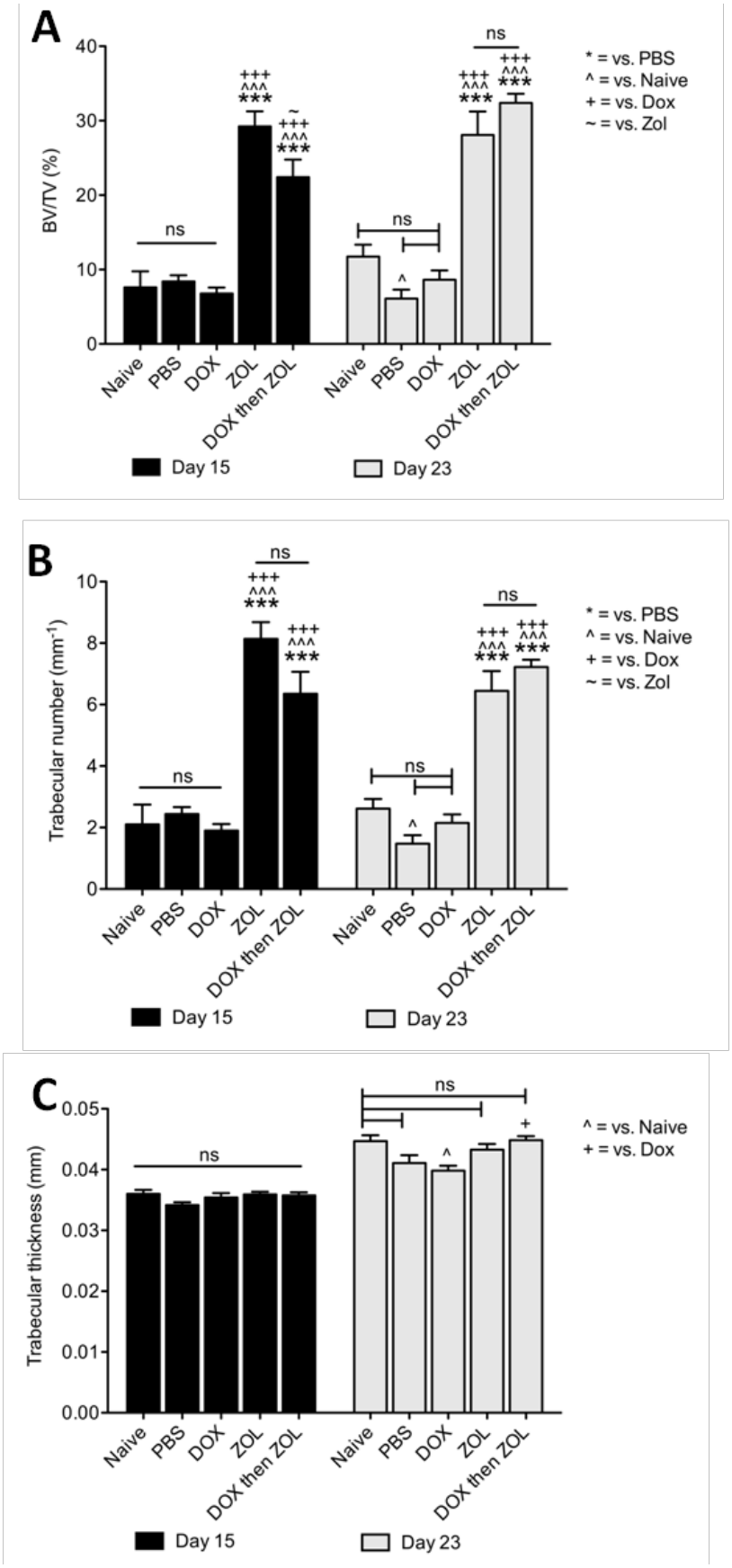

Figure 5.4 Quantification of trabecular bone volume, number and thickness
Analysis of osteolytic bone disease was carried out for the proximal tibia and the distal femur. Quantification of A) trabecular bone volume per tissue volume (BV/TV) B) trabecular number and C) trabecular thickness for animals sacrificed on day 15 and day 23. One way ANOVA and Tuckey's post test, * is $p<0.05$, ** is $p<0.01$, *** is $p<0.001$.

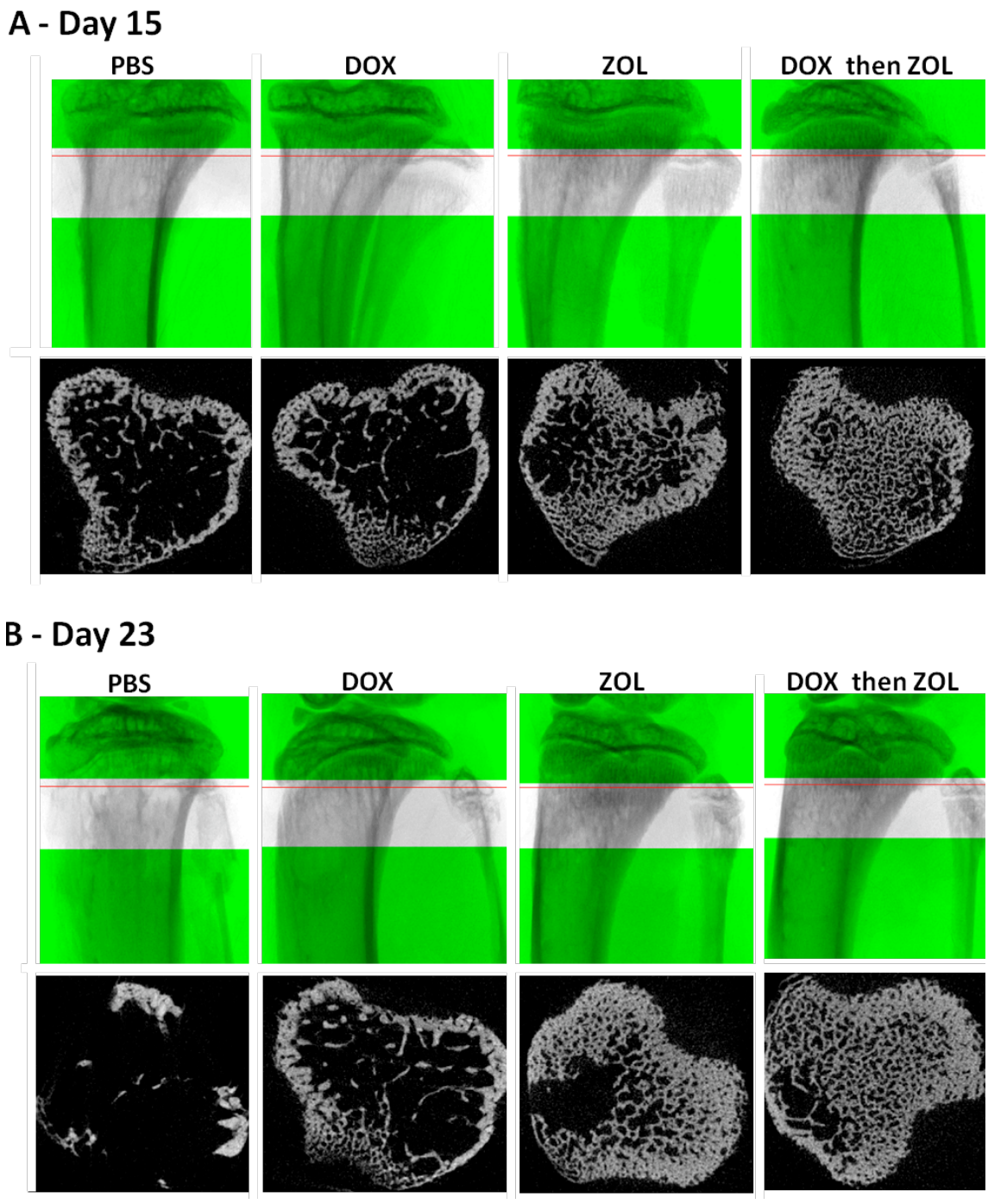

Figure 5.5 Representative µCT radiographs and cross sections
X-ray images taken from µCT scans of the proximal tibia are shown for A) day 15 and B) day 23. The bottom panels depict the corresponding cross sections (indicated by the red line on the radiograph).

5.5.2 A single dose of combination therapy induces sustained inhibition of tumour growth

Previous *in vivo* studies have shown that doxorubicin followed 24 hours later by zoledronic acid induced a significant reduction of tumour growth at various sites (Table 5.1). However, the majority of studies used a repeated dosing regimen with a total of 6 doses. As shown in Figure 5.6, a single, early dose of combination treatment was sufficient to effectively reduce bone associated tumour growth on day 15 compared to mice treated with PBS or zol alone (PBS 0.16mm^2 vs. dox then zol 0.03mm^2, $p<0.05$, Fig. 5.6A) and this was, importantly, also maintained on day 23 (PBS 0.97mm^2 vs. dox then zol 0.17mm^2, $p<0.001$, Fig. 5.6A), while single agents had no effect. The combination treatment was the only therapeutic strategy used in this study that induced a sustained anti-tumour effect. Doxorubicin alone inhibited total tumour growth transiently (day 15, PBS 0.16mm^2 vs. dox 0.04mm^2, $p<0.05$, Fig. 5.6A), but a single dose of the chemotherapeutic agent was not sufficient to affect later stages of tumour progression (day 23). Differential analysis of intra- vs. extraosseous tumour growth showed that the combination treatment had a major effect on intraosseous tumour growth with only 1 animal out of 6 having detectable tumour foci in the bone marrow cavity on day 23. In addition, extraosseous tumour growth in the combination group at day 15 was reduced by 29% ($p<0.05$) compared to that in animals receiving PBS. It is important to mention that the tumours in the combination group were separate tumour foci growing either inside or outside the bone marrow cavity, in the absence of osteolytic lesions, possibly suggesting that tumour growth was redirected from an intra- to an extraosseous site (Fig. 5.7 and 5.8). Surprisingly, mice receiving dox only injections had increased extraosseous tumour growth on day 23 compared to all other groups (dox 1.21mm^2 vs. PBS 0.3mm^2, $p<0.001$, Fig. 5.6 C).

Taken together, the data suggest that administration of combination treatment induced a sustained reduction in tumour growth, mainly affecting intraosseous tumours.

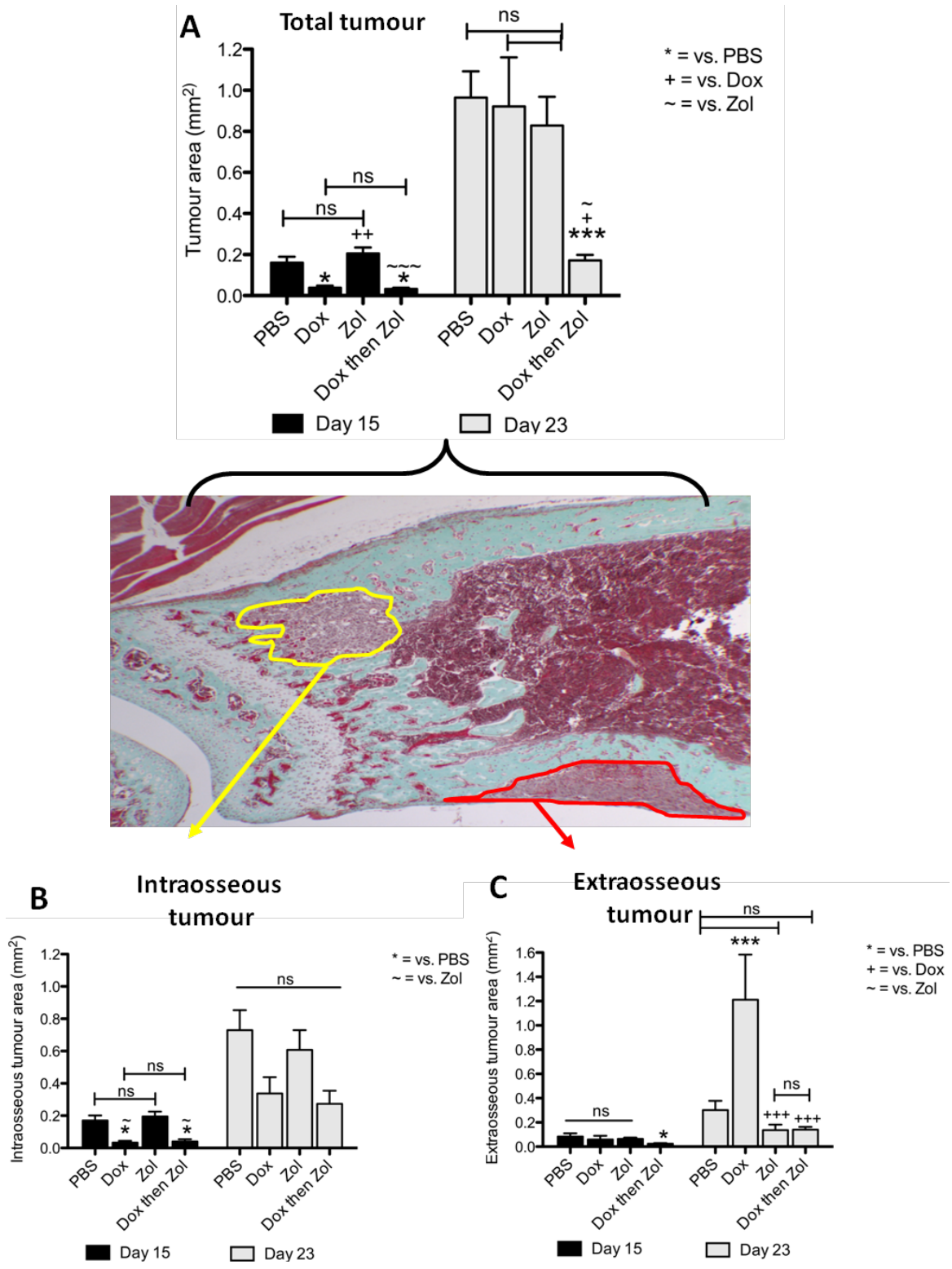

Figure 5.6 Treatment effects on MDA-MB-231-GFP tumour growth in bone

Analysis of tumour area (mm^2) was performed on a minimum of 2 non-serial sections per sample using a 4x objective. A) Total tumour, B) intraosseous tumour and C) extraosseous tumour area were measured. One way ANOVA and Tuckey post test, * is $p<0.05$,** is $p<0.01$, *** is $p< 0.001$, ns=not significant.

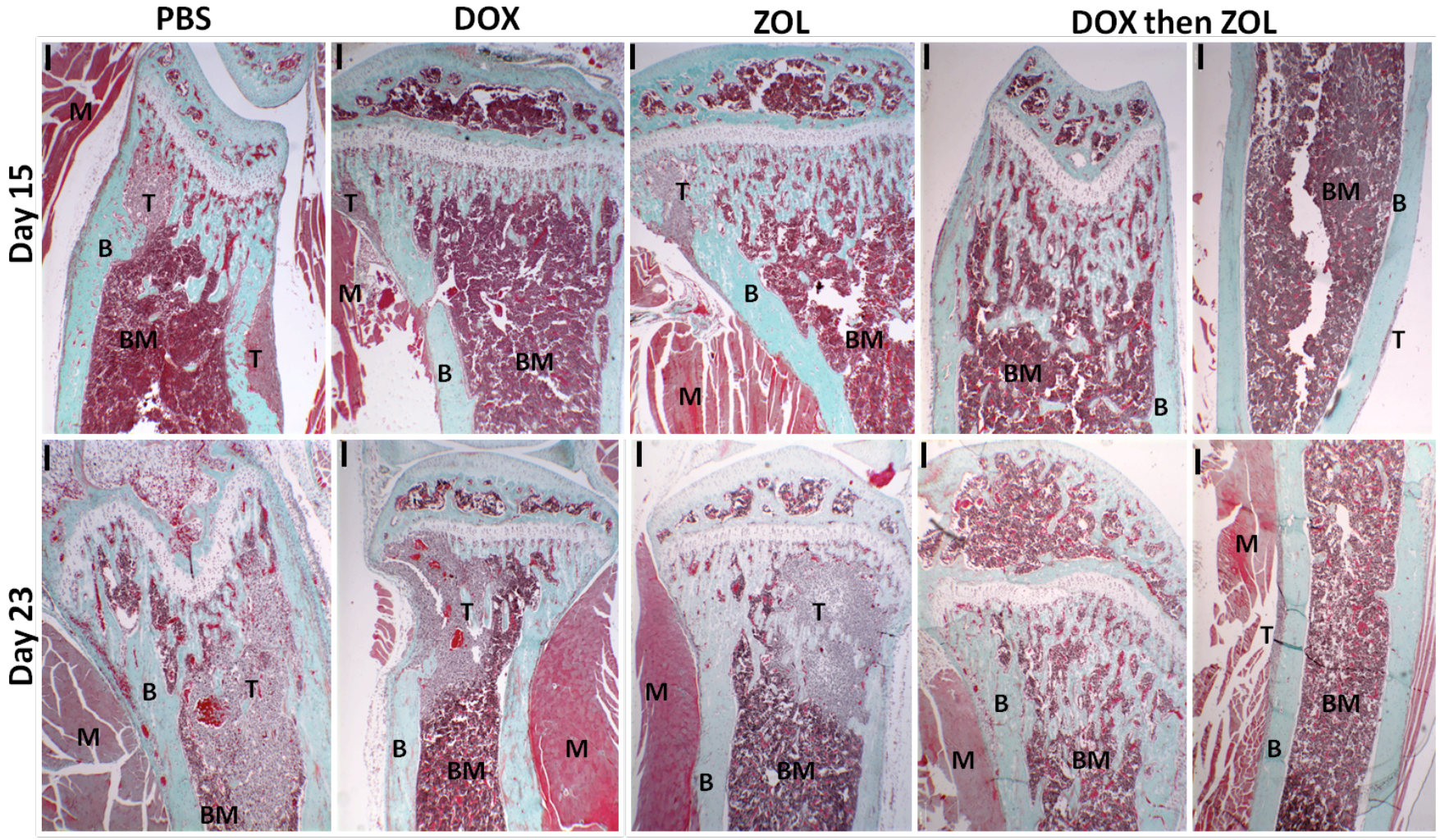

Figure 5.7 Visualisation of tumour growth on histological sections

Goldner's trichrome stained sections of tumour bearing bones depict size and location of tumour growth in bone (T=tumour, B=bone, BM=bone marrow, M=muscle). Note that tumours in the combination group where mostly localised on the periosteal surface along the diaphysis. Images of combination group shown here have only extraosseous tumour colonies. Scale bar=100µm, 1.6x objective.

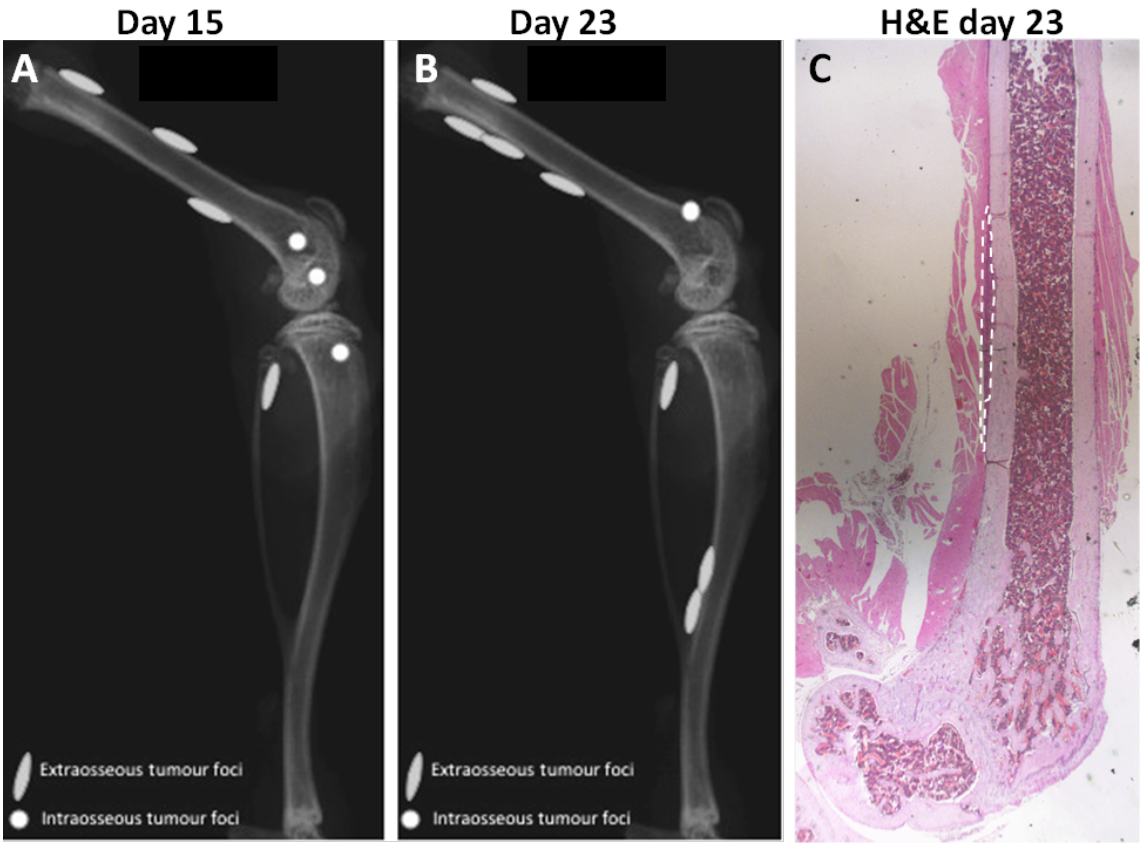

Figure 5.8 Schematic illustrations of approximate tumour foci distribution in mice receiving combination treatment

Schematic overview of tumour location in dox then zol treated mice on A) day 15 and B) day 23. Grey ellipses represent tumour foci detected outside the bone marrow cavity and white circles represent intraosseous tumour colonies. Note that the figure only shows the approximate location of the tumour and is not indicative of tumour size. C) H&E stained section of a femur taken on day 23 illustrating the location of an extraosseous tumour typically found in the combination treatment group (white dotted line).

5.5.3 Treatment-induced changes of the bone microenvironment – effects on osteoblasts and osteoclasts

In vivo studies investigating combination therapy have so far focussed on the treatment effect on human tumour cells (Table 5.1). The indirect anti-cancer effects of the schedule, like treatment-induced cellular alterations in the bone microenvironment, have been studied less extensively. In addition, it is unclear to which degree the combination treatment affects a tumour-free bone microenvironment. The present study therefore aimed to determine the effects of a single dose of combination therapy on bone cell numbers in a tumour free and a tumour bearing setting.

Non-tumour bearing animals administered with PBS, dox or zol alone or the combination treatment did not show any changes in either osteoblast or osteoclast number per mm trabecular bone surface on day 10. In contrast, there was a dramatic reduction in Ob number/mm bone in the zol only and the combination group on day 15 (PBS 10.21 vs. zol 1.63 and combination 1.74, both $p<0.001$, Fig. 5.9A, non-tumour bearing). Similar effects were seen in tumour bearing bones where zoledronic acid treatment inhibited the tumour-induced increase in osteoblast number seen in PBS control (zol 5.43 vs. PBS 13.59, $p<0.001$, Fig. 5.9A, tumour bearing) and induced further reductions at day 23 (zol 0.86 vs. PBS 3.04, $p<0.05$, Fig. 5.9A, tumour bearing).

In line with the reported anti-resorptive activity, zoledronic acid caused a reduction in osteoclast numbers in animals without tumour on day 15 (zol 4.22 vs. PBS 6.75, $p<0.05$, Fig. 5.9B, non-tumour bearing). However, this effect was not seen in animals with osseous tumours (Fig. 5.9B, day 15, tumour bearing), suggesting a delayed effect on cell number due to the presence of the tumour. This was surprising considering the zol-induced increase in trabecular bone volume detected by µCT at this time point (Fig. 5.4A). When investigating the later time point (day 23) osteoclast numbers of mice treated with zol or the combination treatment were found to be reduced with a significant change in the zol treated group compared to PBS control (zol 1.59 vs. 3.04, $p<0.01$, Fig. 5.7B, tumour bearing). Noticeably, and in agreement with the µCT data, a single dose of doxorubicin did not change the numbers of osteoblast or osteoclasts at any of the investigated time points when compared to PBS control.

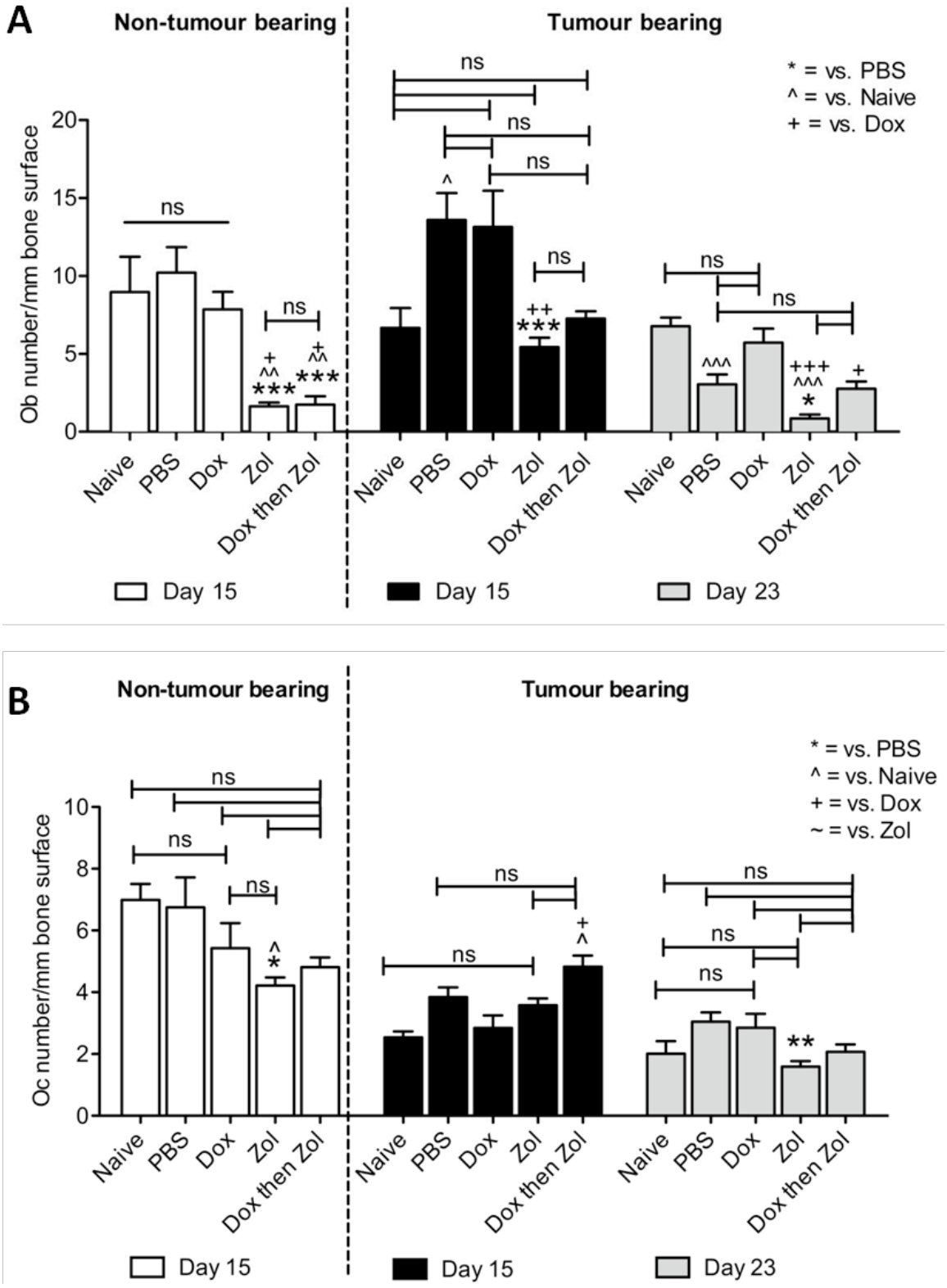

Figure 5.9 Treatment effects on osteoblasts and osteoclasts in a non-tumour bearing and a tumour bearing setting

Animals were treated with 2mg/kg dox, 100µg/kg zol or combination therapy on day 2. Osteoblast A) and osteoclast B) numbers were analysed per mm trabecular bone surface on a minimum of 2 non-serial TRAP stained sections per sample. One way ANOVA and Tuckey post test, * is $p<0.05$, ** is $p<0.01$ and *** is $p<0.001$ compared to PBS control, ns=not significant.

The % of trabecular bone surface in contact with osteoclasts may be a better representation of active bone resorption. However, when the data was presented in this way (Fig. 5.10A), a significant increase in osteoclast area in contact with bone was detected in zol only treated animals compared to the PBS controls on day 15 followed by no significantly different changes in any treatment group on day 23. The reason for this discrepancy may be due to the zoledronic acid-induced changes in osteoclast activity rather than number. Furthermore, the presence of large, multinucleated osteoclasts was noted when analysing the zol only and combination treated mice. Determination of osteoclast area in the total osteoclast population showed that zoledronic acid treated animals had significantly larger osteoclasts (measured in mm^2) compared to those of PBS control animals (PBS $1.9x10^{-4}mm^2$ vs. $3.3x10^{-4}mm^2$ on day 15, $p<0.001$ and PBS $2.3x10^{-4}mm^2$ vs. $3.7x10^{-4}mm^2$ on day 23, $p<0.01$, Fig. 5.10B). Location dependent analysis distinguishing between osteoclasts in contact or not in contact with tumour cells revealed that this effect was independent of osteoclast-tumour cell contact. Significantly larger osteoclasts in contact with tumour cells were detected following zol treatment on day 15 ($4.2x10^{-4}mm^2$) compared to control mice ($2.9x10^{-4}mm^2$, $p<0.001$) and on day 23 ($3.8x10^{-4}mm^2$ vs. $2.7x10^{-4}mm^2$, $p<0.01$, Fig. 5.10C). Furthermore, increased osteoclast area was found in cells away from the tumour in the zol group versus PBS treated mice (day 15: $2.9x10^{-4}mm^2$ vs. control at $1.6x10^{-4}mm^2$ and on day 23 with $2.6x10^{-4}mm^2$ vs. control at $1.6x10^{-4}mm^2$, both $p<0.001$, Fig. 5.10D). The administration of combination therapy only increased the size of those osteoclasts that were <u>not</u> in direct contact with the tumour on both day 15 ($2.2x10^{-4}mm^2$ vs. PBS: $1.6x10^{-4}mm^2$) and day 23 ($2.2x10^{-4}mm^2$ vs. PBS: $1.6x10^{-4}mm^2$, both $p<0.05$, Fig. 5.10D) when compared to PBS controls. The lack of changes in those cells in contact with the tumour can be attributed to the low sample number in the combination group at day 23. Collectively the data indicate an initial effect of zoledronic acid on osteoclast activity connected with morphological changes rather than a decrease in osteoclast viability. Example images of TRAP stained sections are shown in Figure 5.11.

Taken together, the data show that the bone targeting bisphosphonate has a substantial effect on bone cell numbers independent of the presence of malignant cells and may therefore counteract the tumour induced cellular changes to the bone microenvironment.

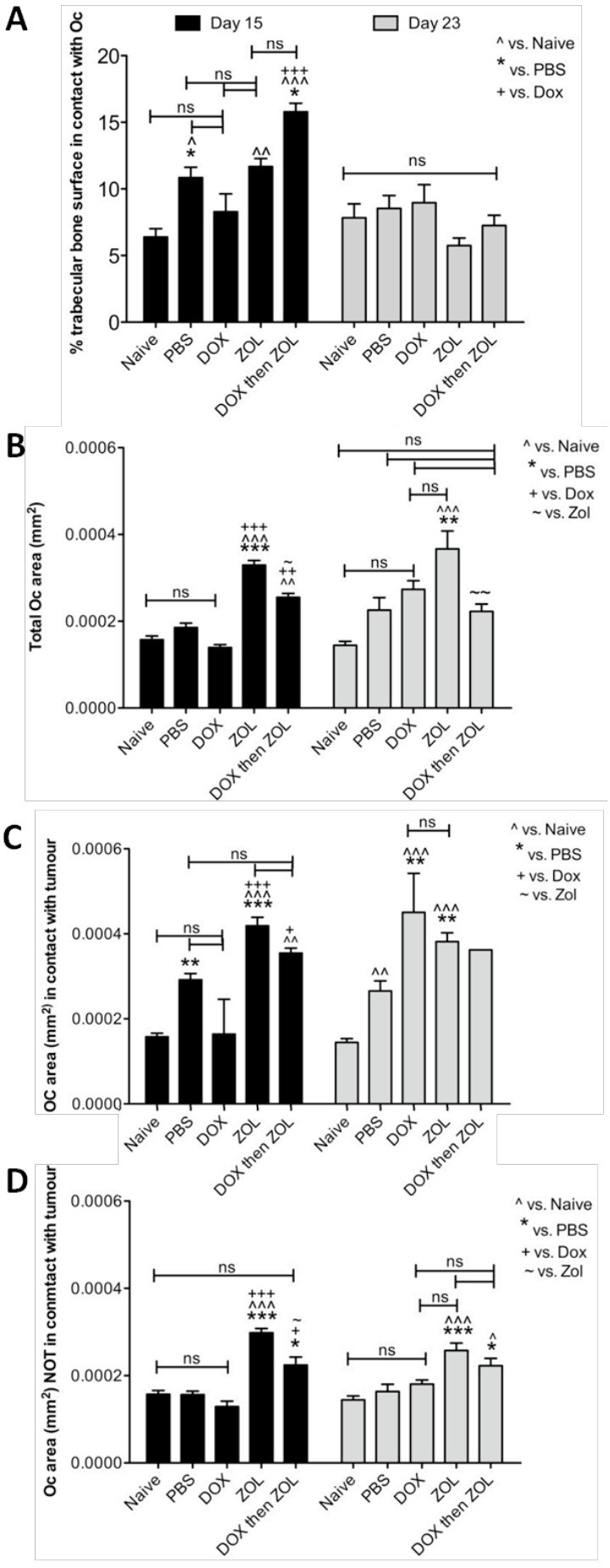

Figure 5.10 Investigation of treatment effects on osteoclast surface in contact with trabecular bone and osteoclast size

A) Analysis of the percentage of trabecular bone surface in contact with osteoclasts. B) Measurement of osteoclast size (expressed as mean area in mm^2) for the total

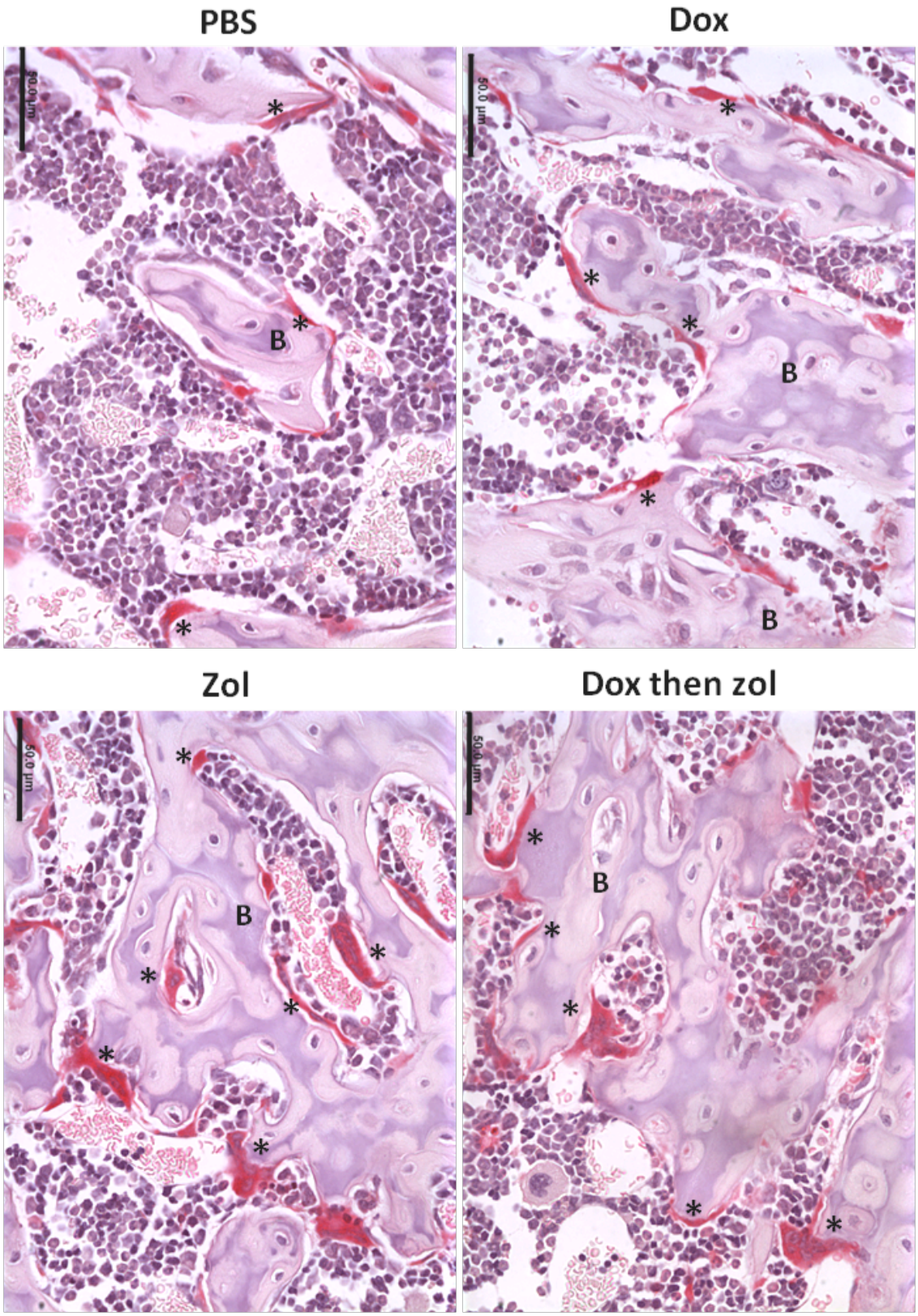

Figure 5.11 Example TRAP images

Example images of TRAP stained bone sections in the PBS, dox, zol, and combination group taken on day 23. B=bone, *=osteoclast, scale bar=50µm, 40x objective.

5.5.4 Treatment effects on bone cell activity – measurements of bone remodelling markers in serum

Although the detected changes in bone cell numbers following treatment give information on a cellular level, the data are not sufficient to conclude changes in bone remodelling activity. CTX and PINP ELISAs were therefore used to measure active bone resorption and formation, respectively, in serum from animals in each treatment group. Surprisingly, mice treated with zol alone had increased CTX levels on both day 15 and day 23 (Fig. 5.12A), although variability in the zol treated samples was high and no statistical significance was detected. The CTX data can therefore not explain the discrepancy between the increased trabecular bone volume (μCT) and the unchanged osteoclast numbers on day 15. When investigating the treatment effects on systemic PINP concentrations, significantly reduced levels were detected in zol only vs. PBS treated mice on day 15 (zol 22.8ng/ml vs. PBS 42.17ng/ml, $p<0.05$, Fig. 5.12B). This effect was, however, only transient since bone formation was restored on day 23. No change in osteoblast activity was seen after administration of combination therapy. Doxorubicin did not alter CTX or PINP levels at either time point, indicating that a single dose does not affect bone turnover. The data for zol only treated mice are in agreement with the histomorphometric quantification of osteoblast numbers on day 15 showing a drug-induced reduction in Ob number.

In summary the data suggest that PINP, but not CTX, may be used as a marker of treatment-induced bone remodelling in this model of metastatic bone disease. The results imply that zoledronic acid treatment alone induces a transient decrease in bone formation on day 15.

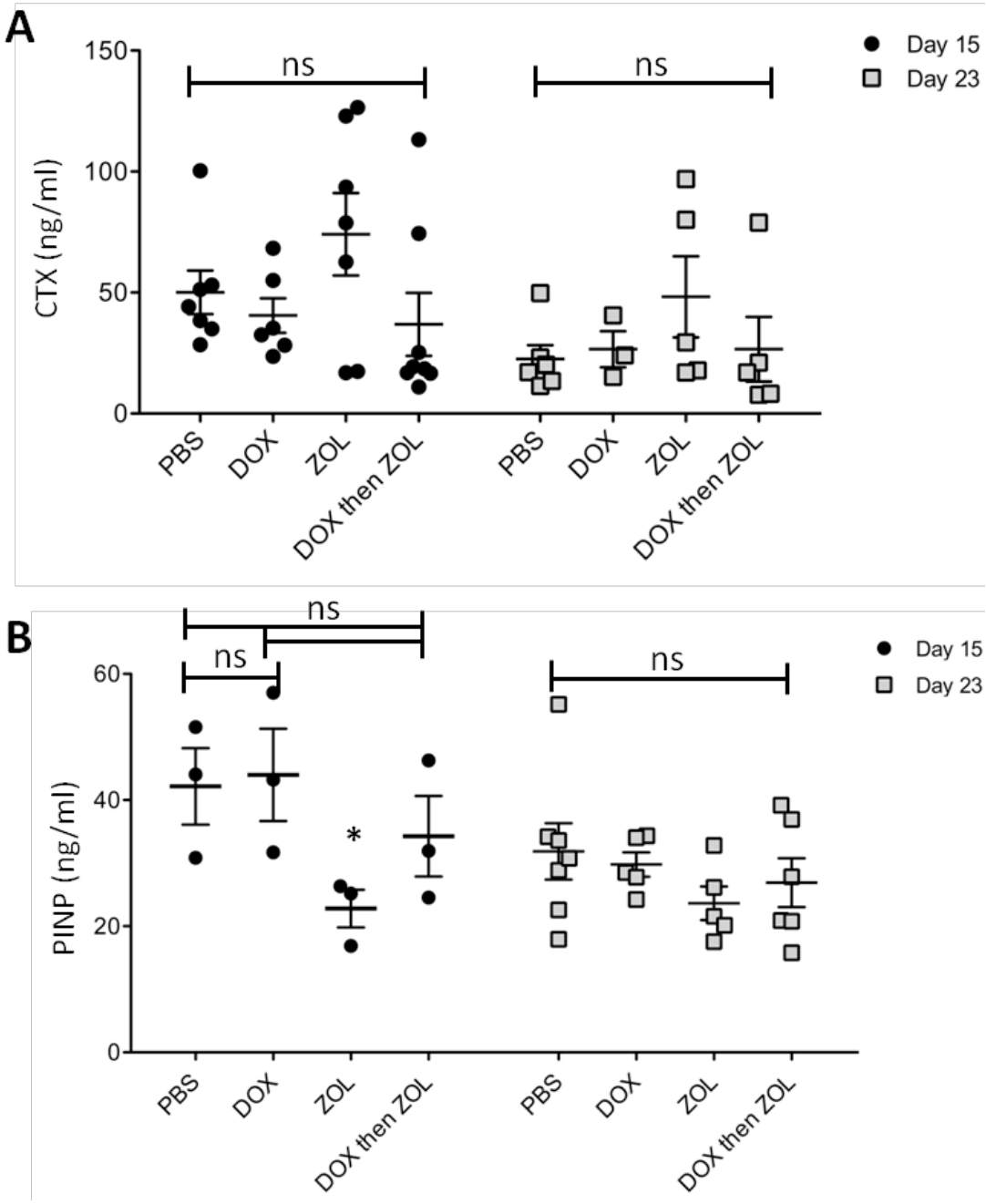

Figure 5.12 Serum levels of bone remodelling markers CTX and PINP

ELISA were performed on serum from starved animals for quantification of CTX A) and PINP B) levels. One way ANOVA, * is $p<0.05$ zol vs. PBS, ns=not significant. Each symbol represents the measurements from one mouse.

5.5.5 Effects of early sequential treatment with dox then zol on tumour cell proliferation and apoptosis

As shown in paragraph 5.5.2, a single dose of doxorubicin followed by zoledronic acid was sufficient to significantly inhibit breast tumour growth in bone over the course of the experiment. In order to investigate whether the observed reduction in tumour size was due to treatment-induced changes in apoptosis and/or proliferation, caspase-3, Ki67 and BrdU immunohistochemistry were performed. Quantification of active caspase-3 positive tumour cells on day 15 showed that only the combination treatment caused a significant increase in the number of apoptotic tumour cells (dox then zol 166.62 vs. PBS 83.64, $p<0.01$, Fig. 5.13A). This effect was lost over time as no difference between any of the groups was detected on day 23 (Fig. 5.13B). Differential analysis of intra- and extraosseous tumour areas showed that the increase in overall tumour cell death in the combination group was due to an increase in apoptosis in tumours growing outside the bone marrow cavity on day 15. The data are in agreement with the observed decrease in extraosseous tumour area on this day (Fig. 5.6B). In addition, doxorubicin mono-therapy increased the number of apoptotic tumour cells in the intra- but not the extraosseous tumour foci (Table 5.3), again mirroring the effects on tumour size on day 15 (Fig. 5.6B and C). No change in the number of caspase-3 positive tumour cells was observed in any treatment group on day 23 indicating that the effect on tumour cell apoptosis was only transient. Example images of caspase-3 stained sections are shown in Figure 5.14 and Figure 5.15.

	Day 15				Day 23			
	PBS	**Dox**	**Zol**	**Dox/Zol**	**PBS**	**Dox**	**Zol**	**Dox/Zol**
Apoptotic cells/mm^2 intra-osseous tumour	80.01 (11.83)	133.7* (19.14)	97.87 (6.66)	83.61 (23.18)	52.21 (5.41)	83 (10.58)	60.4 (6.70)	57.01 (0.35)
Apoptotic cells/mm^2 extra-osseous tumour	90.17 (16.71)	29.43 (14.03)	133.4 (43.19)	266.2* (45.15)	71.08 (7.24)	85.85 (12.54)	46.04 (21.02)	88.68 (15.99)

Table 5.3 Differential analyses of tumour cell apoptosis in intra- and extraosseous tumour areas

The table shows mean values and standard deviation (SD) of caspase-3 positive tumour cells/mm^2 intra or extraosseous tumour area. * is $p<0.05$ vs. the respective PBS control, one way ANOVA and Tuckey post test.

When analysing the effects of treatment on tumour cell proliferation, no change could be detected at any of the two time points investigated (Fig. 5.16 and Fig. 5.17). In addition, analysis of actively proliferating tumour cells in areas in or outside the bone marrow cavity showed no change compared to control or single treatments (Table 5.4).

	Day 15 –BrdU				Day 23 – Ki67			
	PBS	**Dox**	**Zol**	**Dox/Zol**	**PBS**	**Dox**	**Zol**	**Dox/Zol**
Proliferating cells/mm^2 intra-osseous tumour	769.5 (52.8)	990.7 (109.1)	894.3 (52.56)	733.4 (94.34)	1217 (68.53)	1051.0 (160.1)	1504.0 (133.3)	821 (34.64)
Proliferating cells/mm^2 extra-osseous tumour	1027 (162.7)	1272 (61.06)	1115 (146.2)	1104 (112.3)	2119 (168.6)	1983 (209.7)	1799 (255.5)	1972 (144.6)

Table 5.4 Differential analyses of tumour cell proliferation in intra- and extraosseous tumour areas

The table shows mean values and standard deviation (SD) of BrdU (day 15) and Ki67 (day 23) positive tumour cells/mm^2 intra and extraosseous tumour area. No significant difference between groups by One way ANOVA and Tuckey post test.

Collectively, anti-tumour activity was detected in the combination treatment group at day 15 in form of significantly increased apoptotic cell numbers as indicated by detection of active caspase-3, suggesting that a single dose of combination therapy is not sufficient to induce sustained effects on the tumour itself or that they may be transient and not be captured by the time points analysed in this study.

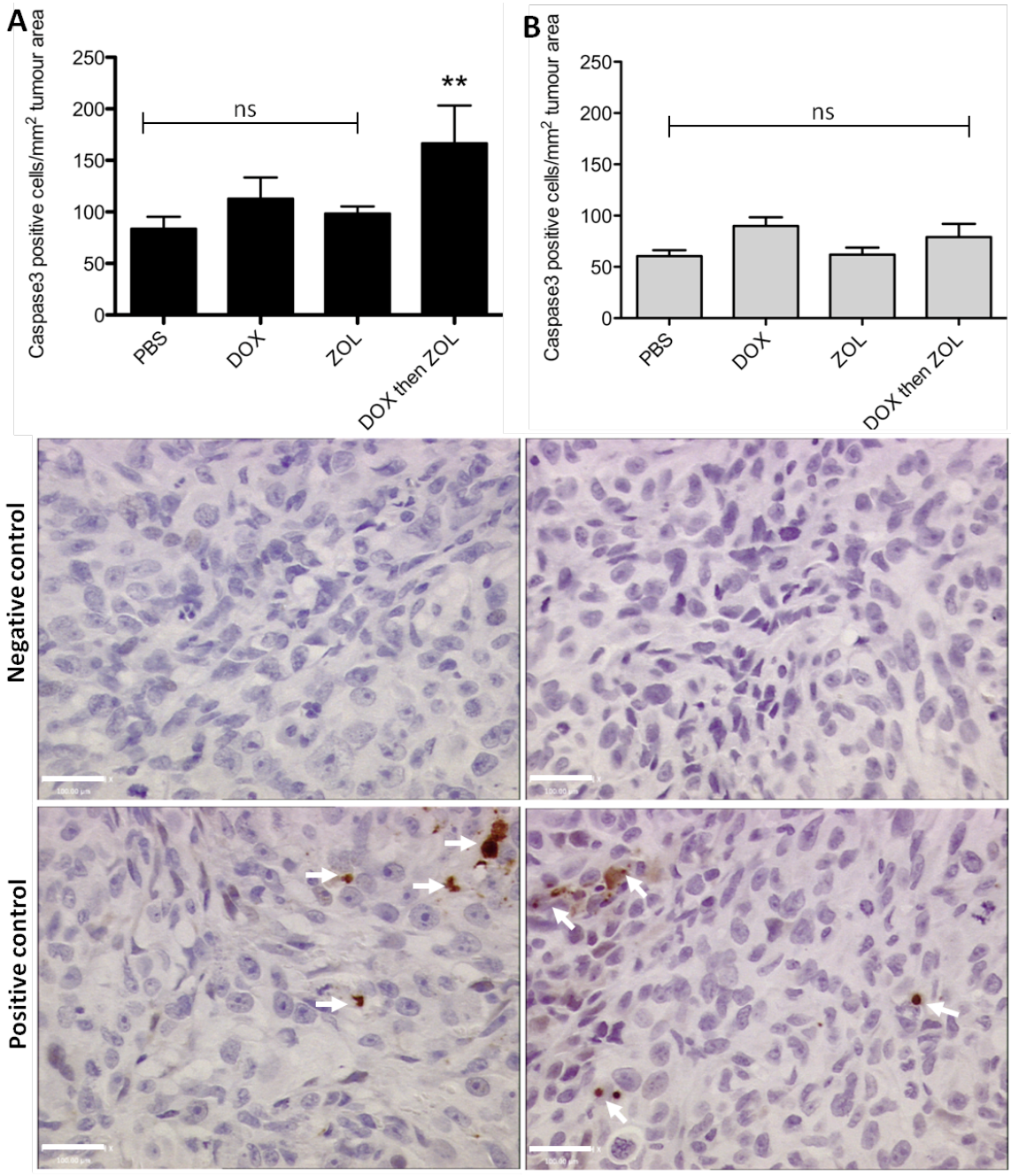

Figure 5.13 Quantification of treatment-induced changes in tumour cell death

Histological sections were stained for human active caspase-3 to detect apoptotic tumour cells. At least 2 non-serial sections per sample were analysed. Data are expressed as number of caspase-3 positive cells per tumour area in mm^2. A) Day 15, B) day 23. One way ANOVA and Tuckey post test, ** is $p<0.01$ vs. PBS control, ns=not significant. Representative images of the negative (no primary antibody) and positive control (osseous tumour sections known to be positive for caspase-3) are shown. 40x objective, scale bar=100µm). Arrows indicate apoptotic tumour cells.

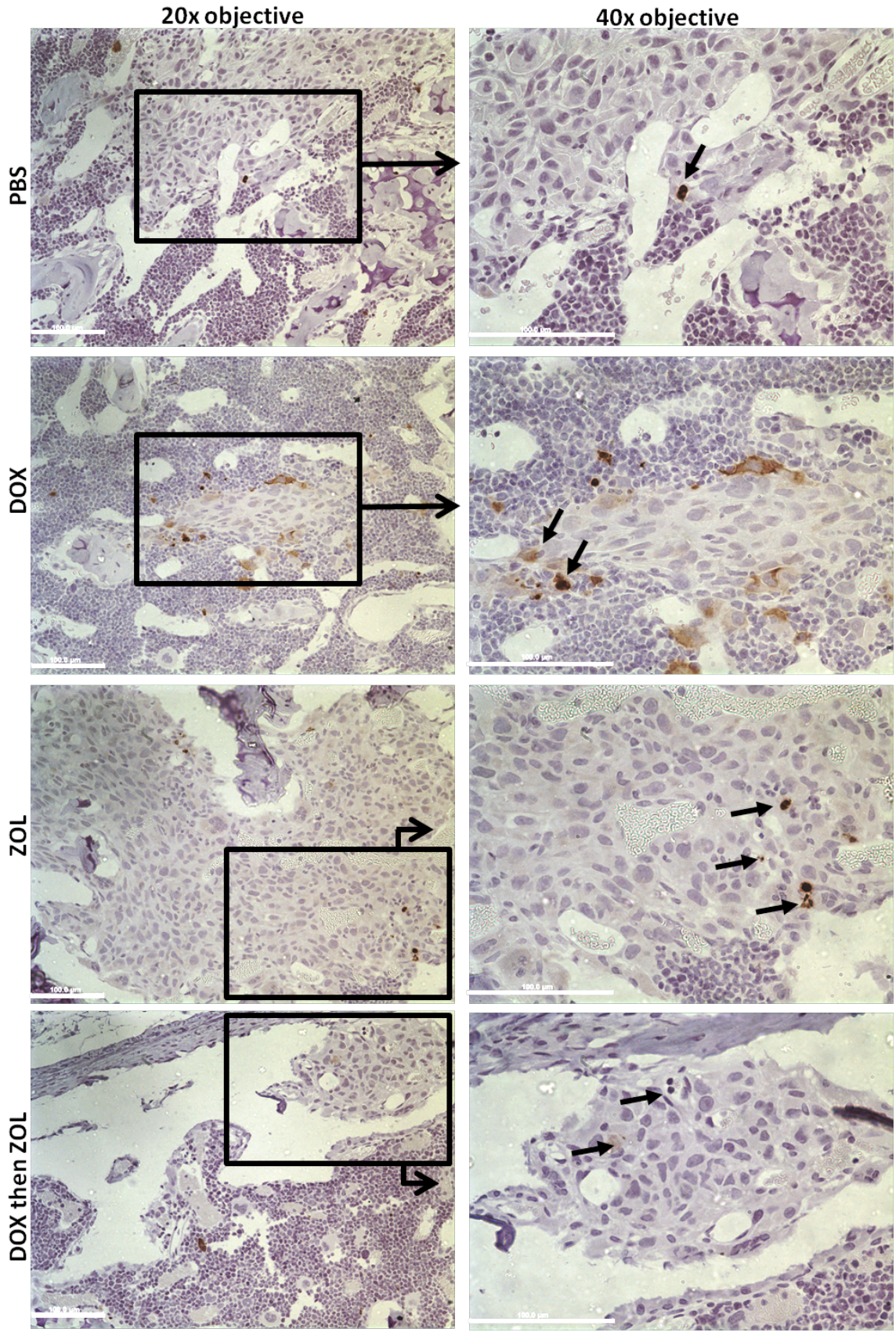

Figure 5.14 Example images of caspase-3 stained sections (day 15)
Example images are shown for PBS, dox, zol and combination group stained for active caspase-3. Scale bar=100µm, black box=area of magnification; arrows indicate caspase-3 positive cells.

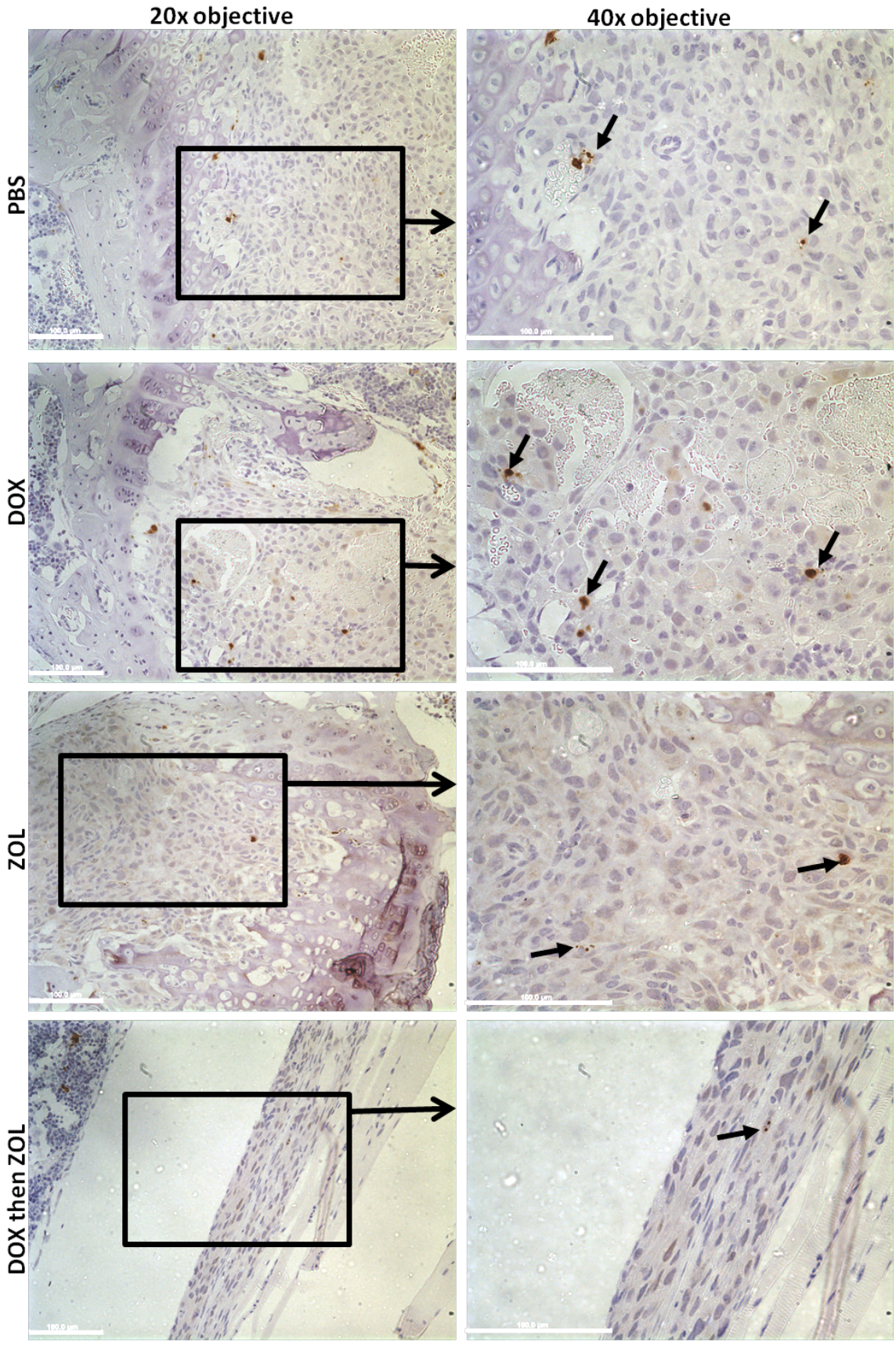

Figure 5.15 Example images of caspase-3 stained sections (day 23)
Example images are shown for PBS, dox, zol and combination group stained for caspase-3 taken with a 20x and a 40x objective. Scale bar=100µm, box indicates area of inset; arrows in 40x images show caspase-3 positive cells.

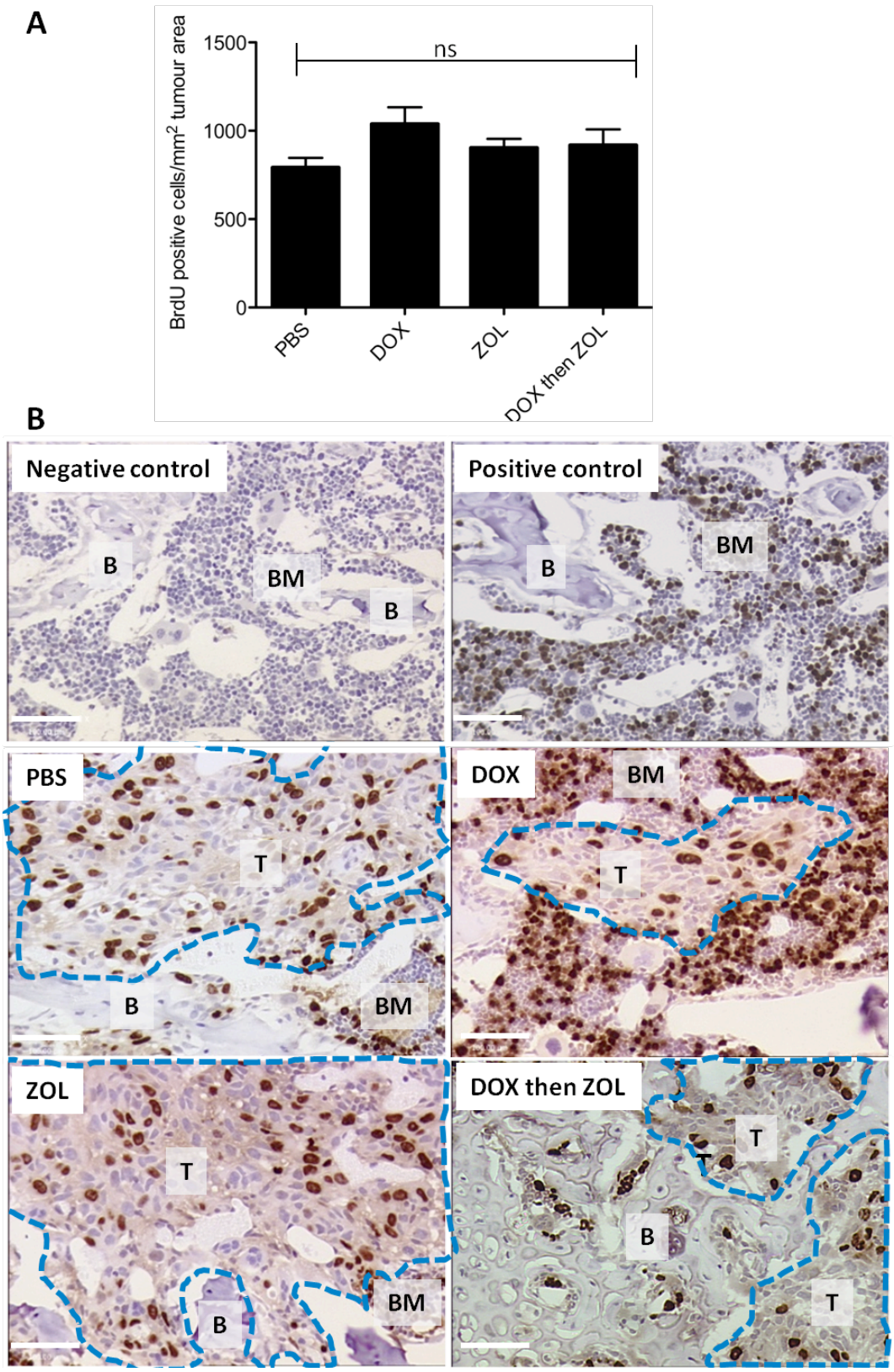

Figure 5.16 Quantification of treatment-induced changes in tumour cell proliferation on day 15

Histological sections were stained for BrdU to detect proliferation. A) At least 2 non-serial sections per sample were analysed (10x objective). B) Representative images of BrdU staining (10x objective, scale bar=100µm, T=tumour, B=bone, BM=bone marrow, dotted line=tumour circumference). No significant change between treatment groups was detected by one way ANOVA and Tuckey post test, ns=not significant.

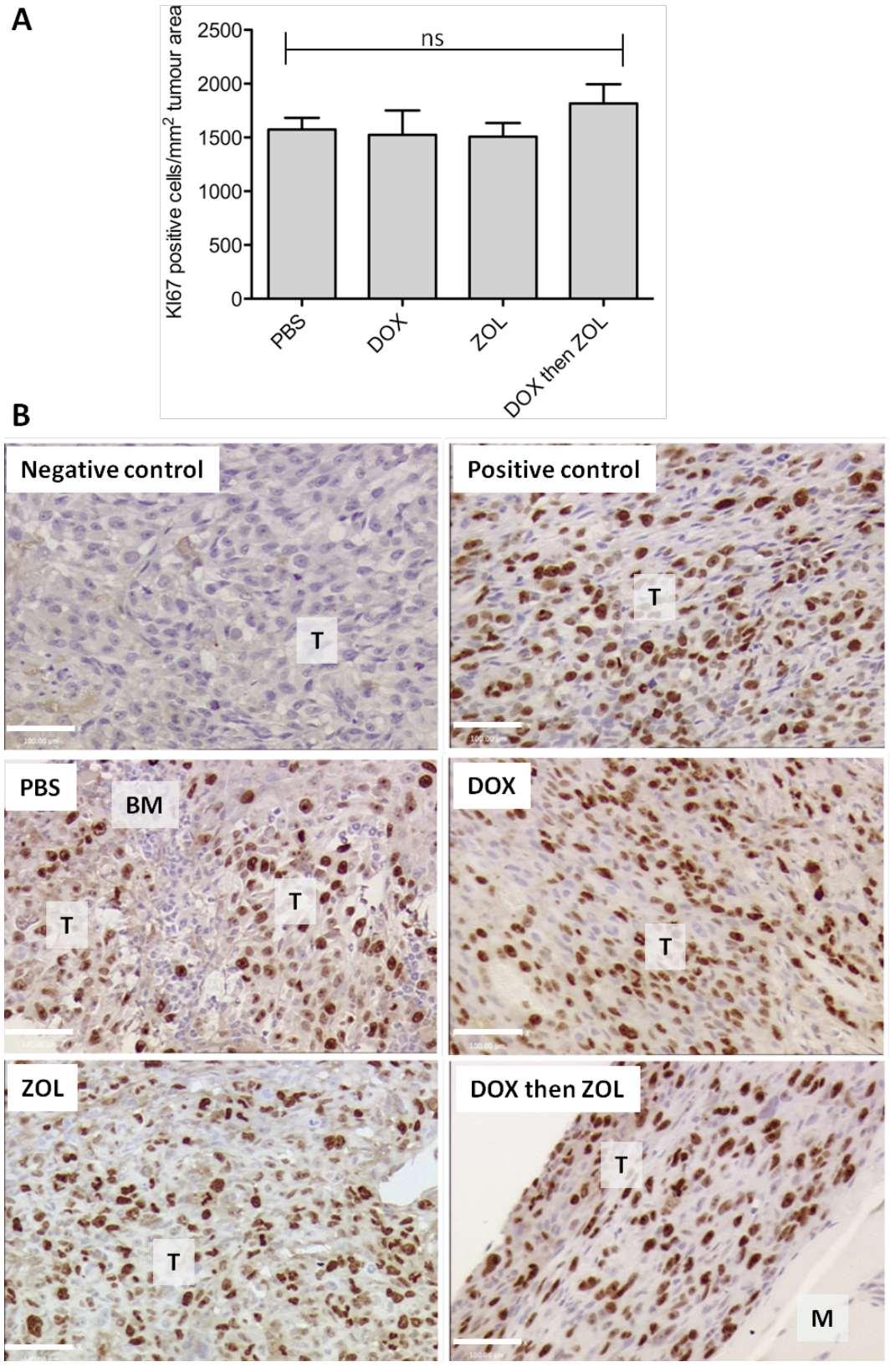

Figure 5.17 Quantification of treatment-induced changes in tumour cell proliferation on day 23

Histological sections were stained for Ki67 to detect tumour cell proliferation. A) At least 2 non-serial sections per sample were analysed (10x objective). B) Representative images of Ki67 staining (10x objective, scale bar=100µm, T=tumour, B=bone, BM=bone marrow, M=muscle). No significant change between treatment groups was detected by one way ANOVA and Tuckey post test, ns=not significant.

5.5.6 Analysis of tumour gene expression by quantitative real time PCR (qRT-PCR specific to human genes)

In order to investigate if the molecular changes induced by administration of early treatment could be assessed in more detail, I performed gene expression studies using qRT-PCR on bone tumour samples collected at day 23. Initial experiments using the Tri-reagent method showed insufficient RNA product for qRT-PCR analysis. Thus a pre-amplification step was performed prior to qRT-PCR analysis. The efficiency and unbiased amplification of a selected gene (ß-actin) compared to GapdH was tested on *in vitro* and *in vivo* samples prior to use of the study material. Ottewell et al. have previously published significant changes in gene expression of genes involved in tumour cell apoptosis and proliferation post combination treatment with doxorubicin followed by zoledronic acid in models of subcutaneous (Ottewell et al., 2008b) and intraosseous Ottewell et al., 2009) tumour growth. Genes analysed in this study included the cell cycle related genes cyclinD1, cyclinD3, p21 and p53 as well as the apoptosis related genes BCL2, BAX, CRADD and FADD. Gene expression analysis in the present study reflected the results on apoptosis and proliferation determined by immunohistochemistry, with no significant changes detected at day 23 (Fig. 5.13 to 5.17). Not all genes were detectable post amplification. BCL2 and CRADD, both involved in apoptosis, were shown to be unchanged when compared to PBS control. Gene products known to be involved in proliferation, including P21 and CyclinD1, were also found to be not significantly different following treatment when compared to control. Only CyclinD3 showed a significant increase in the combination group when compared to PBS control tumours with a 2.63 fold increase with $p<0.05$ (Fig. 5.18)

Next, analysis of bone related genes (Table 4.1) was performed since site comparison studies in Chapter 4 showed significant changes of specific genes in osseous compared to peripheral tumours. Only two genes, SFRP1 and OPG were detectable even after pre-amplification of the samples, emphasising that analysis of bone tumours by this method is challenging due to the limited amount of material available. Pooling of the samples was not carried out due to the small n numbers. SFRP1 and OPG gene expression was significantly increased in zol only and combination treatment groups when compared to PBS control, suggesting suppression of osteoblasts as seen by histology (Fig. 5.19).

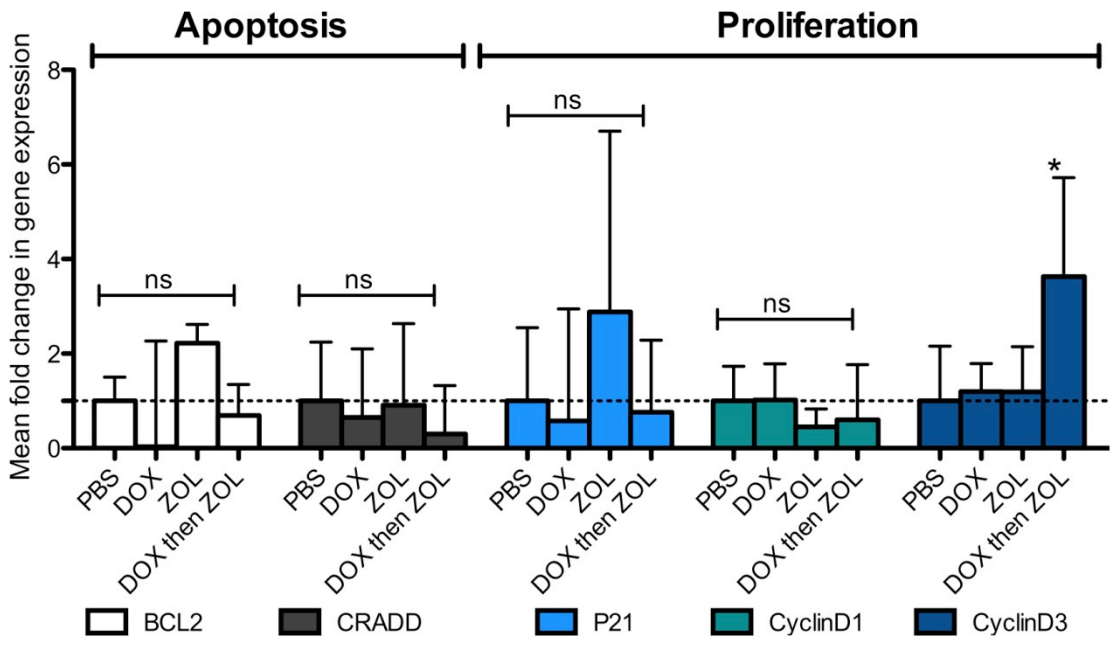

Figure 5.18 Gene expression analysis of human genes involved in tumour cell apoptosis and proliferation

qRT–PCR analysis was performed on osseous tumours taken 23 days post tumour cell injection. Species specificity to detect human genes only was previously shown in Ottewell et al. (2009). Data are expressed as the relative expression of the gene of interest to GapdH (2^-(ΔΔCT) with $\Delta\Delta CT=\Delta CT_{treatment} - \Delta CT_{control}$). Mean±SEM, one way ANOVA and Tuckey post test, * is p<0.05, ns = not significant, all compared to PBS control. PBS, n=5, dox n=4, zol, n=4, combination n=3.

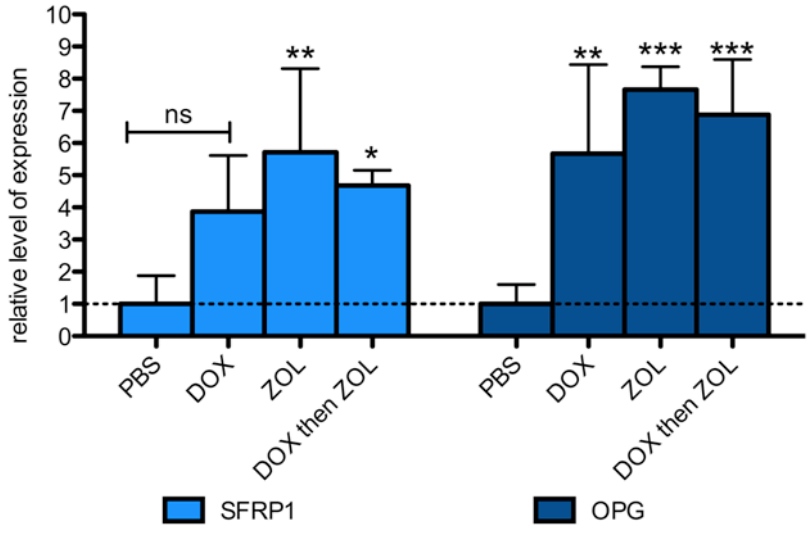

Figure 5.19 Species specific (human) quantitative real time PCR of bone related genes

qRT–PCR analysis was performed on osseous tumours collected 23 days post tumour cell injection. Relative expression of the gene of interest to GapdH (2^-(ΔΔCT) with $\Delta\Delta CT=\Delta CT_{treatment} - \Delta CT_{control}$). Mean±SEM, one way ANOVA and Tuckey post test, * is p<0.05,** is p<0.01, *** is p<0.001, ns = not significant, all compared to PBS control. PBS: n=5, dox: n=4, zol: n=4, combination: n=3. Species specificity of the primers has been assessed.

In summary the data underline the results of the previous analysis showing that single treatment at an early time point does not have significant effects on tumour cells death and growth 21 days post administration. However, treatment did affect bone related genes significantly emphasising the treatment-induced effects on the bone microenvironment. These data require confirmation due to the necessity to pre-amplify the targets of interest.

5.5.7 Investigation of treatment-induced alterations on host serum cytokine levels

Several cytokines including IL-1 and IL-6 have been proposed to be pro-tumourigenic and part of the vicious cycle driving metastatic bone disease but investigation of cytokine changes post combination treatment has not been performed previously. In order to determine if treatment-induced changes in levels of murine cytokines involved in osteoclast activity were detectable in animals 15 and 23 days after tumour cell injection, serum concentrations were analysed by cytometric bead array. The use of ELISAs for cytokine measurements has been performed previously (Dr PD Ottewell, University of Sheffield) but was found to be not sensitive enough for serum measurements. Thus, it was investigated whether the cytometric bead array was suitable.

On day 15 serum concentrations of mouse IL-1α and IL-1β were below the detection limit of 10pg/ml in all treatment groups. However, significantly lower levels of IL-1β were detected when comparing doxorubicin to zoledronic acid treated animals (5.54 pg/ml vs. 8.26 pg/ml, $p<0.05$, Fig. 5.20B). Furthermore, analysis of IL-6, KC (IL-8) and MCP-1 revealed lower levels in dox treated mice compared to the other treatment groups and PBS control animals although no significantly different concentrations were reached (Fig. 5.20C-E). Analysis of cytokine levels on day 23 revealed a different pattern compared to day 15. IL-1α, IL-1β and MCP-1 levels were unchanged in all treatment groups although levels in the combination group were always the lowest. IL-6 levels were significantly increased in zol treated mice compared to PBS, dox only and the combination group (zol: 3890.52 pg/ml vs. PBS: 794.69; vs. dox: 998.87 and vs. dox then zol: 207.01, all $p<0.01$, Fig. 5.21C). In addition, combination therapy induced a significant reduction in KC levels compared to dox only and zol only treated mice (dox then zol: 138.05 pg/ml vs. dox: 1153.6, $p<0.05$ and vs. zol: 1306.92, $p<0.01$, Fig. 5.21E).

In summary, the data show that the osteoclast enhancing cytokines IL-6 and KC are reduced after combination treatment, suggesting a therapy-induced alteration of systemic cytokine levels.

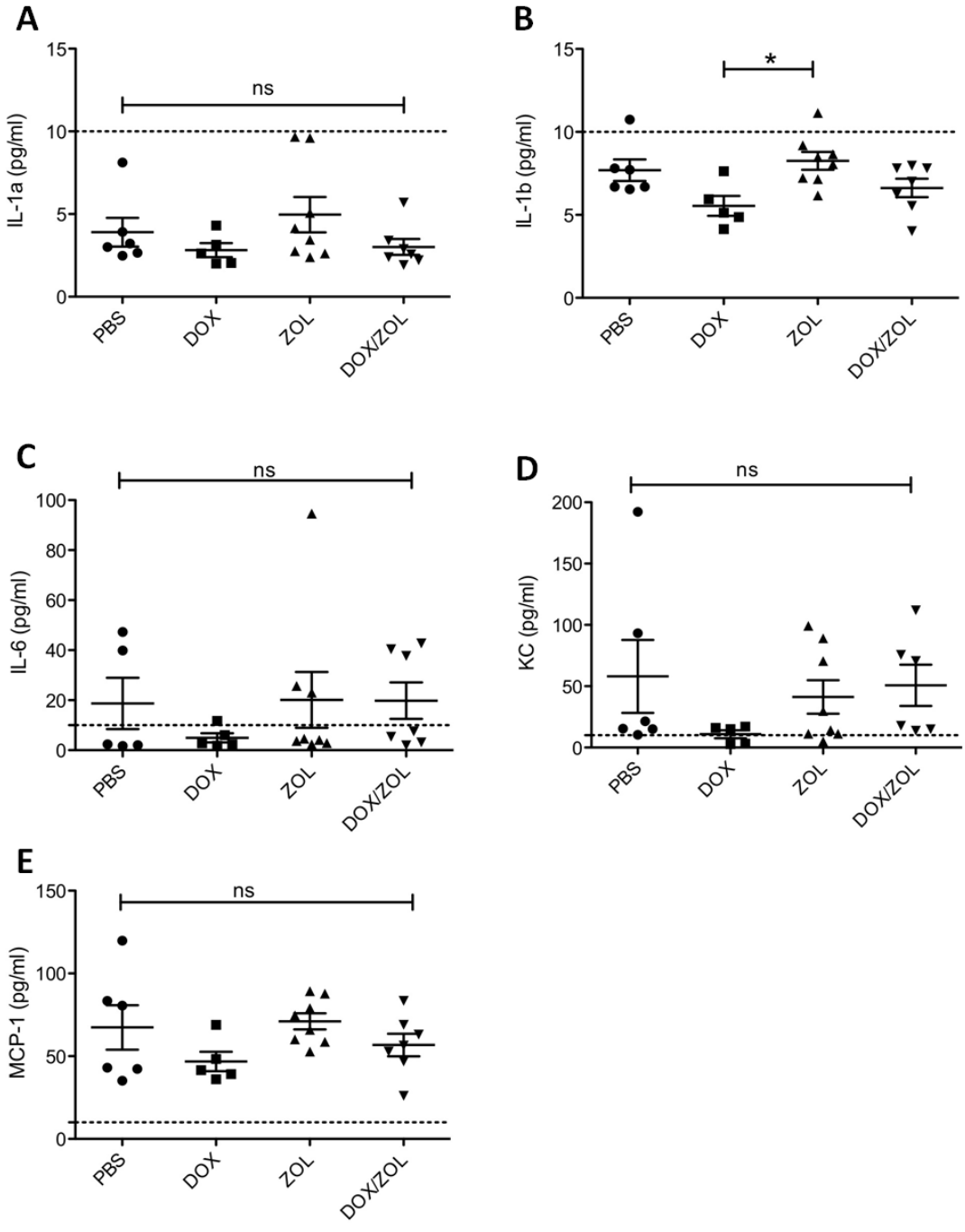

Figure 5.20 Measurements of mouse cytokines in serum 15 days post tumour cell injection

Serum from animals sacrificed 15 days post tumour cell injection was analysed for the mouse cytokines A) IL-1α, B) IL-1β, C) IL-6, D) KC (IL-8) and E) MCP-1 levels by cytometric bead array. Data are presented as mean ± SEM, one way ANOVA and Tuckey post test, * is $p<0.05$, ** is $p<0.01$. Lower detection limit for all cytokines was 10pg/ml. Each symbol represents serum obtained from one mouse. Dotted line indicates detection limit of 10pg/ml.

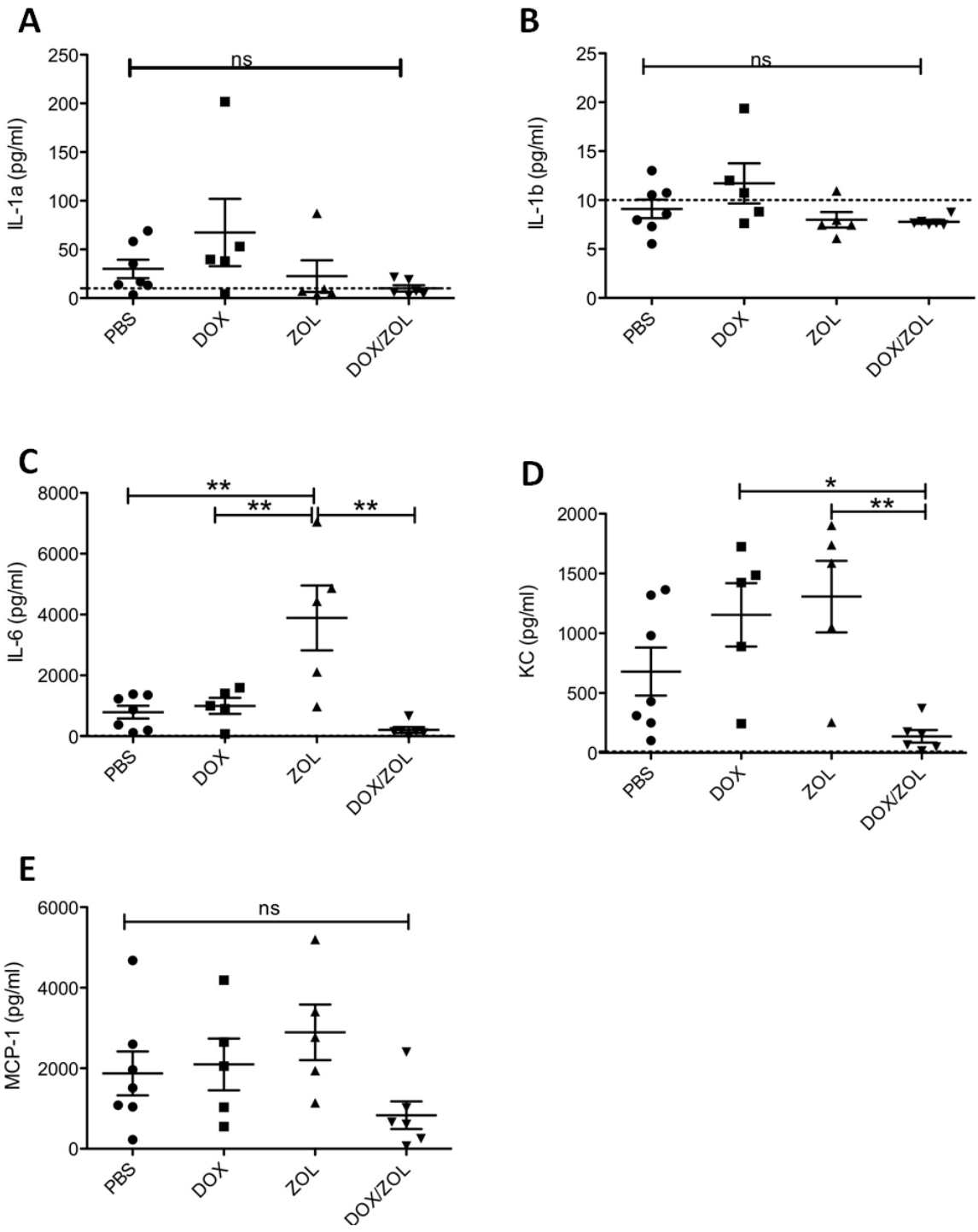

Figure 5.21 Measurements of murine cytokines in serum 23 days post tumour cell injection

Serum from animals sacrificed 23 days post tumour cell injection was analysed for the murine cytokines A) IL-1α, B) IL-1β, C) IL-6, D) KC (IL-8) and E) MCP-1 levels by cytometric bead array. Data are presented as mean ± SEM, one way ANOVA and Tuckey post test, * is $p<0.05$, ** is $p<0.01$. Lower detection limit for all cytokines was 10pg/ml. Each symbol represents serum obtained from one mouse. Dotted line indicates detection limit of 10pg/ml.

5.6 Discussion

The present study is the first to show that a single administration of sequential dox then zol at an early time point (day 2 following tumour cell injection) induced sustained inhibition of osseous tumour growth as well as improved bone integrity compared to single treatments and vehicle control.

Treatment studies in xenograft models of bone metastases often neglect the impact of the therapeutic agents on the host. In order to fully understand the effects of the drugs under investigation, the treatment-induced changes on the host-microenvironment in addition to the tumour xenograft need to be taken into account. I therefore firstly investigated the local effect of combination therapy on the host microenvironment in the absence of tumour. A single dose of zoledronic acid, alone or in combination with doxorubicin, did not induce changes in bone cell numbers on day 10 but significantly reduced osteoclast numbers on day 15 in tumour-free bones. The zol (+/- dox) therapy also induced a major reduction in osteoblast numbers on day 15. However, the data cannot decipher if the effect on osteoblast numbers is due to a direct drug-induced inhibition of osteoblast development or if it is taking place via a downstream effect of inhibition of the osteoclast.

Next, the effects of therapy were analysed in a tumour bearing setting. µCT analysis on tumour bearing bones showed significant bone protection after zol alone or combination treatment compared to PBS control on day 15 and 23, confirming the anti-resorptive activity of the bisphosphonate. Despite this, the effect on bone cell numbers in a tumour-bearing environment was not as prominent compared to the non-tumour bearing bones, possibly underlining the strong influence the tumour cells have on the metastatic site. No reduction in osteoclast number was detected on day 15 although µCT analysis clearly showed a dramatic increase in bone volume. In agreement with Ottewell's study of dox then zol treatment (6 week regimen) on intratibial MDA-MB-436 tumours (Ottewell et al., 2009) was the analysis of the day 23 samples showing decreased osteoclast numbers in zol and combination treatment compared to PBS control. No reduction in osteoclast surface in contact with trabecular bone was detected at either time point. This could be due to a zoledronic acid-induced formation of large osteoclasts in the zol treated animals, as was shown by scoring of mean osteoclast area. The presence of "giant" osteoclasts has also been reported after

long-term alendronate treatment in an osteoporotic setting (Jain and Weinstein, 2009). The authors concluded that aminobisphosphonates effectively inhibited osteoclast activity and prolonged the lifespan of the cells ultimately leading to an increase in cell size due to continuous fusion of the osteoclast with mononuclear precursors. In addition, apoptosis was detected in about 30% of the "giant" cells (Weinstein et al., 2009). The data therefore suggest that the bisphosphonate decreases osteoclast activity and changes cell morphology before reducing viability. CTX analysis did, however, not confirm this although the interpretation of the CTX data is difficult due to high variation in sample values in the zol and combination group. Furthermore, it may be too late to measure a detectable change in CTX levels in mice at the relatively late time point (day 15 and 23) post zoledronic acid administration.

Similar to the results observed in the tumour-free bones, albeit less extensive, was that the main bone cell affected by zoledronic acid was the osteoblast with major reductions in cell number and activity (PINP) detectable on day 15 and 23 compared to PBS control. Zoledronic acid treatment may therefore effectively counteract the tumour-induced changes in both osteoblast and osteoclast numbers as seen in PBS controls and in the longitudinal study described in Chapter 4. Noticeably, the effects on the bone microenvironment were due to the presence of zoledronic acid since dox only treatment had no effect on bone cell numbers and combination treatment did not result in a synergistic effect. The role of the osteoblast in the initiation of osseous breast cancer cell growth is not well established and there is currently no published data looking into the effects of an osteoblast-deficient bone microenvironment on breast tumour growth in bone (this is currently an area of active research within our unit). Although the literature is frequently questioning the *in vivo* effect of bisphosphonate treatment on cells other than osteoclasts (Roelofs et al., 2009; Brown et al., 2011), the data shown in this study suggest that a single, clinically achievable dose of zoledronic acid may affect osteoblasts or other cell types directly or indirectly. Evidence that bisphosphonates can be internalised by osteoblasts *in vivo* was reported by Idris et al. (2008). The group investigated the uptake of alendronate into bone forming cells in mice after a single dose of 0.1mg/kg alendronate was injected 24 hours prior to sacrifice. *Ex vivo* analysis of isolated mouse calvarial osteoblasts showed

detectable levels of unprenylated Rap1A, indicating uptake of the drug in this short period of time and subsequent inhibition of the mevalonate pathway.

Taken together, the data shown here suggest indirect anti-tumour effects of zoledronic acid, most likely taking place via impairment of the tumour-driven alterations to the bone microenvironment. However, this effect is not sufficient to reduce tumour growth on its own, since the group receiving zol only did not show a reduction in tumour size at any time point compared to PBS. The detected reduction in osteoclasts and osteoblasts post zoledronic acid treatment could, however, render the intraosseous bone microenvironment unfavourable for metastatic tumour cell growth, redirecting it to other metastatic sites such as the periosteal surface as seen in the combination group. In fact, there is preclinical evidence that bisphosphonate treatment exhibits stronger anti-tumour effects in the bone marrow cavity compared to the extraosseous bone-associated soft tissue when given alone or in combination with cytotoxic agents (Brown and Holen, 2009). Studies investigating the effects of bisphosphonates as a single agent have reported either no effect on extraosseous tumour growth post pamidronate or olpadronate treatment (van der Pluijm et al., 2005) or increased bone-associated soft tissue tumours after risedronate (Sasaki et al., 1995) or YH529 (a third generation bisphosphonate) administration (Sasaki et al., 1998). Collectively the data from these studies suggest that the bisphosphonate-induced inhibition of bone remodelling may lead to redirection of the tumour growth to the extraosseous site. As described by Ottewell et al. (2008a), the use of combination therapy (doxorubicin given 24 hours post zoledronic acid) only increased the anti-tumour effect on the intraosseous MDA-MB-231/B02 tumour areas but had no effect on the extraosseous parts. The present data are in agreement with these reports showing that a single dose of combination treatment effectively reduced tumour growth inside the bone marrow cavity with only one out of six animals having detectable intraosseous tumours on day 23, but treatment did not eliminate extraosseous tumour growth. Importantly, this is the first study to show that the tumour colonies growing along the periosteal surface are not part of an intraosseous tumour spilling through osteolytic lesions but that these are separate tumour colonies. This could suggest that during the process of tumour cell injection, cancer cells seed to multiple sites but remain dormant until triggered to proliferate or that cells previously

settled in the bone marrow cavity disseminated to other sites. In addition, there are currently few reports published investigating how bisphosphonate treatment could affect the cells of the periosteum (Allen et al., 2004).

The basis of combination therapy is to effectively reduce tumour growth by targeting both the tumour and the microenvironment at the metastatic site. Assessment of anti-cancer effects on the tumour showed that only the combination group exhibited significant differences in tumour cell apoptosis on day 15, mirroring the reduction in tumour area detected on the same day. No changes in active tumour cell proliferation were detected at either time point. While the results of tumour cell death agree with previously published preclinical studies using dox then zol, the proliferation data do not (Ottewell et al., 2008a; Ottewell et al., 2008b; Ottewell et al., 2010; Ottewell et al., 2009). In addition, apoptosis and proliferation candidate genes that were significantly altered in a study by Ottewell et al. (2009) were unchanged after a single dose of combination therapy at day 2. This is probably due to differences in treatment scheduling as most of the previous studies used a frequent dosing regimen with a total of 6 doses and animals were sacrificed 24 hours after the last treatment. The published reports suggest that the apoptotic cell death and reduction in proliferation is an acute effect of combination therapy detectable 24 hours post treatment. It is therefore possible that the here observed increase in tumour cell death, which was evident many days post completion of treatment, is due to an indirect anti-tumour effect on the microenvironment rather than on the tumour cells directly.

Although the increased anti-tumour effect of combination treatment inside the bone marrow cavity remains to be elucidated a possible explanation may be a treatment-induced reduction in growth factors from the bone matrix as well as a change in bone cells at the intra- compared to the extraosseous site. Indeed, an *in vitro* study carried out by Derenne et al. showed that zoledronic acid treatment of human bone marrow stromal cells reduced interleukin-6 levels as well as interleukin-1 stimulated production of MMP-1 (Derenne et al., 1999). These cytokines, as well as IL-8 and MCP-1, have been shown to play a role in bone metastasis and are therefore worth investigating as a possible mediator of the increased anti-tumour activity of combination treatment. The serum concentrations of IL-1α, IL-1β, IL-6, KC (mouse IL-8) and MCP-1 were therefore analysed by cytometric bead array. Although the

inflammatory cytokines, such as IL-6, have been shown to be up regulated during the acute phase response induced by first time NBP treatment (Thiebaud et al., 1997) it is unlikely that the increase in IL-6 detected in this study is due to a similar reaction. Firstly, the acute phase response has been characterised as a transient complication, which is usually limited to the first 3 days post zoledronic acid administration. And secondly, the associated cytokine release is thought to be connected to the activation of a subpopulation of T cells, the γδT-cells (Kunzmann et al., 1999), cells which are not present in the nude mouse used in this study (Girardi et al., 2006). It is therefore more likely that the changes in IL-6 and KC seen on day 23 are due to changes in bone marrow stromal cells, osteoblasts or other cytokine producing cells. Since the levels in the combination treatment group were lowest for all investigated cytokines, it is possible that the combination of a chemotherapeutic and a bisphosphonate is partly responsible for the protection of the bone microenvironment from tumour growth. It may be that, on a more local level, the reduction in inflammatory cytokines is more prominent inside the bone marrow cavity, possibly contributing to the increased efficacy of the combination treatment at the intraosseous site.

This is the first study to report that early administration of a single, clinically achievable dose of combination treatment is effective in significantly reducing breast tumour growth and improving bone integrity compared to single agents or control. Despite the superior effect of the combination therapy on tumour size, it is not possible to pinpoint whether this effect is due to direct or indirect anti-tumour effects or both.

6. Evidence of bisphosphonate localisation into peripheral breast tumour cells *in vivo* – a pilot study

6.1 Summary

Nitrogen-containing-bisphosphonates (NBPs) are known to rapidly bind to the bone matrix where the drugs exert their bone-sparing activity. In addition to the effects on bone resorption, indirect and direct anti-tumour effects have been reported *in vitro* and *in vivo*. However, it remains unclear which cell types apart from osteoclasts are capable of internalising NBPs *in vivo* and especially the question whether tumour cells take up bisphosphonates is of great interest. This chapter assessed whether subcutaneous human breast tumour xenografts and host soft tissues are able to internalise the fluorescently labelled NBP, AF647-RIS.

$5x10^5$ MDA-G8 (MDA-MB-436-GFP) cells were subcutaneously injected into the right flank of 8-week old female balb/c nude mice and allowed to develop into tumours over 4-5 weeks. 400µg/kg AF647-RIS, AF647 or PBS was injected s.c. 24 hours prior to sacrifice. Non-invasive imaging of drug distribution was monitored every 2 minutes for 20 minutes and then at 2 and 24 hours post injection using an IVIS® imaging system. Cells of the peritoneal cavity, tumour, bone marrow, spleen, liver, lung, kidney and forelimbs were collected for analysis by confocal microscopy and flow cytometry.

Optical imaging demonstrated the rapid uptake of AF647-RIS into the skeleton 2-20 minutes after injection, whilst uptake of AF647-RIS into tumour tissue, cells of the peritoneal cavity and bone surfaces was visualised by confocal microscopy 24 hours after injection. Flow cytometric analysis showed detectable AF647-RIS uptake in cell suspensions of the subcutaneous tumour and the peritoneum but no significant change was seen in bone marrow samples. A proportion of GFP-positive tumour cells appeared to be AF647-RIS-positive suggesting uptake of the drug by tumour cells.

This study demonstrates that cells within s.c. breast tumour xenografts and of other non-osseous tissues are capable of internalising AF647-RIS 24 hours following a single administration of the compound *in vivo*. The co-localisation of GFP and AF647-RIS in MDA-G8 cells remains to be confirmed but suggests direct uptake of the drug.

6.2 Introduction

Nitrogen-containing-bisphosphonates (NBPs) are known to exert bone-sparing effects and are commonly used to treat osteolytic bone disease. In addition to the inhibition of bone remodelling, indirect and direct anti-tumour effects have been reported (Neville-Webbe et al., 2002). *In vitro* studies have shown that NBPs are internalised by the highly endocytic osteoclasts (Coxon et al., 2008) as well as a variety of cells types including breast tumour cells (Jagdev et al., 2001) and macrophages (Monkkonen et al., 2007). The mechanism of action of NBPs is executed through the inhibition of FPP-synthase in the mevalonate pathway, thus depleting cells of prenylated proteins such as Ras, Rho and Rac (Luckman et al., 1998; Dunford et al., 2001). The accumulation of unprenylated Rap1A and the reversal through the downstream product GGOH (geranylgeranylgeraniol) is therefore commonly used as a surrogate marker for cellular NBP uptake *in vitro*. However, the determination of cell or tissue specific bisphosphonate distribution and uptake *in vivo* is more difficult to investigate, which is partly due to the drugs' rapid clearance from the circulation to the skeleton. For example, clinical zoledronic acid administration (4mg i.v. every 3-4 weeks), results in peak plasma concentrations of 1-2µM for only a few hours after injection (Chen et al., 2002). After 24 hours, the total plasma levels declined to only 1%. In bone, however, zoledronic acid concentrations of up to 1000µM have been detected in the resorption pits of active osteoclasts (Sato et al., 1991), a level high enough to have potential cytotoxic effects. However, the concentration of BPs outside the sealed resorption pit remains to be established.

Studies investigating the biodistribution of NBPs *in vivo* have focused on different tissues and cell types. Osteoclasts have been commonly investigated by histomorphometry in *in vivo* studies using bisphosphonates and the effects on the cells are often expressed in changes in cell number or osteoclast surface/mm bone surface. Direct measurement of BP uptake and inhibition of the mevalonate pathway on a cellular level is difficult *in vivo* and often require isolation of the cell types of interest or use of labelled bisphosphonates. The injection of 0.4mg/kg [3H] labelled alendronate into newborn rats was shown to cause intracellular accumulation of the bisphosphonate in osteoclasts, but no other cell type in the bone marrow, when assessed 1 day post injection of the drug (Sato et al., 1991). It is possible that active

bone resorption leads to a release of the drug into the surrounding environment but it is unclear if the maximum concentration of free bisphosphonate would reach sufficiently high levels to affect any other cell type than the actively resorbing osteoclast. Monkkonen et al. (1990) showed that administration of a single dose of the ^{14}C-labelled bisphosphonates clodronate, etidronate and amidronate resulted in accumulation in the skeleton and the kidney, with amidronate also detectable in the liver and spleen for up to 6 months post injection. In a more recent study it was furthermore shown that bisphosphonates are readily internalised into peritoneal macrophages *in vivo* (Monkkonen et al., 2007). There is evidence of bisphosphonates exerting anti-tumour effects in bone and at peripheral sites in preclinical models, although the underlying indirect and direct mechanisms remain unclear. The question whether bisphosphonates are internalised by tumour cells *in vivo* is therefore of great interest. Because of the high concentration of NBPs at skeletal sites it is thought that bone residing cancer cells may be exposed to a potentially cytotoxic drug level, compared to peripheral tumours. A key outstanding question is therefore whether drug levels outside bone can reach cytotoxic concentrations.

Several studies investigating *in vivo* bisphosphonate distribution have been carried out using radiolabelled bisphosphonates, but currently there is no commercial access to most of these compounds. The recent development of fluorescently labelled bisphosphonates has allowed further investigation of the drugs biodistribution. The fluorescent tag allows the application of more sensitive imaging techniques than the commonly used detection of unprenylated Rap1A. A downside of a fluorescently tagged bisphosphonates in comparison to Rap1A detection is that no measure of drug activity is possible. A few studies using bisphosphonates labelled with fluorochromes have been published including IRDye78-pamidronate (Zaheer et al., 2001), FAM-RIS (carboxyfluorescein-risedronate), AF647-RIS (Alexa Fluor 647-risedronate) (Roelofs et al., 2009), and the commercially available pamidronate analogues Osteosense680 and Osteosense750 (Kozloff et al., 2007). The compound used for this study, a risedronate analogue conjugated to the near infrared fluorochrome AF647 (AF647-RIS, kindly provided by Professor M Rogers, University of Aberdeen, UK) has recently been shown to inhibit the accumulation of hydroxyapatite crystals *in vitro* (Roelofs et al., 2009). In addition, it was reported that the biodistribution of the compound is comparable to

unconjugated bisphosphonates, indicating that the fluorescent label has little effect on the drugs activity.

To my knowledge, no study has been published investigating the cellular uptake of NBPs into peripheral breast tumours at a clinically relevant dose. The work described in this chapter investigated the *in vivo* distribution of the fluorescently labelled bisphosphonate AF647-RIS following a single administration of the compound in subcutaneous tumour-bearing mice. Soft tissues including tumour, liver, lung, kidney as well as bone marrow cells, cells of the peritoneal cavity and bone samples were assessed for AF647-RIS uptake by non-invasive imaging, confocal microscopy and flow cytometry.

6.3 Aims

The main aims of the present chapter were as follows:

- Can AF647-RIS distribution be detected by non-invasive imaging (IVIS®) and are soft tissues as well as bone labelled?
- Can AF647-RIS localisation on a cellular level be assessed *ex-vivo* by flow cytometry and microscopy?
- Do cells of a peripheral tumour (MDA-G8 cells) and cells of host soft tissues internalise AF647-RIS?

6.4 Materials and Methods

6.4.1 *In vivo* experiments

All experiments were carried out in accordance with local guidelines and with Home Office approval under project license 40/2972 held by Professor N.J. Brown, University of Sheffield, United Kingdom.

Five separate *in vivo* experiments were carried out with a total of 11 mice. $5x10^5$ MDA-G8 (MDA-MB-436-GFP) cells were s.c. injected into the right flank of 8-week old female balb/c nude mice and were allowed to develop into tumours for 4-5 weeks (approximately 8mm in diameter). 400µg/kg AF647-RIS, 400µg/kg AF647 or PBS was injected s.c. 24 hours before sacrifice (Fig. 6.1). AF647-RIS was kindly provided by Professor M Rogers, University of Aberdeen, UK. The compound has a molecular weight of 1198g/mol compared to 305.10g/mol for unlabelled risedronate. The dose used for *in vivo* experiments was therefore 400µg/kg, which is the molar equivalent to 100µg/kg risedronate.

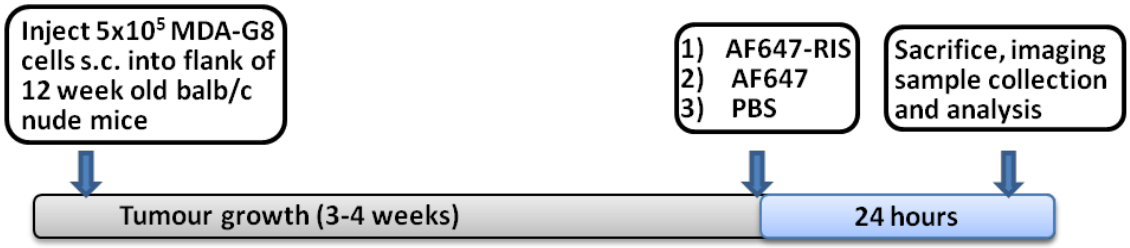

Figure 6.1 Schematic overview of *in vivo* experiment
MDA-MB-436-GFP (MDA-G8) cells were injected s.c. into the right flank of nude balb/c mice and left to grow for approximately 30 days. Twenty-four hours before sacrifice, 100µl PBS, AF647 or AF647-RIS (400µg/kg) was injected subcutaneously. A total of 5 separate *in vivo* experiments were performed with a total of n=5 for AF647-RIS and n=6 in the control group (PBS n=5, AF647 n=1).

The presence of AF647-RIS was detected by non-invasive *in vivo* imaging (IVIS®) before the subcutaneous tumour; bone marrow of the hind legs, forelimbs, spleen, liver, lung and kidney were collected. Because cells of the peritoneal cavity were previously shown to internalise BPs *in vivo* (Monkkonen et al., 2007), these cells were used as a positive control for cellular bisphosphonate uptake. Tissues were processed for the

different analysis methods including microscopy and flow cytometry as described in Materials and Methods (Chapter 2). Because only limited amounts of the drug were available (sufficient for 5 animals), not all techniques were performed on all experiments as the best possible way to investigate the distribution was optimised. Table 6.1 summarises the different experiments and analyses performed.

Experiment	Number of mice	Injected compounds	Analysis methods
1	n=2	AF647-RIS (400µg/kg), PBS	Microscopy
2	n=2	AF647-RIS (400µg/kg), PBS	Microscopy, flow cytometry
3	n=2	AF647-RIS (400µg/kg), PBS	Microscopy, flow cytometry, IVIS®
4	n=3	AF647-RIS (400µg/kg), PBS, AF647 (400µg/kg)	Microscopy, flow cytometry, IVIS®
5	n=2	AF647-RIS (400µg/kg)	Microscopy, flow cytometry, IVIS®

Table 6.1 Overview of performed experiments

6.4.2 Non-invasive *in vivo* imaging of MDA-G8 cells and of AF647-RIS distribution

In three experiments, non-invasive imaging of drug distribution was monitored every 2 minutes for 20 minutes and then at 2 and 24 hours post injection using an IVIS® imaging system. PBS or AF647 injected tumour-bearing control mice were imaged at the same time to adjust for fluorescence background levels. The excitation and emission wavelengths for GFP and AF647 are shown in Figure 6.2, indicating that the two spectra do not overlap.

6.4.3 Flow cytometry

Soft tissues and cells of the bone marrow and the peritoneal cavity were used for preparation of single cell suspensions. Samples from vehicle treated mice were used as controls for background fluorescence. Data acquisition was carried out on a MoFlo® Flow Cytometer and analysis was done using Summit software. Dr M Jones, University of Sheffield performed all Flow cytometry analyses.

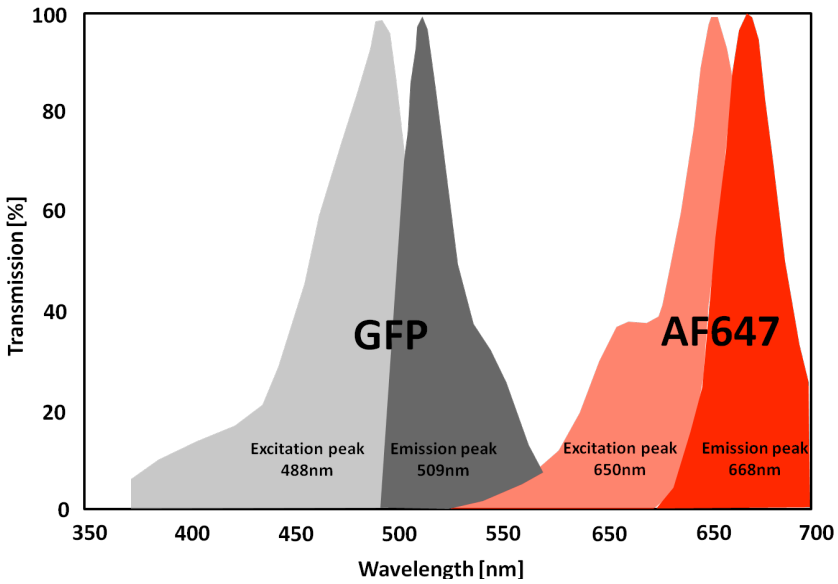

Figure 6.2 Excitation and emission spectra of GFP and AF647

6.4.4 Multiphoton microscopy of MDA-G8 cells and AF647-RIS

Confocal and multiphoton microscopy of soft tissue and front legs was performed for all 5 experiments (n=5 mice for AF647-RIS and n=5 mice for PBS control). The detection of AF647-RIS was assessed in bone, cells of the peritoneal cavity and subcutaneous tumour tissue. In some experiments, soft tissues and cytospins of cell suspensions were visualised. Excitation of AF647 was performed using a 633nm laser and band pass filter BP 650-710 IR. Second harmonic generation was used to visualise bone (900nm, Chameleon laser) and GFP positive tumour cells were detected by either the Chameleon laser at 900nm or a 488nm laser (BP 500-550 IR). Samples from vehicle or AF647 treated mice were used as controls for background fluorescence.

6.4.5 Statistical analysis

Prism GraphPad (Version 5.0a) was used for all statistical analysis. Analysis was by T-test. All data are shown as mean±SEM and differences have been interpreted as being significant at $p \leq 0.05$.

6.5 Results

6.5.1 Non-invasive *in vivo* imaging of AF647-RIS and MDA-G8 cells

The uptake of amino-bisphosphonates into the skeleton is one of the most studied areas of the drugs biodistribution. The non-invasive imaging system IVIS® allows real time *in vivo* imaging of fluorescent markers and was therefore used to assess the location of AF647-RIS at 2-20 minutes; 2 hours and 24 hours post injection. Negative controls were either vehicle control (PBS) or the fluorescent tag AF647. Imaging of mice for a duration of 20 minutes (images were taken every 2 minutes) after injection of the compounds showed that AF647-RIS was visible at site of injection and appeared to be distributed along the spine from as little as 8 minutes post injection (Fig. 6.3). This was more apparent after 12 minutes and from 14 minutes onwards the drug was visible in the scull, the tail and the hind legs. The free label was only visible at site of injection throughout the time course. The PBS injected mouse was free of any signal in the red channel over the entire 20 minutes. These data clearly indicate that the bisphosphonate determined the AF647 distribution, as the free label was only visible at site of injection.

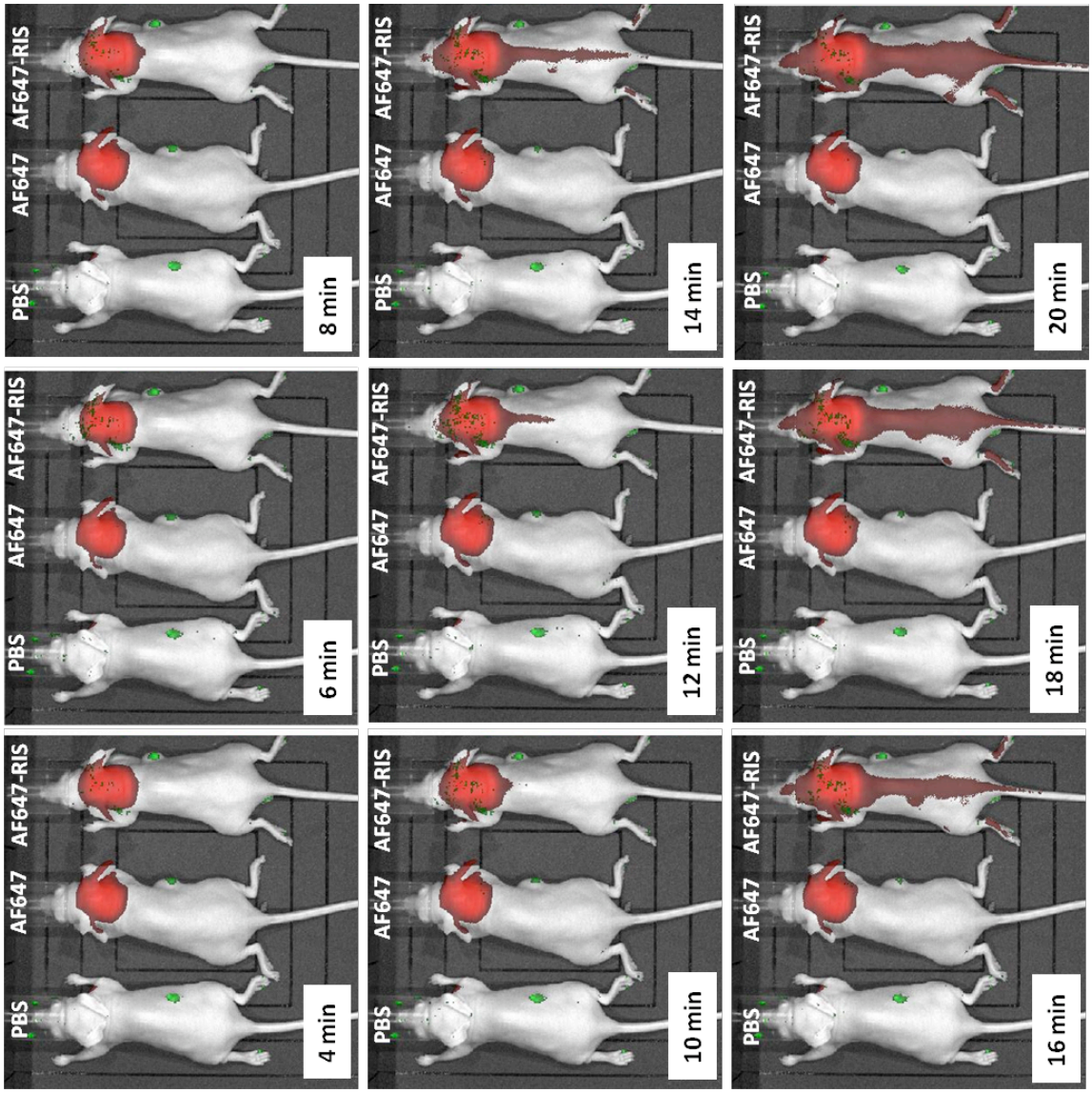

Figure 6.3 IVIS® imaging of AF647 uptake over 20 minutes post administration
Images depict dorsal view of mice bearing MDA-G8 subcutaneous tumours (green, right flank). Mice were either injected subcutaneously with PBS, AF647 (400µg/kg, red) or AF647-RIS (400µg/kg, red). Distribution of compound uptake was visualised by capturing images of the green and red channel every 2 minutes post injection.

Animals were imaged again 2 hours after administration of the compounds, essentially showing the same distribution of AF647-RIS and AF647 as seen at 20 minutes (Fig. 6.4). For unknown reasons, the mouse injected with AF647 only died to unknown causes prior to sacrifice (no adverse effects were visible on the day the tag was injected). The tag was not used for further experiments.

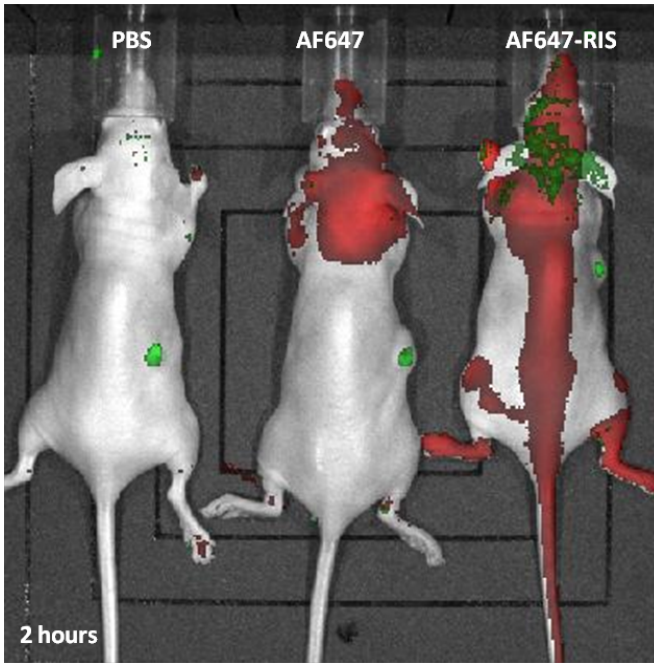

Figure 6.4 IVIS® imaging of AF647 uptake 2 hours post administration
Image shows dorsal view of mice bearing MDA-G8 subcutaneous tumours (green, right flank). Mice were either injected subcutaneously with PBS, AF647 (400µg/kg, red) or AF647-RIS (400µg/kg, red). Distribution of compound uptake was visualised 2 hours post injection.

Visualisation by IVIS® 24 hours after injection of AF647-RIS and PBS showed no change in the distribution of the bisphosphonate (Fig. 6.5). It was furthermore noticeable that the tumour tissue was always free of AF647 signal. After the animals were sacrificed, the tumour, liver, lungs, spleen and kidney were removed and placed into a 6-well plate containing ice cold PBS prior to imaging by IVIS®. When comparing soft tissue organs from AF647-RIS injected mice to PBS control animals it was shown that the drug was detected in the tumour, kidney, liver and lungs but not in the spleen (Fig. 6.6). It was furthermore shown that the highest concentration of the drug was detected in the liver, the tumour and the kidney (Fig. 6.7).

The skeletal distribution of AF647-RIS was detected at similar time points in two further experiments as well as the detection of the drug in the soft tissues as described here. Together the data indicate that AF647-RIS is rapidly localised to the skeleton but that some soft tissues, including the tumour, also take up the drug when imaged 24 hours post injection. The inability to detect soft tissue AF647-RIS uptake during live imaging is possibly due to the strong signal from the labelled bone.

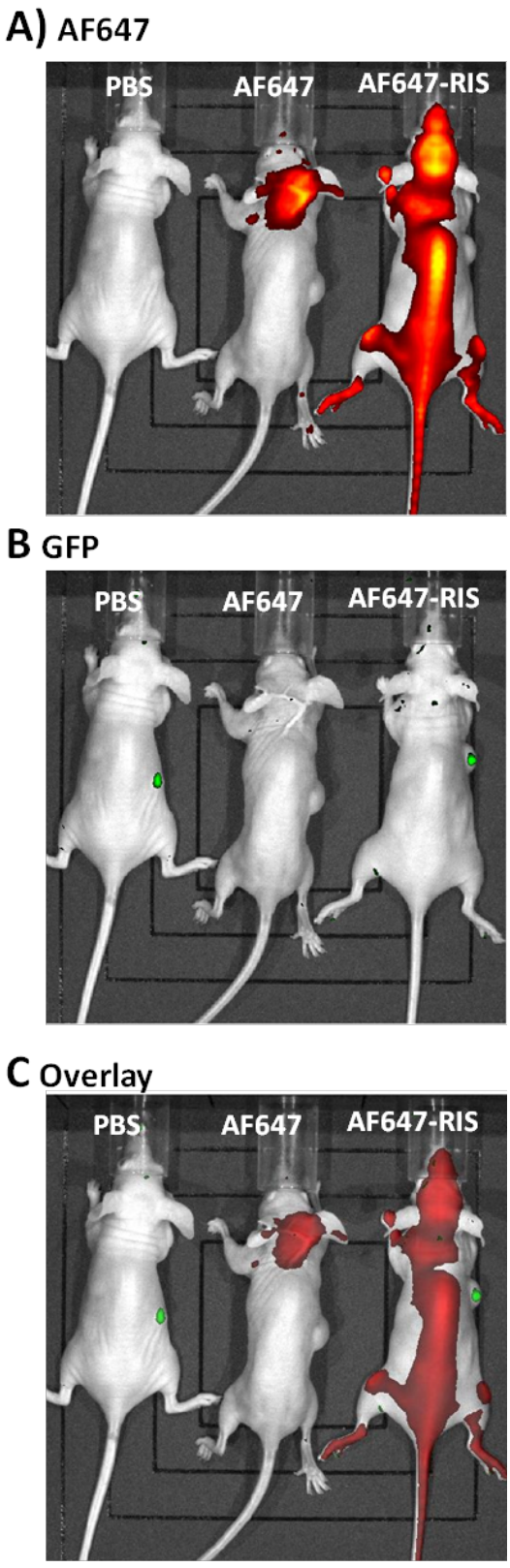

Figure 6.5 IVIS® imaging of AF647 uptake 24 hours post administration
Image shows dorsal view of mice bearing MDA-G8 subcutaneous tumours. Mice were injected once subcutaneously with PBS, AF647 or AF647-RIS (400µg/kg) 24 hours prior to sacrifice. A) Image depicts detection of AF647 (red). B) Image depicts detection of GFP (green). C) Image depicts overlay of the AF647 (red) and GFP (green).

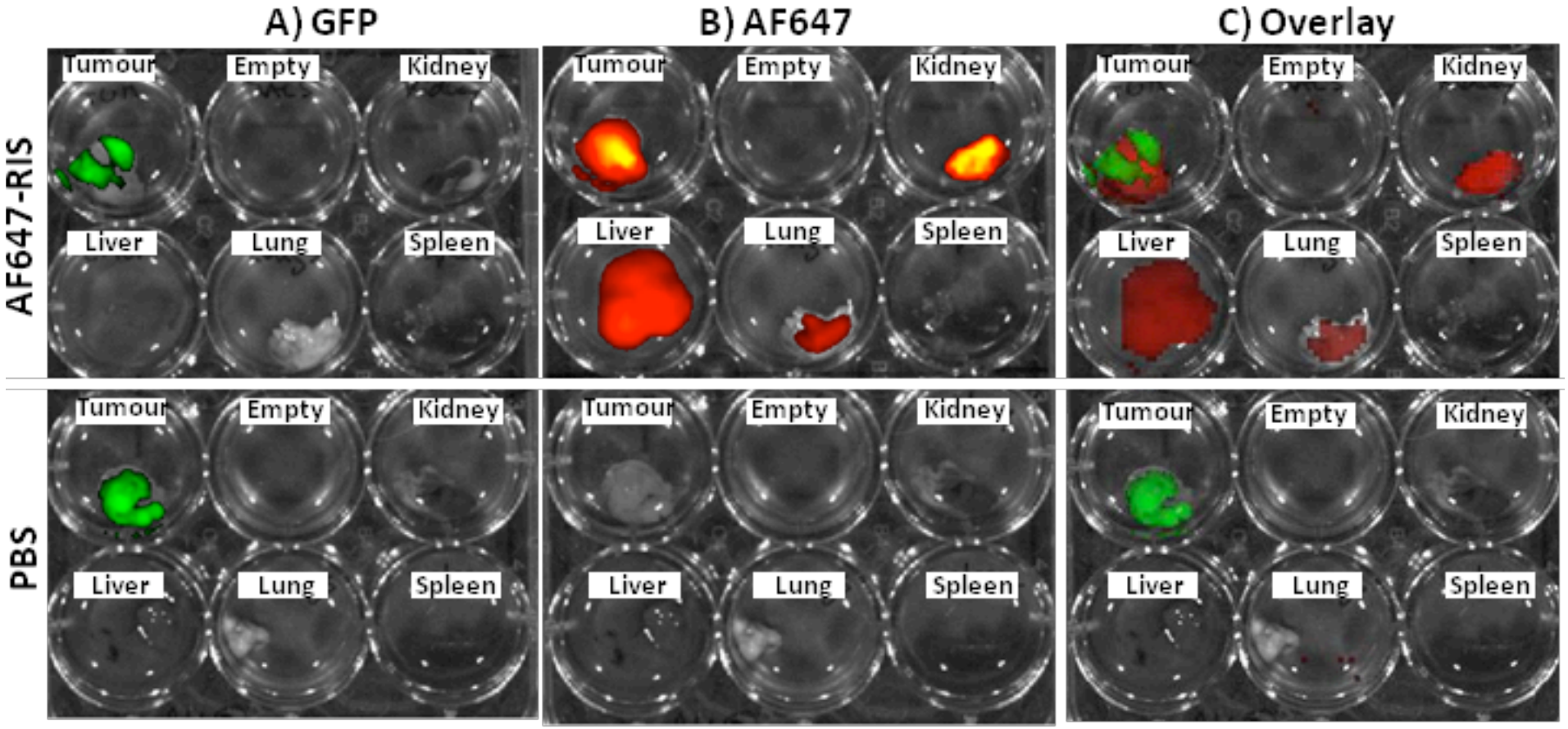

Figure 6.6 Visualisation of AF647-RIS and GFP by IVIS® imaging

IVIS imaging for AF647 and GFP was performed on excised organs taken from mice sacrificed 24 hours post s.c. injection of either PBS (bottom row) or AF647-RIS (400µg/kg, top row). Subcutaneous tumour tissue, kidney, liver, lung and spleen were placed into a 6-well plate with PBS before imaging for A) GFP and B) AF647. C) Overlay of AF647 and GFP signals.

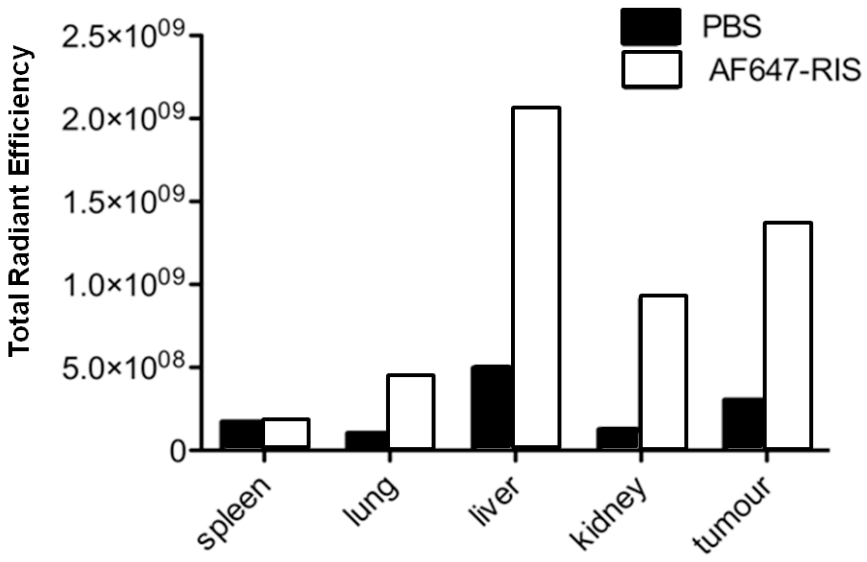

Figure 6.7 Quantification of AF647-RIS uptake into soft tissues using IVIS® imaging
Soft tissues (subcutaneous tumour, kidney, liver, lung and spleen) of PBS or AF647-RIS (400µg/kg) injected mice were placed into a 6-well plate and imaged using Living Image software 24 hours post injection of the compound. Regions of interest (ROI) were defined using the software and quantification was carried it for each ROI separately. Graphical representation of the measurements taken from each ROI expressed as total radiant efficiency. Each bar represents the value from the respective organ of one experiment.

6.5.2 Determination of AF647-RIS uptake on a cellular level – analysis by flow cytometry

The results from this chapter have so far indicated that AF647-RIS not only localises to the skeleton but is also detectable in soft tissues such as the subcutaneous tumour. However, analysis of the drug distribution on a whole tissue level only gives limited information on the percentage and type of cells that may have taken up the drug. Samples from two experiments have therefore been analysed by flow cytometry. Tumour tissue, bone marrow and cells of the peritoneal cavity were prepared as single cell suspensions and run on a MoFlow® flow cytometer to detect AF647 in all samples as well as GFP in the tumour cell suspension. The use of the GFP expressing cancer cells allowed direct quantification of tumour cells (GFP positive) that have taken up the bisphosphonate. Samples from 2 mice per treatment group were split in half before processing, resulting in a replicate of n=4/tissue for PBS control and AF647-RIS injected mice. Details on gating are described in the respective Figure legends. Analysis of the cells of the peritoneal cavity showed a significant increase in AF647 detection with 26.73% AF647 positive cells in the AF647-RIS mice compared to a background level of 1.10% in the PBS control animals (Fig. 6.8C, $p<0.0003$). Furthermore, the analysis of

bone marrow samples revealed no significant difference in AF647 fluorescence between samples from PBS and AF647-RIS injected animals (0.97% vs. 1.36%, p<0.2558, Fig. 6.9).

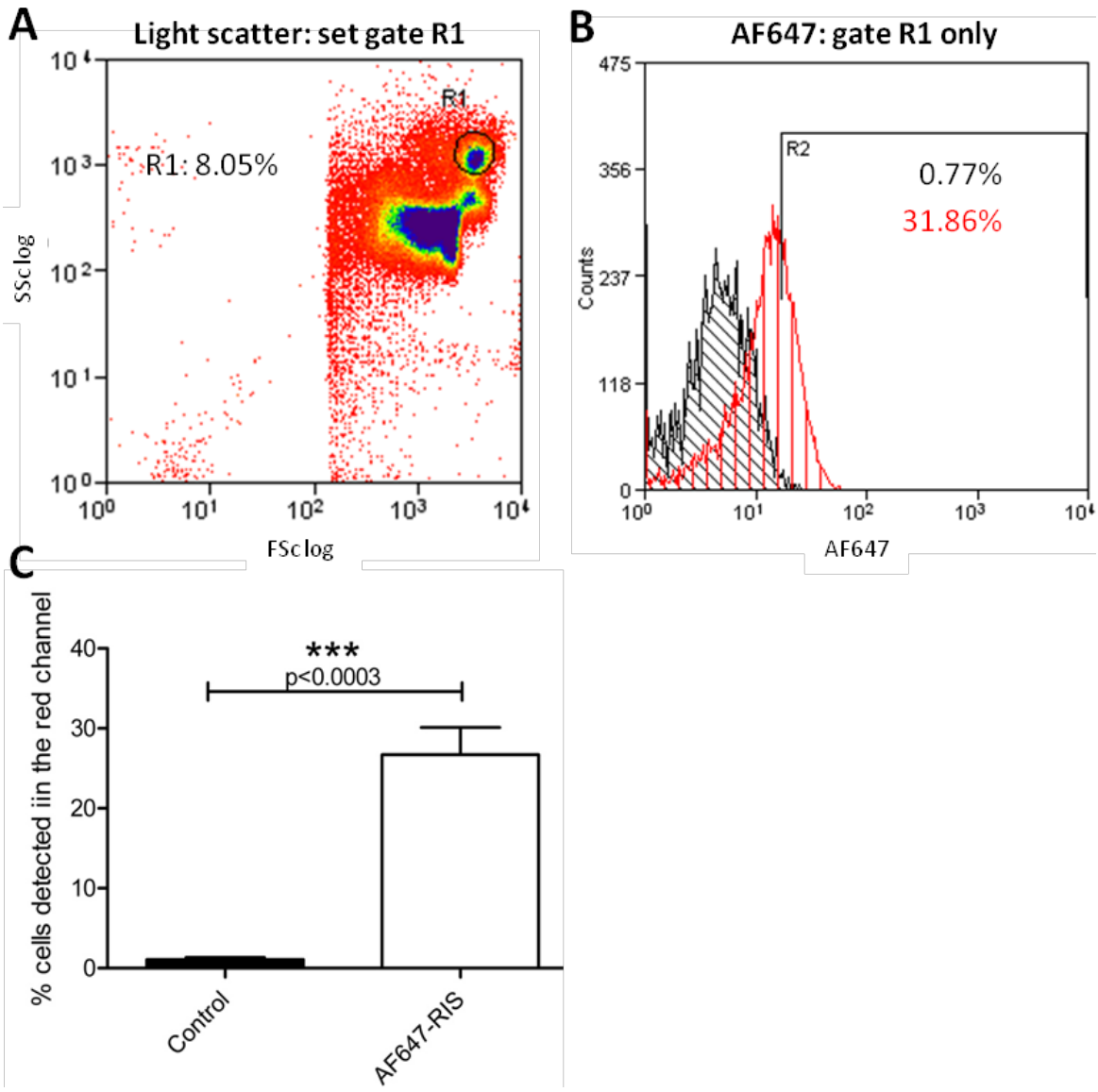

Figure 6.8 Flow cytometric analysis of cell suspensions taken from the peritoneal cavity

Cells of the peritoneal cavity were analysed (n=2 mice) in the PBS control and the AF647-RIS group. Samples were divided resulting in n=4 samples/group. Cell suspensions were analysed by flow cytometry for AF647. A) Light scatter histogram depicting the total cell population and the gate R1 (to exclude cell debris and because the main cell population appeared to be present within this area). B) Overlay histogram of cells in gate R1 of PBS control and AF647-RIS sample. Red=AF647-RIS, black=PBS. C) Bar graph of the mean cell frequency (%) detected in the red channel (AF647). Mean±SEM, T-test, *** is p<0.0003.

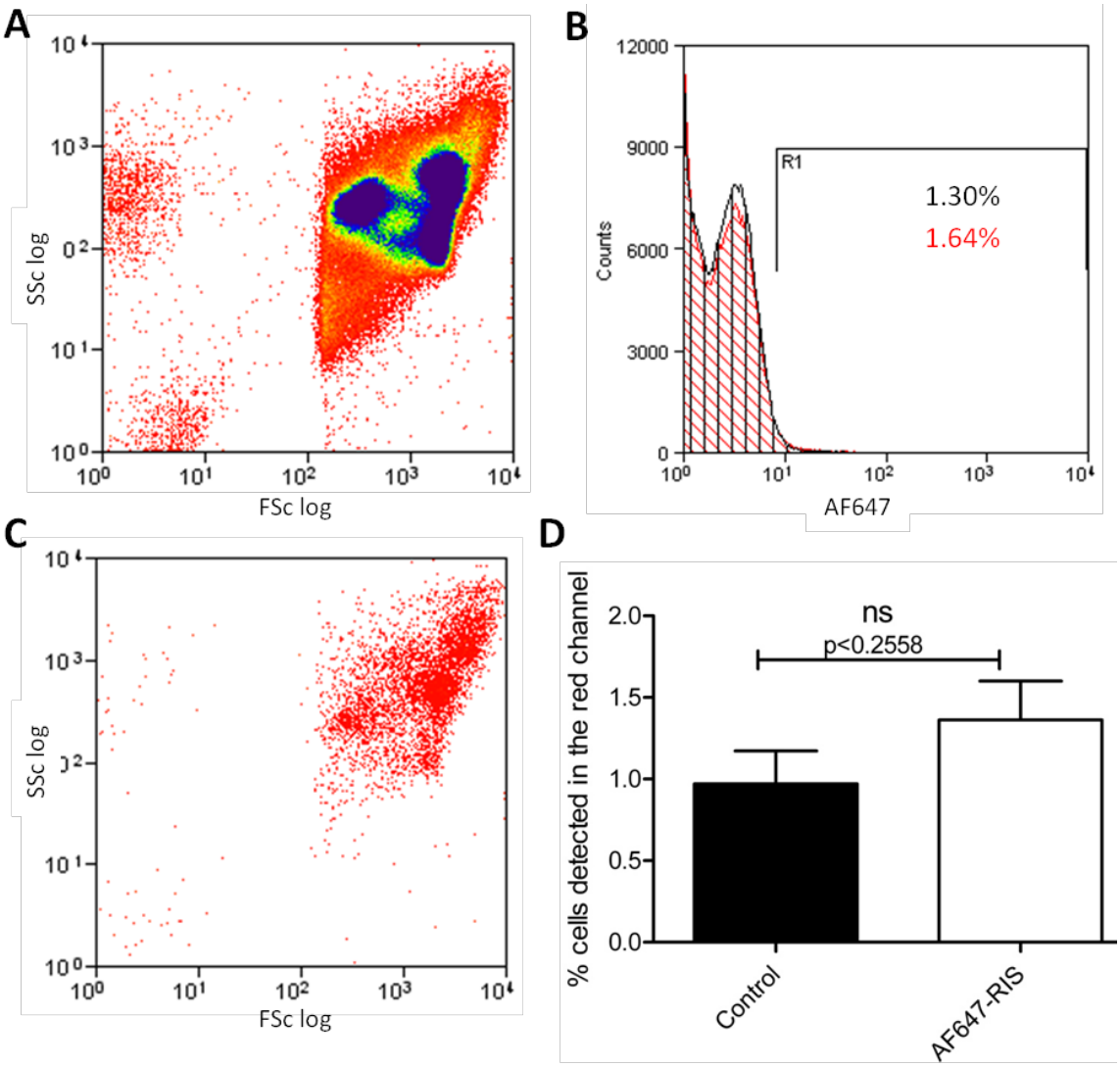

Figure 6.9 Flow cytometric analysis of bone marrow cell suspensions

Bone marrow cell suspensions were analysed for two mice in the PBS control and two mice in the AF647-RIS group. Samples were divided into two prior to processing resulting in n=4 samples/group. Cell suspensions were then analysed by flow cytometry for the presence of AF647. A) Example of a light scatter dot plot depicting the total cell population. No gate was set for the bone marrow samples because of the heterogeneity in cell types and because no single major population was distinguishable by size and granularity alone. B) Overlay histogram of one PBS control and one AF647-RIS sample. Red=AF647-RIS and black=PBS. C) Light scatter dot plot of the AF647 positive cells (R1) in histogram B) showing the location of these cells in the total cell population in the AF647-RIS sample. D) The graph depicts the mean frequency (%) of cells detected in the red channel (AF647) for the PBS control (black) and the AF647-RIS (white) samples. Mean±SEM, T-test, ns=not significant with p<0.2558.

The solid tumour tissue was dissociated enzymatically as well as manually prior to acquisition on the flow cytometer. A gate (R1) was therefore set according to *in vitro* MDA-G8 cells to exclude cell debris (Fig. 6.10A). For the analysis of tumour samples, the percentage of GFP positive tumour cells was determined showing similar percentages in both groups ($p<0.9448$, Fig. 6.10B). Next, the same cell population (R1) was analysed for AF647 to assess the total number of AF647-RIS positive cells. PBS control animals had a low background of 2.34% in the AF647 channel while the percentage increased significantly in the AF647-RIS injected mice up to 9.96% (Fig. 6.10C, $p<0.0134$), indicating that the drug was present in the subcutaneous tumour tissue. While this gives some information on the frequency of RIS positive cells in the analysed tumour samples, it does not identify the cell type(s) that have taken up the compound. The main question asked in this pilot project was to determine whether a bisphosphonate (AF647-RIS) was internalised by subcutaneously growing MDA-G8 tumour cells. Thus, the percentages of AF647 positive cells in the GFP positive cell population (gate R1 and R4) were analysed. It was shown that the drug was detectable in AF647-RIS injected mice with 9.04% of GFP and AF647 positive cells compared to the PBS control animals with 1.90% (Fig. 6.10D, $p<0.0003$). The data therefore suggest that a proportion of tumour cells at a peripheral site are capable of taking up AF647-RIS following a single administration of the drug.

Figure 6.10 Flow cytometric analysis of tumour cell suspensions for GFP and AF647-RIS (page 219)

Subcutaneous tumour cell suspensions were analysed for two mice in the PBS control and two mice in the AF647-RIS group. Samples were divided into two prior to processing resulting in n=4 samples/group. Cell suspensions were then analysed by flow cytometry for the presence of AF647 and GFP. A) Example of light scatter dot plots depicting the total cell population derived from subcutaneous tumours. Gate R1 was set according to *in vitro* MDA-G8 samples. B) Example histograms of GFP positive cells in gate R1 for a PBS and AF647-RIS sample. Mean % of GFP positive cells is shown in the bar graph. C) Example histograms depicting the detection of AF647 positive cells in gate R1 for PBS and AF647-RIS samples. The bar graph is showing the mean percentage of AF647 positive cells. D) Example histograms of AF647 positive cells in gate R1 and R4 for PBS and AF647-RIS samples. The mean % of AF647 and GFP positive cells is presented in the bar graph. All graphs show mean±SEM, T-test, ns=not significant with $p<0.9447$. * is $p<0.0134$ and *** is $p<0.0008$.

A) Light scatter: set gate R1

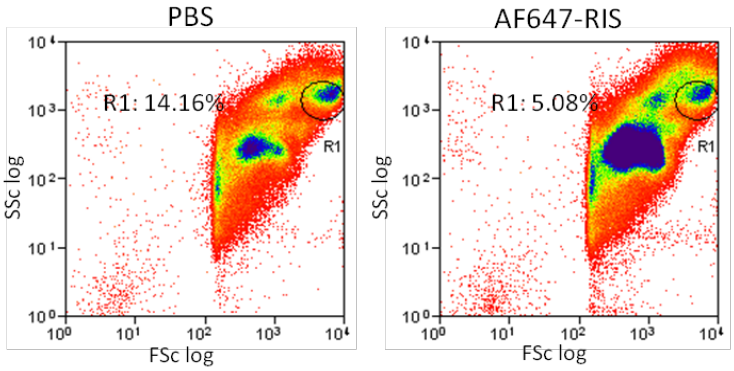

B) GFP: gate R1 only

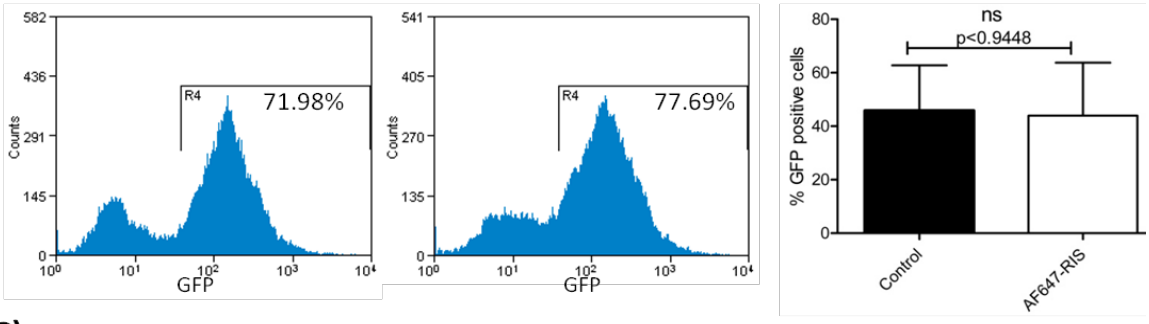

C) AF647: gate R1 only

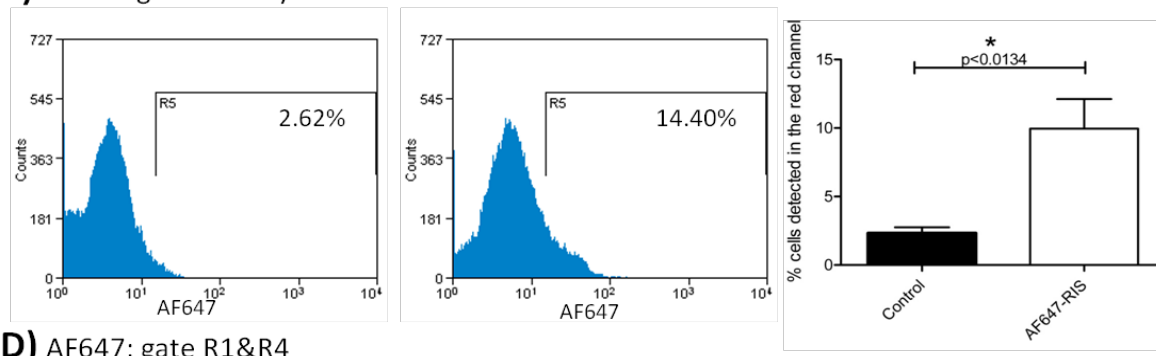

D) AF647: gate R1&R4

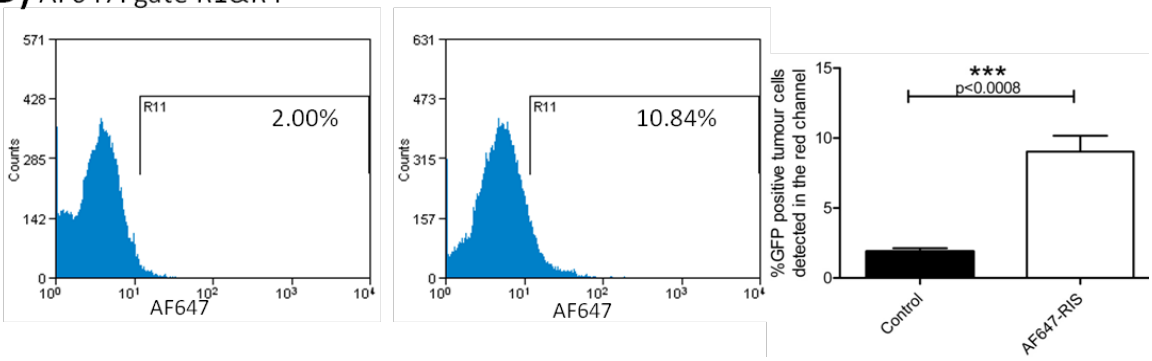

6.5.3 Visualisation of AF647-RIS uptake on a cellular level – analysis by microscopy

Confocal microscopy was used to further confirm the internalisation of the drug into the different soft tissues and the skeleton. Firstly the front legs of PBS and AF647-RIS injected mice were imaged using a 633nm laser to visualise AF647 and a multiphoton laser set at 900nm to visualise bone collagen by second harmonic generation. As expected, AF647-RIS was clearly visible along bone surfaces in the bisphosphonate injected mice but not in the vehicle treated animals (Fig. 6.11). Next, cytospins of the cells collected from the peritoneal cavity and bone marrow cell suspensions were analysed using transmitted light and a 633nm laser to detect AF647. Imaging confirmed the flow cytometry results with a high proportion of cells of the peritoneal cavity being AF647-RIS positive (Fig. 6.12) and only very few visible in the bone marrow samples (Fig. 6.13)

Figure 6.11 Multiphoton images of long bones (page 221)

Multiphoton microscopy images showing representative images of bone (front legs) from animals injected with either PBS (column A and B) or AF647-RIS (column C and D). Images were captured using a 20x objective and the tile scan option of the software. First row depicts AF647 (red) imaged using a 633nm laser, second row shows images taken using the multiphoton laser (Chameleon) at 900nm to visualise bone (white, second harming generation=sgh) and third row shows the overlay images. Scale bar=100μm, white box=area of magnification (20x objective).

A) PBS control (tile scan)
B) PBS control (inset)
C) AF647-RIS (tile scan)
D) AF647-RIS (inset)
AF647
Shg
Overlay
100 µm

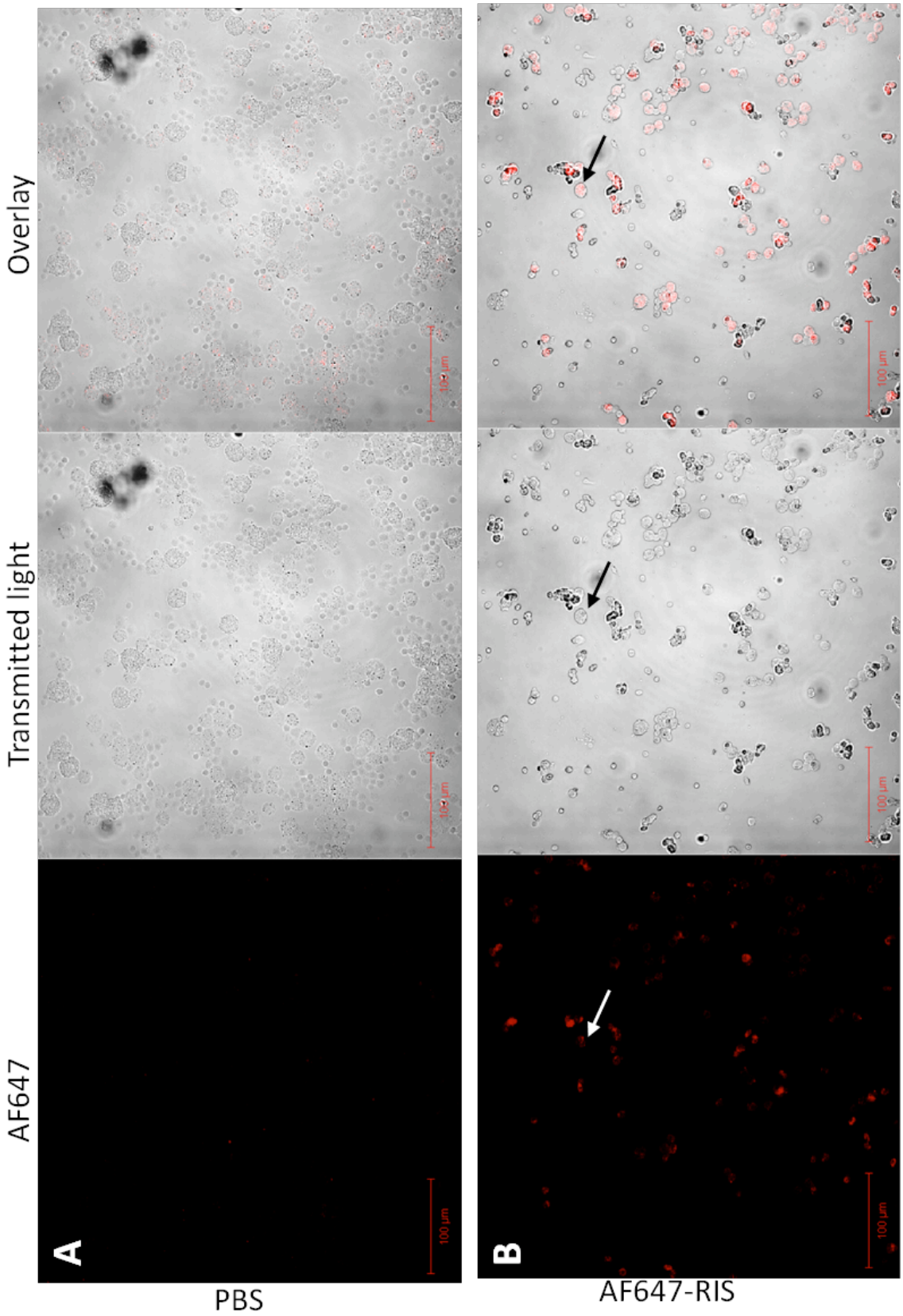

Figure 6.12 Microscopy images of cells of the peritoneal cavity

Images were taken with a 20x objective of cells of the peritoneal cavity from mice injected with A) PBS or B) AF647-RIS (400µg/kg) 24 hours prior to sacrifice. Cells were cytospun onto microscope slides directly post collection and imaged on the same day using transmitted light and a 633 nm laser to visualise AF647 (red). Scale bar=100µm, 20x objective.

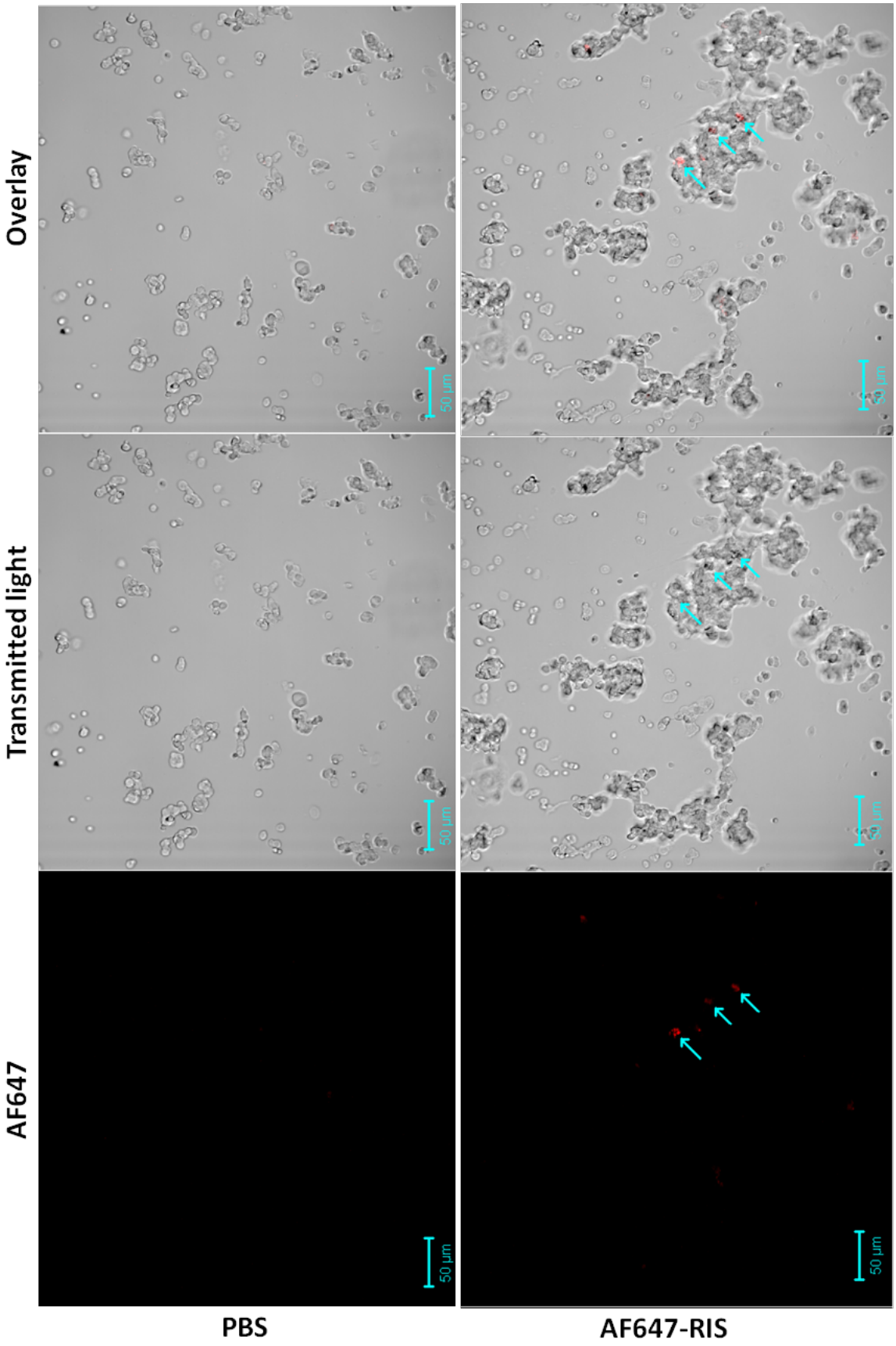

Figure 6.13 Visualisation of AF647-RIS in cells of the bone marrow

The image depicts bone marrow cells taken from hind legs of either PBS or AF647-RIS (400µg/kg) injected mice 24 hours post injection. Images were taken with a 20x objective using transmitted light and a 633nm laser to visualise AF647 (red, arrows). Scale bar=50µm.

Tumour pieces taken from drug treated mice also showed clear staining in some areas (Fig. 6.14) while the tumours from PBS treated mice were negative for the AF647 signal. Because imaging of a tumour piece did not allow discrimination between GFP positive tumour cells and other cells within the tumour (due to high background from the surrounding tissue layers), cell suspensions of subcutaneous tumours were analysed. Figure 6.15 depicts images taken from the tumour cell suspensions showing that GFP positive tumour cells do co-localise with distinct AF647 signals, indicating that the tumour cells have internalised the drug. In addition, other cell types that appeared smaller than the GFP positive tumour cells were AF647 positive.

In an attempt to further characterise AF647 labelled cells that were not GFP positive, F4/80 staining was performed using a pacific blue-labelled antibody. Staining was, however, not specific enough to draw any conclusions and was therefore not taken forward.

Together the data indicate that AF647-RIS is internalised by cells residing in the peritoneal cavity, cells of the bone marrow and also by a proportion of GFP positive tumour cells as well as other cell types in the tumour tissue.

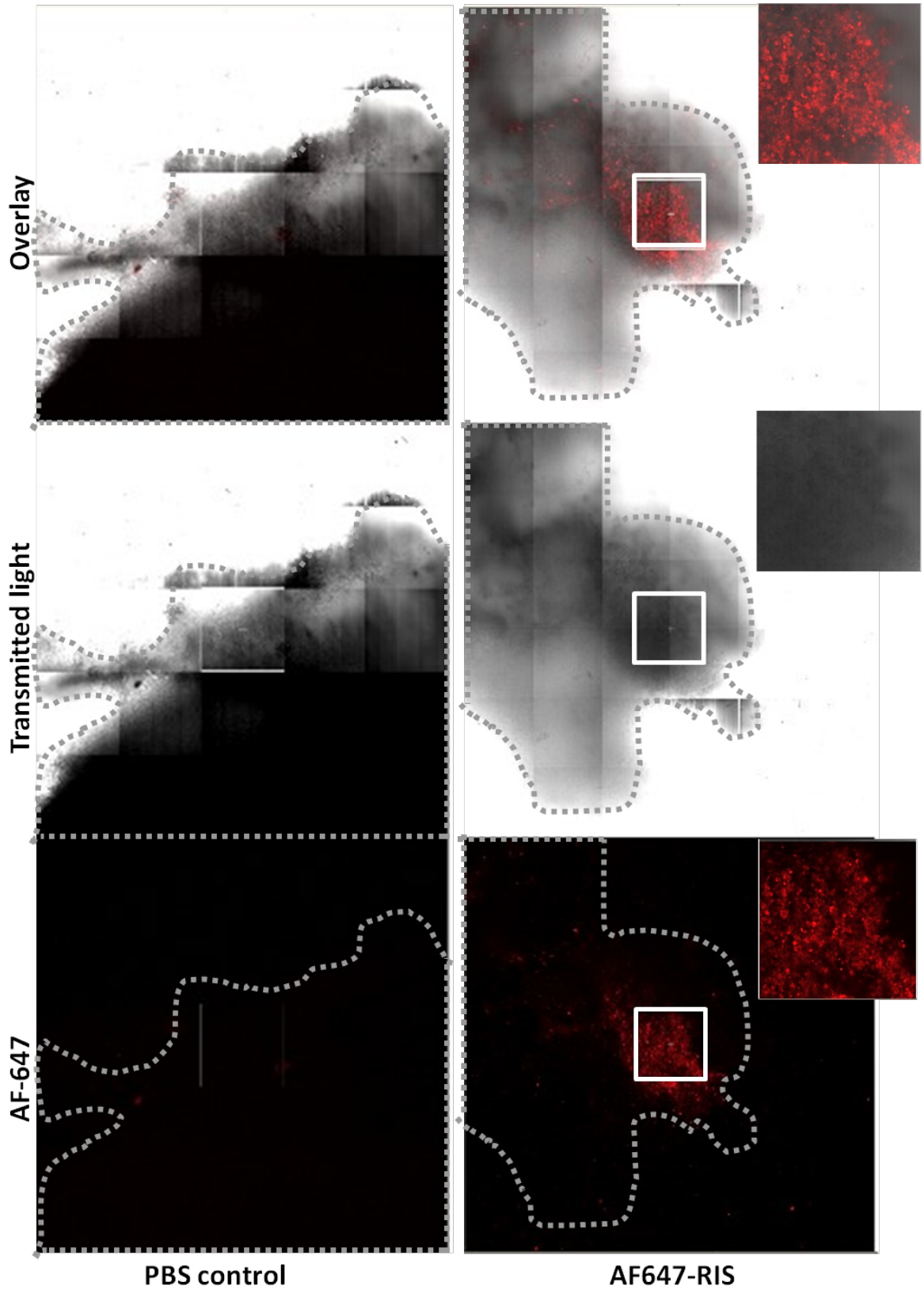

Figure 6.14 Imaging of subcutaneous tumour tissue by confocal microscopy
Tumours that were excised from AF647-RIS or PBS treated mice were snap frozen in liquid nitrogen, embedded in OCT and then visualised by microscopy. A 633nm laser was used to detect AF647 (red) and transmitted light to visualise the tumour. Images depict tile scans captured with a 20x objective. Inset in AF647-RIS represents one tile (white box, 20x objective).

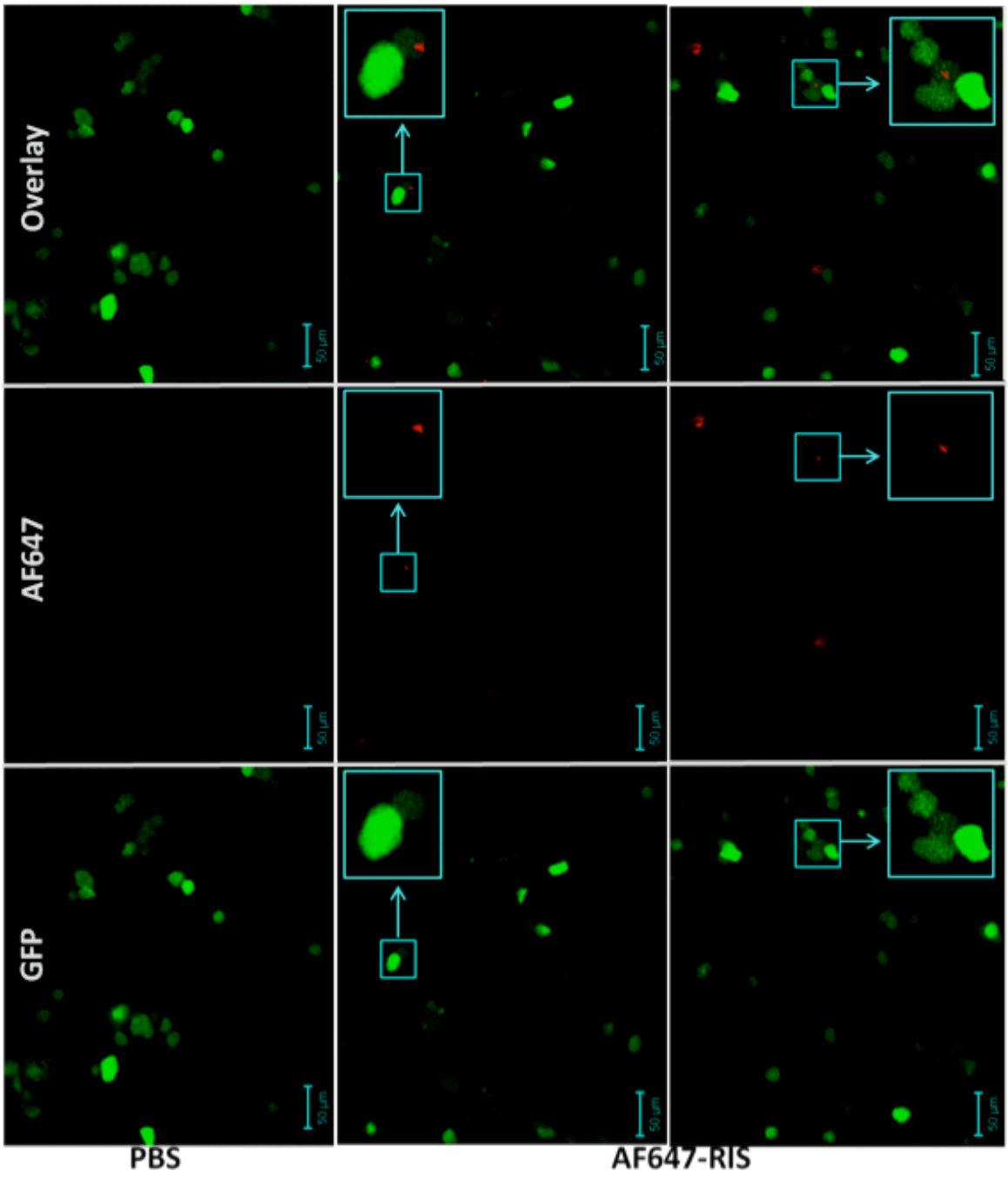

Figure 6.15 Microscopy imaging of tumour cell cytospins

Cytospin preparations of subcutaneous tumour tissue were imaged by confocal microscopy for PBS and AF647-RIS samples. GFP (green), AF647 (red). Scale bars are 50µm, 20x objective. Blue boxes indicate area of inset showing colocalisation of a GFP positive tumour cell and AF647-RIS.

6.6 Discussion

Due to the high affinity for bone and rapid clearance the main target of bisphosphonates are bone cells. However, many groups have reported anti-tumour effects of the agents, with some showing effects on extraskeletal tumours, but it is unclear whether these are of direct or indirect nature. I have therefore investigated the skeletal and soft tissue distribution of the AF647 tagged risedronate analogue AF647-RIS in a mouse model of peripheral breast tumour growth. Animals bearing subcutaneous MDA-G8 (MDA-MB-436-GFP) tumours were injected with PBS, AF647 or AF647-RIS (400µg/kg) and the distribution of the drug was analysed 24 hours later by non-invasive *in vivo* imaging, flow cytometry and confocal microscopy. This is the first study showing that a proportion of GFP positive cells in a peripheral solid tumour mass are capable of taking up AF647-RIS after 24 hours.

IVIS® imaging of animals at 2-20 minutes, 2 hours and 24 hours after injection of the compound showed rapid distribution from the site of injection along the spine from 8 minutes onwards. The bisphosphonate appeared to be visible in skeletal structures rather than soft tissues suggesting that the signal of the drug in the circulation is too low to be detected with the used settings and only accumulation at skeletal sites is visible. This may explain why the AF647 tag was only visible at site of injection when given on its own, supporting the conclusion that any signal in AF647-RIS treated mice is not by free label. In agreement with other published studies in tumour-free animals, AF647-RIS was detected in the liver, kidney and lung but not in the spleen after sacrifice of the animals. Most importantly, the drug was also detected in subcutaneous tumours 24 hours post injection. Roelfos et al. (2009) investigated the uptake of AF647-RIS into tibia and femur as well as the soft tissues liver, kidney and spleen of 3-month-old MF1 mice injected with 0.9mg/kg AF647-RIS and sacrificed either 1 or 7 days post injection. Analysis of the tissues using a 680nm laser on an Infrared Imager showed a significant uptake of the drug into the tibia and femur on both day 1 and 7 as well the kidney at one day post injection. All other organs were found to be negative for the drug when compared to organs from control animals. The discrepancy between the data presented here showing detection of AF647-RIS in liver kidney and lung but not the spleen and that of Roelofs et al. could be due to limitations of the imaging tools used for analysis on a whole tissue level. In addition, the retention of BPs in

extra-skeletal tissues may be dose dependent since it has been reported by Lin et al. (1992) that a high dose of alendronate (30mg/kg) is present in the liver, spleen and kidney of young rats for a longer period of time compared to the 1mg/kg dose, with approximately 25% of drug being present in the non-calcified tissues 48 hours post 30mg/kg alendronate administration.

I further analysed cells isolated from peritoneal cavity and bone marrow by flow cytometry, which showed a significantly higher percentage of AF647 positive cells in samples taken from the peritoneal cavity, but not in bone marrow cells, when compared to control. Due to the very limited amount of drug available in this pilot study I was not able to further identify the cells detected to be AF647 positive, although other groups have identified bisphosphonate internalising cells predominantly to be of the macrophage lineage. Roelofs et al. (2009) have assessed the uptake of bisphosphonates into osteoclasts *in vivo* after injection of a single dose of FAM-RIS and AF647-RIS (day 1 post injection) by imaging either bone sections or isolated osteoclasts by microscopy. The results demonstrated intracellular uptake of the drugs into osteoclasts *in vivo* and the activity of FAM-RIS was confirmed by an increase in unprenylated Rap1A. Investigation of BP uptake into rabbit and human bone marrow cells *in vitro* showed that AF647-RIS was readily internalised after 24 hours. Further immunofluorescence staining showed detection of the drug predominantly in CD14 positive monocytes. The intracellular uptake and inhibition of the mevalonate pathway were further confirmed in bone marrow cell suspensions taken from 3 month old rabbits injected with 0.9mg/kg or 5mg/kg AF647-RIS 24 hours prior to sacrifice. CD14 positive cells have also been shown to be associated with other tissues and it may therefore be possible that the soft tissue associated AF647-RIS cells detected in the present study are, at least in part, monocytes. A study investigating the *in vivo* accumulation of NBP-induced IPP and ApppI could confirm the presence of either compound in peritoneal macrophages but not in bone marrow cells (Monkkonen et al., 2007).

Tumour cell suspensions were also analysed for the presence of AF647, with the GFP positive cell population having a significant proportion of cells that had internalised the drug. The flow cytometry data was therefore in agreement with the IVIS® results; however, flow cytometry alone cannot confirm the internalisation of the drug into the

cancer cells per se since it is possible that the drug is bound to the tumour cell membrane or that other AF647 positive cell types are attached to the cancer cells. When assessing whole tumour tissue by microscopy only localised staining for AF647 was detectable, which is in agreement with a study carried out by Shay et al. (2011) showing that only parts of a peripheral tumour were positive for AF647. In contrast to the present data showing clear internalisation of the drug into GFP positive tumour cells, Shay et al. did not find any GFP positive tumour cells that had internalised AF647-RIS but could show that a population of myeloid cells (CD11b+F4/80+ monocytes/macrophages and Gr1+CD11b+ myeloid-suppressor cells) were AF647 positive. The discrepancy between the studies could be due to the use of different mouse models. Shay et al. used the syngeneic 4T1 mouse model, which was found to exhibit a significant tumour-induced increase in Gr1+CD11b+ myeloid cells (from 5-80% in the spleen and from 20-70% in the bone marrow), the cell type that was further shown to internalise the bisphosphonate.

The effect on soft tissue cells may ultimately be determined by the drug concentration in these tissues. Weiss et al. (2008) have investigated the biodistribution of zoledronic acid in male rat soft tissues and the skeleton. It was shown that there was a slow, albeit low release of ^{14}C-labelled zoledronic acid from bone with levels in soft tissues and plasma being below 0.4nmol/g, 96 hours after the last dose was given (0.15mg/kg, 16x on consecutive days). The authors concluded that the detection of zoledronic acid (up to 240 days after the last injection) in plasma and non-calcified tissues reflects a slow release of the drug from the skeleton, rather than systemic clearance. In addition, Roelofs and colleagues have suggested that the endocytic activity of cells *in vivo* is more relevant to the internalisation of bisphosphonates than the location within bone (Roelofs et al., 2009). Whether these systemic low concentrations of bisphosphonates released from the bone are sufficient to exert biological effects remains to be established. But as the anti-resorptive effect wears off after 3-4 weeks (even when administering the most potent bisphosphonate zoledronic acid) it is unlikely to have significant impact when used as single agents.

To date no published study is available investigating the cellular uptake of a clinically relevant dose bisphosphonates in peripheral tumour tissue. A study by Ottewell et al. (2009) investigated whether zoledronic acid is internalised into intratibial MDA-MB-

436-GFP tumours *in vivo*. Treatment commenced one week after tumour cell implantation for a total of six weeks with PBS, doxorubicin (2mg/kg), zoledronic acid (100µg/kg) or doxorubicin followed 24 hours later by zoledronic acid (once weekly administration) and were sacrificed 24 hours after the last treatment. It was shown by western blot analysis that unprenylated Rap1A was only detectable in tumours from animals treated with the chemotherapeutic agent (doxorubicin) 24 hours prior to zoledronic acid, but not in animals treated with zoledronic acid alone. The data suggest that zoledronic acid concentrations are not sufficient to significantly affect the mevalonate pathway in peripheral tumour cells when administered alone or that the method was not sensitive enough to detect low levels of unprenylated Rap1A. In addition, the frequent dosing regimen results in a relatively high-accumulated zoledronic acid concentration, not mimicking the clinical situation of a single dose every 3-4 weeks.

Taken together the data presented in this chapter show that the bisphosphonate AF647-RIS is internalised by a small proportion of GFP positive tumour cells at a subcutaneous site. The findings suggest that the bisphosphonate does reach tumour cells outside the skeleton without requiring repeated dosing regimens. Despite this, the number of tumour cells found to have internalised the drug are unlikely to be high enough to cause a substantial reduction in tumour growth.

7. Discussion

Advanced breast cancer is associated with a high mortality rate and approximately 70% of patients will develop secondary disease with a high prevalence of bone associated tumour growth. Currently, the metastatic tumour spread cannot be effectively impeded due to lack of effective treatment regimens. Predictive markers for metastatic disease are not available and patients with bone metastases will therefore often present with symptomatic disease caused by already established osseous lesions. Previous preclinical work has contributed greatly to the detection of factors involved in the vicious cycle; and most studies have mimicked the clinical setting by investigating end stage disease with overt bone destruction. It has become clear that investigation of earlier stages, prior to bone destruction, is required for the development of new treatment targets. More recent studies have proposed the concept of the pre-metastatic and metastatic niche as a potential target of early stage cancer in bone (Kaplan et al., 2005; Shiozawa et al., 2011). Stromal cells, osteoblasts, osteoclasts and other factors of the tumour microenvironment have therefore become increasingly investigated. In addition, preclinical data is accumulating in support of earlier treatment regimens (including preventive strategies) (Sasaki et al., 1995; Sasaki et al. 1998) and enhanced anti-cancer effects of combination therapies to target both the tumour and the microenvironment (Hiraga et al., 2003; Ottewell et al., 2008a).

Work presented in this thesis has utilised a number of novel *in vivo* studies and analysis methodologies to help determine bone cell-tumour cell interactions during disease progression and the effects of early combination treatment. Initially, analysis methodologies to investigate the tumour as well as the bone microenvironment, as for example differential analyses of histological sections or the use of multiphoton microscopy for detection of tumour cells in bone, were assessed. While the latter method has the benefit of high resolution and detection of even single tumour cells in the bone compartment, it is not feasible to investigate the surrounding bone cells. Histology and bone histomorphometry therefore remain invaluable tools for identification of the complex cellular interactions within bone and other tissues. New imaging techniques are continuously emerging and will, in combination with other methods, help to elucidate the early stages of tumour cell colonisation and growth in bone. The increasingly sensitive imaging modalities in combination with enhanced firefly luciferase reporters (luciferase2) (van der Horst G, 2011) and for example *in vivo*

activated fluorescent probes such as Prosense®680 (Weissleder et al., 1999) or photoswitchable fluorescent proteins (PsmOrange) (Subach et al., 2011) will furthermore add important information to standard methods. Especially the increased ability to visualise small numbers of tumour cells at great tissue depths will be beneficial. A downside of relying on histology alone is that only snapshots of the *in vivo* situation are available and extrapolation of three-dimensional interactions from two-dimensional images is required. The identification of single tumour cells on histological sections was proven to be difficult (Chapter 3). Detection of disseminated tumour cells in the bone marrow would greatly benefit from identification through a specific marker; however the expression levels of human tumour cell-associated antigens like GFP, beta-galactosidase, luciferase, cytokeratin and EpCAM may vary greatly *in vivo*. A recent study reported that antibodies to the human HLA antigen, which is highly expressed by human cancer cell lines, allow detection of disseminated tumour cells in the murine bone marrow (Shiozawa et al., 2011). The application of this antibody in breast cancer metastases to bone is currently under investigation in our unit and could add significant value to future studies.

Chapter 4 describes the first longitudinal *in vivo* study reporting the detailed spatial and temporal relationship between bone and breast cancer cells and revealed that the dynamic between these cell types is more complex than previously described. The study provided strong evidence that differential analysis of osteoblasts and osteoclasts is required to decipher the tumour-induced changes in detail. The spatial proximity of bone cells to the tumour is currently not taken into account in many studies investigating the tumour bearing bone microenvironment. Osteoblast numbers were drastically altered in the presence of the tumour, strongly suggesting a major role of this cell type in metastatic breast tumour development. This data supports current reports identifying the osteoblast as a crucial factor of tumour cell homing and progression in bone. For example, *in vitro* analyses using a 3-dimensional osteogenic tissue model grown from the murine MC3T3-E1 pre-osteoblast cell line showed direct interactions between osteoblasts and MDA-MB-231 cells (Dhurjati et al., 2008). Interestingly, immature culture conditions were found to be more beneficial to cancer cell colonisation while mature osteoblast cultures were required for tumour formation. An *in vivo* study furthermore reported that intratibial co-injection of the pre-

osteoblastic MC3T3-E1 cell line and MDA-MB-231 cells induced significantly higher tumour burden compared to athymic mice injected with the cancer cells alone (Bodenstine et al., 2011). In addition, the recently published study by Shiozawa et al. (2011), showed that prostate cancer cells home specifically to the HSC niche, in which the osteoblast is an important component, and that niche expansion (PTH administration) or reduction (SDF-1 inhibitors like AMD3100) enhanced or decreased tumour cell numbers in the bone marrow, respectively. While most recent research has focused on the osteoblast-tumour cell interactions at the homing stage of metastatic disease, the intermediate stages of tumour growth like the escape from quiescence and the switch from microenvironment-dependent to -independent tumour growth are equally important areas of interest. The data from this thesis furthermore add to the understanding of these processes by showing that osteoblasts, in addition to osteoclasts, may also be relevant during the transition of micro- to macro-metastatic growth. This is in agreement with a study investigating bone biopsies of breast cancer patients (Vukmirovic-Popovic et al., 2002). Comprehensive analysis showed increased osteoclast and osteoblast numbers on biopsies with small to medium cancer colonies (bone marrow cavity covered to 7.5% or 24.4% by tumour) compared to non-tumour bearing control. Biopsies with larger tumours (tumour covering 47.1% of the bone marrow cavity) had decreased osteoblast and osteoclast numbers compared to tumour-free biopsies. This discrepancy in osteoclast numbers in comparison to the present data could be explained by differences between a mouse model and human biopsies and that total tumour burden in the biopsy cannot be assessed due to the relatively small area available for investigation. In addition, osteoclast and osteoblast distribution may vary depending on location within the bone (Chapter 3). Published information on early stage breast cancer and the related changes to the bone microenvironment is largely limited to the report of Phadke et al. (2006), who reported tumour progression-dependent reduction of osteoclast and osteoblast numbers four weeks after tumour cell implantation. The decrease in osteoblast number was shown to be associated with an increase in osteoblast apoptosis. In the present study osteoblast numbers were also reduced at later stages of tumour growth but levels of cell death were not analysed. Future *in vitro* studies could determine whether tumour cells directly affect osteoblast numbers and whether this is due to cell-cell contact or secreted molecules.

The present work is furthermore the first to comprehensively assess *in vivo* whether the changes in bone cell numbers were of a local or systemic nature. The lack of bone loss in the opposite non-tumour bearing leg strongly suggested the involvement of local interactions (within the affected bone compartment), which was supported by the unaffected serum marker concentrations in tumour bearing compared to naive animals. In addition, the analysis of tumour gene expression indicated that bone related genes, such as the osteoblast inhibitors DKK1 and SFRP-1 as well as the osteoclast stimulating RANKL and GMCSF, were upregulated in tumours growing in bone compared to the same cells grown *in vitro* or as subcutaneous tumours. Thus a direct effect on the surrounding cells is likely but requires further investigation. The present study therefore strongly suggests that tumour cells influence bone cells through direct cell-cell contact as well as via secretion of factors to affect more distal cells. Tumour-induced angiogenesis, which is strongly associated with both the osteoclast and the osteoblast (Parfitt, 2000) could also be investigated in future studies. Little is known about tumour angiogenesis in bone due to lack of suitable analysis methodologies, however the association of blood vessels with the HSC niche emphasises the need to explore the dynamics between the endothelium, bone and tumour cells in more detail (Roche et al., 2012). The possible application of new techniques like the three-dimensional perfusion model (allowing 3-D reconstruction of the vasculature, visualisation and quantification of vessels) in metastatic bone disease may give further insight into the spatial and temporal relationship between tumour, bone and blood vessels.

The data from the longitudinal study indicate that early treatment regimens may be more beneficial than those currently in clinical practice. This has been shown previously in preclinical treatment studies (Brown and Holen, 2009), although the association with the detected changes in bone cells is novel to the present study. The rise in total osteoblast numbers that is taking place before the onset of bone degradation and its associated increase in total osteoclast numbers (Chapter 4) may be the turning point in the highly complex initiation process of microenvironment independent tumour growth. It was therefore investigated whether tumour progression in bone could be prevented by early combination treatment targeting the bone microenvironment and the tumour. Therapy using doxorubicin followed 24 hours

later by zoledronic acid has previously been shown to be effective in reduction of subcutaneous (Ottewell et al., 2008b; Ottewell et al., 2010), advanced bone (Ottewell et al., 2008a; Ottewell et al., 2009) and spontaneous mammary fat pad tumours (Ottewell et al., 2011). The synergistic anti-tumour effect is suggested to be exerted through alterations in apoptotic and cell cycle gene pathways as well as through increased bisphosphonate uptake after doxorubicin treatment (Ottewell et al., 2009). However, the effects of the treatment on the bone microenvironment were not investigated in detail.

The present study is the first to show that clinically relevant treatment at an early stage of tumour growth (day 2 following tumour cell implantation) almost completely abolished intraosseous tumours, which was associated with a significant reduction in osteoblast numbers and osteoclast activity. In addition, extraosseous tumour growth was inhibited but not eliminated. The site dependent reduction of MDA-MB-231 growth indicates an indirect anti-cancer effect through the bone microenvironment. In fact, a single dose of zoledronic acid, alone or in combination with dox, caused a dramatic change in osteoblast numbers on day 15. While the effects of bisphosphonates on osteoclasts are well established, the findings of reduced osteoblast numbers are the first reported after administration of a single dose *in vivo*. Currently few data are published investigating the effects of bisphosphonates on osteoblasts. In a recent study, primary rat osteoblast numbers growing on bisphosphonate-coated bone slices were significantly reduced compared to untreated control, suggesting active cellular internalisation (Cornish et al., 2011). Furthermore, an *in vivo* study undertaken by Pozzi et al. (2009) investigated the effects of zol (weekly for three weeks) on C57BL6 mice. The group detected a decrease in osteoblast and osteoclast numbers by histomorphometric analyses, which were reflected in decreased serum measurements of osteocalcin (bone formation marker) and TRAP5b (bone resorption marker). The inhibitory effect of zol (10µM, twice/week) on osteoblast viability and activity was confirmed *in vitro* showing that inhibition was only detectable after 7 days of culture. The delayed effect of zol on osteoblasts *in vivo* in the present study is in agreement with these data suggesting that the low endocytic activity of osteoblasts compared to osteoclasts may be responsible. In contrast, there is also literature suggesting that the drugs exhibit differential effects on osteoblasts, including

increased activity at low doses, depending on the exposed concentration *in vitro* (Corrado et al., 2010). First *in vivo* evidence that zoledronic acid-induced reduction of melanoma tumour burden is independent of osteoclast related effects was shown in src-/- mice, which lack functional osteoclasts (Hirbe et al., 2009). The data suggest that the bisphosphonate either directly affected the tumour cells or acted through different cell types in the tumour environment, such as endothelial cells or osteoblasts. Ongoing research in our unit is investigating the effects of osteoblast deficiency on osseous breast tumour growth *in vivo*. A single dose of zoledronic acid with or without doxorubicin was also shown to reduce osteoclast activity and increase cell size but numbers were unchanged until twenty-one days after treatment. The data are in agreement with a recent case study report by Jain and Weinstein (2009) suggesting that primarily osteoclast activity is inhibited by BP treatment.

In order to decipher the microenvironment-dependent and independent anti-tumour mechanisms in more detail, a selection of genes involved in apoptosis and cell cycle regulation were analysed by quantitative real time PCR. The genes had previously been shown to be altered in advanced bone tumours after combination therapy with dox then zol (Ottewell et al., 2009). Analysis of the small tumour colonies in the present study was problematic even after pre-amplification. The successfully assessed genes confirmed the immunohistochemistry data showing lack of direct effects on the tumour at the later time point (day 23). This suggests immediate cytotoxic activity of the combination therapy since I investigated tumour tissue 21 days after completion of treatment compared to 24 hours in the study by Ottewell et al. (2009). Also, gene signatures and response to treatment may differ between the two cell lines used (MDA-MB-231 vs. MDA-MB-436).

The present study is the first to show that a single dose of early combination treatment induced almost complete elimination of intraosseous tumour growth (in 6 out of 7 mice) and that single agents had no effect on overall tumour burden. Despite this, small, separate extraosseous tumours were detected along the periosteum of these mice. The findings indicate that alterations to the bone microenvironment may cause a diversion of cells to other sites. This could also occur at extra-skeletal organs and although at the time not possible, could now easily be investigated with the new imaging modalities (IVIS®). However, differential analysis that requires higher

resolution like the intra- vs. extraosseous tumour foci would still need to be performed by other means. The data from this thesis further confirm findings from *in vivo* studies reporting similar bone restricted anti-tumour effects of bisphosphonate treatment alone (Sasaki et al., 1995, van der Pluijm et al., 2005) or in combination with cytotoxic drugs (van Beek et al., 2009).

The predictive significance of preclinical treatment studies is not always clear since drugs often fail or cause differential effects in clinical studies compared to those demonstrated using *in vivo* models. An example is the recent AZURE trial (Coleman et al., 2011), which was partly based on the promising preclinical data from the sequence- and schedule-dependent combination studies with doxorubicin followed by zoledronic acid (Neville-Webbe et al., 2005; Ottewell et al., 2008a; Ottewell et al., 2008b; Ottewell et al., 2010). Importantly, AZURE as well as the ABCSG-12 (Gnant et al., 2009) and the NSABP-34 (Paterson et al., 2011) trial reported the relevance of reproductive hormone levels for the observed anti-tumour effects, with post-menopausal women benefiting from the addition of zoledronic acid. Importantly, the hormone receptor status was reported to be of no significance for disease outcome. The AZURE trial furthermore indicated that inhibition of the vicious cycle may also carry the risk of relocating the metastatic processes to areas outside bone, an observation that was also made in the present preclinical study. Early treatment (adjuvant) of breast cancer patients should therefore be assessed with caution and further preclinical research is required to investigate the treatment effects on bone remodelling and tumour growth in more detail. While these important data were not yet available during my PhD, the interactions between reproductive hormones and treatment of osseous cancer is currently investigated in our unit.

Although bisphosphonates are frequently used in preclinical and clinical studies the biodistribution, half-life and tissue concentrations of BPs are difficult to measure and the effects of the drugs on non-osseous tissues *in vivo* are not well understood. This is mainly due to difficulties in detection of the drug with the main two methods being detection of unprenylated Rap1A by western blot and the use of radiolabelled compounds. The recent development of fluorescently tagged risedronate (Roelofs et al., 2009) has, however, increased the sensitivity of detection greatly. A pilot study performed in this thesis is the first to show that peripheral MDA-MB-436 tumours

actively internalise fluorescently labelled risedronate (AF647-RIS). The near-infrared tag allows imaging with a good signal to noise ratio and thus analyses by IVIS®, flow cytometry and microscopy was successfully performed. Benzaid et al. (2011) were the first to report IPP and ApppI detection in T47D subcutaneous tumours twenty-four hours after treatment with IL-2 + zoledronic acid + PBMC (peripheral blood mononuclear cells). The group concluded that the IPP and ApppI accumulation was due to inhibition of the mevalonate pathway in T47D cells rather than tumour-associated cells like macrophages, since phosphoantigens were undetectable in B02 xenografts after identical treatment. The present data are in agreement with this finding and significantly add to it by showing detection of AF647-RIS on a cellular level. Furthermore, a study by Guenther et al. (2010) showed increased quantities of human unprenylated Rap1A in homogenised plasmacytoma tumours 24 hours after zoledronic acid treatment. Animals were treated either once or thrice with zoledronic acid (8µg/mouse) and were culled 24, 48 or 72 hours after the last injection. While the work arising from my thesis strongly complements these two studies in favour of active bisphosphonate uptake into peripheral tumour cells *in vivo*, a study by Shay et al. (2011) did not. In this study, the 4T1 murine breast cancer model was used to assess AF647-RIS distribution *in vivo*. AF647-RIS uptake was detected in a proportion of tumour-associated macrophages 24 hours after injection of the drug but not in GFP-tagged cancer cells. In conclusion, the few studies investigating the internalisation of bisphosphonates into peripheral tumours *in vivo* have reported controversial data. However, the use of different tumour models suggests great variation in the *in vivo* distribution of the compounds. Whether these data are applicable to the clinical setting and whether sufficient amounts of the drugs are internalised to cause detectable cytotoxic effects remains to be established.

Bisphosphonates have been used in clinic since the 1990s and are the standard of care for bone-associated diseases and the interactions between the bone microenvironment and the tumour cells in bone have been the research focus of the last year. The present thesis has contributed to this field of knowledge in several aspects as has been described above. The importance of the microenvironment in the development of new treatment targets has recently been exemplified by the

development of denosumab, a human anti-RANKL antibody with superior anti-resorptive activity (delayed first on study SRE in breast cancer) compared to zoledronic acid (Stopeck et al., 2010). The underlying mechanisms of treatment-induced alterations to the bone microenvironment, the potential associated risks and the target group of patients remain to be established in future studies.

8. Bibliography

Allavena, P., Sica, A., Solinas, G., Porta, C., and Mantovani, A. (2008). The inflammatory micro-environment in tumor progression: the role of tumor-associated macrophages. Crit Rev Oncol Hematol 66, 1-9.

Allen, M.R., Hock, J.M., and Burr, D.B. (2004). Periosteum: biology, regulation, and response to osteoporosis therapies. Bone 35, 1003-1012.

Arguello, F., Baggs, R.B., and Frantz, C.N. (1988). A murine model of experimental metastasis to bone and bone marrow. Cancer Res 48, 6876-6881.

Bendre, M.S., Montague, D.C., Peery, T., Akel, N.S., Gaddy, D., and Suva, L.J. (2003). Interleukin-8 stimulation of osteoclastogenesis and bone resorption is a mechanism for the increased osteolysis of metastatic bone disease. Bone 33, 28-37.

Benzaid, I., Monkkonen, H., Stresing, V., Bonnelye, E., Green, J., Monkkonen, J., Touraine, J.L., and Clezardin, P. (2011). High phosphoantigen levels in bisphosphonate-treated human breast tumors promote Vgamma9Vdelta2 T-cell chemotaxis and cytotoxicity *in vivo*. Cancer Res 71, 4562-4572.

Bingle, L., Brown, N.J., and Lewis, C.E. (2002). The role of tumour-associated macrophages in tumour progression: implications for new anticancer therapies. The Journal of Pathology 196, 254-265.

Blanchard, F., Duplomb, L., Baud'huin, M., and Brounais, B. (2009). The dual role of IL-6-type cytokines on bone remodeling and bone tumors. Cytokine Growth Factor Rev 20, 19-28.

Bodenstine T.M., Beck B.H., Cao X., Cook L.M., Ismail A., Powers S.J., Powers J.K., Mastro A.M., Welch D.R. (2011). Pre-osteoblastic MC3T3-E1 cells promote breast cancer growth in bone in a murine xenograft model. Chin J Cancer 30, 189-96.

Boyce, B.F., and Xing, L. (2007). Biology of RANK, RANKL, and osteoprotegerin. Arthritis Research & Therapy 9 Suppl 1, S1.

Boyle, W.J., Simonet, W.S., and Lacey, D.L. (2003). Osteoclast differentiation and activation. Nature 423, 337-342.

Brown, H.K., and Holen, I. (2009). Anti-tumour effects of bisphosphonates--what have we learned from *in vivo* models? Curr Cancer Drug Targets 9, 807-823. **Permission for reproduction granted by Bentham Science Publishers Ltd.**

Brown, H.K., Ottewell, P.D., Coleman, R.E., and Holen, I. (2011). The kinetochore protein Cenp-F is a potential novel target for zoledronic acid in breast cancer cells. J Cell Mol Med 15, 501-513.

Brown, J.E., Ellis, S.P., Lester, J.E., Gutcher, S., Khanna, T., Purohit, O.P., McCloskey, E., and Coleman, R.E. (2007). Prolonged efficacy of a single dose of the bisphosphonate zoledronic acid. Clin Cancer Res 13, 5406-5410.

Caraglia, M., Santini, D., Marra, M., Vincenzi, B., Tonini, G., and Budillon, A. (2006). Emerging anti-cancer molecular mechanisms of aminobisphosphonates. Endocrine-Related Cancer 13, 7-26.

Chambers, A.F. (2009). MDA-MB-435 and M14 cell lines: identical but not M14 melanoma? Cancer Res 69, 5292-5293.

Chantry, A.D., Heath, D., Mulivor, A.W., Pearsall, S., Baud'huin, M., Coulton, L., Evans, H., Abdul, N., Werner, E.D., Bouxsein, M.L., et al. (2010). Inhibiting activin-A signaling stimulates bone formation and prevents cancer-induced bone destruction *in vivo*. J Bone Miner Res 25, 2633-2646.

Chen, T., Berenson, J., Vescio, R., Swift, R., Gilchick, A., Goodin, S., LoRusso, P., Ma, P., Ravera, C., Deckert, F., et al. (2002). Pharmacokinetics and pharmacodynamics of zoledronic acid in cancer patients with bone metastases. J Clin Pharmacol 42, 1228-1236.

Clezardin, P. (2005). Anti-tumour activity of zoledronic acid. Cancer Treatment Reviews 31 Suppl 3, 1-8.

Clohisy, D.R., Ogilvie, C.M., Carpenter, R.J., and Ramnaraine, M.L. (1996a). Localized, tumor-associated osteolysis involves the recruitment and activation of osteoclasts. J Orthop Res 14, 2-6.

Clohisy, D.R., Palkert, D., Ramnaraine, M.L., Pekurovsky, I., and Oursler, M.J. (1996b). Human breast cancer induces osteoclast activation and increases the number of osteoclasts at sites of tumor osteolysis. J Orthop Res 14, 396-402.

Clyburn, R.D., Reid, P., Evans, C.A., Lefley, D.V., and Holen, I. (2010). Increased anti-tumour effects of doxorubicin and zoledronic acid in prostate cancer cells *in vitro*: supporting the benefits of combination therapy. Cancer Chemother Pharmacol 65, 969-978.

Coleman, R.E. (2001). Metastatic bone disease: clinical features, pathophysiology and treatment strategies. Cancer Treatment Reviews 27, 165-176.

Coleman, R.E., Body, J.J., Gralow, J.R., and Lipton, A. (2008). Bone loss in patients with breast cancer receiving aromatase inhibitors and associated treatment strategies. Cancer Treatment Reviews 34 Suppl 1, S31-42.

Coleman, R.E., Winter, M.C., Cameron, D., Bell, R., Dodwell, D., Keane, M.M., Gil, M., Ritchie, D., Passos-Coelho, J.L., Wheatley, D., et al. (2010). The effects of adding zoledronic acid to neoadjuvant chemotherapy on tumour response: exploratory evidence for direct anti-tumour activity in breast cancer. British Journal of Cancer 102, 1099-1105.

Coleman R.E., Marshall H., Cameron D., Dodwell D., Burkinshaw R., Keane M., Gil M., Houston S.J.,Gaunt C., Rea U., Peterson J., Davies C., Hiley V., Gregory W., Bell R.; AZURE Investigators. Breast-cancer adjuvant therapy with zoledronic acid. N Engl J Med. 2011 Oct 13;365(15):1396-405.

Conte, P., and Frassoldati, A. (2007). Aromatase inhibitors in the adjuvant treatment of postmenopausal women with early breast cancer: Putting safety issues into perspective. The breast Journal 13, 28-35.

Corey, E., Brown, L.G., Quinn, J.E., Poot, M., Roudier, M.P., Higano, C.S., and Vessella, R.L. (2003). Zoledronic acid exhibits inhibitory effects on osteoblastic and osteolytic metastases of prostate cancer. Clin Cancer Res 9, 295-306.

Cornish, J., Bava, U., Callon, K.E., Bai, J., Naot, D., and Reid, I.R. (2011). Bone-bound bisphosphonate inhibits growth of adjacent non-bone cells. Bone 49, 710-716.

Corrado, A., Neve, A., Maruotti, N., Gaudio, A., Marucci, A., and Cantatore, F.P. (2010). Dose-dependent metabolic effect of zoledronate on primary human osteoblastic cell cultures. Clin Exp Rheumatol 28, 873-879.

Coscia, M., Quaglino, E., Iezzi, M., Curcio, C., Pantaleoni, F., Riganti, C., Holen, I., Monkkonen, H., Boccadoro, M., Forni, G., et al. (2010). Zoledronic acid repolarizes tumour-associated macrophages and inhibits mammary carcinogenesis by targeting the mevalonate pathway. J Cell Mol Med 14, 2803-2815.

Coxon, F.P., Thompson, K., Roelofs, A.J., Ebetino, F.H., and Rogers, M.J. (2008). Visualizing mineral binding and uptake of bisphosphonate by osteoclasts and non-resorbing cells. Bone 42, 848-860.

Croucher, P.I., De Hendrik, R., Perry, M.J., Hijzen, A., Shipman, C.M., Lippitt, J., Green, J., Van Marck, E., Van Camp, B., and Vanderkerken, K. (2003). Zoledronic acid treatment of 5T2MM-bearing mice inhibits the development of myeloma bone disease: evidence for decreased osteolysis, tumor burden and angiogenesis, and increased survival. J Bone Miner Res 18, 482-492.

Daubine, F., Le Gall, C., Gasser, J., Green, J., and Clezardin, P. (2007). Antitumor effects of clinical dosing regimens of bisphosphonates in experimental breast cancer bone metastasis. J Natl Cancer Inst 99, 322-330.

Deleu, S., Lemaire, M., Arts, J., Menu, E., Van Valckenborgh, E., Vande Broek, I., De Raeve, H., Coulton, L., Van Camp, B., Croucher, P., et al. (2009). Bortezomib alone or in combination with the histone deacetylase inhibitor JNJ-26481585: effect on myeloma bone disease in the 5T2MM murine model of myeloma. Cancer Res 69, 5307-5311.

Derenne, S., Amiot, M., Barille, S., Collette, M., Robillard, N., Berthaud, P., Harousseau, J.L., and Bataille, R. (1999). Zoledronate is a potent inhibitor of myeloma cell growth and secretion of IL-6 and MMP-1 by the tumoral environment. J Bone Miner Res 14, 2048-2056.

Dhurjati, R., Krishnan, V., Shuman, L.A., Mastro, A.M., and Vogler, E.A. (2008). Metastatic breast cancer cells colonize and degrade three-dimensional osteoblastic tissue *in vitro*. Clin Exp Metastasis 25, 741-752.

Diel, I.J., Jaschke, A., Solomayer, E.F., Gollan, C., Bastert, G., Sohn, C., and Schuetz, F. (2008). Adjuvant oral clodronate improves the overall survival of primary breast cancer patients with micrometastases to the bone marrow: a long-term follow-up. Ann Oncol 19, 2007-2011.

Diel, I.J., Solomayer, E.F., Costa, S.D., Gollan, C., Goerner, R., Wallwiener, D., Kaufmann, M., and Bastert, G. (1998). Reduction in new metastases in breast cancer with adjuvant clodronate treatment. N Engl J Med 339, 357-363.

Doroshow, J.H. (1983). Cancer Res 43, 4543-4551.

Duivenvoorden, W.C., Vukmirovic-Popovic, S., Kalina, M., Seidlitz, E., and Singh, G. (2007). Effect of zoledronic acid on the doxycycline-induced decrease in tumour burden in a bone metastasis model of human breast cancer. British Journal of Cancer 96, 1526-1531.

Dunford, J.E., Thompson, K., Coxon, F.P., Luckman, S.P., Hahn, F.M., Poulter, C.D., Ebetino, F.H., and Rogers, M.J. (2001). Structure-activity relationships for inhibition of farnesyl diphosphate synthase *in vitro* and inhibition of bone resorption *in vivo* by nitrogen-containing bisphosphonates. The Journal of pharmacology and experimental therapeutics 296, 235-242.

Ellis, S.L., Grassinger, J., Jones, A., Borg, J., Camenisch, T., Haylock, D., Bertoncello, I., and Nilsson, S.K. (2011). The relationship between bone, hemopoietic stem cells, and vasculature. Blood 118, 1516-1524.

Erler, J.T., Bennewith, K.L., Cox, T.R., Lang, G., Bird, D., Koong, A., Le, Q.T., and Giaccia, A.J. (2009). Hypoxia-induced lysyl oxidase is a critical mediator of bone marrow cell recruitment to form the premetastatic niche. Cancer Cell 15, 35-44.

Fili, S., Karalaki, M., and Schaller, B. (2009). Mechanism of bone metastasis: the role of osteoprotegerin and of the host-tissue microenvironment-related survival factors. Cancer Lett 283, 10-19.

Fornari, F.A., Randolph, J.K., Yalowich J.C., Ritke, M.K., Gerwitz, D.A. (1994). Interference by doxorubicin with DNA unwinding in MCF-7 breast tumour cells. Mol Pharmacol 45, 649-656.

Fromigue, O., Lagneaux, L., and Body, J.J. (2000). Bisphosphonates induce breast cancer cell death *in vitro*. J Bone Miner Res 15, 2211-2221.

Garcia, T., Jackson, A., Bachelier, R., Clement-Lacroix, P., Baron, R., Clezardin, P., and Pujuguet, P. (2008). A convenient clinically relevant model of human breast cancer bone metastasis. Clin Exp Metastasis 25, 33-42.

Gebauer, G., Fehm, T., Merkle, E., Beck, E.P., Lang, N., and Jager, W. (2001). Epithelial cells in bone marrow of breast cancer patients at time of primary surgery: clinical outcome during long-term follow-up. J Clin Oncol 19, 3669-3674.

Girardi, M. (2006). Immunosurveillance and immunoregulation by gammadelta T cells. J Invest Dermatol 126, 25-31.

Gnant, M., Mlineritsch, B., Schippinger, W., Luschin-Ebengreuth, G., Postlberger, S., Menzel, C., Jakesz, R., Seifert, M., Hubalek, M., Bjelic-Radisic, V., et al. (2009). Endocrine therapy plus zoledronic acid in premenopausal breast cancer. N Engl J Med 360, 679-691.

Gober, H.J., Kistowska, M., Angman, L., Jeno, P., Mori, L., and De Libero, G. (2003). Human T cell receptor gammadelta cells recognize endogenous mevalonate metabolites in tumor cells. J Exp Med 197, 163-168.

Guenther, A., Gordon, S., Tiemann, M., Burger, R., Bakker, F., Green, J.R., Baum, W., Roelofs, A.J., Rogers, M.J., and Gramatzki, M. (2010). The bisphosphonate zoledronic acid has antimyeloma activity *in vivo* by inhibition of protein prenylation. Int J Cancer 126, 239-246.

Harada, S., and Rodan, G.A. (2003). Control of osteoblast function and regulation of bone mass. Nature 423, 349-355.

Hattner R., Epker B.N., Frost, H.M. (1965). Suggested sequential mode of control of changes in cell behaviour in adult bone remodelling. Nature 206, 489-90.

Heath, D.J., Chantry, A.D., Buckle, C.H., Coulton, L., Shaughnessy, J.D., Jr., Evans, H.R., Snowden, J.A., Stover, D.R., Vanderkerken, K., and Croucher, P.I. (2009). Inhibiting Dickkopf-1 (Dkk1) removes suppression of bone formation and prevents the development of osteolytic bone disease in multiple myeloma. J Bone Miner Res 24, 425-436.

Hiraga, T., Ueda, A., Tamura, D., Hata, K., Ikeda, F., Williams, P.J., and Yoneda, T. (2003). Effects of oral UFT combined with or without zoledronic acid on bone metastasis in the 4T1/luc mouse breast cancer. Int J Cancer 106, 973-979.

Hiraga, T., Williams, P.J., Ueda, A., Tamura, D., and Yoneda, T. (2004). Zoledronic acid inhibits visceral metastases in the 4T1/luc mouse breast cancer model. Clin Cancer Res 10, 4559-4567.

Hirbe, A.C., Roelofs, A.J., Floyd, D.H., Deng, H., Becker, S.N., Lanigan, L.G., Apicelli, A.J., Xu, Z., Prior, J.L., Eagleton, M.C., et al. (2009). The bisphosphonate zoledronic acid decreases tumor growth in bone in mice with defective osteoclasts. Bone 44, 908-916.

Hoffman, R.M. (1999). Orthotopic metastatic mouse models for anticancer drug discovery and evaluation: a bridge to the clinic. Invest New Drugs 17, 343-359.

Holen, I., and Coleman, R.E. (2010). Anti-tumour activity of bisphosphonates in preclinical models of breast cancer. Breast Cancer Res 12, 214.

Idris, A.I., Rojas, J., Greig, I.R., Van't Hof, R.J., and Ralston, S.H. (2008). Aminobisphosphonates cause osteoblast apoptosis and inhibit bone nodule formation *in vitro*. Calcif Tissue Int 82, 191-201.

Jagdev, S.P., Coleman, R.E., Shipman, C.M., Rostami, H.A., and Croucher, P.I. (2001). The bisphosphonate, zoledronic acid, induces apoptosis of breast cancer cells: evidence for synergy with paclitaxel. British Journal of Cancer 84, 1126-1134.

Jain, N., and Weinstein, R.S. (2009). Giant osteoclasts after long-term bisphosphonate therapy: diagnostic challenges. Nat Rev Rheumatol 5, 341-346.

Jones, D.H., Nakashima, T., Sanchez, O.H., Kozieradzki, I., Komarova, S.V., Sarosi, I., Morony, S., Rubin, E., Sarao, R., Hojilla, C.V., et al. (2006). Regulation of cancer cell migration and bone metastasis by RANKL. Nature 440, 692-696.

Joyce, J.A., and Pollard, J.W. (2009). Microenvironmental regulation of metastasis. Nat Rev Cancer 9, 239-252.

Jurasz, P., Alonso-Escolano, D., and Radomski, M.W. (2004). Platelet-cancer interactions: mechanisms and pharmacology of tumour cell-induced platelet aggregation. British Journal of Pharmacology 143, 819-826.

Kalluri, R., and Weinberg, R.A. (2009). The basics of epithelial-mesenchymal transition. J Clin Invest 119, 1420-1428.

Kalluri, R., and Zeisberg, M. (2006). Fibroblasts in cancer. Nat Rev Cancer 6, 392-401.

Kaplan, R.N., Riba, R.D., Zacharoulis, S., Bramley, A.H., Vincent, L., Costa, C., MacDonald, D.D., Jin, D.K., Shido, K., Kerns, S.A., et al. (2005). VEGFR1-positive haematopoietic bone marrow progenitors initiate the pre-metastatic niche. Nature 438, 820-827.

Kinder, M., Chislock, E., Bussard, K.M., Shuman, L., and Mastro, A.M. (2008). Metastatic breast cancer induces an osteoblast inflammatory response. Exp Cell Res 314, 173-183.

Kohno, N., Aogi, K., Minami, H., Nakamura, S., Asaga, T., Iino, Y., Watanabe, T., Goessl, C., Ohashi, Y., and Takashima, S. (2005). Zoledronic acid significantly reduces skeletal complications compared with placebo in Japanese women with bone metastases from breast cancer: a randomized, placebo-controlled trial. J Clin Oncol 23, 3314-3321.

Kopp, H.G., Hooper, A.T., Shmelkov, S.V., and Rafii, S. (2007). Beta-galactosidase staining on bone marrow. The osteoclast pitfall. Histol Histopathol 22, 971-976.

Kozloff, K.M., Weissleder, R., and Mahmood, U. (2007). Noninvasive optical detection of bone mineral. J Bone Miner Res 22, 1208-1216.

Kunzmann, V., Bauer, E., Feurle, J., Weissinger, F., Tony, H.P., and Wilhelm, M. (2000). Stimulation of gammadelta T cells by aminobisphosphonates and induction of antiplasma cell activity in multiple myeloma. Blood 96, 384-392.

Kunzmann, V., Bauer, E., and Wilhelm, M. (1999). Gamma/delta T-cell stimulation by pamidronate. N Engl J Med 340, 737-738.

Liapis, H., Flath, A., and Kitazawa, S. (1996). Integrin alpha V beta 3 expression by bone-residing breast cancer metastases. Diagn Mol Pathol 5, 127-135.

Lin, J.H., Chen, I.W., and Duggan, D.E. (1992). Effects of dose, sex, and age on the disposition of alendronate, a potent antiosteolytic bisphosphonate, in rats. Drug Metab Dispos 20, 473-478.

Luckman, S.P., Hughes, D.E., Coxon, F.P., Graham, R., Russell, G., and Rogers, M.J. (1998). Nitrogen-containing bisphosphonates inhibit the mevalonate pathway and prevent post-translational prenylation of GTP-binding proteins, including Ras. J Bone Miner Res 13, 581-589.

Martin, M.B., Arnold, W., Heath, H.T., 3rd, Urbina, J.A., and Oldfield, E. (1999). Nitrogen-containing bisphosphonates as carbocation transition state analogs for isoprenoid biosynthesis. Biochemical and Biophysical Research Communications 263, 754-758.

Masarachia, P., Weinreb, M., Balena, R., and Rodan, G.A. (1996). Comparison of the distribution of 3H-alendronate and 3H-etidronate in rat and mouse bones. Bone 19, 281-290.

Mendoza-Villanueva, D., Zeef, L., and Shore, P. (2011). Metastatic breast cancer cells inhibit osteoblast differentiation through the Runx2/CBFbeta-dependent expression of the Wnt antagonist, sclerostin. Breast Cancer Res 13, R106.

Mestas, J., and Hughes, C.C. (2004). Of mice and not men: differences between mouse and human immunology. J Immunol 172, 2731-2738.

Michigami, T., Hiraga, T., Williams, P.J., Niewolna, M., Nishimura, R., Mundy, G.R., and Yoneda, T. (2002). The effect of the bisphosphonate ibandronate on breast cancer metastasis to visceral organs. Breast Cancer Res Treat 75, 249-258.

Mohanty, S.T., Kottam, L., Gambardella, A., Nicklin, M.J., Coulton, L., Hughes, D., Wilson, A.G., Croucher, P.I., and Bellantuono, I. (2010). Alterations in the self-renewal and differentiation ability of bone marrow mesenchymal stem cells in a mouse model of rheumatoid arthritis. Arthritis Research & Therapy 12, R149.

Monkkonen, H., Auriola, S., Lehenkari, P., Kellinsalmi, M., Hassinen, I.E., Vepsalainen, J., and Monkkonen, J. (2006). A new endogenous ATP analog (ApppI) inhibits the mitochondrial adenine nucleotide translocase (ANT) and is responsible for the apoptosis induced by nitrogen-containing bisphosphonates. British Journal of Pharmacology 147, 437-445.

Monkkonen, H., Ottewell, P.D., Kuokkanen, J., Monkkonen, J., Auriola, S., and Holen, I. (2007). Zoledronic acid-induced IPP/ApppI production *in vivo*. Life Sci 81, 1066-1070.

Monkkonen, J., Koponen, H.M., and Ylitalo, P. (1990). Comparison of the distribution of three bisphosphonates in mice. Pharmacol Toxicol 66, 294-298.

Muller, A., Homey, B., Soto, H., Ge, N., Catron, D., Buchanan, M.E., McClanahan, T., Murphy, E., Yuan, W., Wagner, S.N., et al. (2001). Involvement of chemokine receptors in breast cancer metastasis. Nature 410, 50-56.

Mundy, G.R. (1997). Mechanisms of bone metastasis. Cancer 80, 1546-1556.

Murdoch, C., Giannoudis, A., and Lewis, C.E. (2004). Mechanisms regulating the recruitment of macrophages into hypoxic areas of tumors and other ischemic tissues. Blood 104, 2224-2234.

Neudert, M., Fischer, C., Krempien, B., Bauss, F., and Seibel, M.J. (2003). Site-specific human breast cancer (MDA-MB-231) metastases in nude rats: model characterisation and *in vivo* effects of ibandronate on tumour growth. Int J Cancer 107, 468-477.

Neville-Webbe, H.L., Evans, C.A., Coleman, R.E., and Holen, I. (2006). Mechanisms of the synergistic interaction between the bisphosphonate zoledronic acid and the chemotherapy agent paclitaxel in breast cancer cells *in vitro*. Tumour Biol 27, 92-103.

Neville-Webbe, H.L., Holen, I., and Coleman, R.E. (2002). The anti-tumour activity of bisphosphonates. Cancer Treatment Reviews 28, 305-319.

Neville-Webbe, H.L., Rostami-Hodjegan, A., Evans, C.A., Coleman, R.E., and Holen, I. (2005). Sequence- and schedule-dependent enhancement of zoledronic acid induced apoptosis by doxorubicin in breast and prostate cancer cells. Int J Cancer 113, 364-371.

Niehrs, C. (2006). Function and biological roles of the Dickkopf family of Wnt modulators. Oncogene 25, 7469-7481.

Ottewell, P., Brown, H., Jones, M., Rogers, T., Cross, S., Brown, N., Coleman, R., and Holen, I. (2011). Combination therapy inhibits development and progression of mammary tumours in immunocompetent mice. Breast Cancer Res Treat [Epub ahead of print].

Ottewell, P.D., Coleman, R.E., and Holen, I. (2006). From genetic abnormality to metastases: murine models of breast cancer and their use in the development of anticancer therapies. Breast Cancer Res Treat 96, 101-113.

Ottewell, P.D., Deux, B., Monkkonen, H., Cross, S., Coleman, R.E., Clezardin, P., and Holen, I. (2008a). Differential effect of doxorubicin and zoledronic acid on intraosseous versus extraosseous breast tumor growth *in vivo*. Clin Cancer Res 14, 4658-4666.

Ottewell, P.D., Lefley, D.V., Cross, S.S., Evans, C.A., Coleman, R.E., and Holen, I. (2010). Sustained inhibition of tumor growth and prolonged survival following sequential administration of doxorubicin and zoledronic acid in a breast cancer model. Int J Cancer 126, 522-532.

Ottewell, P.D., Monkkonen, H., Jones, M., Lefley, D.V., Coleman, R.E., and Holen, I. (2008b). Antitumor effects of doxorubicin followed by zoledronic acid in a mouse model of breast cancer. J Natl Cancer Inst 100, 1167-1178.

Ottewell, P.D., Woodward, J.K., Lefley, D.V., Evans, C.A., Coleman, R.E., and Holen, I. (2009). Anticancer mechanisms of doxorubicin and zoledronic acid in breast cancer tumor growth in bone. Mol Cancer Ther 8, 2821-2832.

Paget, S. (1889). The distribution of secondary growths in cancer of the breast. The Lancet 133, 571-573.

Parfitt, A.M. (1988). Bone histomorphometry: standardization of nomenclature, symbols and units (summary of proposed system). Bone 9, 67-69.

Parfitt, A.M. (2000). The mechanism of coupling: a role for the vasculature. Bone 26, 319-323.

Paterson, et al., (2011). NSABP-34. Annual San Antonio Breast Cancer Symposium Abstract S2-3.

Pecheur, I., Peyruchaud, O., Serre, C.M., Guglielmi, J., Voland, C., Bourre, F., Margue, C., Cohen-Solal, M., Buffet, A., Kieffer, N., et al. (2002). Integrin alpha(v)beta3 expression confers on tumor cells a greater propensity to metastasize to bone. Faseb J 16, 1266-1268.

Peyruchaud, O., Winding, B., Pecheur, I., Serre, C.M., Delmas, P., and Clezardin, P. (2001). Early detection of bone metastases in a murine model using fluorescent human breast cancer cells: application to the use of the bisphosphonate zoledronic acid in the treatment of osteolytic lesions. J Bone Miner Res 16, 2027-2034.

Phadke, P.A., Mercer, R.R., Harms, J.F., Jia, Y., Frost, A.R., Jewell, J.L., Bussard, K.M., Nelson, S., Moore, C., Kappes, J.C., et al. (2006). Kinetics of metastatic breast cancer cell trafficking in bone. Clin Cancer Res 12, 1431-1440.

Pozzi, S., Vallet, S., Mukherjee, S., Cirstea, D., Vaghela, N., Santo, L., Rosen, E., Ikeda, H., Okawa, Y., Kiziltepe, T., et al. (2009). High-dose zoledronic acid impacts bone remodeling with effects on osteoblastic lineage and bone mechanical properties. Clin Cancer Res 15, 5829-5839.

Psaila, B., and Lyden, D. (2009). The metastatic niche: adapting the foreign soil. Nat Rev Cancer 9, 285-293.

Reinholt, F.P., Hultenby, K., Oldberg, A., and Heinegard, D. (1990). Osteopontin-a possible anchor of osteoclasts to bone. Proc Natl Acad Sci U S A 87, 4473-4475.

Roche, B., David, V., Vanden-Bossche, A., Peyrin, F., Malaval, L., Vico, L., and Lafage-Proust, M.H. (2012). Structure and quantification of microvascularisation within mouse long bones: What and how should we measure? Bone 50, 390-399.

Roelofs, A.J., Coxon, F.P., Ebetino, F.H., Lundy, M.W., Henneman, Z.J., Nancollas, G.H., Sun, S., Blazewska, K.M., Lynn, F.B.J., Kashemirov, B.A., et al. (2009). Fluorescent risedronate analogs reveal bisphosphonate uptake by bone marrow monocytes and localization around Osteocytes i*n vivo*. J Bone Miner Res 25, 606-616.

Roelofs, A.J., Thompson, K., Ebetino, F.H., Rogers, M.J., and Coxon, F.P. (2010). Bisphosphonates: molecular mechanisms of action and effects on bone cells, monocytes and macrophages. Curr Pharm Des 16, 2950-2960.

Rogers, M.J., Gordon, S., Benford, H.L., Coxon, F.P., Luckman, S.P., Monkkonen, J., and Frith, J.C. (2000). Cellular and molecular mechanisms of action of bisphosphonates. Cancer 88, 2961-2978.

Rogers, T.L., and Holen, I. (2011). Tumour macrophages as potential targets of bisphosphonates. J Transl Med 9, 177.

Roodman, G.D. (2001). Biology of osteoclast activation in cancer. J Clin Oncol 19, 3562-3571.

Rosen, L.S., Gordon, D.H., Dugan, W., Jr., Major, P., Eisenberg, P.D., Provencher, L., Kaminski, M., Simeone, J., Seaman, J., Chen, B.L., et al. (2004). Zoledronic acid is superior to pamidronate for the treatment of bone metastases in breast carcinoma patients with at least one osteolytic lesion. Cancer 100, 36-43.

Ross, F. P., Chappel, J., Alvarez, J. I, Sander, D., Butler, W. T., Farach-Carson, M. C., Mintz, K. A., Robey, P. G., Teitelbaum, S. L., Cheresh, D. A. (1993). Interactions between the bone matrix proteins osteopontin and bone sialoprotein and the osteoclast integrin alpha v beta 3 potentiate bone resorption. J Biol Chem 268, 9901-7.

Saarto, T., Blomqvist, C., Virkkunen, P., and Elomaa, I. (2001). Adjuvant clodronate treatment does not reduce the frequency of skeletal metastases in node-positive breast cancer patients: 5-year results of a randomized controlled trial. J Clin Oncol 19, 10-17.

Saarto, T., Vehmanen, L., Virkkunen, P., and Blomqvist, C. (2004). Ten-year follow-up of a randomized controlled trial of adjuvant clodronate treatment in node-positive breast cancer patients. Acta Oncol 43, 650-656.

Santini, D., Vincenzi, B., Dicuonzo, G., Avvisati, G., Massacesi, C., Battistoni, F., Gavasci, M., Rocci, L., Tirindelli, M.C., Altomare, V., et al. (2003). Zoledronic acid induces significant and long-lasting modifications of circulating angiogenic factors in cancer patients. Clin Cancer Res 9, 2893-2897.

Santini, D., Vincenzi, B., Galluzzo, S., Battistoni, F., Rocci, L., Venditti, O., Schiavon, G., Angeletti, S., Uzzalli, F., Caraglia, M., et al. (2007). Repeated intermittent low-dose therapy with zoledronic acid induces an early, sustained, and long-lasting decrease of peripheral vascular endothelial growth factor levels in cancer patients. Clin Cancer Res 13, 4482-4486.

Sasaki, A., Boyce, B.F., Story, B., Wright, K.R., Chapman, M., Boyce, R., Mundy, G.R., and Yoneda, T. (1995). Bisphosphonate risedronate reduces metastatic human breast cancer burden in bone in nude mice. Cancer Res 55, 3551-3557.

Sasaki, A., Kitamura, K., Alcalde, R.E., Tanaka, T., Suzuki, A., Etoh, Y., and Matsumura, T. (1998). Effect of a newly developed bisphosphonate, YH529, on osteolytic bone metastases in nude mice. Int J Cancer 77, 279-285.

Sato, M., Grasser, W., Endo, N., Akins, R., Simmons, H., Thompson, D.D., Golub, E., and Rodan, G.A. (1991). Bisphosphonate action. Alendronate localization in rat bone and effects on osteoclast ultrastructure. J Clin Invest 88, 2095-2105.

Sato, N., Yamabuki, T., Takano, A., Koinuma, J., Aragaki, M., Masuda, K., Ishikawa, N., Kohno, N., Ito, H., Miyamoto, M., et al. (2010). Wnt inhibitor Dickkopf-1 as a target for passive cancer immunotherapy. Cancer Res 70, 5326-5336.

Schwaninger, R., Rentsch, C.A., Wetterwald, A., Van der Horst, G., van Bezooijen, R.L., van der Pluijm, G., Lowik, C.W.G.W., Ackermann, K., Pyerin, W., Hamdy, F.C., Thalmann, G.N., Cecchini, M.G. (2007). Lack of noggin expression by cancer cells is a determinant of the osteoblast response in bone metastases. American Journal of Pathology 170, 160-175.

Sebti, S.M. (2005). Protein farnesylation: implications for normal physiology, malignant transformation, and cancer therapy. Cancer Cell 7, 297-300.

Secondini. C., Wetterwald, A., Schwaninger, R., Thalmann, G.N., Cecchini, M.G. (2011). The role of the BMP signalling antagonist noggin in the development of prostate cancer osteolytic bone metastasis. PLoS ONE 6, e16078.

Shay G., Hornick M., Heys S., McKenna C., Ebetino F., Weilbaecher K., Rogers M. (2011). Nitrogen-containing Bisphosphonates are Internalised by Myeloid Derived Suppressor Cells (MDSCs) and Macrophages in a Mouse Breast Cancer Model. 11th International Conference of Cancer-Induced Bone Disease, poster 58.

Shi, R., Huang, C.C., Aronstam, R.S., Ercal, N., Martin, A., and Huang, Y.W. (2009). N-acetylcysteine amide decreases oxidative stress but not cell death induced by doxorubicin in H9c2 cardiomyocytes. BMC Pharmacology 9, 7.

Shiozawa, Y., Patel, L., Mishra A., Jung Y., Joseph J., Kim J.K., Wang J., Pienta K., Taichman R.(2011). The CD133+/CD44+ poulation is Enriched in Desseminated Human Prostate cance

Cells Isolated from Murine Marrow. 11th International Conference on Cancer-Induced Bone Disease, poster 51.

Shiozawa, Y., Pedersen, E.A., Havens, A.M., Jung, Y., Mishra, A., Joseph, J., Kim, J.K., Patel, L.R., Ying, C., Ziegler, A.M., et al. (2011). Human prostate cancer metastases target the hematopoietic stem cell niche to establish footholds in mouse bone marrow. J Clin Invest 121, 1298-1312.

Silber, R., Liu, L.F., Israel, M., Bodley, A.L., Hsiang, Y.H., Kirschenbaum, S., Sweatman, T.W., Seshadri, R., Potmesil, M. (1987). Metabolic activation of N-acylanthracyclines precedes their interaction with DNA topoisomerase II. NCI Monogr 4, 111-115.

Stopeck, A.T., Lipton, A., Body, J.J., Steger, G.G., Tonkin, K., de Boer, R.H., Lichinitser, M., Fujiwara, Y., Yardley, D.A., Viniegra, M., et al. (2010). Denosumab compared with zoledronic acid for the treatment of bone metastases in patients with advanced breast cancer: a randomized, double-blind study. J Clin Oncol 28, 5132-5139.

Subach OM, Patterson GH, Ting L, Wang Y, Condeelis JS, Verkhusha VV (2011). A photoswitchable orange-to-far-red fluorescent protein, PSmOrange. Nature Methods, 8,771–777

Takayama, S., Ishii, S., Ikeda, T., Masamura, S., Doi, M., and Kitajima, M. (2005). The relationship between bone metastasis from human breast cancer and integrin alpha(v)beta3 expression. Anticancer Res 25, 79-83.

Talmadge, J.E., Donkor, M., and Scholar, E. (2007). Inflammatory cell infiltration of tumors: Jekyll or Hyde. Cancer Metastasis Reviews 26, 373-400.

Teitelbaum, S.L. (2000). Bone resorption by osteoclasts. Science (New York, NY 289, 1504-1508.

Thiebaud, D., Sauty, A., Burckhardt, P., Leuenberger, P., Sitzler, L., Green, J.R., Kandra, A., Zieschang, J., and Ibarra de Palacios, P. (1997). An *in vitro* and *in vivo* study of cytokines in the acute-phase response associated with bisphosphonates. Calcif Tissue Int 61, 386-392.

Thomas, R.J., Guise, T.A., Yin, J.J., Elliott, J., Horwood, N.J., Martin, T.J., and Gillespie, M.T. (1999). Breast cancer cells interact with osteoblasts to support osteoclast formation. Endocrinology 140, 4451-4458.

Thompson, K., Rogers, M.J., Coxon, F.P., and Crockett, J.C. (2006). Cytosolic entry of bisphosphonate drugs requires acidification of vesicles after fluid-phase endocytosis. Molecular Pharmacology 69, 1624-1632.

Trebec, D.P., Chandra, D., Gramoun, A., Li, K., Heersche, J.N., and Manolson, M.F. (2007). Increased expression of activating factors in large osteoclasts could explain their excessive activity in osteolytic diseases. J Cell Biochem 101, 205-220.

van Beek, E., Pieterman, E., Cohen, L., Lowik, C., and Papapoulos, S. (1999). Farnesyl pyrophosphate synthase is the molecular target of nitrogen-containing bisphosphonates. Biochemical and Biophysical Research Communications 264, 108-111.

van Beek, E.R., Lowik, C.W., van Wijngaarden, J., Ebetino, F.H., and Papapoulos, S.E. (2009). Synergistic effect of bisphosphonate and docetaxel on the growth of bone metastasis in an animal model of established metastatic bone disease. Breast Cancer Res Treat 118, 307-313.

van der Horst G., v.d.Hoogen .C., Cheung H., Pelger R., van der Pluijm G. (2011). An Optimised Firefly Luciferase Reporter Allows Superior Real-Time Prostate Cancer Cell Tracking in

Preclinical Metastasis Models. 11th International Conference on Cancer-Induced Bone Disease, poster 67.

van der Pluijm, G., Que, I., Sijmons, B., Buijs, J.T., Lowik, C.W., Wetterwald, A., Thalmann, G.N., Papapoulos, S.E., and Cecchini, M.G. (2005). Interference with the microenvironmental support impairs the de novo formation of bone metastases *in vivo*. Cancer Res 65, 7682-7690.

Verdijk, R., Franke, H.R., Wolbers, F., and Vermes, I. (2007). Differential effects of bisphosphonates on breast cancer cell lines. Cancer Lett 246, 308-312.

Voorzanger-Rousselot, N., Goehrig, D., Journe, F., Doriath, V., Body, J.J., Clezardin, P., and Garnero, P. (2007). Increased Dickkopf-1 expression in breast cancer bone metastases. British Journal of Cancer 97, 964-970.

Vukmirovic-Popovic, S., Colterjohn, N., Lhotak, S., Duivenvoorden, W.C., Orr, F.W., and Singh, G. (2002). Morphological, histomorphometric, and microstructural alterations in human bone metastasis from breast carcinoma. Bone 31, 529-535.

Wai, P.Y., and Kuo, P.C. (2008). Osteopontin: regulation in tumor metastasis. Cancer Metastasis Reviews 27, 103-118.

Weinstein, R.S., Roberson, P.K., and Manolagas, S.C. (2009). Giant osteoclast formation and long-term oral bisphosphonate therapy. N Engl J Med 360, 53-62.

Weiss, H.M., Pfaar, U., Schweitzer, A., Wiegand, H., Skerjanec, A., and Schran, H. (2008). Biodistribution and plasma protein binding of zoledronic acid. Drug Metab Dispos 36, 2043-2049.

Weissleder, R., Tung, C.H., Mahmood, U., and Bogdanov, A., Jr. (1999). *In vivo* imaging of tumors with protease-activated near-infrared fluorescent probes. Nat Biotechnol 17, 375-378.

Widler L, Jaeggi KA, Glatt M, Müller K, Bachmann R, Bisping M, Born AR, Cortesi R, Guiglia G, Jeker H, Klein R, Ramseier U, Schmid J, Schreiber G, Seltenmeyer Y, Green JR (2002). Highly potent geminal bisphosphonates. From pamidronate disodium (Aredia) to zoledronic acid (Zometa). J Med Chem., 45(17):3721-38.

Wilson, C., and Coleman, R.E. (2011). Adjuvant therapy with bone-targeted agents. Curr Opin Support Palliat Care 5, 241-250.

Winter, M.C., Holen, I., and Coleman, R.E. (2008). Exploring the anti-tumour activity of bisphosphonates in early breast cancer. Cancer Treatment Reviews 34, 453-475.

Wood, J., Bonjean, K., Ruetz, S., Bellahcene, A., Devy, L., Foidart, J.M., Castronovo, V., and Green, J.R. (2002). Novel antiangiogenic effects of the bisphosphonate compound zoledronic acid. The Journal of Pharmacology and Experimental Therapeutics 302, 1055-1061.

Woodward, J.K., Coleman, R.E., and Holen, I. (2005). Preclinical evidence for the effect of bisphosphonates and cytotoxic drugs on tumor cell invasion. Anti-Cancer Drugs 16, 11-19.

Yao, W., Cheng, Z., Shahnazari, M., Dai, W., Johnson, M.L., and Lane, N.E. (2010). Overexpression of secreted frizzled-related protein 1 inhibits bone formation and attenuates parathyroid hormone bone anabolic effects. J Bone Miner Res 25, 190-199.

Yoneda, T., Michigami, T., Yi, B., Williams, P.J., Niewolna, M., and Hiraga, T. (1999). Use of bisphosphonates for the treatment of bone metastasis in experimental animal models. Cancer Treatment Reviews 25, 293-299.

Yoneda, T., Michigami, T., Yi, B., Williams, P.J., Niewolna, M., and Hiraga, T. (2000). Actions of bisphosphonate on bone metastasis in animal models of breast carcinoma. Cancer 88, 2979-2988.

Zaheer, A., Lenkinski, R.E., Mahmood, A., Jones, A.G., Cantley, L.C., and Frangioni, J.V. (2001). *In vivo* near-infrared fluorescence imaging of osteoblastic activity. Nat Biotechnol 19, 1148-1154.

9. Appendix

Publications and meeting abstracts arising from this thesis

Publications

Brown H.K., Ottewell P.D., Coleman R.E., Holen I. A single administration of combination therapy inhibits breast tumour progression in bone and modifies both osteoblasts and osteoclasts (2012). Journal of Bone Oncology, under review.

Brown H.K., Ottewell P.D., Evans C.A., Holen I. (2012). Location matters – osteoblast and osteoclast distribution is modified by the presence and proximity to breast cancer cells in vivo. Clin Exp Metastasis. 2012 May 6. [Epub ahead of print]. **Permission for reproduction granted.**

Brown H.K. and Holen I. (2009). Anti-tumour effects of bisphosphonates--what have we learned from *in vivo* models? Curr Cancer Drug Targets 9, 807-23. This review has been used in part in this thesis. **Permission for reproduction granted.**

Abstracts and presentations

Brown H.K., Wind N., Jones M., Shay G., Rogers M., McKenna C., Ebetino F., Holen I., (2011). Evidence of bisphosphonate internalisation by subcutaneous breast tumours in vivo – a pilot study. 11th International Conference on Cancer-Induced Bone Disease, Chicago, Illinois, USA. Poster 94.

Brown H.K., Ottewell P.D., Evans A., Coleman R.E., Holen I (2011). Early intervention with a single dose of doxorubicin followed by zoledronic acid induces sustained inhibition of breast cancer-induced bone disease in a mouse model. 3rd Joint Meeting of the ECTS/IBMS, Athens, Greece. Poster NIPP12, PP493, *New Investigator Session.*

Brown H.K., Wind N., Jones M., Rodgers M., Holen I. (2011). Distribution of the fluorescent risedronate-AF-647 in s.c. breast tumours and soft tissues *in vivo* – a pilot study. Mellanby Centre Research Day, University of Sheffield, UK. *Oral presentation.*

Brown H.K., Ottewell P.D., Evans A., Holen I (2010). Changes in osteoblast and osteoclast number rely on direct contact with breast cancer cells – evidence from a longitudinal study of bone metastasis. 10th International Conference Cancer-Induced Bone Disease, Sheffield, UK. Poster 58. *Winner of travel award.*

Brown H.K., Ottewell P.D., Evans A., Coleman R.E., Holen I (2010). Combination vs single agent treatment: the effects of zoledronic acid +/- doxorubicin on breast tumour growth in bone prior to development of osteolytic bone disease. 10th International Conference Cancer-Induced Bone Disease, Sheffield, UK. Poster 60**.**

Brown H.K., Ottewell P.D., Lefley D.V., Coleman R.E., Holen I. (2009). Effects of doxorubicin followed by zoledronic acid on early, medium and late stage breast tumour growth in bone. IX International Meeting on Cancer Induced Bone Disease, Arlington, Virginia, USA. Poster 87.

Brown H.K., Ottewell P.D., Holen I. (2009). Effects of sequential treatment with doxorubicin followed by zoledronic acid on breast tumour growth in bone. Mellanby Centre Opening, University of Sheffield, UK. Poster.

Publications and meeting abstracts produced during PhD studies

Publications

Holen I., Whitworth J., Nutter F., **Brown H.K.,** Evans C.A., Barbaric I., Jones M., Ottewell P.D., (2011). Plakoglobin mediates the metastatic potential of breast cancer cells in vitro and in vivo. Submitted to Breast Cancer Research. Under review.

Ottewell P.D., **Brown H.K**., Jones M., Rogers T.L., Cross S.S., Brown N.J., Coleman R.E. and Holen I., (2011). Combination therapy inhibits development and progression of mammary tumours in immunocompetent mice. Breast Cancer Res Treat. [Epub ahead of print].

Brown H.K., Ottewell P.D., Coleman R.E., Holen I., (2011). The kinetochore protein Cenp-F is a potential novel target for zoledronic acid in breast cancer cells. J Cell Mol Med 15, 501-13.

Michailidou M., **Brown H.K.,** Lefley D.V., Evans A., Cross S.S., Coleman R.E., Brown N.J., Holen I., (2010). Microvascular endothelial cell responses *in vitro* and *in vivo*: modulation by zoledronic acid and paclitaxel? J Vasc Res 47, 481-93.

Abstracts and presentations

Ottewell P.D., **Brown H.K.**, Rogers T., Lefley D.V., Evans C.A., Wind N.S., Brown N.J., Coleman R.E., Holen I. (2011). Prevention of spontaneous tumour growth by sequential administration of doxorubicin and zoledronic acid in an immunocompetent mouse model. Annals of Oncology 22, Poster 30.

Ottewell P.D., **Brown H.K.,** Evans C.A., Wind N.S., Brown N.J., Coleman R.E., Holen I. (2010). First evidence for anti-tumour effects of doxorubicin and zoledronic acid from an immunocompetent mouse model. 10th International Conference Cancer-Induced Bone Disease, Sheffield, UK. Poster 62.

Wind N.S., **Brown H.K.**, Ottewell P.D., Sadej R., Romanska H., Berditchevski F., Holen I. (2010). Does differential expression of CD151 affect the ability of breast cancer cells to establish tumours in bone? 10th International Conference Cancer-Induced Bone Disease, Sheffield, UK. Poster 70.

Brown H.K. and Holen I. (2008). The Effect of Zoledronic Acid on the Kinetochore Protein Cenp-F in Breast Cancer Cells. Annual Meeting of the European Bisphosphonate Network, University of Aberdeen, UK. Oral presentation.